An investigation into the importance of the ATM protein in the myocardial pathology associated with insulin resistance and type 2 diabetes

by

Yolandi Espach

Dissertation presented for the degree of Doctor of Philosophy (Medical Physiology)

in the Faculty of Medicine and Health Sciences

at Stellenbosch University

Supervisor: Prof. Barbara Huisamen

Co-Supervisors: Prof. Hans Strijdom and Prof. Anna-Mart Engelbrecht

March 2017

Declaration

By submitting this dissertation electronically, I declare that the entirety of the work contained therein is my own, original work, that I am the sole author thereof (save to the extent explicitly otherwise stated), that reproduction and publication thereof by Stellenbosch University will not infringe any third party rights and that I have not previously in its entirety or in part submitted it for obtaining any qualification.

Yolandi Espach

March 2017

Abstract

Introduction: Ataxia-telangiectasia (A-T) is an autosomal, recessive disorder that is caused by mutations in the ataxia-telangiectasia mutated (*ATM*) gene. The gene product, ATM, is a 350 kDa serine/threonine protein kinase with a large number of substrates in various pathways. Patients suffering from A-T display a high incidence of insulin resistance or type 2 diabetes mellitus (T2DM) and are more susceptible to ischaemic heart disease. Although it is known that the ATM protein is expressed in the heart and that structural and functional changes are observed in the hearts of ATM knock-out mice, very little research has been done on ATM and its role in insulin signalling in the cardiovascular context.

This project aimed to identify and characterise an obese, insulin resistant animal model in which myocardial ATM expression is altered; to use this model to determine the effect of ATM manipulation on myocardial function and response to ischaemia/reperfusion injury (IRI); and to determine the effect of ATM manipulation on insulin signalling networks.

Methodology: Male Wistar rats received a high caloric diet (HCD) or standard rat chow (control) for 16 weeks after which biometric data was collected. ATM was manipulated in perfusion studies prior to ischaemia using insulin (activator) and KU-60019 (inhibitor). Hearts perfused using the Langendorff balloon model were subjected to global ischaemia followed by reperfusion and Western blots were performed to evaluate insulin signalling intermediates. Hearts were also perfused using the working mode and subjected to regional ischaemia. Following reperfusion, infarct size (IFS) was determined. Aortic ring isometric tension studies were performed to determine the effect of KU-60019 on vasodilation.

Results: The HCD resulted in significantly increased body mass, visceral fat mass, glucose levels, insulin levels and HOMA-IR index compared to the control diet and ATM expression was

reduced in the HCD hearts. Cardiac function and IFS were comparable in the control and HCD hearts. In control hearts, insulin administration activated the insulin signalling network prior to ischaemia and cardiac function was improved during reperfusion. Insulin had no effect on the insulin signalling network or cardiac function in the insulin resistant HCD hearts. High concentrations of insulin increased IFS in both the control and HCD hearts.

ATM inhibition improved cardiac function in control and HCD hearts during early reperfusion but had no effect on cardiac function during later reperfusion. ATM phosphorylation was increased by insulin and decreased by KU-60019 in control hearts, but could not be manipulated in HCD hearts. Insulin-stimulated PKB/Akt activation is not ATM-dependent in the heart. However, ATM inhibition appears to down-regulate insulin signalling via PI3K, PTEN and GSK-3β. ATM inhibition caused NO-dependent vasodilation in control hearts, suggesting a role for ATM in vasoconstriction.

Conclusion: ATM is a complex signalling regulator with numerous substrates. In our study, we found that acute cardiac ATM inhibition did not result in significant cardiac dysfunction or complete abrogation of insulin signalling. However, we found that ATM possibly plays a significant role in vasoconstriction. More research needs to be done to fully understand the cardiac role of ATM in insulin signalling.

Opsomming

Inleiding: Ataxia-telangiectasia (A-T) is ‘n autosomale, resesiewe siekte wat deur mutasies in die *ATM* geen veroorsaak word. Die geenproduk, ATM, is ‘n 350 kDa serien/treonien proteïenkinase met ‘n groot aantal substrate wat in verskeie molekulêre paaie aktief is. Daar is ’n hoë insidensie van insulienweerstandigheid en tipe 2 diabetes mellitus onder A-T pasiënte en hulle ontwikkel ook meer iskemiese hartsiektes. Alhoewel dit bekend is dat ATM in die hart uitgedruk word en dat struktruele en funksionele veranderinge gesien kan word in die harte van muise wat nie die *ATM* geen het nie, is daar baie min bekend oor ATM se rol in insulien-seintransduksie in die hart.

Hierdie projek het beoog om ‘n vetsugtige, insulienweerstandige rotmodel te identifiseer waarin ATM vlakke verander is; om te bepaal hoe die hart reageer op iskemie/herperfusie wanneer ATM gemanipuleer word, en om te bepaal hoe ATM manipulasie insulien-seintransduksie beïnvloed.

Metodiek: Manlike Wistar rotte wat vir 16 weke ‘n hoë-kalorie dieet (HCD) of standaard rotkos (kontrole) gevoer is, is gebruik. ATM uitdrukking en/of aktivering is in die harte gemanipuleer deur hulle voor iskemie met insulien (aktiveerder) of KU-60019 (inhibitor) te perfuseer. Harte is met die Langendorff ballonmodel aan globale iskemie blootgestel en na herperfusie is proteïene van die insulien-seintransduksiepaaie met behulp van die Western-klad tegniek ge-analiseer. Harte is ook deur middel van die werkharttegniek aan streeksiskemie/herperfusie blootgestel waarna infarktgrootte bepaal is. Isometriese spanningsondersoeke is op aortaringe uitgevoer om die effek van KU-60019 op verslapping te bepaal.

Resultate: HCD diere het beduidende hoër liggaamsmassas en visserale vet massas; hoër glukosevlakke en insulienvlakke; ‘n verhoogde HOMA-IR indeks en laer ATM vlakke gehad as

die kontrole diere. Miokardiale funksie en infarktgroottes het nie verskil tussen kontrole en HCD harte nie. Insulien kon insulien-seintransduksie voor iskemie in kontrole harte stimuleer en het hartfunksie tydens herperfusie verbeter. Daarteenoor het insulien geen effek op hartfunksie of insulien-seintransduksie in die HCD harte gehad nie. In beide die kontrole en HCD harte het hoë konsentrasies insulien infarkte vergroot.

In kontrole en HCD harte het ATM inhibisie hartfunksie vroeg tydens herperfusie verbeter, maar het geen effek op hartfunksie later in herperfusie getoon nie. Alhoewel ATM fosforilering deur insulien verhoog is en deur KU-60019 verlaag is in kontrole harte, was daar geen verandering in ATM fosforilering in HCD harte nie. Insulien-gestimuleerde aktivering van PKB/Akt was nie afhanklik van ATM aktivering in die hart nie. ATM inhibisie het wel gelei tot onderdrukking van insulien-seintransduksie deur effekte op PI3K, PTEN en GSK-3β. ATM inhibisie het ook verslapping in aortaringe op ’n stikstofoksied-afhanklike manier veroorsaak wat ‘n aanduiding is dat ATM betrokke is by vasokonstriksie.

Gevolgtrekkings: Deur ‘n groot aantal substrate te beïnvloed, speel ATM ‘n belangrike rol in die regulering van seintranduksiepaaie. Ons het bevind dat akute inhibisie van ATM in die hart nie ‘n beduidende negatiewe effek op hartfunksie gehad het of insulien-seintransduksie onderdruk het nie. Ons het wel bevind dat ATM moontlik ‘n beduidende rol speel in vasokonstriksie. Verdere studies is nodig om die kardiovaskulêre rol van ATM in insulien-seintransduksie ten volle te verstaan.

Acknowledgements

I would like to extend my sincere gratitude towards the following people and institutions for their assistance and contributions during this study:

- I am so thankful for the Grace of God, without which I would never have finished.
- My promotor, Prof. Barbara Huisamen for guidance, insight and support throughout the study.
- My co-promotors Profs. Anna-Mart Engelbrecht and Hans Strijdom for critical reading of my dissertation.
- Sonia Genade for her patience and willingness to train me in the perfusion technique and for her technical input.
- Mignon van Vuuren for always lending a helping hand when it was needed and for her continual moral support.
- Ascentia Seboko, for her contribution to the western blots.
- Roseanne Allanson and Dr. Corli Westcott for their contributions to the aortic ring work.
- Dr. Sven Friedrich for his assistance with the FACS analysis.
- My sister, Noëlene Brits, for the design of Figures 2.2, 2.4, 2.6, 2.7 and 3.3.
- Colleagues and friends in the Division of Medical Physiology, for the supportive working environment.
- The NRF, Stellenbosch University and the Division of Medical Physiology for funding. The financial assistance of the National Research Foundation (NRF) towards this research is hereby acknowledged. Opinions expressed and conclusions arrived at, are those of the author and are not necessarily to be attributed to the NRF.
- Family and friends for their endless love, encouragement and support.
- I want to especially thank my parents for taking over night feeds so I can get enough sleep and for looking after Logan during the day so that I could complete my dissertation during my maternity leave. It would not have been possible without your help and support! Thank you Christo for your patience, help and sacrifice, especially after Logan's birth. I love you!

List of Figures

List of Tables

List of Abbreviations

2-DG	2-deoxy-D-[3H]glucose
AAR	Area at risk
ACC	Acetyl-CoA carboxylase
ACh	Acetylcholine
AMPK	AMP-activated protein kinase
ANOVA	Analysis of variance
AO	Aortic output
AP-1	Activator protein 1
AS160	Akt substrate of 160 kDa
A-T	Ataxia-telangiectasia
ATM	Ataxia-telangiectasia mutated
ATP	Adenosine triphosphate
BPM	Beats per minute
BSA	Bovine serum albumin
CF	Coronary flow
CoA	Coenzyme A
CVD	Cardiovascular disease
DC	Diabetic cardiomyopathy
DDR	DNA damage response
DIO	Diet induced obesity
DNA	Deoxyribonucleic acid
DNA-PK	DNA-dependent protein kinase
DP	Diastolic blood pressure
DSB	Double strand DNA breaks
eIF-4E	Eukaryotic initiation factor 4E
ELISA	Enzyme-linked immunosorbent assay

eNOS	Endothelial nitric oxide synthase
ER	Endoplasmic reticulum
$FADH_2$	Flavin adenine dinucleotide
FFA	Free fatty acid
GLUT4	Glucose transporter type-4
GS	Glycogen synthase
GSK-3	Glycogen synthase kinase-3
HCD	High caloric diet
HIF-1	Hypoxia inducible factor-1
IFS	Infarct size
IGF-I	Insulin-like growth factor-I
IKKβ	Iκβ kinase B
IR	Insulin receptor
IRI	Ischaemia/reperfusion injury
IRS	Insulin receptor substrate
JNK	Jun N-terminal kinase
KHB	Krebs-Henseleit buffer
LDL	Low density lipoprotein
LVDevP	Left ventricular developed pressure
MAPK	Mitogen-activated protein kinase
MAP2K	Mitogen-activated protein kinase kinase
MAP3K	Mitogen-activated protein kinase kinase kinase
MMPs	Matrix metalloproteinases
MRN	MRE11-RAD50-NBS1
mTORC1	Mammalian target of rapamycin complex-1
mTORC2	Mammalian target of rapamycin complex-2
NADH	Nicotinamide adenine dinucleotide
NADPH	Nicotinamide adenine dinucleotide phosphate
NO	Nitric oxide

OGTT	Oral glucose tolerance test
PDK1	3-phosphoinositide-dependent protein kinase-1
PE	Phenylephrine
PI	Propidium iodide
PI3K	Phosphatidylinositol 3-kinase
PIKK	Phosphatidylinositol 3-kinase-related kinase
PIP_2	Phosphatidylinositol (3,4)-bis-phosphate
PIP_3	Phospatidylinositol (3,4,5)-tris-phosphate
PKB	Protein kinase B
PP2A	Protein phosphatase 2A
PPP	Pentose phosphate pathway
PRAS40	Proline-rich Akt substrate of 40 kDa
PTEN	Phosphatase and tensin homolog
ROS	Reactive oxygen species
RPP	Rate pressure product
SEM	Standard error of the mean
SH2	Src Homology 2
SOS	Son-of-sevenless
SP	Systolic pressure
SPIKE	Signaling Pathway Integrated Knowledge Engine
T2DM	Type 2 diabetes mellitus
TAG	Triacylglycerol
TBST	Tris-buffered saline Tween-20
TNF-α	Tumour necrosis factor-alpha
TSC	Tuberous sclerosis complex
TTC	Triphenyl tetrazolium chloride
UPR	Unfolded protein response
VEGF	Vascular endothelial growth factor
VLDL	Very low density lipoproteins

WHO	World health organization

Units of Measurement

° C	Degree Celsius
µCi	Microcurie
µg	Microgram
µL	Microlitre
µm	Micrometre
%	Percentage
g	Gram
kDa	Kilodalton
kJ	Kilojoules
mg	Milligram
mL	Millilitre
mm	Millimetre
mM	Millimolar
N	Normality
ng	Nanogram
nM	Nanomolar
rpm	Revolutions per minute
U	Units

Table of Contents

Chapter 1: Introduction

1.1 General Introduction

Cardiovascular disease (CVD) is the leading cause of death globally, with approximately 31% of all deaths being attributed to CVD in 2012 as reported by the World Health Organization (WHO, Fact Sheet 317). In the same year, diabetes was ranked as the eighth leading cause of death in the world (WHO, Fact Sheet 310). Additionally, it is estimated that 387 million people were living with diabetes in 2014 and that 77% of these people are living in low- and middle-income countries (International Diabetes Federation, 2014). Alarmingly, the incidence of both CVD and diabetes is on the rise. This places a tremendous financial burden on governments, both for the treatment and management of these conditions and for the loss in productivity in individuals affected by CVD and diabetes.

Diabetes is a major contributing factor to the development of CVD, with 50% of diabetic individuals eventually dying of CVD (Morrish et al., 2001). Although a number of molecular mechanisms have been proposed to explain how diabetes can lead to CVD (reviewed in Bugger and Abel, 2014), new insights are continuously coming to light.

Ataxia-telangiectasia mutated (ATM) is a protein kinase well known for its nuclear role in the response to double-stranded deoxyribonucleic acid (DNA) breaks. In recent years, it has become apparent that ATM also plays important metabolic roles outside of the nucleus and that defective ATM signalling can lead to a clinical picture resembling that of the metabolic syndrome.

1.2 Problem Identification

Although it is known that ATM is expressed in the heart, very little scientific literature is available on ATM in the cardiovascular pathology context. It is as yet unknown how ATM participates in signalling networks in the heart. Additionally, the effect of the insulin resistant state on the expression or activation of ATM in the myocardium is unknown as well as the contribution of altered ATM signalling in the development of cardiovascular pathology associated with insulin resistance. The main purpose of this study was, therefore, to investigate the role of ATM in the myocardium, specifically in the insulin resistant state. We hypothesise that ATM plays a currently unrecognised role in the development of the cardiovascular pathology associated with the insulin resistant state.

1.3 Aims and Objectives

The aims of the study were as follows:

- To determine the myocardial expression of ATM in different rat models.

  Objective 1: Select the most suitable model to study the effects of the protein on cardiovascular function.

  Objective 2: Determine the whole-body glucose homeostasis in the chosen model as well as the myocardial insulin resistance.

- To determine the effects of manipulation of the expression or activation of ATM on myocardial function and resistance to IRI.

  Objective 1: Manipulate the expression and/or activation of ATM with insulin/chloroquine and the inhibitor KU-60019 using the *ex vivo* working heart perfusion model and

measure myocardial function and the ability of the hearts to recover contractile function after a period of regional ischaemia followed by reperfusion.

Objective 2: Use the same interventions but measure the IFS induced by regional ischaemia in hearts perfused using the *ex vivo* working heart model.

- To determine the effects of manipulation of the expression or activation of ATM on relevant myocardial signalling networks following IRI.

  Objective 1: Use the same interventions as in the previous aim in Langendorff *ex vivo* perfused hearts using the balloon model and subject the hearts to global ischaemia followed by reperfusion.

  Objective 2: Determine the expression and activation of signalling intermediates of the insulin network.

Chapter 2: Literature Review

2.1 Insulin Signalling

2.1.1 The history and structure of insulin

Insulin has been one of the most intensely studied proteins and has led to great technical advances in science. It was the first protein ever to be sequenced and has served as a model protein to help study the structure, properties and characteristics of other proteins. The term "insuline" (derived from the Latin *insula,* meaning island) was first used in 1909 by Jean De Meyer to describe "the internal secretion of the pancreas" (De Meyer, 1909). It was not until 13 years later that insulin was successfully purified by Frederick G. Banting and Charles H. Best (Banting et al., 1922). Frederick Sanger and colleagues were responsible for determining the protein sequence of the B and A chains of insulin in 1951 and 1953 respectively (Sanger and Thompson, 1953a,b; Sanger and Tuppy, 1951a,b), and in 1955 the primary protein structure of insulin was elucidated (Figure 2.1) (Ryle et al., 1955). Another decade later, scientists were able to successfully synthesise insulin for therapeutic use. Today, no other peptide or protein is more in use as a therapy than insulin and millions of people globally are dependent on insulin for the treatment of diabetes (Mayer et al., 2007).

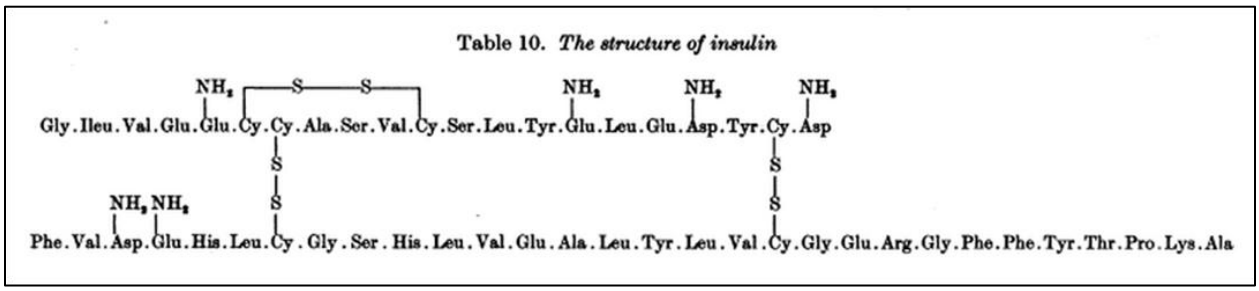
Table 10. *The structure of insulin*

NH₂ S—S NH₂ NH₂ NH₂

Gly.Ileu.Val.Glu.Glu.Cy.Cy.Ala.Ser.Val.Cy.Ser.Leu.Tyr.Glu.Leu.Glu.Asp.Tyr.Cy.Asp

S S

NH₂ NH₂ S S

Phe.Val.Asp.Glu.His.Leu.Cy.Gly.Ser.His.Leu.Val.Glu.Ala.Leu.Tyr.Leu.Val.Cy.Gly.Glu.Arg.Gly.Phe.Phe.Tyr.Thr.Pro.Lys.Ala

Figure 2.1: The primary protein structure of insulin as it appeared in Ryle et al., 1955.

Insulin is a peptide hormone secreted by the β-cells of the islands of Langerhans in the pancreas. Insulin consists of two polypeptide chains held together by two disulphide bonds. Chain A consists of 21 amino acid residues while chain B is longer, consisting of 30 amino acid residues.

2.1.2 Normal insulin signalling

Although plasma glucose levels rise and fall during the day due to meal ingestion, fasting and exercise, it is important that the levels are maintained in a narrow range as both hypo- and hyperglycaemia have severe consequences. Insulin is one of the very important hormones responsible for maintaining glucose homeostasis. Tissues that are responsive to insulin include skeletal and cardiac muscle, adipose tissue and the liver. Insulin is described to have both an excitatory and an inhibitory action in these tissues as it increases the uptake of glucose in muscle and fat tissue, and decreases glucose production and release by the liver (Saltiel and Kahn, 2001; Sonksen and Sonksen, 2000). After food is ingested, the resulting rise in plasma glucose will trigger the release of insulin from the β-cells in the pancreas, causing a three- to fourfold increase in insulin levels within 60 minutes. In fact, an increase in plasma glucose levels as small as 10 mg/dL (0.55 mmol/L) will result in the secretion of insulin (Shrayyef and Gerich, 2010). Insulin secretion may also be stimulated by increased amino acids and free fatty acids (FFA). By binding to receptors in its target tissues, insulin activates a cascade of signalling events that results in the glucose to either be immediately stored as glycogen or undergo oxidative or non-oxidative glycolysis.

Insulin never enters the cells. It simply binds to the alpha subunit of the transmembrane insulin receptor (IR) tyrosine kinase to initiate the signalling cascade inside the cell. The IR is activated through trans-autophosphorylation, after which it recruits and phosphorylates any one of six members of the insulin receptor substrate (IRS) family. This results in activation of either the

metabolic phosphatidylinositol 3-kinase (PI3K)-protein kinase B (PKB)/Akt pathway or the mitogenic Ras-mitogen-activated protein kinase (MAPK) pathway (Taniguchi et al., 2006). The IRS family are scaffolding proteins that recruit and dock downstream proteins (White, 1998). Of the six known IRS isoforms, IRS-1 and IRS-2 are the most widely distributed and the most important. Both IR and IRS are activated by tyrosine phosphorylation, but inhibited by serine phosphorylation. A third pathway, the CAP-Cbl-TC10 pathway, is also activated in response to insulin stimulation following IR activation (Figure 2.2).

The PI3K-PKB/Akt pathway

The PI3K-PKB/Akt pathway is a highly conserved pathway (Hemmings and Restuccia, 2012). The class 1A PI3K is a heterodimer, consisting of a 110 kDa (p110) catalytic subunit and an 85 kDa (p85) regulatory subunit (Carpenter et al., 1990). Once IRS-1 is activated, the phosphorylated tyrosine residues create sites that can associate with proteins containing Src Homology 2 (SH2) domains. PI3K is activated via the p85 regulatory subunit that contains SH2 domains that can dock to tyrosine phosphorylated IRS-1. The catalytic subunit converts the membrane bound lipid, phosphatidylinositol (3,4)-bis-phosphate (PIP_2), to phosphatidylinositol (3,4,5)-tris-phosphate (PIP_3), which in turn recruits both PKB/Akt and 3-phosphoinositide-dependent protein kinase-1 (PDK1) to the plasma membrane, allowing PKB/Akt to be phosphorylated in the kinase domain, at threonine 308, by PDK1 (Alessi et al., 1997; Hemmings and Restuccia, 2012). This association is mediated by the plecstrin homology domains of proteins which allow them to associate with specific phosphorylated inositide lipids in specific membrane structures. The conversion of PIP_2 to PIP_3 is negatively regulated by the tumour suppressor, phosphatase and tensin homolog (PTEN) (Maehama and Dixon, 1998). Full activation of PKB/Akt is only achieved after phosphorylation in the regulatory domain, at serine 473, possibly mediated by mammalian target of rapamycin complex 2 (mTORC2), DNA-

dependent protein kinase (DNA-PK) or ATM (Bozulic and Hemmings, 2009; Sarbassov et al., 2005; Viniegra et al., 2005).

Activated PKB/Akt contributes to a number of processes, including cell survival, cell growth, proliferation, angiogenesis, cell migration and metabolism (Manning and Cantley, 2007). By negatively regulating pro-apoptotic proteins such as BAD and deactivating pro-apoptotic transcription factors such as FOXO and p53, PKB/Akt promotes cell survival (Datta et al., 1997; Tran et al., 2003). Cell growth is achieved by the activation of Mammalian target of rapamycin complex-1 (mTORC1) and the downstream effects of p70S6K and 4EBP1/eIF-4E (Laplante and Sabatini, 2012). PKB/Akt phosphorylates tuberous sclerosis complex (TSC) 2 on multiple sites, which destabilizes the TSC1/TSC2 complex which usually inhibits mTORC1 (Inoki et al., 2002). Additionally, PKB/Akt has also been shown to phosphorylate proline-rich Akt substrate of 40 kDa (PRAS40) causing PRAS40 to dissociate from mTORC1 and lifting the inhibitory effect on mTORC1 (Wiza et al., 2012). The activation of mTORC1 also results in cell proliferation through the translation of proteins involved in cell-cycle progression (Manning and Cantley, 2007). Glycogen synthase kinase-3 (GSK-3) phosphorylates proteins responsible for cell-cycle progression which results in proteasomal degradation of these proteins and thus, inhibition of cell-cycle progression. Therefore, by phosphorylating and inactivating GSK-3, PKB/Akt contributes to cell-cycle progression and proliferation (Diehl et al., 1998). Angiogenesis, as well as vasodilation and vascular remodelling is the result of nitric oxide (NO) being released after PKB/Akt phosphorylates and activates endothelial NO synthase (eNOS) (Dimmeler et al., 1999; Morbidelli et al., 2003). PKB/Akt additionally affects angiogenesis by increasing the production of hypoxia inducible factor-1 (HIF-1), a transcription factor that leads to the expression of vascular endothelial growth factor (VEGF), which is responsible for angiogenesis (Lee et al., 2007).

Metabolically, PKB/Akt plays an important role in glucose uptake in adipose tissue and muscle and in the inhibition of glucose production by the liver in response to insulin. Glucose transporter type-4 (GLUT4) levels at the plasma membrane rise at least 10-fold in response to insulin (Welsh et al., 2005). In muscle, PKB/Akt has been shown to phosphorylate the Akt substrate of 160 kDa (AS160) on multiple sites, causing it to stimulate GLUT4 translocation to the cell membrane and glucose to be taken up by the cells (Manning and Cantley, 2007; Sakamoto and Holman, 2008). Both GSK-3α and -β are phosphorylated and thus, inactivated, by PKB/Akt, causing an increased conversion of glucose to glycogen by glycogen synthase (GS) in muscle and liver (Cross et al., 1995). Plasma glucose levels are further reduced by PKB/Akt by increasing the rate of glycolysis, the process by which glucose is broken down to pyruvate (Elstrom et al., 2004).

The CAP/Cbl/TC10 pathway

Although the PI3K-PKB/Akt pathway is required for GLUT4 translocation, it is not sufficient on its own (Chiang et al., 2001). Once the IR is activated, the adaptor protein, APS, binds to the IR and recruits CAP, which in turn recruits the proto-oncogene, Cbl to the IR and a CAP/Cbl complex is formed. Upon phosphorylation of Cbl, the CAP/Cbl complex is released from the IR and gets translocated to lipid rafts. Lipid rafts are areas in the plasma membrane that are enriched in cholesterol and specific lipids and proteins such as sphingolipids, lipid-modified signalling proteins, glycosylphosphotidylinositol-anchored proteins and glycolipids (Pike, 2009). Once at the lipid raft, Cbl recruits the CrkII-C3G complex and C3G activates TC10, leading to GLUT4 translocation and the subsequent uptake of glucose in response to insulin stimulation (Chiang et al., 2001; Tomasovic et al., 2012). The CAP/Cbl/TC10 pathway takes place in parallel to the PI3K-PKB/Akt pathway, but is PI3K-independent (See Figure 2.2).

The MAPK pathway

The MAPK pathway is a signalling cascade that amplifies an extracellular signal and achieves proliferation, differentiation and development (Seger and Krebs, 1995). The signalling pathway consists of a MAPK kinase kinase (MAP3K), MAPK kinase (MAP2K) and a MAPK, and each of these phosphorylates and activates the next protein in the signalling pathway (i.e. MAP3K phosphorylates and activates MAP2K, which then phosphorylates and activates MAPK). In response to insulin stimulation, and the consequent activation of the IR, son-of-sevenless (SOS) is recruited to the IR and activates a small GTPase, namely Ras (Geiβler et al., 2013). Ras leads to the sequential activation of Raf (a MAP3K), MEK1/2 (a MAP2K) and ERK1/2, the MAPK (Kim and Choi, 2010). The MAPK pathway results in cell proliferation, cell-cycle regulation, differentiation, cell migration and cell survival in response to insulin (Peyssonnaux and Eychène, 2012).

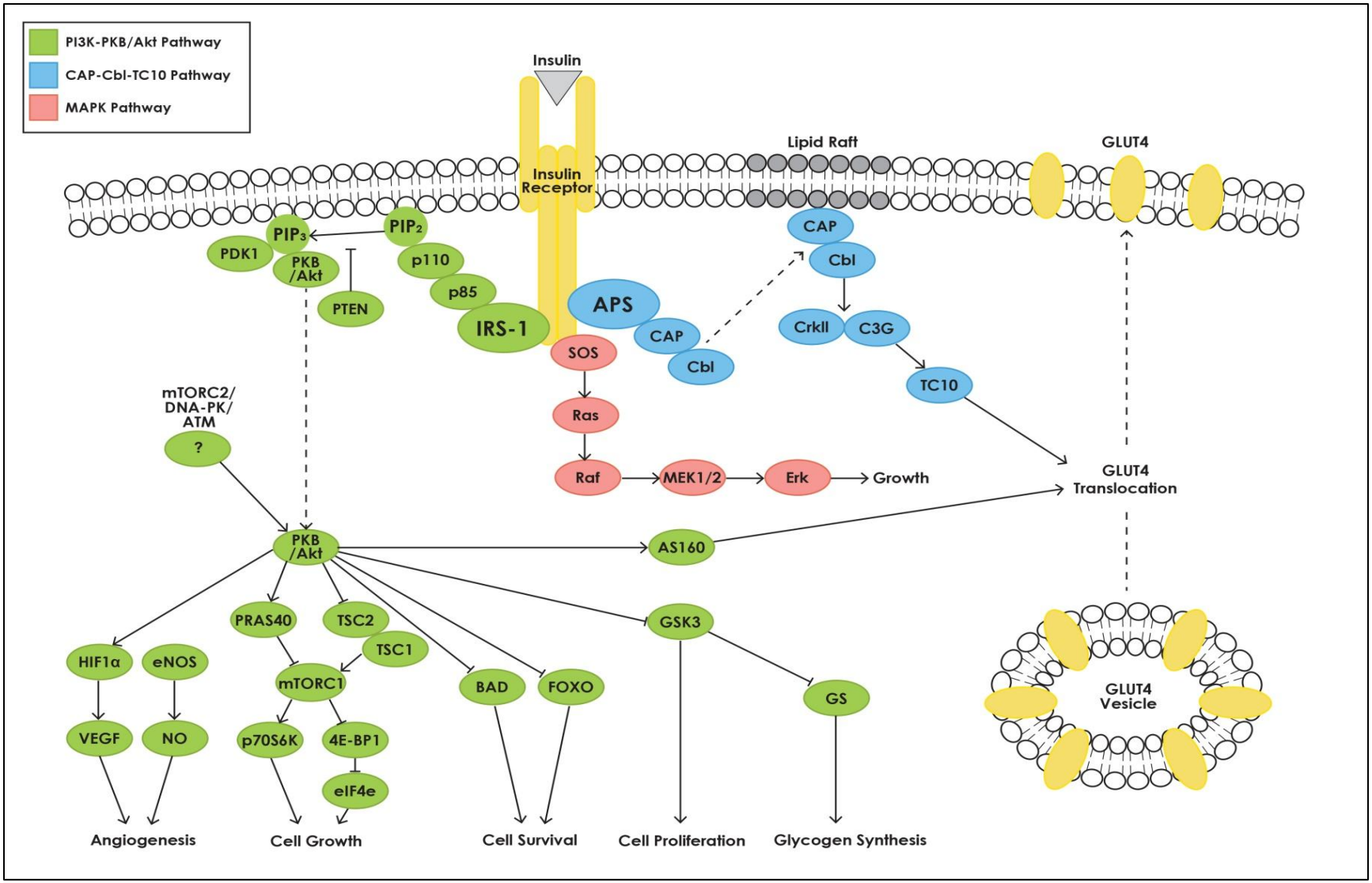

Figure 2.2: Binding of insulin to the insulin receptor results in the activation of three different pathways, namely the PI3K-PKB/Akt pathway, the CAP-Cbl-TC10 pathway and the MAPK pathway. These pathways result in a range of different processes such as angiogenesis, cell growth, cell survival, cell proliferation, glycogen synthesis and glucose uptake.

2.1.3 The development of insulin resistance

Insulin resistance is defined as a decreased ability of cells to respond to insulin (Nieto-Vazqiez et al., 2008). To compensate for this effect, the pancreas secretes more insulin, leading to hyperinsulinemia. However, this can only be tolerated for a short period of time, after which it leads to β-cell failure and ultimately, T2DM (White, 2003). Insulin resistance has a complicated aetiology in which a number of different pathways have been shown to play a role.

Obesity and insulin resistance

Thirteen percent of the global population, accounting for 600 million people, were obese in 2014 according to the WHO (WHO, Fact Sheet 311). Obesity is considered the most common contributor to the development of insulin resistance in humans (Johnson and Olefsky, 2013). An individual is classified as obese when their body mass index, calculated as weight in kilograms divided by height in meters squared (kg/m^2) is higher than 30 kg/m^2. Obesity is the result of surplus energy being stored as fat when more energy is consumed in food than what is needed and used (Bray, 2004). Adipose tissue, made up of fat cells, is recognized as a metabolic and endocrine organ. During obesity, the function of adipose tissue is altered, resulting in increased release of fatty acids, hormones and pro-inflammatory cytokines (Weisberg et al., 2003).

Obese individuals are considered to experience chronic low-level inflammation as macrophages infiltrate adipose tissue and pro-inflammatory cytokine levels increase in the obese state (Tzanavari et al., 2010). One of the pro-inflammatory cytokines that is elevated during obesity, is tumour necrosis factor-alpha (TNF-α), which is over-expressed in adipose tissue (Hotamisligil et al., 1993). Elevated TNF-α levels have been shown to be consistent with the degree of obesity as well as hyperinsulinemia (Hotamisligil et al., 1995). Upon treatment with TNF-α, reduced insulin-stimulated autophosphorylation of IR was observed, as well as reduced tyrosine phosphorylation and increased serine phosphorylation of IRS-1 in adipocytes (Hotamisligil et al.,

1996). Improved insulin sensitivity was found to be associated with decreased TNF-α levels that accompanied weight loss in obese individuals (Hotamisligil et al., 1995). Although the insulin resistant effect of cytokines released from adipose tissue is predominantly local, the cytokines could cause a systemic effect in muscle and liver when their levels rise, causing them to leak out from the adipose tissue (Osborn and Olefsky, 2012). It is noted that it is only visceral adipose tissue, and not subcutaneous adipose tissue, that display the increased inflammation and macrophage infiltration and the accompanying negative effect on metabolism (Johnson and Olefsky, 2013).

In addition to an increase in pro-inflammatory cytokines during obesity, increased plasma FFA concentrations are also observed and have been implicated in the development of insulin resistance (Nielsen et al., 2004). In fact, insulin resistance that developed in high-fat diet fed rats was found to be due to FFAs in circulation rather than increased TNF-α levels (Jiao et al., 2008). Free fatty acids are bound to albumin in the plasma and this is how triacylglycerol (TAG), which is usually stored in adipose tissue, is transported to other sites for utilization (Karpe et al., 2011). The main source of FFAs is the abdominal subcutaneous adipose tissue, while a small portion of FFAs is released by visceral fat (Karpe et al., 2011; Vatier et al., 2012). High levels of FFAs were first described to contribute to abnormal carbohydrate metabolism and to lead to the development of insulin resistance in 1963 (Randle et al., 1963). In what is now termed the Randle cycle, Randle and colleagues (1963) explained that dynamic interactions exist between substrates and that glucose and fatty acids compete with each other to be oxidized in muscle and adipose tissue. They thus proposed that high FFA levels are able to inhibit glucose oxidation. Fatty acid oxidation increases the mitochondrial acetyl-coenzyme A (CoA)/CoA and nicotinamide adenine dinucleotide (NADH) /NAD^+ ratios. The increased ratios lead to the inhibition of pyruvate dehydrogenase in order to reduce the production of acetyl-CoA. Furthermore, accumulation of citrate in the cytosol inhibits 6-phosphofructo-1-kinase which

increases glucose-6-phosphate, eventually leading to hexokinase inhibition (summarised in Hue and Taegtmeyer, 2009). It has now been shown that high FFA concentrations reduce glucose uptake by reducing glycogen synthesis and carbohydrate oxidation, by stimulating glycogenolysis and also by increasing hepatic gluconeogenesis, all leading to hyperglycaemia (Boden et al., 1994; Staehr et al., 2003). Insulin sensitivity is improved through weight loss and exercise and this effect is mediated by reduced FFA mobilization and uptake (Schenk et al., 2009). Conversely, others have shown that insulin resistance can develop in the absence of elevated FFA and that high FFA levels are not necessarily associated with insulin resistance, and it is suggested that more dynamic studies are needed to elucidate the relationship between FFA and insulin resistance (Karpe et al., 2011).

A role for GSK-3 in the development of insulin resistance has also been proposed. Although GSK-3 protein levels have been shown to be increased during T2DM, limited studies are available on the regulation of GSK-3 in insulin resistance (Lee and Kim, 2007; Nikoulina et al., 2002). Mice genetically prone to the development of diet-induced obesity and diabetes (C57BL/6J mouse strain), had increased GSK-3 activity levels in adipose tissue compared to mice resistant to diet-induced obesity and diabetes (Eldar-Finkelman et al., 1999). Basally active GSK-3 can contribute to the development of insulin resistance as it is able to oppose the action of insulin by inhibiting glucose uptake and glycogen synthesis as well as inhibiting IRS-1, and thus, the insulin signalling pathway (Liberman and Eldar-Finkelman, 2005).

Ectopic fat accumulation

Besides the role of circulating FFAs, ectopic fat accumulation has also been implicated in the development of insulin resistance. Ectopic fat is the result of storage of triglycerides in insulin responsive tissues other than adipose tissue, such as muscle and the liver (Snel et al., 2012). These lipids accumulate when the supply is bigger than the capacity of the liver and muscle to

oxidize the lipids. Partial oxidation of FFA results in accumulation of metabolites such as long-chain acyl-CoA, diacylglycerol and ceramides that are able to activate protein kinase C, IKB-kinase-β and c-Jun N-terminal kinase (JNK). These proteins phosphorylate serine residues in IRS-1, causing inhibition and ultimately, insulin resistance (reviewed in Morino et al., 2006).

Endoplasmic reticulum stress and activation of the unfolded protein response

The endoplasmic reticulum (ER), together with the attached ribosomes, are responsible for protein and lipid synthesis and the consequent folding of the newly synthesized proteins (Alberts et al., 2002). When problems with the folding of proteins arise, the unfolded protein response (UPR) is launched. The aims of the UPR are to reduce the rate at which mRNA is translated, to enlarge the folding capacity of the ER and to degrade incorrectly folded proteins (Scheuner and Kaufman, 2008). Activation of the UPR has been shown to contribute to insulin resistance via a number of different mechanisms, but a central theme appears to be the alteration of lipid balance through accumulation of lipid intermediates (reviewed in Samuel and Shulman, 2012).

Oxidative stress and insulin resistance

Oxidants are free oxygen or nitrogen radicals that are natural by-products of aerobic metabolism that play significant beneficial physiological roles by acting as second messengers in signalling cascades. However, when the production of oxidants exceeds the antioxidant capacity of the cell, oxidative stress ensues (Sies, 1997). Hyperglycaemia is able to induce both mitochondrial and ER dysfunction, causing an increase in oxidative stress (Fiorentino et al., 2013). Other causes of increased levels of reactive molecules include inflammatory cytokines, hyperinsulinemia and high levels of FFA (Evans et al., 2005). Oxidative stress, in turn activates stress-sensitive molecules such as JNK, PKC, TNF-α and Iκβ kinase B (IKKβ), all of which have been shown to inhibit insulin signalling by inactivating the IR and/or IRS-1 (Evans et al., 2005). Several studies have shown that treating diabetic or insulin resistant patients with antioxidants

such as vitamin C, vitamin E or α-lipoic acid improved insulin sensitivity (Caballero, 1993; Hirashima et al., 2000; Jacob et al., 1999).

2.1.4 The development of diabetes

Insulin resistance is linked to a number of different conditions such as T2DM, hypertension, dyslipidemia, non-alcoholic fatty liver disease, blood coagulation problems and fibrinolysis (Bray, 2004). Insulin resistance can ensue for a long time before the eventual development of T2DM, and during this time blood glucose levels could be maintained in the normal range through compensatory mechanisms such as hyperinsulinemia (Kahn, 2003). Eventually, the β-cells of the pancreas can no longer maintain the increased insulin production required to overcome insulin resistance. The resulting hyperglycaemia and high FFA levels lead to oxidative stress, which is detrimental to β-cell function and structure (Cerf, 2013; Gastaldelli, 2011). T2DM is widely thought to be caused by a combination of insulin resistance and pancreatic β-cell dysfunction. The cardiorenal metabolic syndrome, which is comprised of a number of metabolic abnormalities, is said to drive the T2DM epidemic. These metabolic abnormalities include the following: a HCD accompanied by a sedentary lifestyle that leads to obesity; hyperglycaemia due to insulin resistance; pre-hypertension caused by increased vascular tone; dyslipidemia due to a rise in pro-inflammatory cytokines; kidney dysfunction due to decreased glomerular filtration and microalbuminuria (Mandavia et al., 2013; Sowers et al., 2011). Individuals have an increased risk for the development of T2DM if they display impaired glucose tolerance and/or fasting glucose levels, have hypertension, high triglyceride levels and low high-density lipoprotein-cholesterol (dyslipidemia) levels. Additional factors include having a close relative with T2DM (genetics) or previously having gestational diabetes during pregnancy.

2.2 The heart and insulin resistance

2.2.1 The metabolism of the heart

The heart has a higher metabolic demand per gram than any other organ in the body. It utilizes adenosine triphosphate (ATP) as energy source to fuel basal metabolism, contraction and ionic homeostasis (Lopaschuk et al., 2010). If ATP synthesis were to cease, cardiac ATP stores would be depleted within approximately 15 seconds. In order to maintain adequate ATP levels, the rates at which ATP is produced and used must thus be closely regulated. Because of the high ATP demand, the heart is capable of using a number of different substrates to generate enough ATP. These substrates include fatty acids, carbohydrates, lactate, ketone bodies and amino acids (Weiss and Maslov, 2004). The heart is able to alternate between the choice of substrates and adapt rapidly during exercise, ischaemia and fasting when the supply of substrates or need for ATP is changed (Stanley et al., 2005). Under non-ischaemic conditions, over 95% of the heart's energy is produced through the oxidation of fatty acids and carbohydrates (Lopaschuk et al., 2010). Below is a simplified overview of the use of fatty acids and carbohydrates as substrates as these are the predominant substrates used for energy production in the heart. A schematic representation of myocardial metabolism can be seen in Figure 2.3.

Fatty acid metabolism

The β-oxidation of fatty acids generates the most ATP molecules and fatty acids are thus the predominant substrate used by cardiac cells, producing 50-70% of the ATP in the adult heart (Lopaschuk et al., 2010; Weiss and Maslov, 2004). The fatty acids are either taken up from the plasma or they are released by the breakdown of stored TAG that is already present in the cardiomyocyte (Stanley et al., 1997). Once fatty acids, bound to fatty acid binding proteins, enter the cytosol of cardiomyocytes, they are esterified into long-chain fatty acyl CoA by fatty

acyl-CoA synthetase. The fatty acyl-CoA is transported into the mitochondria with the help of carrier proteins and once in the mitochondria, they enter the β-oxidation cycle. During each cycle, acyl-CoA becomes two carbons shorter and acetyl-CoA, flavin adenine dinucleotide ($FADH_2$) and NADH are produced (Lopaschuk et al., 2010). The reducing agents, $FADH_2$ and NADH, take part in the electron transport chain while acetyl-CoA enters the Krebs cycle (also known as the citric acid cycle or tricarboxylic acid cycle) and both of these processes result in the generation of ATP.

Carbohydrate metabolism

Glucose uptake is dependent on the glucose transmembrane gradient as well as the presence of glucose transporters at the plasma membrane (Stanley et al., 1997). Besides the insulin responsive transporter, GLUT4, GLUT1 has also been shown to be present in the myocardium and to be responsible for a significant amount of basal glucose uptake in the heart (Abel, 2004). During exercise and stresses such as ischaemia and hypoxia, GLUT4 translocation can be stimulated by AMP–activated protein kinase (AMPK) (Coven et al., 2003; Russel et al., 1999). During glycolysis, which takes place in the cytosol, each glucose molecule is converted into two molecules each of pyruvate, ATP and NADH (Mathews et al., 2000). Pyruvate is further metabolised in the mitochondria by decarboxylation to form acetyl-CoA. The acetyl-CoA derived from carbohydrates is subsequently fed into the Krebs cycle similar to the acetyl-CoA derived from fatty acid β-oxidation, in order to produce ATP.

Although fatty acid oxidation produces more ATP molecules than carbohydrate metabolism, glucose is a more oxygen-efficient energy source for producing ATP than fatty acids (Fukushima et al., 2015; Lopaschuk et al., 2010). It has also been shown that cardiac efficiency decreases with an increased utilization of fatty acids as substrate as opposed to glucose as is the case during obesity, insulin resistance, diabetes and reperfusion after an ischaemic period

(Lopaschuk et al., 2010). The efficiency of the heart is determined by comparing the myocardial oxygen consumption with the work performed by the left ventricle (Bing and Michal, 1959).

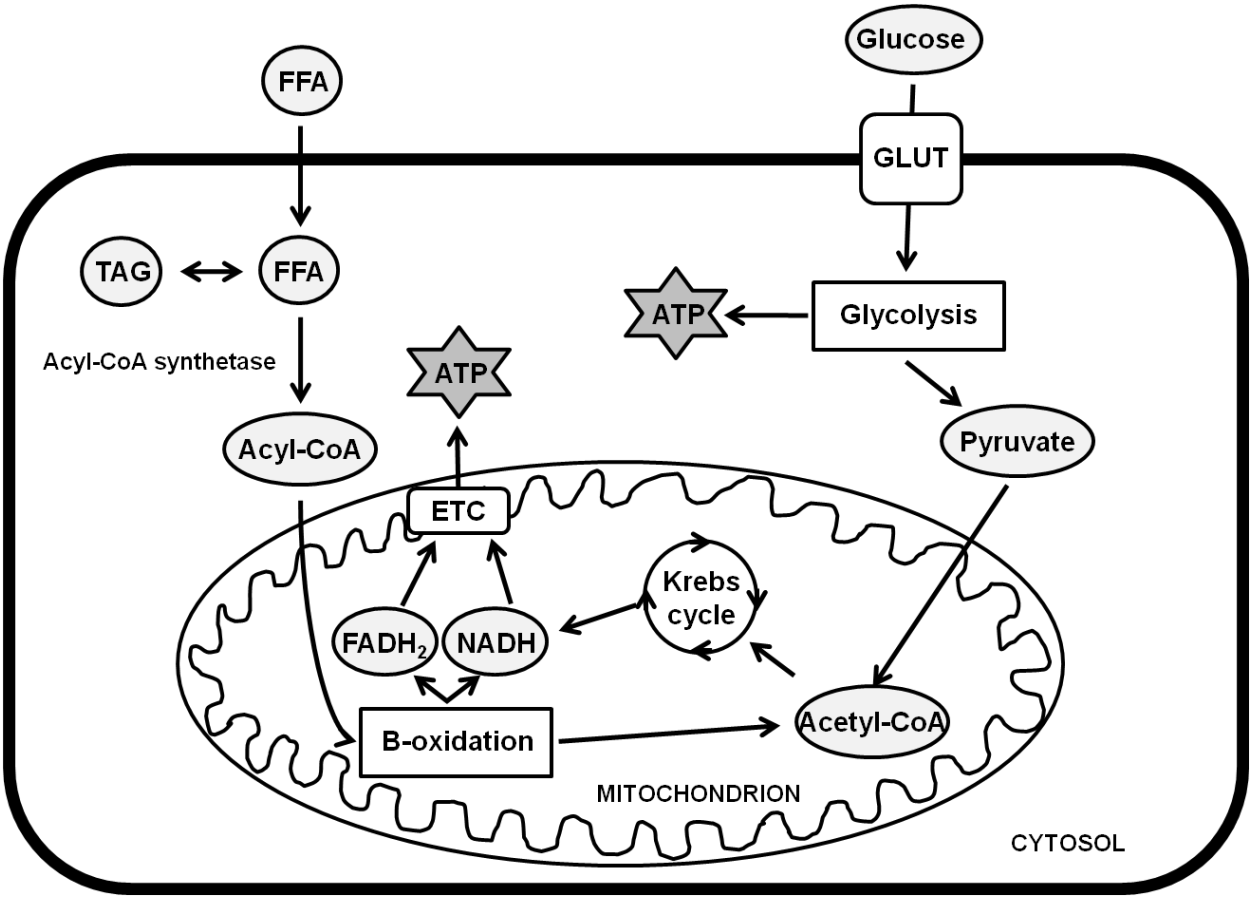

Figure 2.3: Schematic representation of the substrate metabolism of the heart. Free fatty acids, taken up from the plasma or released from TAG, is converted to acyl-CoA before entering the mitochondria where they undergo β-oxidation. This results in the release of acetyl-CoA, NADH and FADH2. The acetyl-CoA enters the Krebs cycle which also results in the release of NADH and FADH2. These reducing agents then enter the electron transport chain for the generation of ATP. Glucose is taken up by cardiomyocytes via the GLUT transporter family and converted to glucose-6-phosphate, which can either be stored as glycogen or enter glycolysis. Glycolysis produces both ATP and pyruvate. Pyruvate is converted into acetyl-CoA, which follows the same fate as acetyl-CoA produced from fatty acid metabolism.

2.2.2 Mechanisms that lead to cardiovascular disease

Cardiovascular disease is an umbrella term used to describe conditions affecting the heart and vascular system. These conditions include hypertensive heart disease, stroke, arrhythmias, coronary artery disease, myocardial infarction, rheumatic heart disease, cardiomyopathy, atrial fibrillation, congenital heart disease, endocarditis, aortic aneurysms, peripheral artery disease, venous thrombosis and cardiac failure (Wattanapitayakul and Bauer, 2001). A number of underlying mechanisms have been defined and these vary depending on the condition in question. Only a few mechanisms that are relevant to this study will be discussed in more detail below.

Substrate usage and cardiovascular disease

Cardiac substrate usage is tightly controlled and the choice of substrate is dependent on their supply, need for energy production, hormones and transcription factors. Metabolic abnormalities such as obesity, and the accompanying high fatty acid levels, insulin resistance, hyperinsulinemia and hyperglycaemia interfere with the normal functioning of the heart and can, therefore, lead to cardiac dysfunction. Hypertensive and ischaemic heart disease are more prevalent in diabetic patients compared to healthy individuals and diabetic cardiomyopathy (DC), which is not associated with hypertension or coronary artery disease, is also a hallmark of diabetes (Mandavia et al., 2013). In fact, the presence of T2DM can increase the likelihood of having CVD up to fivefold (Dagogo-Jack and Santiago, 1997).

A potential mechanism for the development of CVD during T2DM is the increased reliance on fatty acids as substrate during diabetes. Due to the increased oxidation of fatty acids as opposed to glucose, there is a greater oxygen cost for ATP production, which leaves the heart at risk of energy depletion during periods of limited oxygen supply or when workload is increased (McNulty, 2006). Hafstad and colleagues also demonstrated that isolated hearts from

diabetic db/db mice increasingly oxidized fatty acids and showed decreased glucose oxidation compared to non-diabetic db/+ hearts. Additionally, contractile dysfunction, exhibited as reduced peak aortic systolic pressure (SP), cardiac output and work, was also observed in diabetic hearts. Surprisingly, they found that the diabetic db/db hearts were, in fact, responsive to large insulin doses and that insulin increased PKB/Akt phosphorylation, glucose uptake, and glucose oxidation and decreased fatty acid oxidation in these hearts. Insulin had no effect on contractile function in either the diabetic or non-diabetic hearts (Hafstad et al., 2006).

Although it is well known that obesity, insulin resistance and diabetes contribute to the development of CVD, it is becoming evident that the heart is able to tolerate insulin resistance. It is suggested in several studies that hearts of T2DM individuals may have very little to no loss of insulin sensitivity compared to hearts of non-diabetic individuals (Jagasia et al., 2001; Utriainen et al., 1998). Nevertheless, defective systemic insulin signalling, that is comprised of hyperinsulinemia, hyperglycaemia and insulin resistance, gives rise to oxidative stress which is thought to be the basis of the metabolic dysfunction that leads to DC (Aksakal et al., 2011). It is proposed that insulin resistance in the heart and the lack of metabolic flexibility are the main contributing factors to metabolic cardiomyopathy (Mandavia et al., 2013).

Diabetic cardiomyopathy

Diabetic cardiomyopathy was first described in 1972 by Rubler et al. (1972). They noted myocardial changes while performing autopsies on diabetic patients that could not be explained by hypertension, coronary artery complications, valvular or neuromuscular disease, alcoholism, uraemia or renal disease, and concluded that it must be a form of cardiomyopathy associated with diabetes that had not been described previously (Rubler et al., 1972). Only abnormal muscle function is implicated in DC, which is the initial manifestation of heart disease associated with diabetes (Mandavia et al., 2013). Early in DC, diastolic dysfunction and ventricular

hypertrophy are observed, while systolic dysfunction becomes evident later in the condition. A number of mechanisms, causing structural and signalling alterations have been described in DC.

Increased left ventricular mass and wall thickness are seen in individuals with T2DM compared to non-diabetic individuals (Eguchi et al., 2008; Somaratne et al., 2011). Leptin, which is released by adipose tissue, was shown to increase endothelin-1, which in turn stimulated the production of reactive oxygen species (ROS) and led to hypertrophy in cultured neonatal rat cardiomyocytes (Xu et al., 2004). Another cytokine over-expressed during diabetes, both by adipose tissue and the heart, is resistin. Resistin was shown to contribute to the development of hypertrophy in neonatal cardiomyocytes via the activation of ERK and p38 in the MAPK pathway as well as IRS-1 serine phosphorylation (Kim et al., 2008). Diastolic dysfunction is the result of intra-myocardial lipid accumulation during diabetes, obesity, insulin resistance and impaired glucose tolerance. This lipid accumulation is termed cardiac steatosis, is independent from circulating triglyceride levels and exceeds the oxidative capacity of the mitochondria (McGavock et al., 2007). Cardiac steatosis leads to the production of lipotoxic intermediates that cause apoptosis through the increased production of ROS (Zhou et al., 2000). Interstitial and perivascular fibrosis is seen in DC, with significantly increased collagen type III in diabetic patients compared to healthy individuals (Shimizu et al., 1993).

As mentioned earlier, diastolic dysfunction is observed early in DC. Diastolic dysfunction could occur due to increased lipid accumulation in the heart or alterations in the calcium homeostasis (Boudina and Abel, 2010). Since mitochondria play a central role in metabolism, and diabetes is known to alter metabolism, it is no surprise that mitochondrial dysfunction is present and plays a role in the pathogenesis of DC. Potential mechanisms that contribute to the mitochondrial dysfunction in the hearts of diabetic patients include mitochondrial uncoupling and altered energy metabolism, oxidative stress, defective handling of calcium by mitochondria,

mitochondrial-induced cell death and increased mitochondrial biogenesis without improved mitochondrial respiration or ATP production (reviewed in Duncan, 2011). Compromised mitochondrial function during diabetes can thus lead to contractile dysfunction and contribute to the development of DC.

Although all the mechanisms involved in the development of DC have not yet been elucidated, it is clear that DC is associated with structural, functional and metabolic changes that lead to cardiac dysfunction and heart failure that is independent of coronary artery disease or hypertension (Boudina and Abel, 2010).

Endothelial dysfunction and atherosclerosis

Nitric oxide synthase converts L-arginine into L-citrulline in endothelial cells, which is associated with the production of NO. Vascular effects of NO include vasodilation, decreased migration and growth of vascular smooth muscle cells, aggregation of platelets and thrombosis, inflammation and monocyte and macrophage adhesion (Caballero, 2003). During diabetes, both a reduction in the production of NO by endothelial cells and a reduced response to NO in vascular smooth muscle cells are observed (Williams et al., 1996). Endothelial dysfunction develops when there is a loss of balance between vasoconstrictors and vasodilators, promoters and inhibitors of growth, pro- and anti-atherogenic factors and pro- and anti-coagulant factors (Quyyumi, 1998). Endothelial dysfunction has been associated with obesity and insulin resistance and is considered to be a key element in the development of atherosclerosis (Steinberg et al., 1996).

Obesity, and the resulting high plasma FFA levels, leads to increased FFA levels in the liver. The delivery of high FFA levels to the liver, accompanied by hepatic insulin resistance and hyperinsulinemia, results in increased production and secretion of very low density lipoproteins (VLDL) by the liver (reviewed in Julius, 2003; Lewis, 1997). Once in circulation, VLDL are converted to low density lipoproteins (LDL), and high LDL concentrations are associated with an

increased risk for the development of CVD and, specifically, atherosclerosis (McLeod et al., 2004). When oxidized, LDL is phagocytosed by macrophages, forming foam-cells that hinder the degradation of oxidized LDL and perpetuates the high LDL levels (Shashkin et al., 2005; Sowers and Lester, 1999). The accumulation of foam cells in the tunica intima of blood vessels is the hallmark first step in the progression to atherosclerotic lesions (Yu et al., 2013).

Oxidative stress

Superoxide, hydrogen peroxide, hydroxyl radical and NO are all forms of ROS that are involved in the cardiovascular system (Molavi and Mehta, 2004). These free radicals can be produced via nicotinamide adenine dinucleotide phosphate (NADPH) oxidase, xanthine oxidase, NOS or uncoupling of the electron transport chain. A role for ROS in cardiac damage was first identified through IRI and myocardial infarction, where acute periods of reduced perfusion and oxygen deprivation are followed by perfusion and oxygen restoration. This leads to alterations in myocardial metabolism, the production of ROS and cell death. It is interesting to note that more ROS is produced and more ROS-related damage occurs during reperfusion than during the ischaemic or hypoxic state. It is now known that ROS not only contributes to cardiovascular complications during acute ischaemic or hypoxic periods, but also in the progression of chronic CVD states (Wattanapitayakul and Bauer, 2001).

Oxidative stress has been found to be associated with reduced left ventricular function and ventricular remodelling and it is suggested that the amount of free radicals produced is correlated with the severity of the heart failure (Belch et al., 1991; Mallat et al., 1998). A role for oxidative stress has also been described in the development of cardiac hypertrophy (reviewed in Maulik and Kumar, 2011). When superoxide interacts with NO, peroxynitrite is formed. Peroxynitrite is cytotoxic, and can result in lipid peroxidation, protein oxidation, activation of matrix metalloproteinases (MMPs) that are implicated in chamber remodelling, and alterations in

excitation-contraction coupling, leading to impaired contractility (Katori et al., 2006; Pacher et al., 2005).

2.3 Mammalian heart perfusion as a tool to study cardiovascular disease

Ethical considerations, difficulties in obtaining tissue and the inability to control and limit confounding factors limit the use of human subjects in cardiovascular research. Although it is not without shortcomings, the use of animal models has significantly contributed to our understanding of normal and pathogenic biological structures and functions, including the cardiovascular system. Myocardial perfusion of rodent or small mammalian hearts is a particularly useful technique to study and investigate myocardial functioning in the healthy or diseased state or in response to various pharmaceutical substances.

2.3.1 The principles of myocardial perfusion

Langendorff perfused heart model

The isolated perfused mammalian heart technique was initially developed in 1895 by Oskar Langendorff, based on the isolated frog heart perfusion method (Langendorff, 1895). In this method, named Langendorff or retrograde perfusion, oxygenated perfusate is administered via a cannula inserted into the ascending aorta. This forces the aortic valves to close and the perfusate enters the coronary ostia, causing the coronary vasculature of the heart to be perfused. The perfusate then drains into the right atrium via the coronary sinus and flows out of the heart (Figure 2.4a) (Liao et al., 2012; Sutherland and Hearse, 2000). The Langendorff perfused heart continues beating, however, it is not considered a working heart as the heart chambers are not being filled and the perfusate is not ejected by the heart (Liao et al., 2012). Langendorff perfusion experiments can make use of constant pressure or constant flow and can be used to investigate the effect of pharmaceutical compounds on myocardial function, electrical

conduction, reactivity of the vasculature, vascular endothelial and smooth muscle function, myocardial ischaemia, stunning and preconditioning (Liao et al., 2012). Modifications to the Langendorff method include the insertion of an inflatable balloon into the left ventricle to measure isovolumic pressures (Gottlieb et al., 1904) and the use of constant flow to determine changes in pressure during perfusion which signifies vascular resistance (Katz et al., 1939).

Working heart perfusion model

Another modification to the perfusion technique, developed by Neely et al. (1967), enables the perfused heart to have pump action and, thus, to perform mechanical work. This is now known as the working heart or ejecting heart perfusion technique and is a more physiologically relevant perfusion technique compared to the Langendorff technique. In the working heart model, perfusate is administered to the left atrium via the cannulated left pulmonary veins. The perfusate is then transferred to the left ventricle and ejected out the cannulated aorta by the beating heart (Figure 2.4b). The heart works against constant preload and afterload hydrostatic pressure (Liao et al., 2012). This method is preferred for studies investigating substrate usage and metabolic parameters under physiological conditions and the use of a microconductance catheter enables the measurement of the pressure-volume relationship (Liao et al., 2012).

The most commonly used perfusate is Krebs-Henseleit buffer (KHB), which is a crystalloid bicarbonate buffer. Although fatty acids are the preferred metabolic substrate of the heart under normal physiological conditions, glucose is mostly used as substrate in perfusion experiments due to the low solubility of fatty acids and the frothing that occurs as a result of the oxygenation of a fatty acid-containing perfusate (Liao et al., 2012). The perfusate is oxygenated with a 95% O_2 / 5% CO_2 gas mixture.

In spite of some limitations to the technique, such as the absence of neuronal and humoral influences, the perfusate being cell-free and a high coronary flow (CF) (Skrzypiek-Spring et al.,

2007), the many advantages make the mammalian isolated heart perfusion technique a useful tool in the study of the cardiovascular system. Advantages of the technique include its simplicity and relatively low cost, high reproducibility, a large number of measurable parameters and the accuracy at which parameters can be measured (Skrzypiek-Spring et al., 2007). The ability to study the effects of global or regional ischaemia and reperfusion injury using *ex vivo* perfusion experiments makes it a powerful tool in cardiovascular research as the experiments can continue in spite of heart pump failure or lethal arrhythmias, which would otherwise kill the animal in *in vivo* studies (Sutherland and Hearse, 2000).

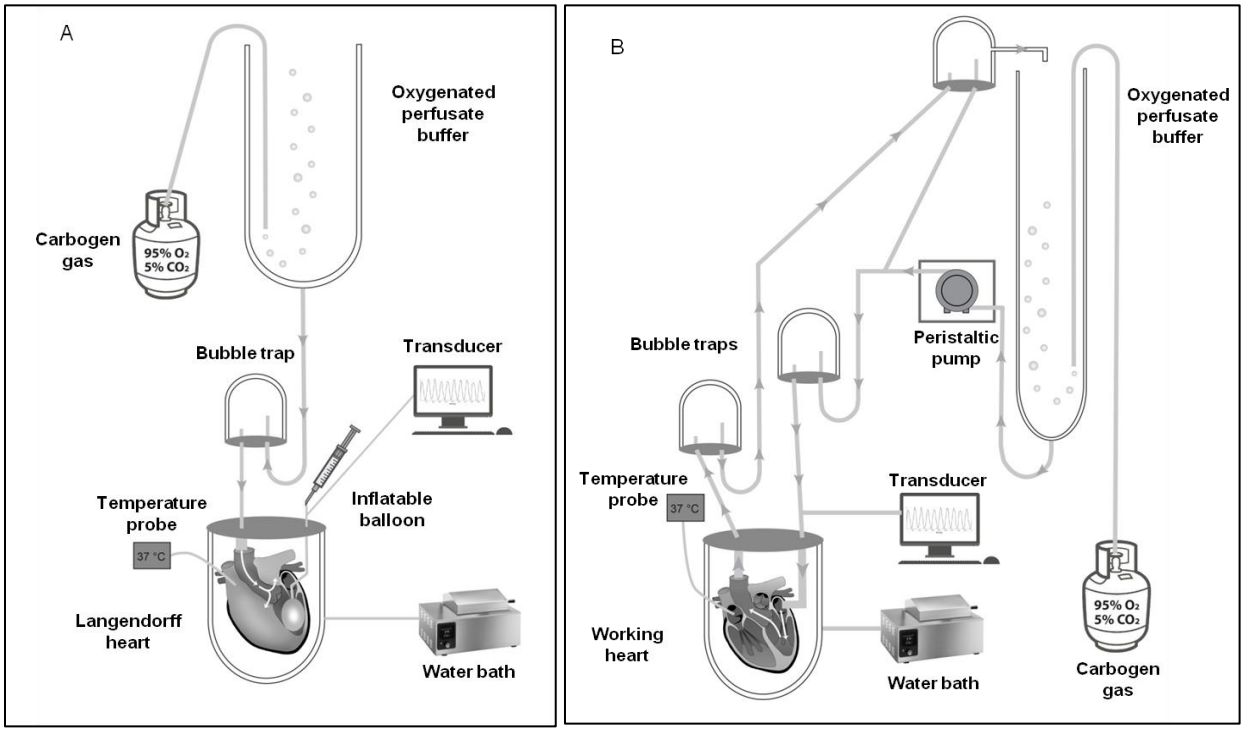

Figure 2.4: Schematic representation of the basic elements of the A) Langendorff perfusion method and B) working heart perfusion method.

2.3.2 Myocardial ischaemia/reperfusion injury

Myocardial ischaemia

When the supply of blood (or perfusate) to the heart is restricted, a lack in both oxygen and nutrients is experienced, while metabolites accumulate as they cannot be removed. This is referred to as myocardial ischaemia. In perfusion experiments, global myocardial ischaemia is induced when the total perfusion supply to the heart is interrupted, while regional ischaemia is induced by ligation of the left descending coronary artery, thereby interrupting perfusion to that part of the myocardium supplied by this artery (Sutherland and Hearse, 2000). In the body, myocardial ischaemia is predominantly caused by coronary artery diseases such as atherosclerosis.

Ischaemia can result in myocardial injury and dysfunction, which is also observed at the molecular level (Ytrehus, 2006). The severity of ischaemia determines the myocardial metabolic response. In response to a mild decrease in blood flow (20-60%), the heart has reduced oxygen consumption and FFA oxidation, and increased anaerobic glycolysis. Although the heart will experience a degree of contractile dysfunction, the remaining blood flow can prevent the heart from undergoing permanent tissue damage. In contrast, during complete ischaemia, ATP levels will be rapidly depleted, lactate will accumulate, the heart will experience acidosis and lose contractile function (Armstrong, 2004). Complete ischaemia eventually results in permanent damage to the heart due to necrosis and myocardial infarction (Stanley et al., 1997). Besides flow-related ischaemia, demand-induced ischaemia also occurs, although it is less used in experimental studies. Demand-induced ischaemia occurs when blood flow, and therefore oxygen and nutrient supply, does not increase in response to increased contractility and the accompanying greater need for oxygen and nutrients (Stanley et al., 1997).

Reperfusion

Once ischaemic tissue is reperfused, the heart reverts from anaerobic glycolysis back to oxidative phosphorylation to produce ATP. However, contractile function takes longer to return to normal upon reperfusion and this is termed myocardial stunning (Stanley et al., 1997). Although ischaemia without reperfusion will inevitably result in cell death, reperfusion of the ischaemic area has also been found to cause major tissue damage and has been termed IRI (Welbourn et al., 1991). Complications that arise due to IRI include arrhythmias, microvascular damage, myocardial stunning and cell death (Dhalla et al., 2000). Cell death is achieved through activation of apoptosis, necrosis or autophagy and multiple death-inducing stimuli, such as ROS production, Ca^{2+}-overload and the activation of proteases can contribute to the activation of these death pathways (Eltzschig and Eckle, 2011; Hotchkiss et al., 2009). However, Ca^{2+}-overload and oxidative stress have been found to be the biggest contributors to IRI (Dhalla et al., 2000).

During ischaemia, the heart becomes acidotic due to the accumulation of H^+. The excess intracellular H^+ is exchanged for Na^+ through the cardiac Na^+/H^+ exchanger (NHE1) during reperfusion, which in turn is exchanged for Ca^{2+} through the Na^+/Ca^{2+} exchanger (NCX), resulting in Ca^{2+}-overload during reperfusion (Stanley et al., 1997). Increased Ca^{2+} plays a crucial role in the initiation of necrosis and is associated with reduced recovery of mechanical functioning of the heart during reperfusion (Tani, 1990).

Kinases that have been shown to be activated upon reperfusion include PKB/Akt, ERK and JNK (Mizukami and Yoshida, 1997; Mockridge et al., 2000; 1997; Omura et al., 1999; Yin et al., 1997). PKB/Akt was shown to be activated via the PI3K pathway, and 4E-BP1, which leads to protein synthesis, was found to be phosphorylated downstream of PKB/Akt, but not GSK-3α

(Mockridge et al., 2000). Reactive oxygen and nitrogen species have been implicated in the mechanism of protein kinase activation (Armstrong, 2004; Mockridge et al., 2000).

During reperfusion, excess ROS and reactive nitrogen species are produced. It was found that the use of antioxidants was able to protect the heart against the contractile dysfunction that is usually seen in IRI, suggesting that oxidative stress significantly contributes to the development of IRI (Dhalla et al., 1999; Temsah et al., 1999).

Myocardial infarction

Myocardial infarction is a pathological state arising from prolonged ischaemia. It is considered to be a dynamic process ischaemic injuries undergo a shift from being reversible to irreversible. As necrosis of the myocardium is only detectible hours after the insult, IRI-stimulated cell death is not immediate. The irreversibly injured myocardium eventually dies and is replaced by fibrous scar tissue, giving rise to the myocardial infarction (Jennings et al., 1995).

Infarcts are classified according to location and the size of the damaged area (Alpert et al., 2000). They can also be further defined as acute, healing or healed. Acute myocardial infarctions contain polymorphonuclear leucocytes, while healing myocardial infarctions contain fibroblasts and mononuclear cells. When no infiltration by other cells are seen and scar tissue is present, the myocardial infarction is defined as healed. A myocardial infarction takes at least five to six weeks from onset to being classified as healed (Thygesen et al., 2007). Myocardial infarction is a major cause of death and disability on a global scale.

2.4 Ataxia-telangiectasia mutated

With the high incidences of obesity, insulin resistance, T2DM and CVD currently being experienced globally, and the role they play in morbidity and mortality rates, researchers are constantly striving to better understand the mechanisms and aetiologies behind these conditions. In 1970 it was noted that ataxia-telangiectasia (A-T) patients were inclined to develop diabetes, but it was not until more recently that the mechanisms in which ATM protein signalling contributes to defective insulin signalling and glucose homeostasis, started to be elucidated (Schalch et al., 1970). Although some studies have shed light on a cardiovascular role for ATM, relatively little is still known about this topic.

2.4.1 Background on the ATM protein kinase

Gene and protein characteristics

The ATM protein is encoded by a single gene of the same name, which is located on chromosome 11q22-23 and encodes a 12 kilobase mRNA transcript (Savitsky et al., 1995). The human ATM protein sequence is 3 056 amino acids in length and has a molecular mass of 350 kDa. The protein belongs to the phosphatidylinositol 3-kinase-related kinase (PIKK) superfamily and regions of interest in the protein include a telomere-length maintenance and DNA damage repair (TAN) domain, a catalytic domain (PIKKc_ATM), a FAT domain and a FATC domain as well as an ATP binding site, a catalytic loop and an activation loop (NCBI, accession number AAB65827; Savitsky et al., 1995).

Tissues in which ATM expression has been identified include the brain, lungs, kidneys, spleen, pancreas, liver, small intestine, colon, placenta, ovary, testis, thymus, leukocytes, skeletal muscle and the heart. ATM has been shown to be localized in the cytoplasm, mitochondria and the nucleus (Zakikhani et al., 2012). In proliferating cells, ATM is predominantly found in the

nucleus and following mitosis, ATM is found in the cytoplasm (Gorr et al., 2012). It has been suggested that DNA-PK is involved in the regulation of ATM expression and activation as ATM levels decrease in response to decreased DNA-PK levels (Peng et al., 2005). Activated ATM phosphorylates substrates on serine or threonine residues that are followed by a glutamine residue (S/TQ motif) (Kim et al., 1999).

Ataxia-telangiectasia

Mutations in the *ATM* gene result in a lack of functional ATM protein and leads to A-T, which is a debilitating, autosomal recessive disease (Su and Swift, 2000). A-T is a rare disease, affecting approximately 1 in 40 000 to 1 in 200 000 people globally, while 2.8% of people are estimated to be A-T carriers (Rasio et al., 1995; Swift et al., 1986). Although affected individuals appear healthy at birth, symptoms appear early on in life. Ataxia becomes evident when the affected child begins to walk and continues to progress, typically leaving the child wheelchair-bound by the age of 10 or 11. Other symptoms typically associated with A-T are cerebellar neurodegeneration, oculocutaneous telangiectasia, immunodeficiency, an increased risk of cancer development, premature ageing and radiosensitivity (Bakkenist and Kastan, 2003; Su and Swift, 2000; Yang et al., 2011). Additionally, A-T patients also experience growth retardation, insulin resistance and glucose intolerance (Yang et al., 2011). One study found that up to 17% of people affected by A-T develop T2DM (Morio et al., 2009). Although carriers are spared these signs and symptoms, it appears as if their life-expectancies are shortened by an average of approximately four years due to the development of cancer and an average of 11 years due to the development of ischaemic heart disease compared to ATM wild-type individuals (Su and Swift, 2000; Swift and Chase, 1983). There is currently no cure for A-T.

Activation of ATM

When present in dimers or higher-order multimers, ATM is inactive as the kinase domains are blocked while in a complex. In response to a number of different stressors, the ATM dimer or multimer complexes will dissociate, leading to the activation of ATM and the phosphorylation of specific substrates by the activated ATM (Guo et al., 2010). Two different mechanisms in which ATM is activated have been elucidated. The first is in response to double-stranded DNA breaks, when ATM is activated via interaction with the MRE11-RAD50-NBS1 (MRN) complex (Uziel et al., 2003). The inactive ATM multimers dissociate into active monomers when the serine 1981 residue in each ATM is autophosphorylated by the kinase domain of a neighbouring ATM molecule in the complex (Bakkenist and Kastan, 2003). Autophosphorylation of ATM has been described as a key event in the activation of ATM (Koslov et al., 2003). *In vitro* studies revealed that ATP is able to increase the kinase activity of ATM up to 10-fold and that the activation is dependent on the presence of Mn^{2+}. The PI3K inhibitor, wortmannin, was shown to inhibit the ATP-dependent activation of ATM (Kozlov et al., 2003). Phosphorylation at serine 1981 is generally regarded as a sign of activated ATM, however, some studies have reported ATM kinase activity in the absence of serine 1981 phosphorylation (Guo et al., 2010; Pellegrini et al., 2006).

Exposure to oxidative stress, and the subsequent oxidation of ATM, is the second known mechanism by which ATM can be activated. Intermolecular disulfide bonds are formed at, amongst others, cysteine 2991, causing conformational changes in oxidized ATM. The formation of disulfide bonds result in ATM becoming activated while still in covalently bound dimers and is essential for the activation of ATM in response to oxidative stress (Guo et al., 2010). Other known activators of ATM include hypoxia and insulin, although their mechanisms are unknown.

Two phosphatases, namely Wip1 and protein phosphatase 2A (PP2A) have been shown to regulate ATM phosphorylation. In unstressed cells, PP2A prevents ATM from being phosphorylated by associating with ATM via its scaffolding and catalytic subunits (Goodarzi et al., 2004). Wip1, on the other hand, dephosphorylates ATM once the initial stressor is no longer present (Sheeram et al., 2006).

2.4.2 The many functions of ATM

A large proteomic study published in 2007 has identified over 490 proteins to be substrates of ATM (Matsuoka et al., 2007). According to the Signaling Pathway Integrated Knowledge Engine (SPIKE), ATM participates in up to 953 regulations and 21 interactions with substrates (Arnon et al., 2011; Elkon et al., 2008) (Figure 2.5). Activated ATM is thus able to regulate a variety of substrates that form part of a number of signalling pathways, making ATM kinase one of the master controllers of signalling networks.

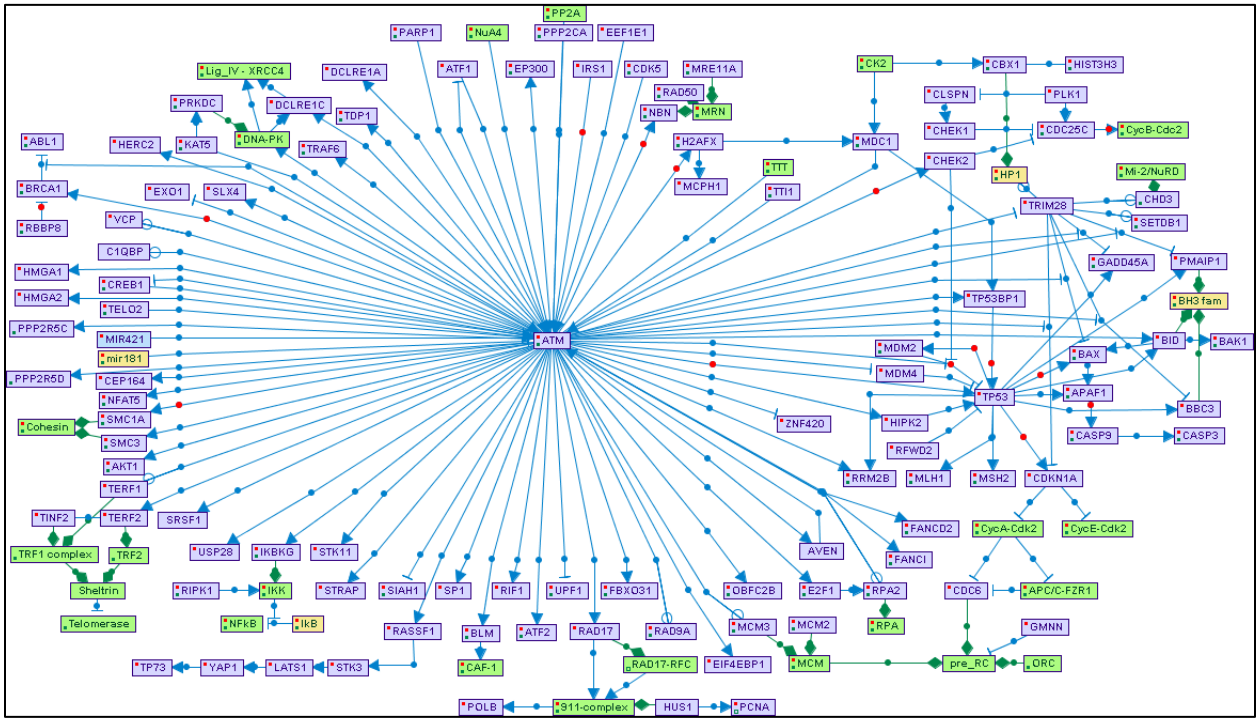

Figure 2.5: ATM regulates and associates with a large number of substrates that form part of a number of signalling networks (ATM Signaling Network (spike00006) image obtained from SPIKE).

The nuclear role of ATM

The most well-known and extensively studied function of ATM is in the nucleus where it plays a significant role in the response to double strand DNA breaks (DSB), termed the DNA damage response (DDR). The MRN complex acts as a sensor of DSB, which subsequently activates ATM, as previously described. Nuclear ATM then phosphorylates downstream substrates, including p53, Chk2, BRCA1 and H2AX that are involved in processes such as cell-cycle arrest, DNA repair or apoptosis in order to maintain genome stability (Banin et al., 1998; Burma et al., 2001; Cortez et al., 1999; Matsuoka et al., 1998).

DNA damage can also affect cytoplasmic ATM. DNA damaging agents, such as topotecan, have been shown to phosphorylate and activate cytoplasmic ATM. The activated ATM directly phosphorylates cytoplasmic PTEN on serine 113, causing it to translocate to the nucleus and initiate autophagy via the p-JUN-SESN2-AMPK pathway (Chen et al., 2015). Although PTEN is a known inhibitor of PKB/Akt, it was found that ATM-dependent phosphorylation of PTEN had no effect on the PKB/Akt pathway (Chen et al., 2015).

It has become apparent that defective DDR signalling alone could not be responsible for the wide range of signs and symptoms observed in A-T patients and roles for ATM outside of the nucleus, involving cellular homeostasis and metabolism, have now been described (Ditch and Paull, 2012). A prominent effect that is believed to contribute to most of the signs and symptoms seen in individuals affected by A-T is the critical role of ATM in maintaining redox homeostasis (Ambrose and Gatti, 2013; Semlitsch et al., 2011).

ATM and oxidative stress

Although the source of the stress has not been properly characterized, cells derived from A-T patients or animal models that lack ATM have been found to be under constant oxidative stress (Ousset et al., 2010; Watters, 2003). Additionally, Reichenbach et al. (1999) determined the antioxidant capacity of A-T patients, and found that their plasma had a lower antioxidant capacity than that of healthy age-matched control individuals. Mitochondria are the primary site for the production of intracellular ROS (Ott et al., 2007), and ATM has been found to localize to mitochondria and to contribute to mitochondrial functioning (Ambrose et al., 2007; Valentin-Vega et al., 2012). In the absence of ATM, thymocytes have been shown to contain mitochondria that are swollen, have a disorganized structure, have decreased activity of complex I of the electron transport chain and have changes in their membrane potentials. Defective mitophagy of the damaged mitochondria was also observed (Valentin-Vega et al., 2012). Additionally, Zakikhani et al. (2012) suggests that ATM could be involved in the functioning of mitochondrial complex II as this complex was found to be dysfunctional in the presence of the ATM inhibitor, KU-55933. The dysfunction of complex II caused decreased oxidative phosphorylation and the accumulation of succinate due to reduced conversion of succinate to fumarate which resulted in inhibition of the Krebs cycle (Zakikhani et al., 2012). It has thus been suggested that the mitochondrial dysfunction observed in A-T cells contributes to the increased amount of oxidative stress observed in these cells (Figure 2.6) (Ambrose et al., 2007; Valentin-Vega et al., 2012). Excessively high levels of ROS have been shown to damage proteins and lipids, to induce oxidation of mitochondrial and nuclear DNA and to contribute to single and double-strand breaks in the DNA (Ambrose and Gatti, 2013). The importance of mitochondria in oxidative phosphorylation and the production of ATP, and the high ATP demand of cardiomyocytes, renders cardiomyocytes particularly susceptible to mitochondrial dysfunction. Mitochondrial dysfunction in cardiomyocytes cause reduced energy production and

contractility as well as changes in electrical properties and cell death (Rosenberg, 2004). Healthy mitochondria are, therefore, crucial for cardiovascular health and it appears as if ATM plays a role in normal functioning of mitochondria.

One of the ways in which ATM contributes to the anti-oxidant response is by altering glucose metabolism in favour of the pentose phosphate pathway (PPP) as opposed to glycolysis in the presence of oxidative stress (Figure 2.7) (Krüger and Ralser, 2011). While both glycolysis and the PPP metabolize glucose, glycolysis produces ATP and leads to the use of oxygen in oxidative phosphorylation while the PPP does not produce ATP or require oxygen (Jalloh et al., 2015). The PPP consists of an oxidative phase and a non-oxidative phase, the former of which is the main source of NADPH production. NADPH is a reducing agent and a cofactor important for anti-oxidants such as glutathione reductase and cytochrome p450 reductase. Glucose-6-phosphate dehydrogenase is the rate limiting enzyme of the PPP. ATM has been shown to phosphorylate Hsp27 which increases the affinity of Hsp27 for glucose-6-phosphate dehydrogenase and in doing so, enhances the rate of the PPP and amount of NADPH produced (Consentino et al., 2011; Krüger and Ralser, 2011). The anti-oxidative effects originating from the activation of the PPP was shown to increase the viability and proliferation of cardiac progenitor cells in diabetic hearts (Katare et al., 2013). In human diabetic hearts that are failing, cardiomyocytes, endothelial cells and fibroblasts are progressively killed by apoptosis and necrosis due to oxidative stress (Frustaci et al., 2000). Pharmaceutical activation of ATM, and consequently the PPP, could be clinically significant in the cardiovascular system due to possible anti-oxidant effects.

The structure and function of the diabetic heart is partly regulated by AMPK as it increases autophagy in damaged cells. It also contributes to the regulation of both cardiac lipid and glucose metabolism (Gray and Kim, 2011; Xie et al., 2011). Improved cardiac metabolism and function have also been reported in mice with T2DM when mTOR has been inhibited, possibly

due to the resultant reduction in oxidative stress (Das et al., 2013). The induction of oxidative stress in cells with the use of H_2O_2, over a period of 60 minutes, activated ATM and consequently caused it to activate AMPK. This was achieved by directly phosphorylating AMPK at threonine 172 as well as by phosphorylating and activating the tumour suppressor, LKB1, a known activator of AMPK (Alexander et al., 2010; Shackelford and Shaw, 2009). Activated AMPK inhibited mTORC1 via phosphorylation of TSC2 at threonine 1271 and serine 1387 (Alexander et al., 2010). When mTORC1 is inhibited, decreased protein synthesis and increased autophagy are achieved in response to oxidative stress (Figure 2.7). Hypoxic conditions have also been shown to induce ATM-dependent inhibition of mTORC1. Although the mechanism is still unclear, hypoxic stress is able to activate ATM, causing it to phosphorylate and activate HIF-1α. This leads to the transcription of REDD1 (REgulated in Development and DNA damage responses) which inhibits the association between 14-3-3 and TCS2, causing TSC2 to inhibit mTORC1 (Figure 2.7) (Cam et al., 2010; DeYoung et al., 2008).

The biosynthesis of both subunits of the HIF-1 transcription factor was shown to be increased as a result of the elevated ROS levels in three different $ATM^{-/-}$ cell models (Ousset et al., 2010). The higher HIF-1 levels lead to the overexpression of both GLUT1 and VEGF, which initiates an anti-oxidant response. It is also possible that the overexpression of these two proteins contributes to the development of insulin resistance and abnormal vascularisation, which are two of the clinical manifestations of A-T. The ubiquitously expressed glucose transporter, GLUT1, is responsible for basal uptake of dehydroascorbic acid (DHA) and glucose, therefore, overexpression of GLUT1 will lead to the increased uptake of these substances (Ousset et al., 2010). Once converted into ascorbic acid, DHA becomes a ROS scavenger and thus has a beneficial anti-oxidant effect (Arrigoni and Tullio, 2002). Overexpression of GLUT1, on the other hand, has been shown to be detrimental as it could lead to the development of insulin resistance in skeletal muscle of mice and potentially plays a role in the development of the

insulin resistant phenotype that is present in A-T patients (Buse et al., 1996). Another symptom of A-T, namely telangiectasia, could be caused by the HIF-1-induced overexpression of VEGF, as VEGF is a crucial factor in angiogenesis (Hoeben et al., 2004). Although it still needs to be confirmed, it has been suggested that increased angiogenesis could contribute to plaque instability and the development of atherosclerotic plaques (Khurana et al., 2005). An angiogenesis-independent effect of VEGF in ischaemic conditions is to increase the expression of myoglobin, an iron- and oxygen-binding protein that is present in both cardiac and skeletal muscle (van Weel et al., 2004). In addition to maintaining oxygen supply through the release of stored oxygen during periods of high oxygen demand, such as ischaemia and strenuous exercise, myoglobin has also been shown to act as a NO and ROS scavenger in cardiac and skeletal muscle (Figure 2.6) (Ordway and Garry, 2004).

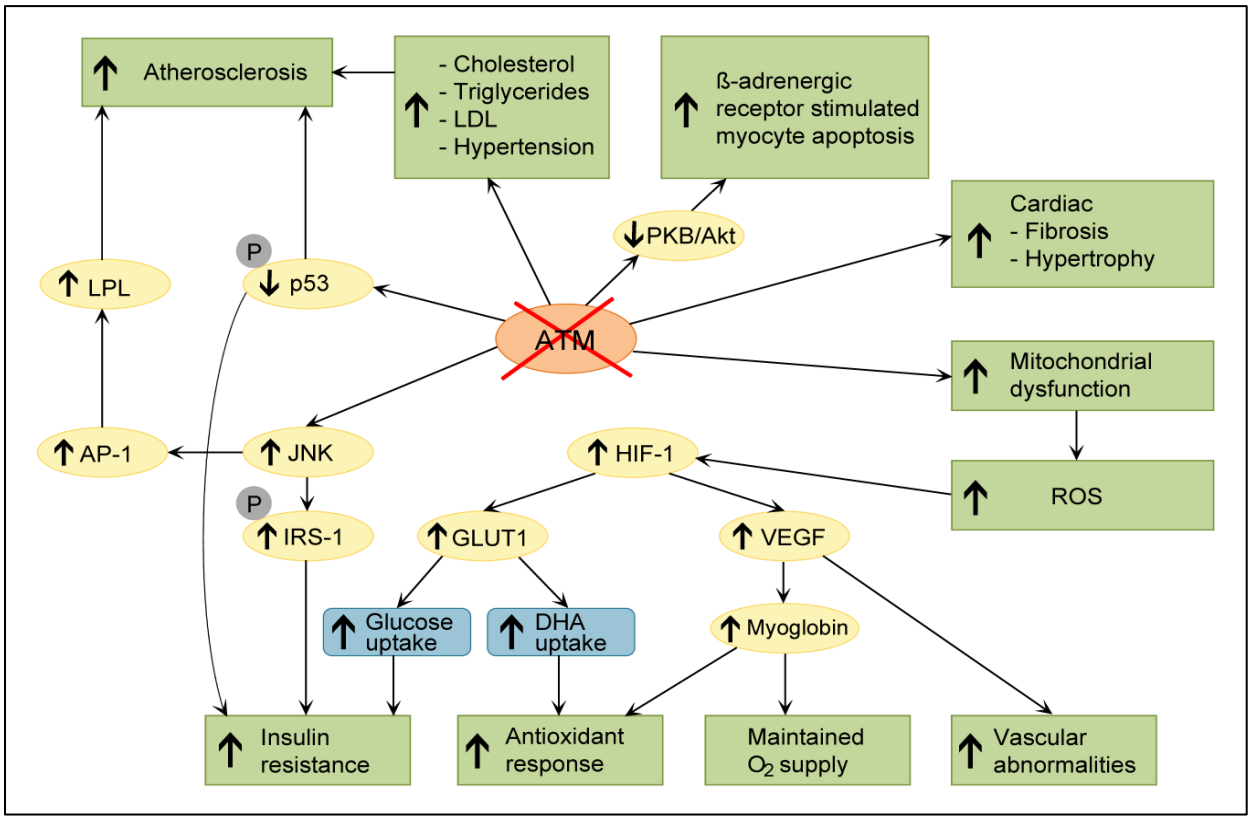

Figure 2.6: A number of metabolic and cardiovascular effects have been observed in the ATM-deficient state. Mitochondrial dysfunction, which contributes to elevated ROS levels, has been observed in ATM deficient cells. Elevated ROS associated with ATM-deficiency lead to increased biosynthesis of HIF-1, which results in an antioxidant response and maintained oxygen supply, but also insulin resistance and vascular dysfunction due to overexpression of GLUT1 and VEGF. ATM deficient mice have been found to have increased JNK levels, which lead to the serine phosphorylation of IRS-1 and ultimately contributes to the development of insulin resistance. Increased JNK levels could also contribute to increased atherosclerosis through increased AP-1 activity and LPL expression. Other pathophysiological consequences of ATM-deficiency are metabolic disturbances consistent with the metabolic syndrome, such as dyslipidaemia (elevated cholesterol, triglycerides and LDL proteins) and hypertension. Furthermore, the disruption of ATM-dependent phosphorylation of p53 has been shown to result in increased insulin resistance and atherosclerosis. Finally, ATM-deficient animals have been shown to have increased cardiac fibrosis and hypertrophy and β-adrenergic receptor stimulation has been associated with increased cardiomyocyte apoptosis due to decreased PKB/Akt activity in these animals. (Image from Espach et al., 2015).

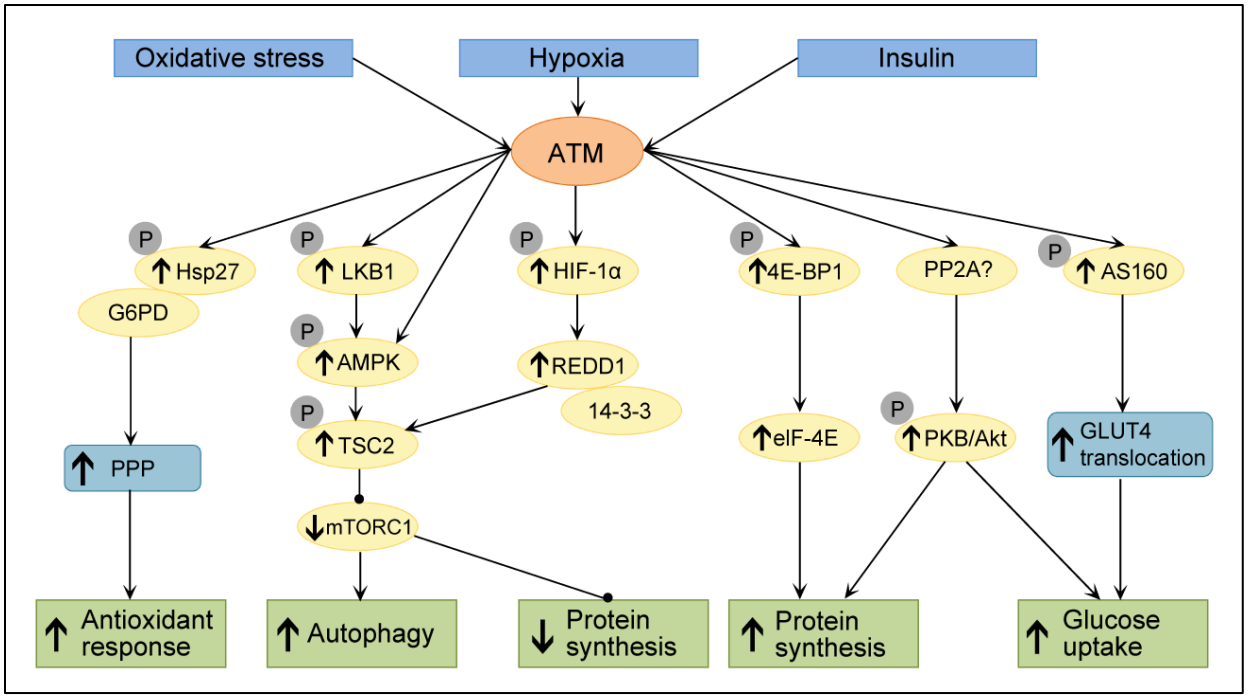

Figure 2.7: ATM has been shown to be activated by oxidative stress, hypoxia and insulin. In response to oxidative stress, ATM increases the rate of the pentose phosphate pathway in order to attain an antioxidant effect and achieves increased autophagy and decreased protein synthesis through activation of the AMPK-mTORC1 pathway. Increased autophagy and decreased protein synthesis are also achieved via HIF-1α phosphorylation in response to hypoxia. By regulating an as yet unidentified phosphatase (possibly PP2A), ATM increases the phosphorylation of PKB/Akt in response to insulin stimulation, leading to increased protein synthesis and glucose uptake. ATM also directly phosphorylates 4E-BP1 in response to insulin stimulation, resulting in increased protein synthesis and it has also been shown that ATM mediates insulin stimulated glucose uptake by phosphorylating AS160, causing GLUT4 externalization. (Image from Espach et al., 2015)

ATM and insulin signalling

Rather than having a single cause, it is thought that the disruption of a number of different ATM-dependent mechanisms contribute to the insulin resistance seen in A-T patients (Viniegra et al., 2005). The ATM/p53 pathway is a mechanism that leads to the development of both insulin resistance and atherosclerosis. The 'guardian of the genome' tumour suppressor, p53, has an ATM-specific phosphorylation site at serine 15 in humans and serine 18 in mice (Nakagawa et al., 1999). Mouse models in which serine 18 was mutated in p53 had increased levels of

inflammatory cytokines as well as reduced levels of anti-oxidants (Armata et al., 2010). Although no effect was observed at three months of age, the mutated mice developed insulin resistance and glucose intolerance by the age of six months. Consequently, it was proposed that the accumulation of oxidative stress and the resulting damage led to the disruption of glucose homeostasis (Armata et al., 2010). Pharmaceutical activation of ATM with the use of chloroquine in high-fat fed mice reduced the size of atherosclerotic plaques, but only in genetically wild-type mice and not in p53-null mice (Razani et al., 2010). This indicates that the presence of functional p53 is required for the beneficial effects of ATM activation. It is still not clear which signalling network downstream of ATM and p53 results in the protection.

Blood glucose levels were found to increase with age in $ATM^{-/-}$ mice while insulin secretion decreased with age, potentially due to dysfunction of β-cells in the pancreas (Miles et al., 2007). Although the mechanism has not yet been elucidated, it has been suggested that it is more likely to be caused by metastatic cancer, which is a common phenomenon in aged $ATM^{-/-}$ mice, rather than a direct effect of ATM in insulin secretion (Halaby et al., 2008). However, it is possible that ATM plays a role in β-cell homeostasis. In response to lipid loading, the pancreas was found to have increased expression levels of ATM (Schneider et al., 2002). Lipids are important for the normal functioning of the pancreatic β-cells and for their regulation of glucose stimulated insulin secretion (Nolan et al., 2006). Mutation of the ATM-specific phosphorylation site in mice contributed to hypertrophy of pancreatic islets, further suggesting a role for ATM in β-cell homeostasis (Armata et al., 2010).

The previous sections described indirect ways in which ATM participates in insulin signalling, but more direct effects of ATM on insulin and its major signalling pathways have also been observed. The kinase activity of ATM is increased up to three-fold in response to insulin (Yang and Kastan, 2000) and insulin-like growth factor-I (IGF-I) was also able to increase the serine 1981 phosphorylation of ATM in mice (Ching et al., 2013a). The activation of ATM upregulates

the promotor activity of the IGF-I receptor, increasing the expression of IGF-I receptor in response to IGF-I stimulation (Peretz et al., 2001). Reinforcing the notion that ATM participates in IGF-I signalling, it was demonstrated that PI3K, PKB/Akt, mTORC1 and S6K phosphorylation was reduced following IGF-I stimulation in skeletal muscle obtained from $ATM^{-/-}$ mice (Ching et al., 2013a). Phosphorylation of IRS-1 was unaffected by ATM deficiency, suggesting that ATM participates in IGF-I signalling downstream of IRS-1 (Ching et al., 2013a; Halaby et al., 2008). The anti-apoptotic and pro-survival effect of IGF-I was diminished in ATM-deficient cells. A deficiency in ATM did not affect IR expression as it did IGF-I receptor expression (Viniegra et al., 2005).

ATM has been shown to play a role in the activation of PKB/Akt, a central protein kinase in the insulin signalling network. An association is formed between the catalytic PIKKc_ATM domain of ATM and PKB/Akt which facilitates the phosphorylation of serine 473 in PKB/Akt in response to insulin stimulation (Viniegra et al., 1999). It is, however, not likely that PKB/Akt is directly phosphorylated at serine 473 by ATM as this is not an S/T-Q motif (Golding et al., 2009; Kim et al., 1999). It has thus been suggested that ATM regulates an okadaic acid-sensitive phosphatase, most likely PP1, PP2A or PP4-6, which then increases dephosphorylation of PKB/Akt (Figure 2.5) (Golding et al., 2009). Phosphorylation at serine 473 in PKB/Akt does not achieve full activation of PKB/Akt, but this ATM-dependent phosphorylation step is essential before phosphorylation at threonine 308 can take place, after which PKB/Akt is fully activated (Halaby et al., 2008; Viniegra et al., 2005). The involvement of ATM in activation of PKB/Akt in response to insulin appears to be cell-type specific as phosphorylation of PKB/Akt was ATM-dependent in some cells, but not in others (Jeong et al., 2010). It was hypothesised by Ching and colleagues (2013a) that the need for ATM in activation of PKB/Akt is determined by the upstream stimulus, as the signal would be stronger through IR activation, but weaker through IGF-I receptor activation.

Apart from affecting the activation of PKB/Akt, ATM also participates in other aspects of insulin signalling that are independent of PKB/Akt. Insulin stimulated phosphorylation of AS160, which is a Rab GTPase-activating protein crucial for the translocation of GLUT4 to the cell membrane, was downregulated in L6 myotubes and soleus muscle of mice in which ATM had been inhibited (Jeong en al., 2010; Sano et al., 2003). This resulted in reduced uptake of glucose, while PKB/Akt and PKC phosphorylation remained unaffected by the inhibition of ATM (Jeong et al., 2010). GLUT4 is found predominantly in skeletal and cardiac muscle and adipose tissue and is responsible for insulin-stimulated glucose uptake. GLUT1, on the other hand, is responsible for basal glucose uptake and is found in most tissue types (Buse et al., 1996). Both GLUT4 and GLUT1-mediated glucose uptake has been found to be affected by ATM. In L6 myoblasts it has been demonstrated that there are different mechanisms that lead to reduced glucose uptake when ATM is inhibited or inactivated. When L6 myoblasts were engineered to contain kinase-dead ATM, reduced translocation of GLUT4 was observed in response to insulin stimulation compared to L6 myoblasts containing functional ATM (Halaby et al., 2008). When ATM was inhibited using KU-55933 and CP466722 in L6 myotubes, less GLUT1 transporters were present at the cell surface compared to in untreated cells. A 48% reduction in basal glucose uptake was observed as well as reduced DHA uptake in response to ATM inhibition (Andrisse et al., 2013). By phosphorylating serine 490 of GLUT1, ATM increases the interaction between the glucose transporter and the binding protein GIPC1 which results in translocation of GLUT1 to the cell membrane (Andrisse et al., 2013; Matsuoka et al., 2007). It seems as if there is a discrepancy between the results obtained by Ousset et al. (2010) and Andrisse et al. (2013). Ousset et al. (2010) reported that they observed ATM deficiency to upregulate GLUT1 transcription while Andrisse et al. (2013) reported that less GLUT1 was externalised to the cell surface during ATM deficiency. We hypothesise that, in order to compensate for the reduced number of GLUT1 transporters at the cell surface, GLUT1 transcription is increased in the absence of ATM. Further investigation is, however, required to validate this hypothesis.

From the above it is clear that ATM plays a significant role in the insulin signalling network and the uptake of glucose. Glucose intolerance and insulin resistance contribute to the eventual development of T2DM, as described previously in section 2.1.4. Although it is still a controversial viewpoint (Birnbaum and Shaw, 2011), ATM has been proposed to be involved in the action of metformin, which is the drug of choice in the treatment of T2DM. A genome-wide association study found that the *ATM* gene is present at the same locus as a gene that is closely associated with the response to metformin treatment. The study highlights that the metformin-dependent activation of AMPK is not observed when ATM has been pharmaceutically inhibited and that the glycaemic response to metformin treatment was influenced by variations in the *ATM* gene (Zhou et al., 2011).

ATM and protein synthesis

It was demonstrated in 293T cells that ATM regulates protein synthesis by phosphorylating 4E-BP1 on serine 111 in response to insulin stimulation. Phosphorylation of serine 111 was not dependent on rapamycin, an inhibitor of mTORC1. However, successive rapamycin-sensitive phosphorylation events must take place on 4E-BP1, causing it to release eukaryotic initiation factor 4E (eIF-4E) and the initiation of translation (Figure 2.5) (Yang and Kastan, 2000). Protein translation is initiated when the released eIF-4E binds to an N^7-methylguanosine cap of an mRNA molecule. Reduced body masses were observed in $ATM^{-/-}$ mice compared to wild-type mice (Barlow et al., 1996). Additionally, cells isolated from A-T patients have a higher requirement for serum growth factors than cells isolated from healthy individuals (Yang and Kastan, 2000). This further suggests a role for ATM in protein synthesis and growth promotion. To our knowledge, no studies have been published on the role of ATM specifically on protein synthesis and growth promotion in the heart.

Metabolic and vascular effects of ATM

Both insulin resistance and atherosclerosis are well known for significantly contributing to the development of serious cardiovascular complications. Insulin resistance is known to be caused, at least in part, by oxidative stress (Bloch-Damti and Bashan, 2005; Evans et al., 2005) while both oxidative stress and DNA damage contribute to the development of atherosclerosis. Both oxidative stress and DNA damage have been shown to activate ATM (Guo et al., 2010; Uziel et al., 2003). A number of studies have demonstrated that ATM is able to protect against atherosclerosis and insulin resistance. Studies have also demonstrated how a clinical picture similar to that seen in the metabolic syndrome emerges when the expression or activation of ATM is downregulated and agents that activate ATM, or that have an antioxidant effect, are able to improve the metabolic signs and symptoms associated with ATM-deficiency (Le Guezennec et al., 2012; Mercer et al., 2012; Schneider et al., 2006).

In ATM-deficient mice, aortas, macrophages, adipose tissue, skeletal muscle and liver was shown to have increased activity of JNK (Schneider et al., 2006). Insulin signalling is disrupted when JNK phosphorylates IRS-1 at serine 307, leading to an insulin resistant state (Figure 2.6). In line with this, mice that were lacking JNK did not develop obesity or insulin resistance (Hirosumi et al., 2002). Another effect of JNK is to increase the activity of the transcription factor activator protein 1 (AP-1). The expression of lipoprotein lipase, which has been shown to be atherogenic, is increased by AP-1 (Figure 2.6) (Mead and Ramji, 2002; Schneider et al., 2006).

Our understanding of the metabolic actions of ATM have significantly been augmented by studying mice that are haploinsufficient for ATM ($ATM^{+/-}/ApoE^{-/-}$) and comparing their metabolic characteristics with ATM wild-type mice ($ATM^{+/+}/ApoE^{-/-}$). Mice that are complete ATM knockdowns have a very short lifespan as they develop thymic lymphoma between the ages of two to four months, according to The Jackson Laboratory, which renders them difficult to use for

experimentation (The Jackson Laboratory mouse strain datasheet). Compared to control animals, the haploinsufficient mice had increased levels of cholesterol, triglycerides and LDL and feeding these animals a high fat diet led to a higher incidence of atherosclerotic plaque formation than in control animals (Mercer et al., 2010; Wu et al., 2005). ATM haploinsufficiency further contributed to hypertension, abnormal lipid and carbohydrate metabolism, and evidence of mitochondrial dysfunction and DNA damage (Figure 2.4) (Mercer et al., 2010). Treating the $ATM^{+/-}/ApoE^{-/-}$ mice with a mitochondria-targeted anti-oxidant, namely MitoQ, for 14 weeks resulted in less fat to be accumulated and thus decreased weight gain, decreased hyperglycaemia, decreased hypercholesterolemia and decreased hypertriglyceridemia than what was observed in untreated $ATM^{+/-}/ApoE^{-/-}$ mice (Mercer et al., 2012). The use of an anti-oxidant was therefore able to reduce the ATM deficiency-induced metabolic effects. Atherosclerotic lesions were also decreased with the use of chloroquine, which has been shown to activate ATM, in $ATM^{+/+}/ApoE^{-/-}$ mice. Other effects of ATM activation with the use of chloroquine as seen in other animal models of insulin resistance included a decrease in blood pressure, JNK activity, glucose and insulin levels (Schneider et al., 2006).

Deletion of Wip1, which is responsible for the dephosphorylation of ATM, caused ATM to be hyperphosphorylated. $ApoE^{-/-}Wip1^{-/-}$ mice had accelerated metabolic rates compared to control animals, which resulted in less atherosclerotic lesions, that were also smaller in size, and less fat deposition than what was observed in $apoE^{-/-}Wip1^{+/+}$ mice. An ATM-mTOR-dependent pathway was suggested for the mechanism in which Wip1-deficiency affected the metabolic rates of the mice (Le Guezennec et al., 2012).

In addition to the metabolic basis for the development of atherosclerosis discussed in section 2.3.2, aging is also emerging as a risk factor for the development of atherosclerosis (Minamino and Komuro, 2007). Cellular senescence and reduced cell proliferation, telomere dysfunction and shortening, increased DNA damage, growth arrest and apoptosis are all aging-related

characteristics that are associated with atherosclerotic plaques and are believed to contribute to the development of atherosclerotic plaques (reviewed in Wang and Bennett, 2012). In endothelial cells, it was found that oxidative stress activated not only ATM, but also downstream targets of ATM such as PKB/Akt, p53 and p21 (Zhan et al., 2010). Increased activation of PKB/Akt has been associated with increased cellular senescence in human endothelial cells via a p53/p21-dependent mechanism (Miyauchi et al., 2004). Furthermore, the activated ATM localised to DSB, initiating the DDR, which is also known to trigger cellular senescence (von Zglinicki et al., 2005; Zhan et al., 2010). Oxidative stress-induced activation of ATM is thus able to induce endothelial senescence via activation of the DDR and PKB/Akt-p53-p21 pathway, finally leading to atherosclerosis.

Oxidized LDL was also shown to induce ATM phosphorylation in a time dependent manner in VA13 fibroblasts and endothelial cells. Additionally, oxidized LDL had a more adverse effect on cell viability of ATM-deficient fibroblasts (AT22 cells) than on normal fibroblasts (VA13 cells), indicating that ATM activation plays a protective role against the toxic effect of oxidized LDL. In line with this, AT22 cells were found to have a higher number of chromosomal breaks due to oxidized LDL treatment compared to treated VA13 cells (Semlitch et al., 2011). These results suggest that ATM activation is a protective mechanism against oxidized LDL and their role in the development of atherosclerosis.

ATM and its cardiac implications

People affected with A-T usually pass away in their twenties due to the severity of symptoms that result from ATM deficiency (Morrel et al., 1986). Although there is evidence of cardiovascular complications that are caused by ATM deficiency, the lifespans of A-T sufferers are usually too short for these signs and symptoms to fully develop and to become life threatening. The majority of A-T research is therefore focused on mechanisms affecting the

more deleterious symptoms of the disease such as cancer, ataxia, immunodeficiency and neurodegeneration. From the previous sections it is clear that ATM significantly contributes to normal metabolism and the response to oxidative stress and hypoxia. Additionally, it appears as if a clinical picture resembling that of the metabolic syndrome is seen when ATM protein kinase is dysfunctional or absent and the metabolic syndrome is very strongly associated with an increased risk for the development of CVD.

Individuals with a single mutated *ATM* copy do not have any of the severe symptoms present in A-T patients, but they also do not appear to be completely unaffected. Carriers of an *ATM* mutation have been shown to die earlier than non-carriers and have a higher rate of mortality due to quicker development of cancer as well as ischaemic heart disease (Su and Swift, 2000). In animal models, it has also been observed that the same metabolic alterations present in ATM homozygous animals are observed in ATM heterozygous animals (Shoelzon, 2002). Additionally, it has been demonstrated that ATM protein kinase levels are significantly downregulated in animals in response to a high fat diet and that this effect was independent of ATM genetics (Halaby et al., 2008). This is of interest as it suggests that a larger portion of the population could be affected by ATM related metabolic dysfunction, and cardiovascular complications, as ATM deficiency can be diet-induced.

Although lipids serve as the heart's primary source of energy substrate, glucose comprises 10-40% of the substrate consumption of the heart and during ischaemic conditions, glucose becomes the substrate of choice (Gertz et al., 1988; Opie and Lopaschuk, 2004; Taegtmeyer, 2000). Cardiac performance, especially during myocardial ischaemia, will thus be compromised if glucose metabolism is dysfunctional. The established role that ATM plays in insulin signalling and glucose uptake, suggests that a deficiency in ATM could exacerbate cell death and cardiac dysfunction. Although there is, to our knowledge, no published material available regarding myocardial substrate metabolism during the ATM-deficient state, it appears as if the cardiac

effects of obesity such as hypertrophy and fibroses are also observed in the ATM-deficient state (Eguchi et al., 2008; Foster et al., 2011).

It is known that ATM is expressed in the heart and that stimulation of the β-adrenergic receptors increases ATM expression up to 2.5 fold (Foster et al., 2011). It has been suggested that this effect is mediated by AP-1 due to the fact that the ATM promotor area contains a fat specific element that is a modified AP-1 site (Ghee et al., 1998; Gueven et al., 2003). Acute β-adrenergic receptor stimulation is beneficial for the heart, but chronic β-adrenergic receptor stimulation is harmful as it can lead to cardiac remodelling and apoptosis of cardiomyocytes (Shizukuda et al., 1998). ATM was found to be protective against chronic β-adrenergic receptor stimulation-induced cardiomyocyte apoptosis and cardiac remodelling in ATM haploinsufficient mice. The ATM deficient mice had increased cardiac hypertrophy, fibrosis and more myocyte apoptosis than mice with normal ATM levels, irrespective of β-adrenergic receptor stimulation (Figure 2.6) (Foster et al., 2011). A role for MMPs was suggested in the development of fibrosis as MMP-2 expression was upregulated and decreased TIMP-2 levels were seen in ATM deficient hearts that were treated with isoproterenol (Foster et al., 2011; Foster et al., 2012). When dysregulated, the proteolytic MMPs can contribute to myocardial extracellular remodelling as they are responsible for the degradation of the extracellular matrix (Spinale, 2002). Irrespective of whether ATM is present or absent, chronic β-adrenergic receptor stimulation results in apoptosis of cardiomyocytes. However, the choice of signalling network that contributes to apoptosis is dependent on whether or not ATM is present (Foster et al., 2012). A mechanism involving p53 and JNK is followed in wild-type hearts, while ATM deficiency results in reduced PKB/Akt activity and this caused the apoptosis in hearts in which ATM was deficient (Figure 2.6). Following myocardial infarction, ATM has been implicated in the modulation of cardiac remodelling. Infarcts were larger seven days post infarction in ATM-deficient mice

compared to controls and the larger infarcts were associated with an increase in apoptosis as well as fibrosis (Foster et al., 2013).

2.4.3 Drugs used to manipulate ATM

Homozygous ATM deficient animal models are difficult to use in studies as they develop lethal lymphomas at a very young age. While some investigators opt to use heterozygous ATM animals, another option is to use pharmaceutical agents to manipulate ATM. Pharmaceutical agents also make it possible to manipulate ATM transiently or at a certain time point rather than having a rigid ATM-deficient state as in knockout models. Agents known to activate ATM are insulin, metformin and chloroquine. Wortmannin, caffeine, CP466722, KU-55933 and KU-60019 act as ATM inhibitors. Agents relevant to the current study are discussed below. Insulin has been omitted here as it has been extensively discussed in the previous sections.

Chloroquine

Chloroquine was initially developed to be used as an antimalarial drug (Slater, 1993). In many areas, the *Plasmodium* parasites responsible for malaria have, however, become resistant to chloroquine treatment (Sidhu et al., 2002). Other uses for chloroquine have also emerged which include the treatment of rheumatic diseases and for the treatment of viral infections (Freedman and Steinberg, 1960; Savarino et al., 2003). Long term use of chloroquine has, however, been shown to have toxic effects, particularly in the eyes and heart (Fragasso et al., 2009; Michaelides et al., 2011). It has been shown that chloroquine is capable of increasing autophosphorylation of serine 1981 and in doing so, activation of ATM is increased up to 2.5-fold (Bakkenist and Kastan, 2003; Lim et al., 2012). The chloroquine-mediated activation of ATM is not mediated by the induction of DNA breaks, but rather by causing changes in the structure of chromatin (Bakkenist and Kastan, 2003). As mentioned in section 2.5.2, chloroquine-mediated activation of ATM has also been shown to improve metabolic and

vascular complications that are caused by reduced ATM levels and that this effect is possibly mediated by p53 (Razani et al., 2010; Schneider et al., 2006).

Wortmannin

Wortmannin is described as a potent and specific inhibitor of members of the PI3K family. The inhibition is covalent, and thus, irreversible, and non-competitive with regards to ATP. The degree of PI3K inhibition was shown to be directly proportional to the time of incubation with wortmannin as well as the concentration of wortmannin (Powis et al., 1994). As a PI3K is one of the first proteins in the insulin signalling cascade, its inhibition will block almost all of the insulin-stimulated processes such as glucose uptake, protein translation and apoptosis (Figure 2.2). Other members of the PI3K family that have been shown to be inhibited by wortmannin when used at higher concentrations include DNA-PK as well as ATM (Chan et al., 2000; Sarkaria et al., 1998). However, the use of wortmannin to inhibit ATM is not ideal in *in vivo* studies as it is not specific for ATM (Rainey et al., 2008).

KU-55933

KU-55933 is an ATP-competitive and ATM-specific inhibitor with an *in vitro* IC_{50} of 13 nM and a Ki of 2.2 nM (Hickson et al., 2004). At a concentration of 10 μM, KU-55933 was unable to inhibit any other kinases in a screen that included 60 kinases and the IC_{50} for ATM was found to be more than 100-fold lower than the IC_{50}-values for other members of the PIKK family such as DNA-PK, PI3K, ATR, PI4K or mTOR (Hickson et al., 2004). ATM inhibition by KU-55933 is maintained for at least eight hours in tissue culture and the inhibition is reversed once KU-55933 is removed (Hickson et al., 2004; Rainey et al., 2008). A number of different effects have been attributed to the use of KU-55933 to inhibit ATM. As was the case with CP466722, KU-55933 did not inhibit the activation of PKB/Akt in response to IGF-I treatment following serum starvation (Rainey et al., 2008). In contrast, when used at high concentrations, KU-55933 was

able to inhibit PKB/Akt phosphorylation at serine 473 and threonine 308 in response to both insulin and IGF-I in cancer cells that had abnormal PKB/Akt activity (Li and Yang, 2010). The authors found a strong correlation between the degree of PKB/Akt activity and the antiproliferative effect of KU-55933 as a bigger effect was observed in cancer cell lines with high basal activity of PKB/Akt (Li and Yang, 2010). KU-55933 was not able to reduce the expression levels of total ATM, but inhibition of ATM activation reduced growth and had an antiproliferative effect in cell cultures (Zakikhani et al., 2012). Zakikhani et al. (2012) further showed that the use of KU-55933 resulted in a significantly reduced number of living cells, decreased respiration and ATP levels, increased AMPK activation, increased production of lactate and glucose consumption and a larger number of necrotic and apoptotic cells compared to untreated controls. It is interesting to note that similar effects were observed with the use of metformin. In MCF-7 and Hela cells, KU-55933 treatment reduced SCO2 levels, a protein required for the assembly of cytochrome c oxidase. However, this effect appears to be tissue specific as the same effect was not observed in HepG2 cells (Zakikhani et al., 2012).

KU-60019

KU-60019 was developed as an improvement on KU-55933 as the two substances share most of the structural, pharmacological and biological effects (Figure 2.8) (Golding et al., 2009). Although KU-60019 is also reversible (Golding et al., 2012), it is more water-soluble and more potent than KU-55933 as the IC_{50}-value for ATM is almost half that of KU-55933, at 6.3 nM. When used at 1 μM, KU-60019 had very few to no non-specific targets when screened against 229 other protein kinases, however, PI3K was inhibited to some degree (i.e. p110β/p85α 9%, p120γ 3% and p110δ/p85α 27%).

KU-60019 was able to block ionizing radiation-induced phosphorylation of PKB/Akt and also reduced basal PKB/Akt phosphorylation levels in unirradiated cells by up to 70% (Golding et al.,

2009). This suggests that the effect of KU-60019 on PKB/Akt activation levels is not dependent on DNA damage. Dephosphorylation of PKB/Akt at serine 473 was noted as early as five minutes after the drug was added. In response to the decreased phosphorylation of PKB/Akt, decreased phosphorylation of BAD and GSK-3β was also observed. The ATM recognition site (S/TQ motif) is not present in PKB/Akt, which indicates that ATM is not responsible for direct phosphorylation of PKB/Akt. The use of okadaic acid, which is known to inhibit phosphatases, blocked the KU-60019-dependent decrease in PKB/Akt phosphorylation (Garcia et al., 2002; Golding et al., 2009). This is indicative of ATM regulating an okadaic acid sensitive phosphatase which dephosphorylates PKB/Akt, however, the identity of the phosphatase is still unknown. KU-60019 reduced basal and radiation- and insulin-induced phosphorylation of PKB/Akt. Golding et al. (2012) were able to observe reduced phosphorylation of p53 at its ATM-specific phosphorylation site at a KU-60019 dose as low as 10 nM in serum-free conditions. In light of this, they propose that KU-60019 is more effective in serum-free conditions as their results suggested that the bioavailability of KU-60019 is reduced by serum.

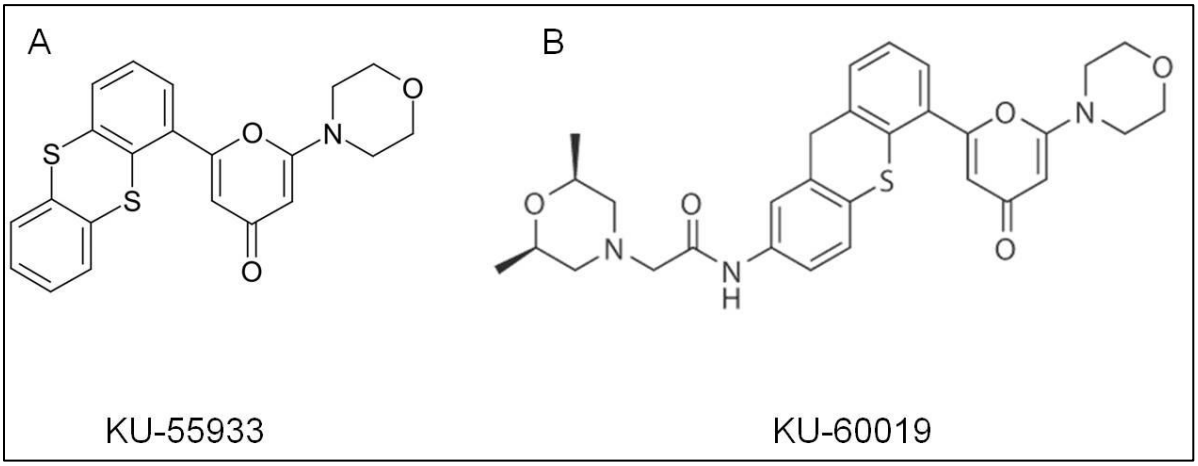

Figure 2.8: The chemical structures of three ATM inhibitors. A. 2-morpholin-4-yl-6-thianthren-1-yl-pyran-4-one (KU-55933; Hickson et al., 2004) C. 2-((2R, 6S)-2, 6-Dimethyl-morpholin-4-yl)-N-[5-(6-morholin-4-yl-4-oxo-4H-pyran-2-yl)-9H-thioxanthen-2-yl]-acetamide (KU-60019; Golding et al., 2009).

Chapter 3: Materials and Methods

In order to investigate the role of ATM in the myocardial pathology associated with insulin resistance, we firstly needed to induce insulin resistance in an animal model. We made use of special diets to induce insulin resistance in a rat model and used different perfusion techniques and Western blotting to determine the effects of ATM on cardiac function and various intracellular signalling networks.

3.1 Animal Models

This study was approved by the Research Ethics Committee: Animal Care and Use (Protocol number SU-ACUM12-00040) and complied with the accepted standards for the use of animals in research as stipulated in the South African National Standards 10386: 2008.

Age and weight matched adult male Wistar rats were used in all animal experiments, unless otherwise stated. All animals had free access to food and water and were housed at the Central Research Facility of Stellenbosch University in a temperature controlled (± 23°C) room with a 12-hour light/dark cycle. Once the rats reached a weight of 190±10 g, they were randomly allocated to control or diet groups. We made use of two different diets. For the first, termed the diet induced obesity (DIO) diet, the rats received standard rat chow supplemented with sugar and condensed milk to increase the carbohydrate content. For the second diet, termed HCD, rats received a standard rat chow diet supplemented with Holsum cooking fat (Malaysian palm oil) in addition to sugar and condensed milk. This diet has an increased carbohydrate and fat content. The protein, fat and carbohydrate compositions of the different diets are indicated in Table 3.1. The rats received these diets for a period of 16 weeks after which further experiments were performed. A total of 380 animals were used in this study: 157 age-matched controls, 159 HCD rats, 12 DIO rats and 52 young control rats.

Table 3.1: Macronutrient compositions of the two different diets used compared to a control rat chow diet.

Diet	Energy (kJ/100 g)	Total fat (g/100 g)	Protein (%)	Carbohydrate (%)
Control	1272	4.8	17.1	34.6
DIO	1173	4.6	9.4	45.8
HCD	1354	11.5	8.3	42.0

3.1.1 The effect of the diets on basal ATM expression levels in the heart

Following the 16 week diet feeding period, three rats from each diet group were anaesthetized by means of an intra-peritoneal administration of 160 mg/kg sodium pentobarbitone (Euthanaze, Bayer). Once the rats showed no pedal reflex in response to a foot pinch, their hearts were excised, the atria were swiftly removed and the ventricles immediately freeze-clamped using tongs pre-cooled in liquid nitrogen. In order to determine if the DIO and/or the HCD reduced basal ATM expression and reduced activation in the hearts, total ATM expression as well as phospho-ATM levels were determined using Western blotting. Total and phospho-PKB/Akt levels were also determined. By cutting and stripping a single membrane, ATM (350 kDa) and PKB/Akt (60 kDa), as well as the phospho-antibodies were assessed on the same membrane. The membrane was stained using Ponceau stain (0.1% (w/v) Ponceau S and 5% (v/v) glacial acetic acid; Sigma-Aldrich) and protein loading was normalised using the Ponceau stain against total proteins in each lane using the ImageLab software 5.0 (Bio-Rad). Please refer to section 3.4 (page 68) for a detailed description of the Western blotting protocol used.

3.1.2 Collection of biometric and metabolic data

Body mass, blood glucose levels and visceral fat mass

Biometric data was collected from 12 rats per diet group. Prior to being sacrificed, unfasted anaesthetised rats were weighed to determine their total body mass and blood glucose levels were determined via a tail prick using a GlucoPlus™ glucometer and disposable test strips (Cipla Dibcare (pty) ltd.). Once the heart was excised, the visceral fat, including the retroperitoneal, perirenal and epididymal fat pads, were removed and weighed. Based on the results obtained, the HCD animals were selected and only the HCD animals and age-matched control animals were used for further experimentations.

Oral glucose tolerance test

A subset of rats (n=15 per group) was subjected to an oral glucose tolerance test (OGTT). After being food-fasted overnight (± 16 hours), the rats were weighed and basal fasting blood glucose levels were determined using a tail prick and a handheld GlucoPlus™ glucometer. The rats were then anaesthetized with a low dose of sodium pentobarbitone (50 mg/kg; Eutha-naze, Bayer). Carotid blood was collected from anaesthetized rats in yellow BD Vacutainer® tubes containing gel and clot activator for serum separation. The blood was allowed to clot on ice for approximately 30 minutes, after which the blood was centrifuged at 3 000 rpm for 10 minutes at 4°C. The serum was removed, aliquoted in Eppendorf tubes and stored at -80°C until needed for the insulin assay.

Following blood collection, the animals were gavaged with a 50% sucrose solution at a concentration of 1 g/kg body mass. Blood glucose levels were measured at regular intervals (3, 5, 10, 15, 20, 25, 30, 45, 60, 90 and 120 minutes). The animals that were subjected to the

OGTT were allowed to recover for at least two weeks before they were used for Langendorff balloon model perfusion experiments.

Insulin assay

In order to quantify the insulin present in the serum samples (n=6), a Rat/Mouse Insulin enzyme-linked immunosorbent assay (ELISA) kit (EMD Millipore Corporation) was used according to the manufacturer's instructions. This is a non-radioactive quantification kit which is based on sandwich ELISA. Control and HCD serum samples were analysed in duplicate. An online ELISA analysis tool (http://www.elisaanalysis.com/) was used to calculate the insulin concentrations in serum samples against a dose-response reference curve of rat insulin standards. The homeostasis model assessment (HOMA) was used to calculate insulin resistance (HOMA-IR) as described by Matthews et al. (1985). Although originally developed for use in human subjects, the use of HOMA-IR was recently validated against the classical insulin tolerance test in Wistar rats (Antunes et al., 2016; Cacho et al., 2008). HOMA-IR is calculated as the product of fasting glucose (mmol/L) and fasting insulin (μU/mL) concentrations divided by 22.5.

3.2 Drug dosage experiments

Before any further experimentation, dose-response studies had to be conducted to determine the correct dosage of substances, including insulin, chloroquine diphosphate salt (further referred to as chloroquine) and KU-60019 to elicit the desired responses (i.e. Insulin – stimulate glucose uptake; chloroquine – stimulate glucose uptake and ATM activation; KU-60019 – inhibit glucose uptake and ATM activation). A total of 52 untreated, young male Wistar rats of approximately 200 – 300 g body mass were used for the dose-response studies. The rats were anaesthetized and the hearts removed as described in section 3.1.1.

3.2.1 Glucose uptake studies

Isolation of adult ventricular cardiomyocytes

Ventricular cardiomyocytes were isolated from untreated young male Wistar rats, weighing approximately 200 – 300 g according to the protocol described by Huisamen et al. (2001). Unheparinised rats were anaesthetized with an intra-peritoneal administration of approximately 160 mg/kg sodium pentobarbitone (Eutha-naze, Bayer), and once no pedal reflex in response to a foot pinch was detected, the hearts were rapidly removed and arrested in ice-cold KHB (pH 7.4; 119 mM NaCl, 24.9 mM $NaHCO_3$, 4.7 mM KCl, 1.2 mM KH_2PO_4, 0.6 mM $MgSO_4 \cdot 7H_2O$, 0.59 mM Na_2SO_4, 1.25 mM $CaCl_2 \cdot 12H_2O$ and 10 mM glucose; Merck Pty. Ltd.).

The hearts were mounted via the aorta onto the aortic cannula of a Langendorff perfusion system. Throughout the perfusion, the buffers were maintained at 37°C and continuously gassed with 100% oxygen. Hearts were perfused with solution A, which is a calcium-free HEPES buffer (6 mM KCl, 1 mM Na_2HPO_4, 0.2 mM NaH_2PO_4, 1.4 mM $MgSO_4$, 128 mM NaCl, 10 mM HEPES, 5.5 mM D-glucose and 2 mM pyruvate; pH 7.4; Sigma-Aldrich) for five minutes to flush out remaining blood. Connective tissue was then digested by perfusion in a re-circulating manner with solution B (solution A plus 0.7% fatty acid free bovine serum albumin (BSA; Roche) fraction V, 1.07 mg/mL type 2 collagenase (Worthington Biomedical Corporation) and 17.6 mM 2, 3 butanedione monoxime (Sigma-Aldrich)). At 15 and 20 minutes, $CaCl_2$ was added to solution B, resulting in final concentrations of 0.1 mM and 0.2 mM respectively. After 35-40 minutes of digestion, or once the effluent was streaming, the hearts were removed from the perfusion system, the atria and connective tissue removed, and the ventricles carefully shredded with tweezers before being incubated in a flat-bottomed flask containing solution C (1:1 dilution of solution A and solution B plus 0.5% fatty acid free BSA fraction V, 0.5 % BSA and 0.2 mM $CaCl_2$) in a 37°C water bath with gentle agitation. After 15 minutes, the $CaCl_2$

concentration was gradually increased over five one-minute intervals to concentrations of 0.4 mM, 0.6 mM, 0.8 mM, 1 mM and finally 1.25 mM respectively.

The isolated ventricular cardiomyocytes were filtered through a 200 μm^2 nylon mesh and gently centrifuged at 100 rpm for three minutes at room temperature (± 23°C). The supernatant was aspirated, the pellet re-suspended in solution D (solution A plus 1.25 mM $CaCl_2$ and 2% fatty acid free BSA fraction V) and allowed to settle into a loose pellet for five to eight minutes. Following this time, the supernatant, containing dead cells, was carefully aspirated and the loose pellet containing live cells re-suspended in fresh solution D in a flat-bottomed flask. The cells were allowed to recover from the isolation process by being incubated at room temperature (± 23°C) under 100% oxygen for one hour with gentle agitation. Following the recovery process, a loose pellet was once again allowed to form, the supernatant aspirated and the remaining living cells washed three times in solution E (6 mM KCl, 1 mM Na_2HPO_4, 0.2 mM NaH_2PO_4, 1.4 mM $MgSO_4$, 128 mM NaCl, 10 mM HEPES, 1.25 mM $CaCl_2$ and 2% fatty acid free BSA fraction V). The cells were gently centrifuged at 100 rpm for three minutes at room temperature (± 23°C) between washes and finally re-suspended in solution E before being used in the 2-deoxy-D-[3H]glucose (2-DG) uptake assays.

2-Deoxy-D-[3H] glucose uptake assay

The ventricular cardiomyocytes were treated with different concentrations of insulin (1/10/100 nM), chloroquine (10/50/100 µM) or KU-60019 (1.5/3/6 µM) and subjected to glucose uptake experiments immediately following isolation. The solution E/cardiomyocyte cell suspension, containing approximately 0.5 mg protein, was added to flat-bottomed tubes along with solution E to reach a final volume of 750 µL. Tubes were prepared to have a negative control set (which only contained solution E, cardiomyocytes and 2-DG), a phloretin-only set and three different drug concentrations. Each of these sets was prepared in duplicate. The GLUT inhibitor,

phloretin (Sigma-Aldrich), was added to the phloretin-only samples at a final concentration of 400 µM in order to determine the basal or GLUT-independent glucose uptake.

The samples were oxygenated and subjected to different protocols, depending on the drug used. Figure 3.1 depicts the treatment protocols followed for insulin, chloroquine (Sigma-Aldrich) and KU-60019 (Selleckchem.com). The samples were incubated in a shaking water bath, set to 37°C, for the entire assay. At the start of the assay, the samples were equilibrated in the water bath for five minutes followed by the addition of the drugs as indicated in Figure 3.1. After the samples were treated with the different drugs, radio-labelled 2-DG (1.5 µCi/mL; Perkin Elmer, Boston, USA), at a final concentration of 1.8 µM, was added to initiate glucose uptake. Glucose uptake continued for 30 minutes until the reaction was stopped by the addition of 400 µM phloretin to all tubes except the phloretin only set (which received phloretin at the start of the assay). The samples were centrifuged at 14 500 rpm for 90 seconds to collect the pellets, the supernatant was discarded, and the pellets were washed twice with solution A. Finally, the pellets were completely dissolved in 500 µL of 1 N NaOH for approximately 30 minutes in a 60°C water bath. After the pellet was completely dissolved, distilled H_2O was added to bring the NaOH concentration to 0.5 N. An aliquot of these samples was then quantified using scintillation counting and the protein concentration in each sample was determined using the Lowry method (Lowry et al., 1951).

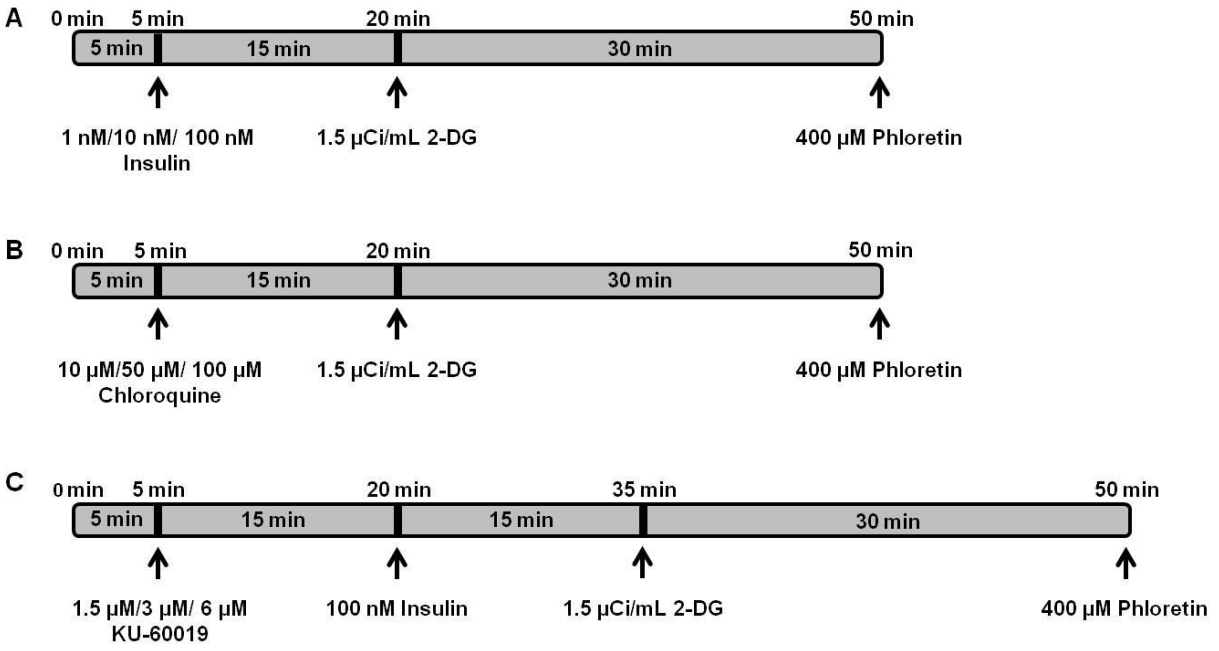

Figure 3.1: Protocols used for the glucose uptake assay in response to different concentrations of A) insulin (n=6) B) Chloroquine (n=3) and C) KU-60019 (n=4). 2-DG 2-deoxy-D-[3H]glucose

Lowry protein determination

The Lowry method (Lowry et al., 1951) was used to determine the protein concentrations in each of the samples. Fifty µL of sample was used in the assay as well as 50 µL of three BSA protein standards with known protein concentrations (namely 0.161 mg/mL, 0.322 mg/mL and 0.644 mg/mL). Each of the samples and standards were assayed in triplicate and a blank containing 0.5 N NaOH and no protein was also included in the assay. Starting with the blank, followed by the protein standards and samples, 1 mL of freshly prepared reaction buffer (1.96% Na_2CO_3, 0.01% $CuSO_4 \cdot 5H_2O$ and 0.02% Na-K-Tartrate) was added to each tube in 10 second intervals. After each addition of reaction buffer, the tubes were rapidly vortexed. The reaction was allowed to proceed for a total duration of 10 minutes after which 100 µL of folin ciocalteu's phenol reagent, diluted 1:2 with distilled H_2O, was added to each tube, again in 10 second time intervals and vortexing after each addition. The reaction was incubated at room temperature (± 23°C) for 30 minutes to allow for colour development and the optical density was measured at

750 nm. The known concentrations of the BSA standards were used to prepare a standard curve from which the unknown protein concentrations of the samples were determined.

Quantification of glucose uptake

Approximately 3 µL scintillation fluid and 100 µL of sample dissolved in 0.5 N NaOH was added to each scintillation vial (this was done in duplicate for each sample). A vial containing only scintillation fluid and another containing scintillation fluid and 25 µL of 1.5 µCi/mL 2-DG was also prepared as blank and total counts respectively. All vials were left in the dark at room temperature (± 23°C) overnight (± 16 hours) to stabilize before being counted in an LS 6500 multi-purpose scintillation counter (Beckman) to determine the disintegrations per minute. Uptake of 2-DG was calculated as pmol 2-DG/mg protein/30 minutes.

3.2.2 Propidium iodide assays to determine cell viability

Propidium iodide (PI; BioLegend) staining was used to assess cell viability following treatment of isolated cardiomyocytes with KU-60019 (n=2 per group) or chloroquine (n=2 per group). The membranes of viable cells are impermeable to PI, which is a nucleic acid intercalating agent. Once PI is bound to the DNA of compromised cells, the resultant increased fluorescence can be detected using flow cytometry.

Cardiomyocytes were prepared as explained in section 3.4.1. For the assay, cell aliquots suspended in 500 µL HEPES buffer (6 mM KCl, 1 mM Na_2HPO_4, 0.2 mM NaH_2PO_4, 1.4 mM $MgSO_4$, 128 mM NaCl, 10 mM HEPES) were stabilized for five minutes in a shaking water bath at 37°C. The cells were then treated with 0.03% DMSO (vehicle control) and 3 µM KU-60019 for the KU study or with 10, 50 and 100 µM chloroquine for the chloroquine study for 45 minutes. Duplicate samples were prepared for each condition. The samples were centrifuged to collect the pellets, the cells were re-suspended in fresh HEPES buffer and 5 µM PI was added to each

sample. The samples were incubated in the dark at room temperature (± 23°C) for 15 minutes to allow for the uptake of PI by compromised cells before fluorescence was measured using flow channel two of a Becton Dickinson FACSCalibur (BD Biosciences). Twenty thousand events were acquired per condition.

3.2.3 Langendorff perfusions

Langendorff perfusions were conducted in order to observe the effect of increasing concentrations of KU-60019 and chloroquine on the hearts. The balloon model was used to assess cardiac function during the chloroquine perfusions. Cardiac function was not assessed during KU-60019 perfusions as these perfusions were performed in the Langendorff mode on a working heart perfusion rig and functional assessments were thus not possible. Hearts were stabilised for 30 minutes after which they were treated with increasing chloroquine or KU-60019 concentrations. KU-60019 treatment was followed by insulin stimulation to determine which KU-60019 concentrations were able to inhibit the effect of insulin stimulation. The protocols used for perfusions are depicted in Figure 3.2. Seven hearts were perfused in each group for the chloroquine study, while only two hearts were perfused in each group for the KU study due to time constraints and a limited number of rats being available. Please refer to section 3.3 (page 64) for a detailed description of the Langendorff perfusion technique. Following the perfusion protocols, the hearts were freeze-clamped and stored at -80°C until they were used in Western blot analysis to determine the effect of the drugs used on total ATM expression and ATM phosphorylation. Please refer to section 3.4 (page 68) for a detailed description of the Western blot technique.

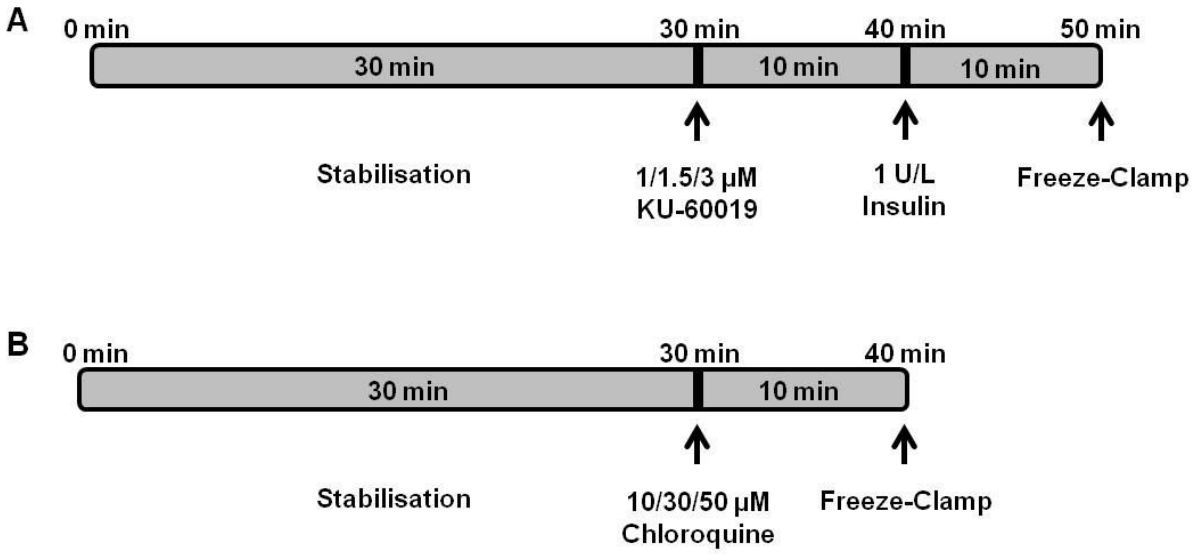

Figure 3.2: Protocols followed for Langendorff dosage perfusions. A) KU-60019 (n=2 per group) B) Chloroquine (n=7 per group except 50 µM Chloroquine n=4).

3.3 Langendorff perfusions

The hearts were cannulated via the aorta and perfused retrogradely with KHB gassed with 95% O_2 and 5% CO_2 and with a constant hydrostatic pressure of 100 cm H_2O. The perfusion buffer was warmed by circulating water heated by a water bath through the double-walled glassware in order to maintain the myocardial temperature at approximately 36.5 – 37°C. The temperature of the heart was continuously monitored with the use of a temperature probe inserted into the coronary sinus.

3.3.1 The balloon model

The balloon model allows for pressure data collection during drug administration in the Langendorff mode. The balloon model was thus utilised as we were interested in determining the effect of pharmacological agents on the heart as they were administered. Furthermore, Langendorff perfused hearts were subjected to global ischaemia as the balloon model enabled

the determination of time to onset of contracture and peak developed pressure during global ischaemia. A syringe inflatable balloon constructed from plastic clingwrap was inserted via the pulmonary vein, through the left atrium and into the left ventricle (Figure 3.3). The balloon was inflated with water to achieve a diastolic blood pressure (DP) of approximately 10 mm Hg. The balloon is connected to a pressure transducer which enabled the measurement of myocardial function. Heart rate, as beats per minute (BPM), SP and DP were measured and the Gentronics chart recorder v1.00 software calculated the left ventricular developed pressure (LVDevP: DP subtracted from the SP) and the rate pressure product (RPP; LVDevP multiplied with BPM). Additional measurements collected at regular intervals during experiments included myocardial temperature and CF.

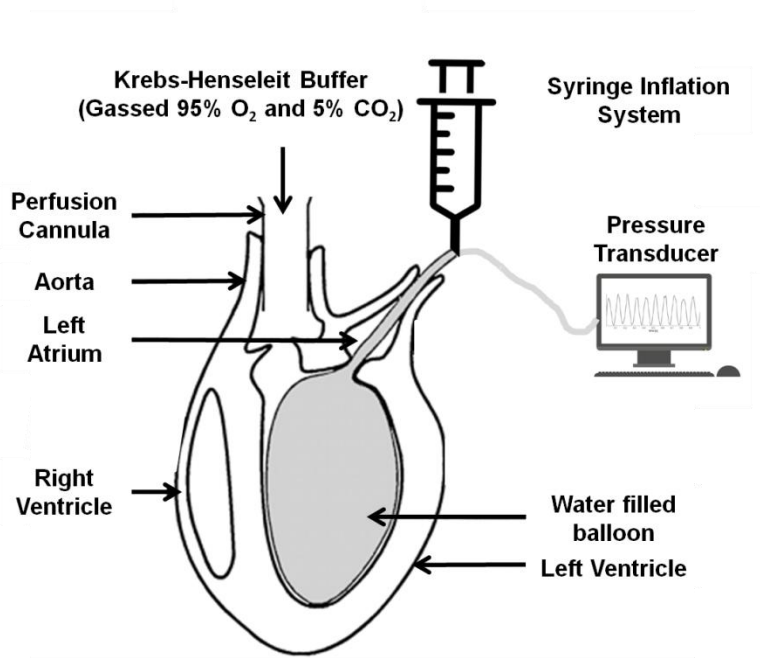

Figure 3.3: Illustration of the inflatable balloon inserted into the left ventricle of a cannulated heart.

3.3.2 Perfusion protocol

Hearts were stabilised for 20 minutes before treatment commenced. The hearts were treated with DMSO (0.033%, vehicle control) insulin (1 U/L), wortmannin (100 nM), insulin and wortmannin combination, KU-60019 (3 μM) and an insulin and KU-60019 combination. The wortmannin concentration was previously optimised and used in our laboratory (Huisamen et al., 2008). Five hearts were perfused per treatment group (The HCD Insulin group, 10 minutes reperfusion had n=4). All treatments were administered in a recirculating manner. For the untreated control group, KHB was recirculated for the duration of the treatment period. Following the 20 minute treatment period, hearts were subjected to 20 minutes of global ischaemia by stopping all perfusion to the hearts, which prevented delivery of substrates and oxygen. The time to onset of contracture and peak developed pressure during global ischaemia was noted. Hearts were reperfused for either five or ten minutes, after which they were freeze-clamped and stored at -80°C for Western blot analysis. Only the hearts that were reperfused for 10 minutes were used for Western blot analysis as previous work in our laboratory has shown that this is the best time to determine differences in protein expression and activation. The hearts reperfused for five minutes remain in storage for future Western blot analysis. Figure 3.4 (page 67) is a schematic representation of the protocol followed for the Langendorff perfusions using the balloon model. Due to an unavoidable delay in the commencement of perfusion studies, animals used for the 10 minute reperfusion group were on the diet longer (approximately 25 weeks). Cardiac function was, however, comparable in animals that were on the diet for 16 and 25 weeks so the data was pooled.

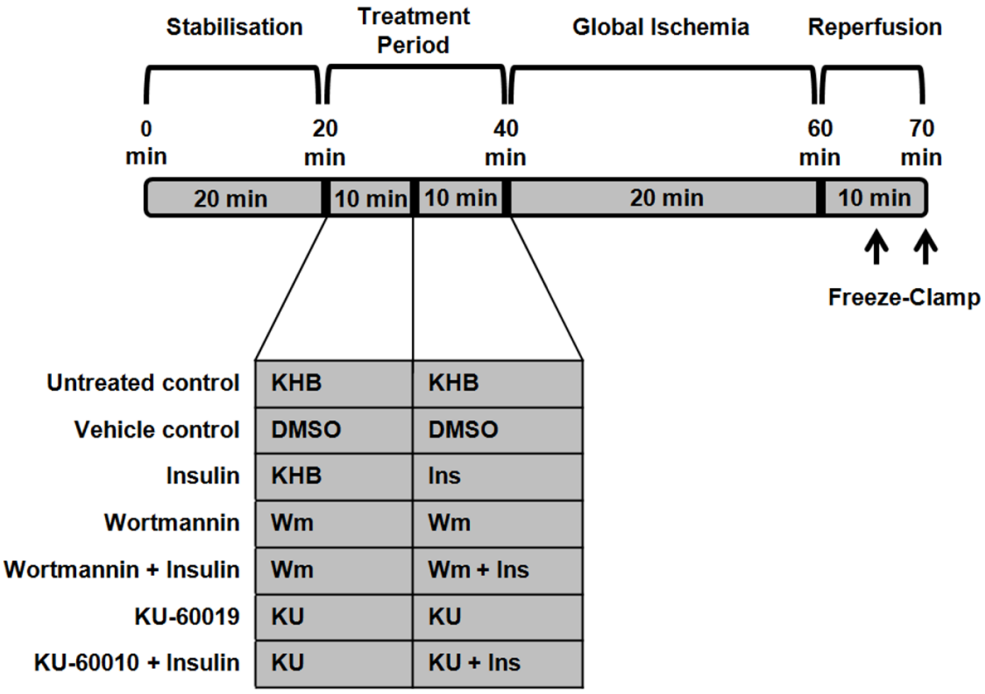

Figure 3.4: Schematic representation of the protocol followed for Langendorff perfusions using the balloon model and the treatment groups used for global ischaemia studies. Hearts were either freeze-clamped following five or ten minutes of reperfusion. (n=5 per group) Ins: insulin, KHB: Krebs-Henseleit buffer, KU: KU-60019, Wm: wortmannin.

3.3.3 Basal effect of ATM manipulation on signalling networks

In order to determine the effect of ATM manipulation on signalling networks in the absence of IRI, additional Langendorff perfusion experiments were conducted. In these experiments, hearts were stabilised for 20 minutes, after which they were treated with insulin (1 U/L), KU-60019 (3 μM) and an insulin and KU-60019 combination over 20 minutes. Three hearts were perfused per treatment group. The hearts were then freeze-clamped and Western blot analysis conducted to determine the expression and activation levels of proteins indicated in Table 3.2. The perfusion protocol used is indicated in Figure 3.5 and the Western blot technique used is described in section 3.4.

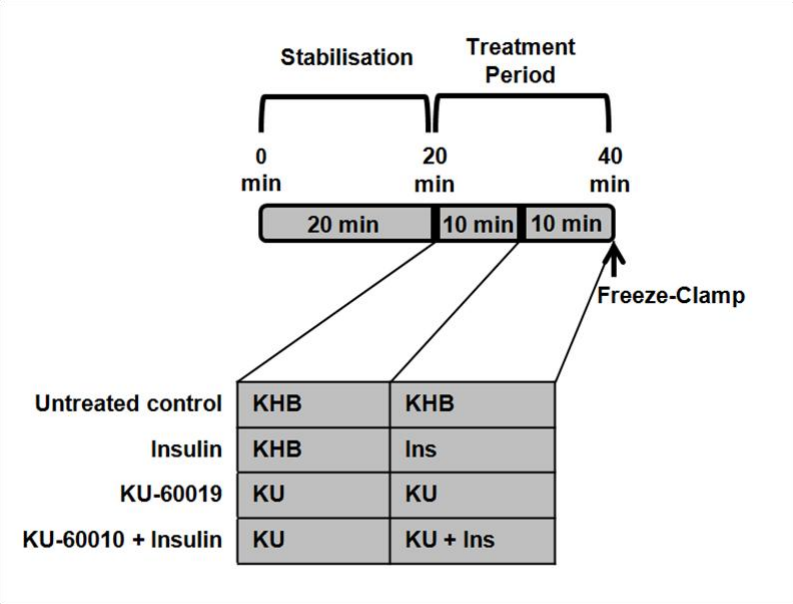

Figure 3.5: Schematic representation of the protocol followed for Langendorff perfusions using the balloon model and the treatment groups used to determine the basal effect of ATM manipulation. (n=3 per group) Ins: insulin, KHB: Krebs-Henseleit buffer, KU: KU-60019.

3.4 Western blotting

3.4.1 Preparing lysates from freeze-clamped heart tissue

All steps for lysate preparation took place on ice. Approximately 0.1 g of freeze-clamped heart tissue was pulverised and homogenised in 700 µL lysis buffer in order to extract protein from the tissue. The lysis buffer consisted of the following components: 20 mM Tris-HCl (pH 7.5), 1 mM EGTA, 1 mM EDTA, 150 mM NaCl, 1 mM β-glycerophospate, 2.5 mM tetra sodium pyrophosphate, 10 mM sodium orthovanadate, 1% Triton X-100, 10 µg / mL leupeptin, 10 µg / mL aprotinin and 50 µg / mL PMSF. The heart tissue was pulverised for two cycles of four seconds each at 20 000 rpm using a Heidolph SilentCrusher-M homogeniser. The lysates were allowed to stand on ice for 15 to 30 minutes after which they were centrifuged at 15 000 rpm for 20 minutes at 4°C to remove the cell debris. The protein-containing supernatant was collected and total protein concentrations were determined using the Bradford method (Bradford, 1976).

3.4.2 Bradford protein determination

The Bradford protein determination method (Bradford, 1976) was used to determine the protein concentrations in the prepared lysates. The lysates were diluted 1:9 with distilled water and 5 µL of the diluted lysates was assayed. A standard curve, using known protein concentrations of BSA was also prepared. A volume of 900 µL of Bradford solution (120 µM coomassie brilliant blue G-250, 4.75% (v/v) ethanol, 8.5% (v/v) phosphoric acid) that has been filtered twice, was added to each sample. The samples were incubated for 15 minutes on the bench to allow for colour development, after which the absorbance was read at 595 nm using a Spectronic® 20 Genesys™ spectrophotometer. Each lysate and protein standard was assayed in duplicate and the standard curve was used to determine the protein concentration in each lysate.

Based on the determined protein concentrations, the lysates were diluted with lysis buffer so that the final lysates each contained 50 µg of protein per 15 µL. A 3X Laemmli sample buffer (2.5 M glycerol, 0.189 M Tris-HCl (pH 6.8), 10.1% SDS, 1.275 mM bromophenol blue, 15% β-mercaptoethanol) was added to each lysate in a 1:2 ratio. The final lysates were incubated in boiling water (100°C) for five minutes in order to denature proteins and stored at -80°C.

3.4.3 SDS-Polyacrylamide gel electrophoresis protein separation and transfer

Before being loaded in SDS-polyacrylamide gels to separate the proteins in terms of size, the lysates were once again incubated in boiling water (100°C) for five minutes to denature proteins. Lysates used to probe for GLUT4 were never incubated in boiling water as hydrophobic membrane proteins such as GLUT4 form aggregates at high temperatures, prohibiting them from entering the gel. Equal amounts of protein (50 ng) were loaded and separated using SDS-polyacrylamide gels. TGX Stain-Free™ FastCast™ Acrylamide Kits (10% and 12%) (BioRad) and 4-15% Mini-PROTEAN® TGX Stain-Free™ Precast Gels (Bio-Rad) were used to separate the proteins. Protein markers used were the PageRuler™ Prestained Protein Ladder (Thermo

Scientific) and HiMark™ Pre-stained Protein Standard (Novex by Life Technologies). The running buffer contained the following: 25 mM Tris, 192 mM glycine and 0.1% (w/v) SDS. The gels were electrophoresed at 200 mA and 200 V for an hour (gradient gels: 1h30) using the Mini Trans-Blot® Cell system from Bio-Rad, after which the gels were Stain-Free activated for one minute and imaged using the ChemiDoc MP system and ImageLab software 5.0 (Bio-Rad).

After separation and gel activation, proteins were transferred to polyvinylidene fluoride membranes (Immobilon®-P, Millipore) at 200 mA and 200 V for one hour (gradient gels: 1h30). The transfer buffer contained 25 mM Tris, 192 mM glycine and 20% (v/v) methanol (transfer buffer for gradient gels contained only 10% (v/v) methanol). After the transfer was completed, the membranes were imaged using the ChemiDoc MP system and ImageLab software 5.0 (Bio-Rad) in order to do whole lane protein normalisation to correct for any unequal loading.

3.4.4 Membrane blocking, antibody incubation and immunodetection

Non-specific binding sites were blocked for one to two hours using 5% (w/v) fat-free milk made up in Tris-buffered saline-Tween-20 (TBST) buffer (20 mM Tris-HCl (pH 7.6), 137 mM NaCl, 0.1% Tween-20). Membranes were then washed thoroughly with TBST for three cycles of 10 minutes on a shaker and incubated overnight (± 16 hours) under constant agitation with primary antibodies at 4°C. Primary antibodies used are indicated in Table 3.2. All primary antibodies were acquired from Cell Signaling Technology and all primary antibodies used, except GLUT4, were raised in rabbit. GLUT4 was raised in mice. The following day the membranes were washed to remove any unbound primary antibody using TBST (three cycles of 10 minutes on a shaker) and incubated with the appropriate horseradish peroxidise-conjugated secondary antibody (either Anti-rabbit or Anti-mouse IgG HRP-linked antibody, Cell Signaling Technology) at room temperature (± 23°C) for one hour. Unbound secondary antibody was washed away using TBST (three cycles of 10 minutes).

In order to visualise the proteins of interest, a chemiluminescent detection system was employed. The membranes were incubated in Clarity™ Western ECL Blotting Substrate (Bio-Rad) for five minutes after which the membranes were exposed using the "Chemi" or "Chemi High Sensitivity" settings as needed of the ChemiDoc MP system (Bio-Rad). Antibodies that required exposure times longer than 15 minutes due to low sensitivity were exposed on autoradiography film in the dark room.

Membranes were always probed with total protein antibodies first, then stripped and probed with the phospho-protein antibodies. The stripping protocol was as follows: Two cycles of five minutes each in distilled water, seven minutes in 0.2 M NaOH, and two cycles of five minutes each in distilled water. All steps took place at room temperature (± 23°C) and with gentle agitation on a shaker.

3.4.5 Western blot data analysis

The ImageLab Software (version 5.0) was used to quantify and analyse the bands of interest. Signal intensities of the relevant protein bands (detected using chemiluminescence) as well as total protein stain-free fluorescence was determined using the "Lane and Bands" function of the ImageLab software. In order to correct for any unequal loading and/or transferring, the blots were normalised against total protein in lanes using the "Normalization" function of the software (Gürtler et al., 2013). The "Normalization" function determines the total protein present in each lane (as opposed to a single house keeping protein) and calculates a normalization factor based on the total protein present in each lane relative to the first lane. A lane with less protein loaded/transferred will have a higher normalization factor and a lane with more protein loaded/transferred will have a lower normalization factor. Unequal loading/transferring is corrected by multiplying the chemiluminescence signal intensities by the normalization factor for each lane.

Table 3.2: Specifications for antibodies used in Western blot analysis.

Protein of interest	Phosphorylation site	Molecular weight	Gel used	Primary AB dilution	Secondary AB dilution
T+P ACC	Ser79	280 kDa	4-15%	1:1000 in TBST	1:4000 in TBST
T+P AMPK	Thr172	62 kDa	4-15%	1:1000 in TBST	1:4000 in TBST/2.5% milk
T AS160		160 kDa	10%	1:1000 in TBST	1:4000 in TBST
P AS160	Thr642	160 kDa	10%	1:1000 in TBST	1:4000 in TBST/2.5% milk
T+P ATM	Ser1981	350 kDa	4-15%	1:667 in SignalBoost*	1:2500 in SignalBoost*
T GLUT4	N/A	45 kDa	12%	1:1000 in SignalBoost*	1:4000 in TBST/2.5% milk
T+P GSK-3β	Ser9	46 kDa	12%	1:1000 in TBST	1:4000 in TBST
T+P IRS-1	Ser307	180 kDa	10%	1:1000 in SignalBoost*	1:4000 in SignalBoost*
T+P JNK	Thr183/Tyr185	47 kDa	10%	1:1000 in TBST	1:4000 in TBST
T+P mTOR	Ser2448	289 kDa	4-15%	1:1000 in TBST	1:4000 in TBST
T PI3K		85 kDa	4-15%	1:1000 in TBST	1:4000 in TBST
P PI3K	Tyr458	85 kDa	4-15%	1:1000 in TBST	1:4000 in TBST/2.5% milk
T+P PKB/Akt	Ser473	60 kDa	12%	1:1000 in TBST	1:4000 in TBST
T+P PTEN	Ser380/Thr382/383	54 kDa	10%	1:1000 in TBST	1:4000 in TBST

* SignalBoost™ Immunoreaction Enhancer Kit (Calbiochem®)

T Total; P Phospho-

3.5 *Ex vivo* working heart perfusions

3.5.1 Perfusion protocol

Excised hearts were arrested in ice-cold KHB (~4°C) and subsequently mounted on a Morgan working heart perfusion system as quickly as possible by cannulation of both the aorta and pulmonary veins. Immediately, once securely cannulated, the hearts were retrogradely perfused with filtered KHB, continuously gassed with 95% O_2 and 5% CO_2 and warmed to maintain physiological temperatures. The Langendorff perfusion occurred at a constant hydrostatic pressure of 100 cm H_2O and the buffer was not circulated. This initial Langendorff perfusion step of 15 minutes was used to wash remaining blood from the heart and to stabilise the heart.

Myocardial temperature, as measured by a temperature probe inserted into the coronary sinus, was continually monitored and maintained at 36.5–37°C. Coronary flow was measured regularly during all phases of the experiment.

The perfusion mode was switched to the working heart mode in which the perfusate enters the left atrium via the cannulated pulmonary veins. The beating heart then ejects the perfusate from the left ventricle through the aorta, working with a preload of 15 cm H_2O and against an afterload of 100 cm H_2O. During the working heart mode, the myocardial mechanical function prior to ischaemia was determined by measuring aortic output (AO), heart rate, SP and DP and by calculating total work performed by the heart. A pressure transducer, connected to the aortic line, was used to determine the pressure measurements. Aortic output was measured manually by measuring the amount of fluid ejected by the aorta over a minute time period.

In order to treat the hearts with different drugs and drug combinations, the perfusion mode was switched back to the Langendorff mode. In addition to an untreated control group, the hearts were treated with insulin (1 U/L), wortmannin (100 nM), insulin plus wortmannin combination,

KU-60019 (3 μM) and an insulin plus KU-60019 combination. DMSO was used to dissolve the KU-60019. In order to compensate for any effect of the vehicle, an equal concentration of DMSO (0.033%) was added to each of the other treatment groups at the same time point when KU-60019 was added. All the drugs were administered in a re-circulating manner. Figure 3.6 depicts the protocols used for working heart perfusions. Hearts from animals on the control diet and the HCD were perfused and six to eight hearts were perfused per treatment group.

Immediately following the treatment period, the left anterior descending coronary artery was temporarily ligated using a silk suture (Ethicon®) to induce regional ischaemia. Care was given to consistently ligate the same area in all hearts. Myocardial temperature was closely monitored and maintained at 36.5°C during the ischaemic period by submerging the heart in warmed KHB. Regional ischaemia lasted for 35 minutes, after which the suture was released and the heart was reperfused in the Langendorff mode for 10 minutes.

In order to determine the degree of recovery in myocardial mechanical function following ischaemia, the hearts were again switched to the working heart perfusion mode for 20 minutes. Mechanical function parameters were noted (AO, BPM, SP, DP and total work). Another 30 minutes of reperfusion in the Langendorff mode was performed after which the hearts were stained for infarct determination.

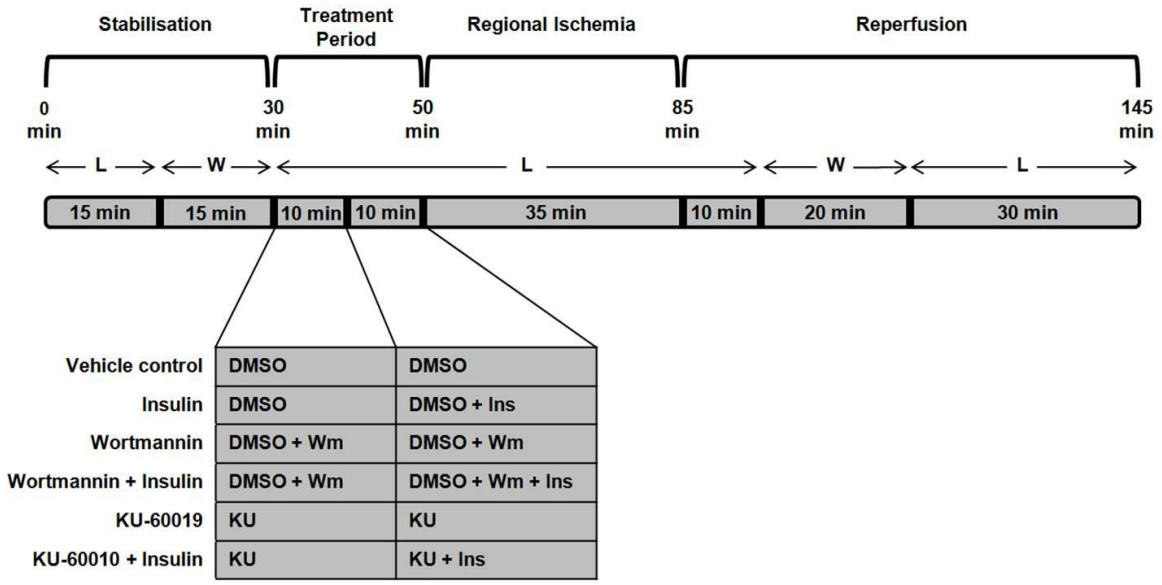

Figure 3.6: Schematic representation of the protocol followed for the working heart perfusions and treatment groups used. (n=6-8 per group) Ins: insulin, KU: KU-60019, L: Langendorff perfusion mode, W: Working heart perfusion mode, Wm: wortmannin

3.5.2 Staining of the heart and infarct determination

Following a total reperfusion time of 60 minutes, the left anterior descending coronary artery was once again ligated and the heart was stained with 0.2% Evans blue (Sigma-Aldrich) dye via the aorta. This was done to determine the viable area that was not affected by ischaemia as the dye only stains the viable tissue. The hearts were then frozen at -20°C before the IFS was determined.

Visualisation of the area at risk (AAR) and IFS was achieved by triphenyl tetrazolium chloride (TTC) staining. The frozen hearts were evenly sliced into approximately 2 mm thick disks from the ligation point to the apex of the heart using a scalpel. The heart disks were incubated at room temperature (± 23°C) in TTC staining solution (20 mM $NaH_2PO_42H_2O$, 80 mM Na_2HPO_4 and 29.9 mM TTC; pH 7.4) for 30 minutes. During this incubation time, metabolically active

tissue (AAR) is stained red due to the reduction of TTC, while necrotic tissue (IFS) remains white/pale due to TTC remaining unreduced (Figure 3.7).

In order to enhance the colour development and terminate the staining reaction, the heart slices were fixed in 10% formaldehyde. The total surface area of the viable tissue, AAR and IFS was then quantified for each heart using UTHSCSA ImageTool for Windows v3.00 (developed by The University of Texas Health Science Center in San Antonio).

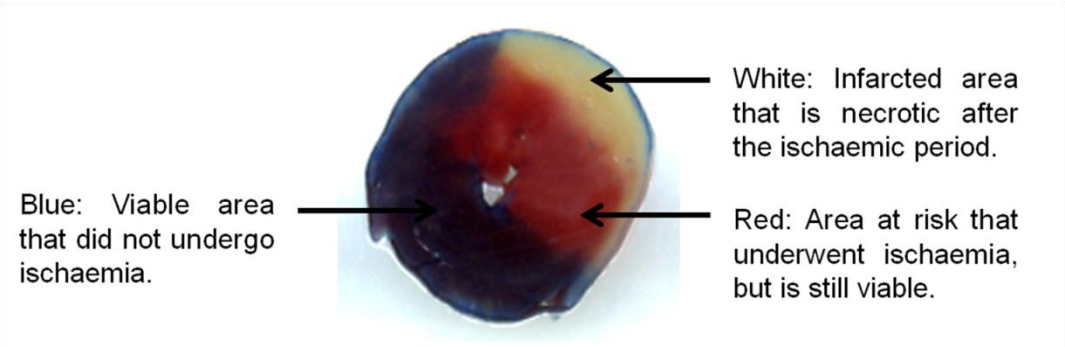

Figure 3.7: Example of a heart stained using Evans blue dye and triphenyl tetrazolium chloride staining. The blue area is stained with Evans blue and was not affected by occlusion of the left anterior descending coronary artery. This is the viable tissue. The red and white areas were subjected to regional ischaemia. The red-stained tissue is viable as the triphenyl tetrazolium chloride has been metabolized while the white tissue is necrotic.

3.5.3 Ex vivo working heart perfusions with reduced insulin concentration

In order to investigate the effect of a reduced insulin concentration, hearts from both control and HCD animals were treated with 0.3 U/L insulin and a combination of 3 μM KU-60019 and 0.3 U/L insulin (n=3 per group). The perfusion protocol was as described in Figure 3.6 and the endpoint was IFS determination as described in section 3.5.2.

3.6 Aortic ring studies

3.6.1 Isolation and mounting of the aortic rings

Thoracic aortas were isolated from the same animals used for the working heart perfusion experiments, however, only age-matched control animals were used due to time constraints. Immediately once the hearts were removed, the trachea and oesophagus were also removed in order to expose the aorta. The portion of the aorta ranging from the aortic arch to just above the diaphragm (thoracic portion of the aorta) was excised and placed in ice-cold KHB in order to maintain the integrity of the tissue. The aorta section was cleaned of perivascular fat and connective tissue and cut into rings of three to four millimetres in length. One of these aorta rings was mounted between two stainless-steel hooks of an organ bath (AD Instruments). The organ bath contained KHB, continuously gassed with 95% oxygen and 5% carbon dioxide and warmed to 37°C. One of the stainless-steel hooks was connected to a 0 – 25 g force transducer (TRI202PAD, Panlab) via a silk suture in order to allow measurement of the contraction and relaxation of the aortic ring. LabChart7 software (Dunedin) was used to record and analyse the aortic ring tension data.

3.6.2 Isometric tension protocol

A previously described isometric tension protocol was modified to study the effect of KU-60019 on vasodilation of aortic rings (Privett et al., 2004). Mounted aortic rings were stabilised at a basal isometric tension of 1.5 g for 30 minutes. During the stabilisation period, the KHB was replaced with fresh, pre-warmed KHB every 10 minutes. Following stabilisation, an initial contraction-relaxation cycle was carried out to assess the viability of the aortas before actual experimentation began.

For the viability assessment, phenylephrine (PE; 100 nM) was added to stimulate contraction of the smooth muscle. Once contraction reached a plateau, relaxation was induced with the addition of acetylcholine (ACh; 10 μM). Phenylephrine is an α_1-adrenergic receptor agonist and causes blood vessels to constrict by selectively binding to $alpha_1$ receptors on the smooth muscle. Acetylcholine causes smooth muscle to relax by activating endothelial NOS, which in turn produces NO. Aortic rings were deemed viable if they had a minimum relaxation of 70% of the maximum PE-induced contraction. Only rings that displayed more than 70% relaxation were included in the study. Following the viability assessment, the viable aortic rings were once again stabilised at 1.5 g tension for 30 minutes. During this time, the organ bath was rinsed by replacing the buffer with fresh, pre-warmed KHB three times, at regular intervals.

A second round of contraction was induced in the rings through the cumulative addition of PE, reaching final PE concentrations of 100 nM, 300 nM, 500 nM, 800 nM and 1 μM. Subsequent PE additions were not dependent on time, but rather when the maximum contraction was achieved by the previous PE concentration. When maximum contraction of the final concentration (1 μM) was achieved, relaxation of the aortic rings was induced using cumulative concentrations of ACh (positive control; 30 nM, 100 nM, 300 nM, 1 μM and 10 μM), DMSO (vehicle control; 0.011%, 0.022%, 0.034%, 0.045% and 0.056%) and KU-60019 (1 μM, 2 μM, 3 μM, 4 μM and 5 μM). In order to determine if observed ACh- and KU-60019-induced relaxation was dependent on endothelial NOS activation and NO release, aortic rings were also pre-treated with L-NAME (100 μM) for 30 minutes prior to PE-induced contraction. Because L-NAME is a NOS inhibitor, it blocks the vasodilatory effects of drugs that act by activating NOS, such as ACh. The relaxation-inducing capacity of each of the treatment groups was calculated as percentage relaxation from the maximum contraction caused by PE. Each group had an n-value of five to seven biological replicates. Figure 3.7 illustrates the protocol followed for the isometric tension experiments and the treatment groups used.

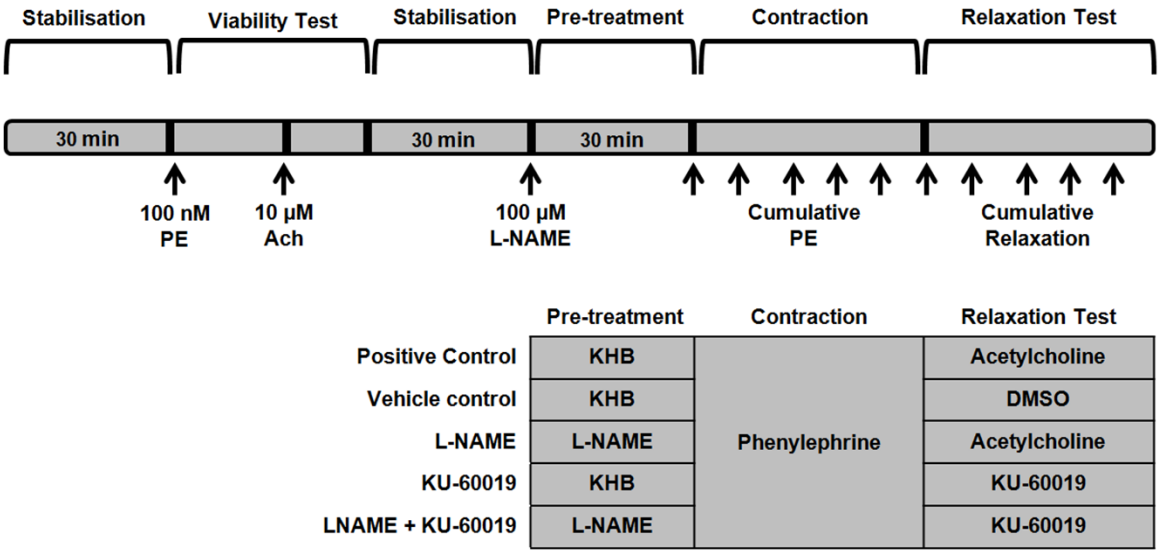

	Pre-treatment	Contraction	Relaxation Test
Positive Control	KHB	Phenylephrine	Acetylcholine
Vehicle control	KHB		DMSO
L-NAME	L-NAME		Acetylcholine
KU-60019	KHB		KU-60019
LNAME + KU-60019	L-NAME		KU-60019

Figure 3.7: Schematic representation of the protocol followed for isometric tension studies on aortic rings and the treatment groups used to achieve relaxation. (n=5-7 per group) ACh: acetylcholine, KHB: Krebs-Henseleit buffer, PE: phenylephrine.

3.7 Critical Appraisal

We made use of animals of the same sex, age and genetic background. This restriction reduces variability and thus reduces the need for very large sample sizes. As previously mentioned, animals were randomly allocated to the different diet groups. This was staggered in order to ensure that all animals were on the diet for the same amount of time at the time of experimentation (i.e. 10 age-matched control and 10 HCD animals were put on the diet each week so that only 20 animals were ready for perfusion each week). Individuals caring for the animals did not know which perfusion groups the animals would be allocated to which reduced the risk of performance bias. Selection bias during perfusion was avoided by randomly allocating animals to treatment groups each day. Perfusions were not conducted systematically where each treatment group was completed before the next was started. Thus, hearts that make up a group were isolated from animals that were put on the diet in different weeks and

they were perfused at different times of day in order to avoid confounding effects. Although the approach to assessing endpoints was objective and the same across treatment groups, there was a risk for detection bias as perfusions were not blinded. Infarct size determination, which could be more subjective, was however blinded. For Langendorff balloon model perfusions, hearts that were still fibrillating when measurements were taken during reperfusion were excluded. Hearts with basal AO values lower than 20 were excluded. For infarcts, hearts were excluded if the percentage viable area was not between 40-60%.

3.8 Statistical analysis

GraphPad Prism 5 software was used to perform statistical analysis. Results are displayed as mean ± standard error of the mean (SEM), unless otherwise stated. When comparing two groups, an unpaired Student's t-test was utilised. When comparing more than two groups, a one- or two-way analysis of variance (ANOVA) with a Bonferroni post-hoc test was utilised, where appropriate. Differences with a p-value of smaller than 0.05 was considered significant.

Chapter 4: Results

4.1 Identification of the diet to be used

4.1.1 Determination of ATM expression levels

Halaby et al. (2008) have shown that rats fed a high fat diet had reduced ATM expression levels in their skeletal muscle compared to chow-fed rats. In order to determine whether either the DIO or the HCD was able to reduce ATM expression, the Western blotting technique was used to determine basal ATM expression and activation in the hearts of animals on the diets compared to chow-fed control animals. Because of its central role in the insulin signalling network, PKB/Akt expression and activation was also determined in the two diets and compared to the hearts of age-matched control animals.

The HCD, but not the DIO diet was found to significantly decrease basal cardiac ATM expression after 16 weeks compared to the chow-fed control animals (Control 1.00 ± 0.06; HCD 0.33 ± 0.11; $p < 0.05$) (Figure 4.1 B). Although ATM activation was not affected by either diet, the P/T ATM ratio was significantly increased by the HCD compared to the control diet (Control 1.00 ± 0.07; HCD 3.38 ± 1.02; $p < 0.01$) (Figures 4.1 C and D). Similarly, the HCD diet significantly decreased total PKB/Akt expression (Control 1.00 ± 0.09; HCD 0.70 ± 0.01; $p < 0.05$), while PKB/Akt phosphorylation (Ser473) was unaltered compared to the control diet (Figures 4.1 E and F). This also resulted in an increased P/T PKB/Akt ratio (Control 1.00 ± 0.01; HCD 1.29 ± 0.08; $p < 0.05$) (Figure 4.1 G).

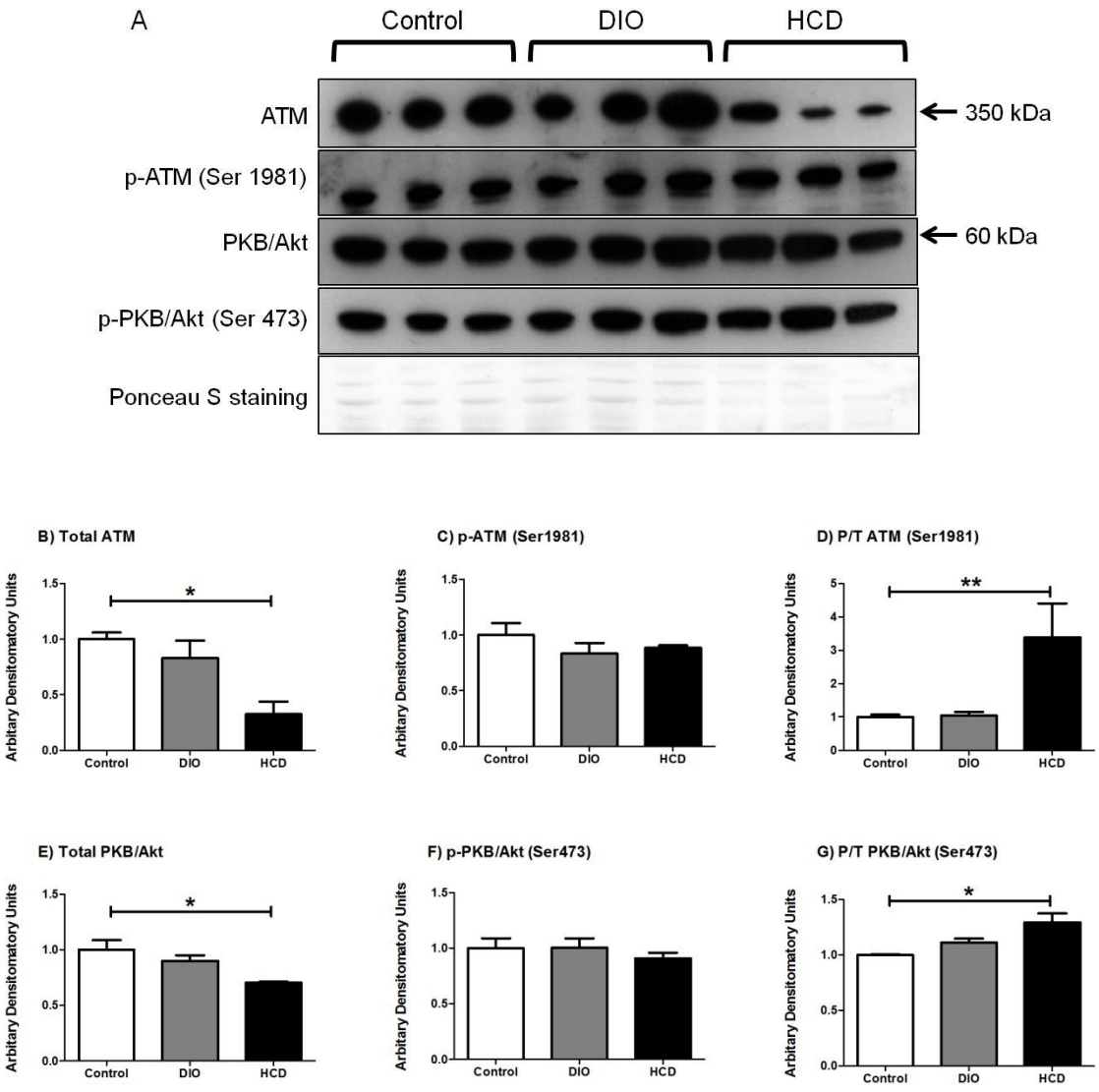

Figure 4.1: The effect of 16 week diet (DIO and HCD) compared to control diet on basal total and p-ATM and PKB/Akt levels in rat hearts. A) Western blot chemiluminescent results of ATM, p-ATM, PKB/Akt and p-PKB/Akt and Ponceau S staining of the membrane against which the chemiluminescent results were normalised. All antibodies were probed on the same membrane. B) Bar graph depicting analysed results for total ATM. C) Bar graph depicting analysed results for p-ATM (Ser1981). D) Bar graph depicting phospho to total ratio of ATM. E) Bar graph depicting analysed results for total PKB/Akt. F) Bar graph depicting analysed results for p-PKB/Akt (Ser473). G) Bar graph depicting phospho to total ratio of PKB/Akt. Results are indicated relative to the control diet. * $p < 0.05$ ** $p < 0.005$ (n=3 per group).

4.1.2 Biometric data

After the 16-week diet feeding program, biometric data including body mass, visceral fat mass and non-fasting glucose levels were measured in DIO, HCD and age-matched control animals in order to determine the ability of the diets to induce obesity and glucose intolerance. The results are summarised in Table 4.1. The DIO diet increased the visceral fat mass by 81.7% compared to the control diet (Control 16.88 ± 1.33 g; DIO 30.74 ± 2.68 g; $p < 0.0001$). Body mass and non-fasting glucose levels were, however, unaffected by the DIO diet compared to the control diet. In contrast, the HCD significantly increased the body mass by 15.1% (Control 444.4 ± 11.4 g; HCD 511.5 ± 15.19 g; $p < 0.05$), the visceral fat mass by 131.4% (Control 16.88 ± 1.33 g; HCD 39.13 ± 2.36 g; $p < 0.0001$) and the non-fasting glucose levels by 11.6% compared to the control diet (Control 6.9 ± 0.15 mmol/L; HCD 7.7 ± 0.28 mmol/L; $p < 0.05$). Taken together, these results suggest that the HCD model has a more pronounced effect on the measured parameters and is thus more successful in inducing obesity and hyperglycemia in the animals compared to the DIO model. We therefore conducted the rest of the experiments using only the HCD model.

Table 4.1: Body mass, visceral fat mass and non-fasting glucose levels of the DIO and HCD animals compared to age-matched control animals following a 16-week diet feeding program. (n=12 per group)

Parameters	Control	DIO	HCD
Body mass	444.4 ± 11.4 g	496.4 ± 19.3 g	511.5 ± 15.2 g (*)
Visceral fat mass	16.9 ± 1.3 g	30.7 ± 2.7 g (***)	39.1 ± 2.4 g (***)
Non-fasting glucose levels	6.9 ± 0.1 mmol/L	7.0 ± 0.2 mmol/L	7.7 ± 0.3 mmol/L (*)

* $p < 0.05$; ** $p < 0.005$; *** $p < 0.0001$

4.1.3 Further characterisation of the high caloric diet

In order to further determine whether the HCD is able to induce insulin resistance and glucose intolerance in the animals, fasting glucose levels and insulin levels were determined, the HOMA-IR index was calculated and an OGTT was performed. The HCD animals had significantly increased fasting glucose levels (Control 4.6 ± 0.1 mmol/L; HCD 5.8 ± 0.2 mmol/L; $p < 0.0001$) as well as significantly higher insulin levels (Control 0.15 ± 0.004 ng/mL; HCD 0.18 ± 0.009 ng/ml; $p < 0.05$) compared to control animals. Furthermore, the HOMA-IR index was also significantly higher in the HCD animals compared to the control animals (Control 0.95 ± 0.10; HCD 1.35 ± 0.14; $p < 0.05$) (Table 4.2).

Results from the OGTT indicated that animals that received the HCD had consistently increased glucose levels compared to animals that were on the control diet (Figure 4.2 A) Additionally, the area under the curve was also significantly bigger for the HCD group compared to the control group (Control 652.9 ± 24.3; HCD 747.9 ± 33.2; $p < 0.05$) (Figure 4.2 B). Taken together, these results indicate that the HCD induced hyperglycemia, hyperinsulinemia and insulin resistance in the animals and is thus a sufficient model to be used in the study.

Table 4.2: Characteristics of animals fed the HCD compared to the control diet.

Parameter	Control	HCD
Fasting glucose levels (n=15)[+]	4.6 ± 0.1 mmol/L	5.8 ± 0.2 mmol/L (***)
Insulin levels (n=6) [+]	0.15 ± 0.004 ng/mL	0.18 ± 0.009 ng/ml (*)
HOMA-IR (n=6) [+]	0.95 ± 0.10	1.35 ± 0.14 (*)

* $p<0.05$; *** $p<0.0001$

[+] n-values are per group

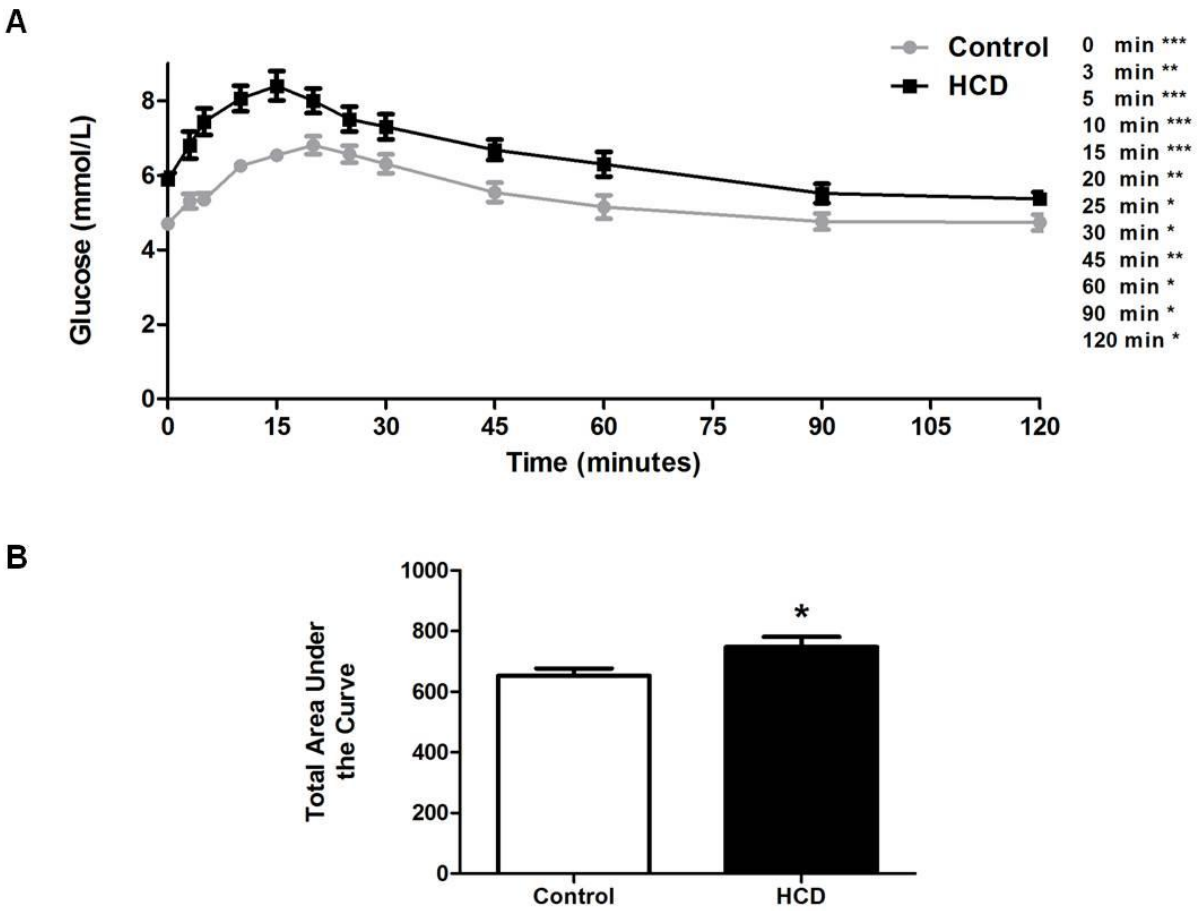

Figure 4.2: Results of the oral glucose tolerance test in the HCD group compared to the control group. A) Glucose concentrations over time (n=12-15 per time point). B) Total area under the curves in the control and HCD animals (n=15 per group). * $p<0.05$; ** $p<0.005$; *** $p<0.0001$

4.2 Drug dosage experiments

4.2.1 Insulin

Glucose uptake

Glucose uptake experiments were done in isolated ventricular cardiomyocytes from control animals using insulin concentrations of 1 nM, 10 nM and 100 nM. Glucose uptake was significantly increased in response to 100 nM insulin compared to the untreated control (Untreated 1.0; 100 nM Ins 2.8 ± 0.5; $p < 0.01$) (Figure 4.3). This indicates that 100 nM insulin is sufficient to significantly stimulate glucose uptake in cardiomyocytes.

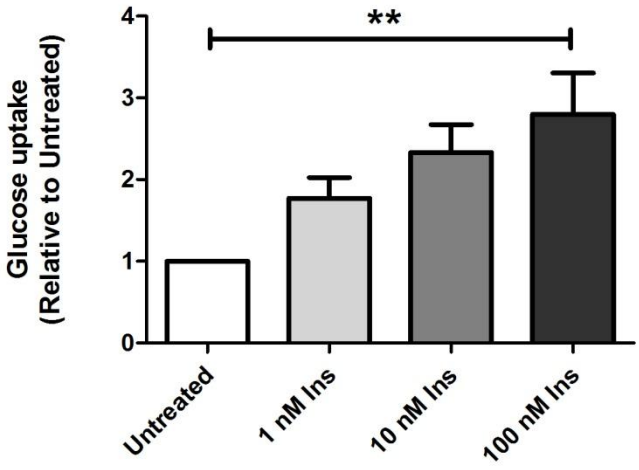

Figure 4.3: Bar graph depicting the glucose uptake, relative to the untreated group, by cardiomyocytes after stimulation with increasing insulin concentrations (1 nM, 10 nM and 100 nM). ** $p<0.01$; (n=6 per group).

4.2.2 Chloroquine

In order to determine whether chloroquine is a viable drug to use to activate cardiac ATM, a number of drug dose-response studies were conducted, including glucose uptake, cell viability assay, Langendorff perfusions to assess cardiac function and Western blot analysis.

Glucose uptake

Firstly, glucose uptake was measured in response to increasing chloroquine concentrations in isolated cardiomyocytes. None of the chloroquine concentrations used, including 10 µM, 50 µM and 100 µM, significantly changed glucose uptake levels compared to untreated levels (Figure 4.4).

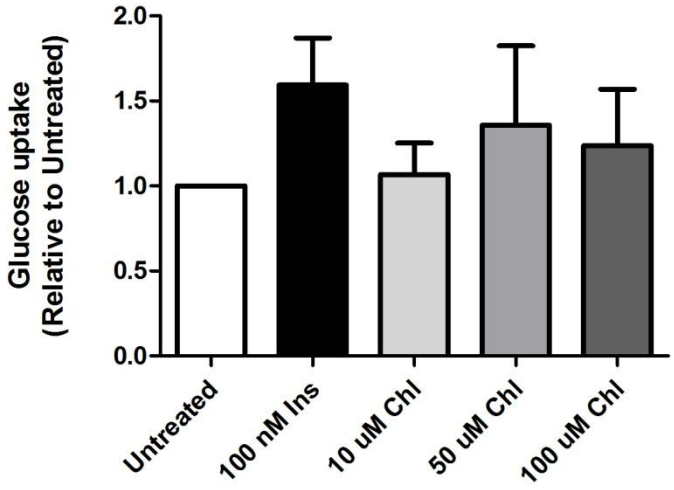

Figure 4.4: Bar graph depicting the glucose uptake, relative to the untreated group, by cardiomyocytes after stimulation with increasing concentrations of chloroquine (10 µM, 50 µM and 100 µM) Chl Chloroquine; Ins Insulin (n=3 per group).

Cell viability

We then performed a PI assay to determine if chloroquine treatment leads to necrosis of isolated cardiomyocytes. Analysed chloroquine concentrations included 10 µM, 50 µM and 100 µM. Compared to the untreated group, significantly more necrosis was measured in cells treated with 10 µM (115.4 ± 0.97%; $p < 0.005$) and 50 µM (108.1 ± 0.22%; $p < 0.05$) chloroquine (Figure 4.5). This indicates that chloroquine has a cardiotoxic effect.

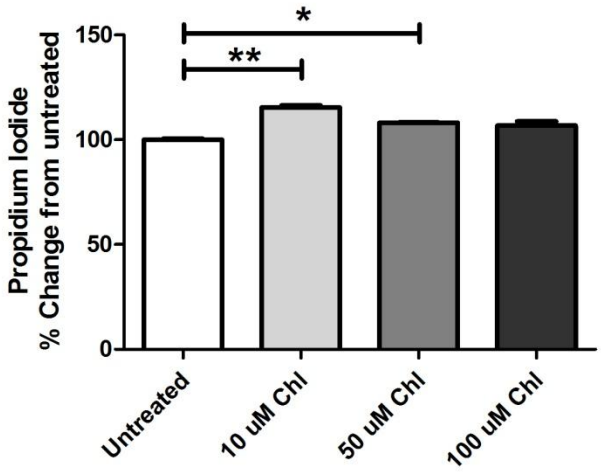

Figure 4.5: Bar graphs showing the percentage change in propidium iodide uptake from untreated cells by isolated cardiomyocytes treated with increasing concentrations of chloroquine. * $p < 0.05$; ** $p < 0.005$ Chl Chloroquine (n=2 per group).

Langendorff perfusion and Western blotting

Lastly, Langendorff perfusion experiments were conducted, after which the hearts were freeze-clamped for total and phospho-ATM determination using Western blot analysis. The RPP was significantly reduced after 10 minutes of treatment with each of the chloroquine concentrations used compared to untreated controls (Figure 4.6 A). The decrease in RPP was caused by both a decrease in LVDevP and in heart rate, as is shown in Figures 4.6 B and C respectively. Fifty percent of hearts treated with 50 µM chloroquine ceased to function within the first five minutes

after being perfused with chloroquine. For this reason, we omitted the highest chloroquine concentration, namely 100 µM, from the perfusion experiments.

None of the chloroquine concentrations used had a significant effect on the total or phosphorylation (Ser1981) levels of ATM and the P/T ATM ratio was also unaffected (Figure 4.7).

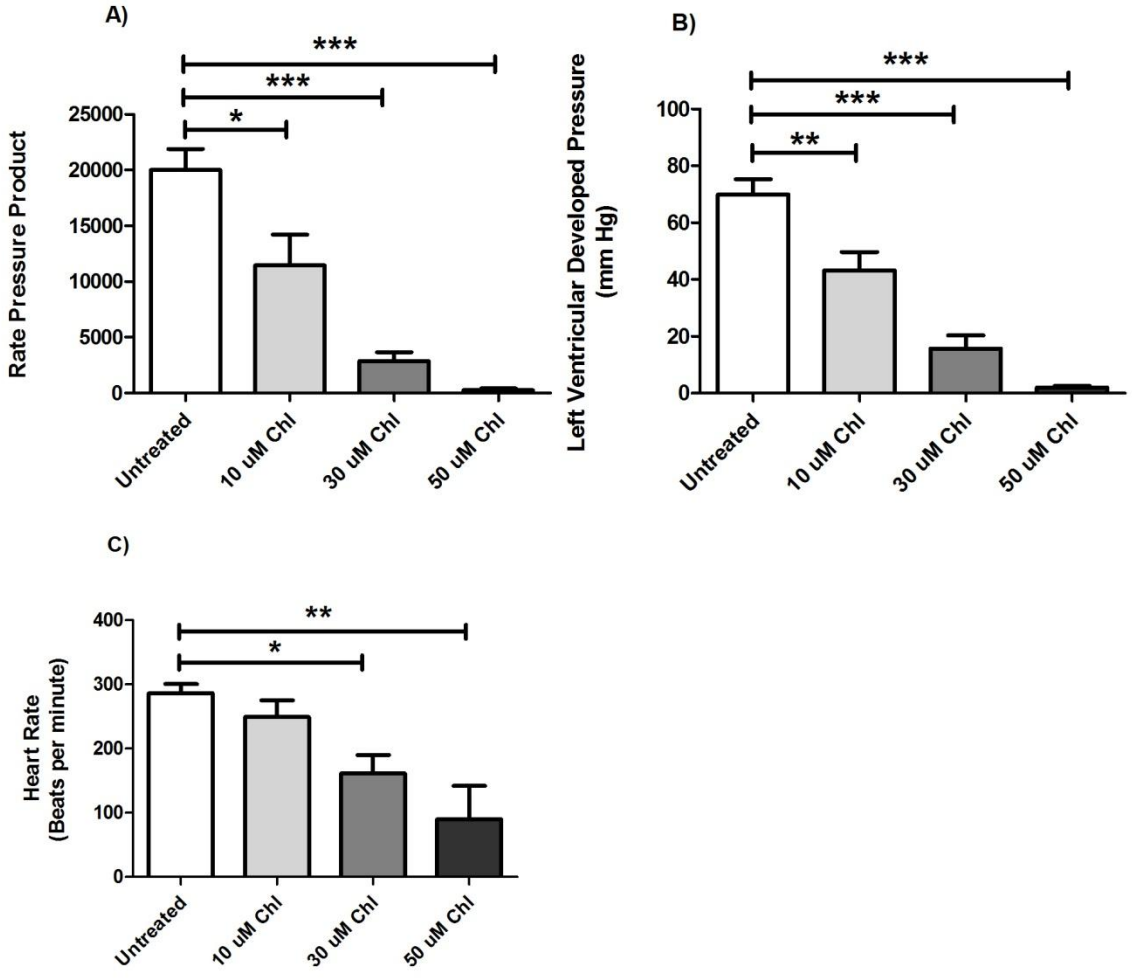

Figure 4.6: Bar graphs showing cardiac function following treatment of Langendorff perfused hearts with 0 µM (untreated), 10 µM, 30 µM and 50 µM chloroquine. A) Rate pressure product (mm Hg beats/minute). B) Left ventricular developed pressure (mm Hg). C) Heart rate (Beats per minute). * $p < 0.05$; ** $p < 0.005$; *** $p < 0.0001$ Chl Chloroquine (n=7 per group except 50 µM Chloroquine n=4).

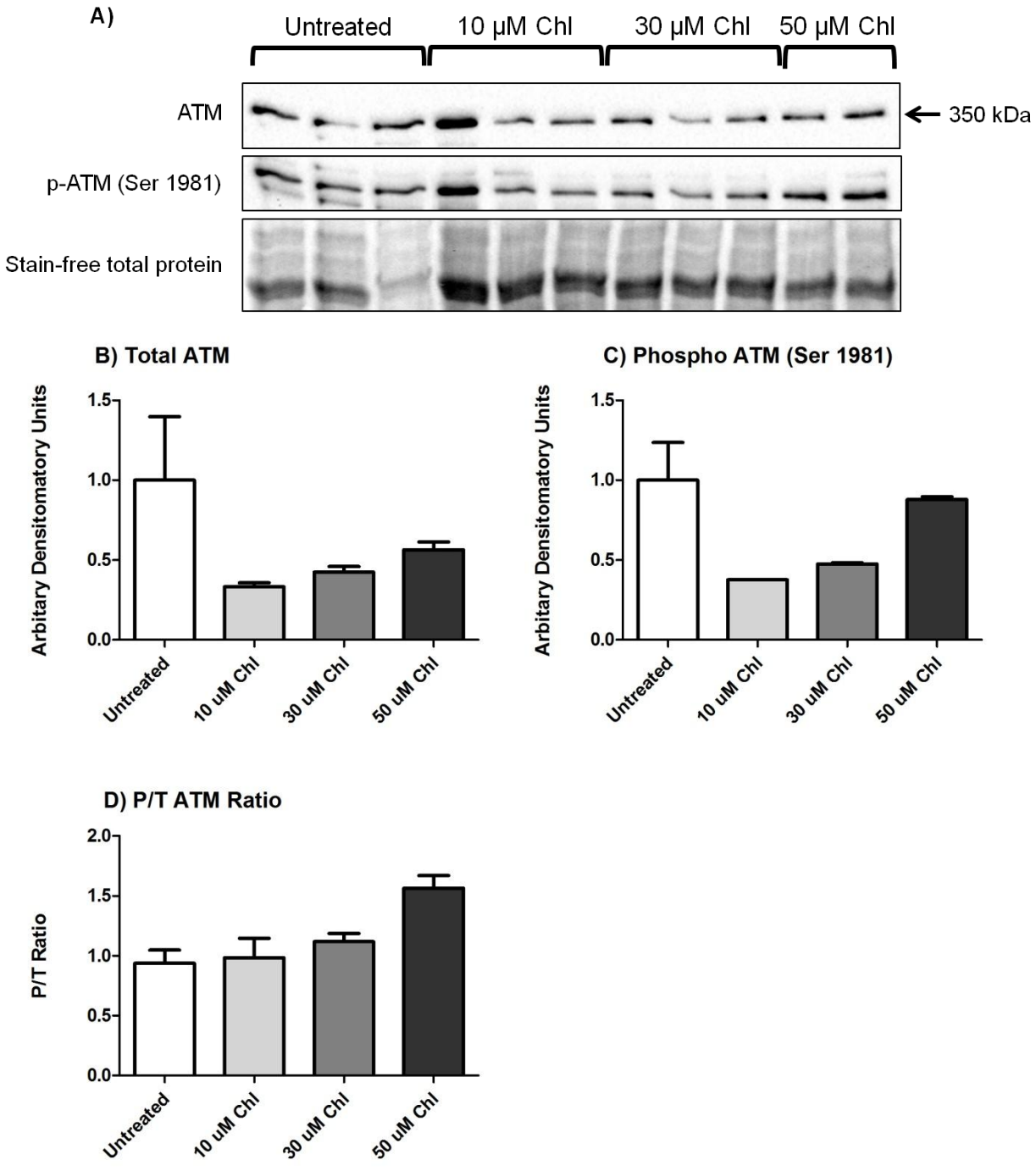

Figure 4.7: The effect of perfusion with increasing chloroquine concentrations on ATM expression and activation. A) Western blot chemiluminescent results of ATM, phospho ATM and stain-free total protein. B) Bar graph depicting analysed results for total ATM. C) Bar graph depicting analysed results for phospho-ATM (Ser 1981). D) Bar graph depicting phospho to total ratio of ATM. Chl Chloroquine (n=3 per group).

4.2.3 KU-60019

Glucose uptake

We measured glucose uptake by cardiomyocytes following treatment with insulin alone, or insulin in combination with increasing concentrations of KU-60019 in order to identify the best dosage of KU-60019. Although glucose uptake appeared to decrease slightly with increasing concentrations of KU-60019, the change in glucose uptake was not significant (Figure 4.8).

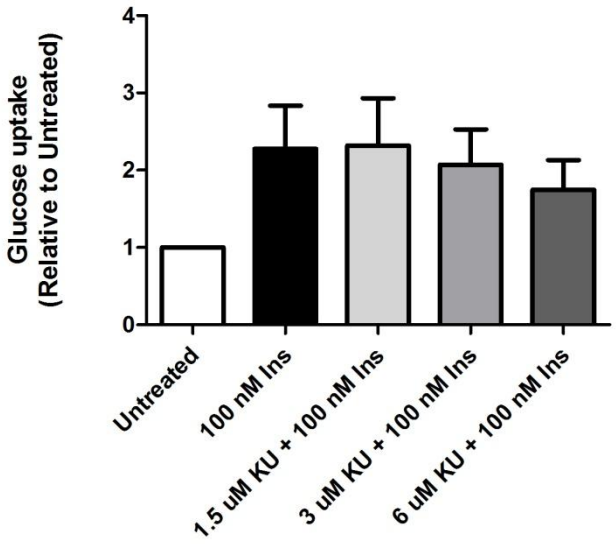

Figure 4.8: Bar graph depicting the glucose uptake, relative to the untreated group, by cardiomyocytes after stimulation with a combination of 100 nM insulin and increasing concentrations of KU-60019 (1.5 µM, 3 µM and 6 µM). Ins Insulin; KU KU-60019. (n=4 per group).

Western blotting

Hearts isolated from young control rats were perfused with insulin and increasing concentrations of KU-60019. Following perfusion, the hearts were freeze-clamped and subjected to Western blotting using total ATM and phospho-ATM antibodies. A significantly lower P/T ATM ratio was observed in hearts perfused with 3 μM KU-60019 in combination with insulin compared to both untreated hearts (Untreated 0.97 ± 0.06; 3 μM 0.67 ± 0.01; $p < 0.05$) and hearts treated with insulin alone (Ins 1.17 ± 0.09; 3 μM 0.67 ± 0.01; $p < 0.05$) (Figure 4.9). A KU-60019 dosage of 3 μM was thus able to decrease ATM phosphorylation to lower levels than what is seen in untreated hearts.

In order to confirm this, age-matched control rats were perfused with 3 μM KU-60019 for 20 minutes and freeze-clamped. Western blots probing for total and phospho-ATM were performed on the freeze-clamped heart tissue. Treatment with 3 μM KU-60019 had no effect on total ATM levels compared to the untreated group (Figure 4.10 A). Treatment with 3 μM KU-60019 significantly reduced phosphorylation of ATM (Ser1981) compared to the untreated group (Untreated 1.09 ± 0.09; 3 μM KU 0.61 ± 0.10; $p < 0.01$) (Figure 4.10 B). A KU-60019 concentration of 3 μM was thus selected to be used in the study.

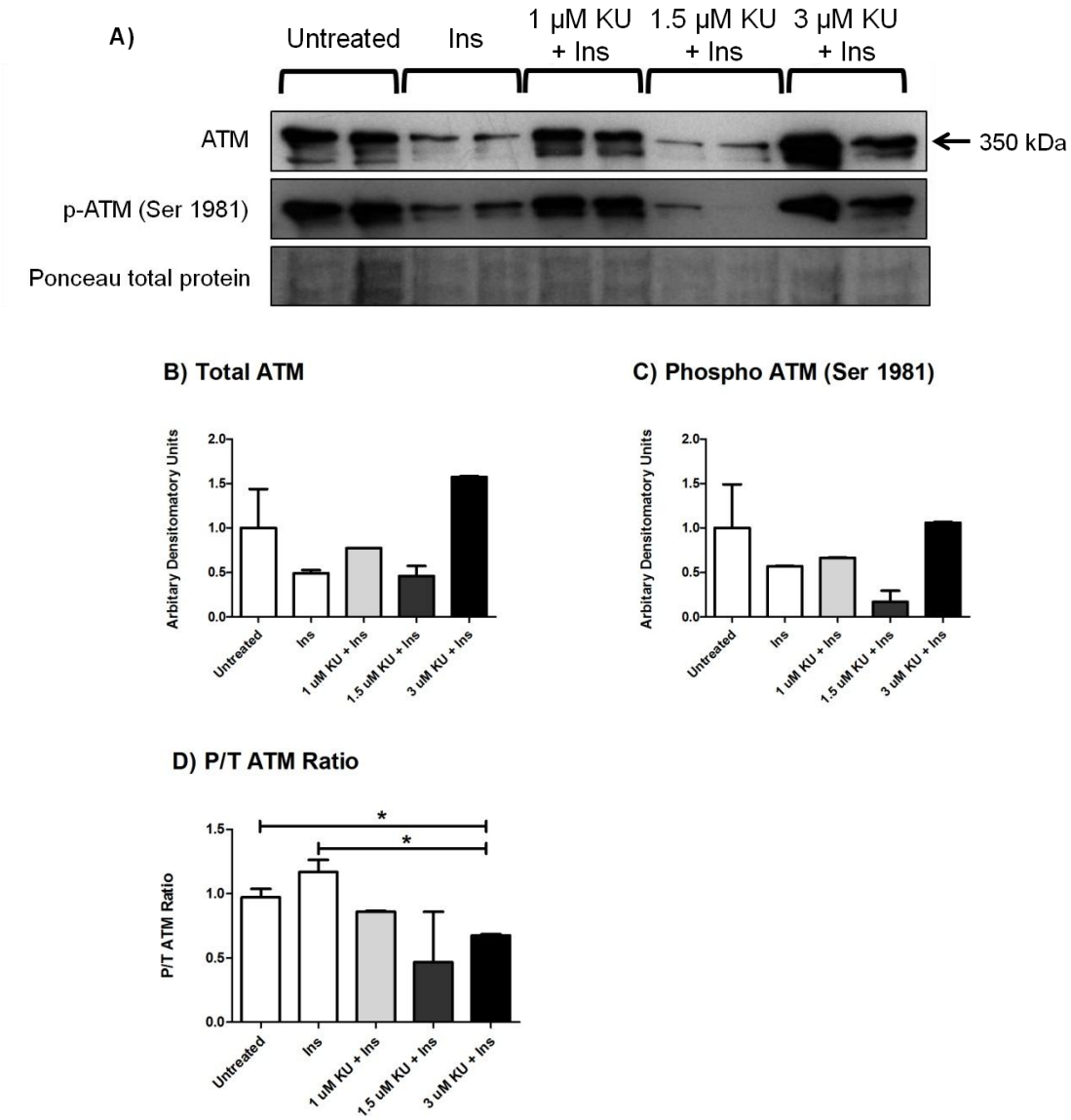

Figure 4.9: The effect of perfusion with increasing KU-60019 concentrations on ATM expression and activation. A) Western blot chemiluminescent results of ATM, phospho-ATM and Ponceau total protein stain. B) Bar graph depicting analysed results for total ATM. C) Bar graph depicting analysed results for phospho-ATM (Ser 1981). D) Bar graph depicting phospho to total ratio of ATM. Ins insulin; KU KU-60019 * $p < 0.05$ (n=2).

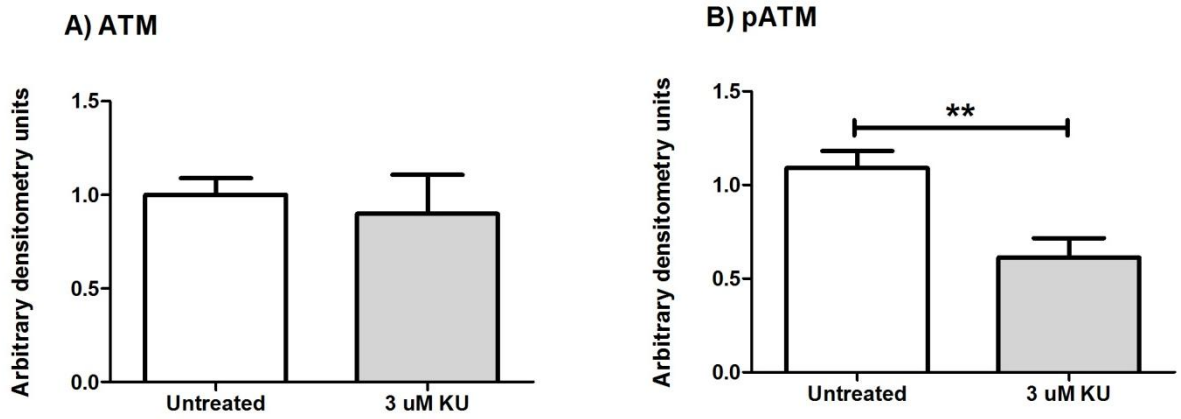

Figure 4.10: Total and phospho-ATM levels in hearts of age-matched control rats that were perfused with 3 μM KU-60019. A) Total ATM. B) Phospho-ATM. ** P < 0.01 KU KU-60019 (n=5 per group).

Cell viability

A PI assay was performed to assess whether 3 μM of KU-60019 or the DMSO vehicle increased necrosis of isolated cardiomyocytes. Cell viability was unaffected by both the DMSO vehicle and the 3 μM KU-60019 (Figure 4.11).

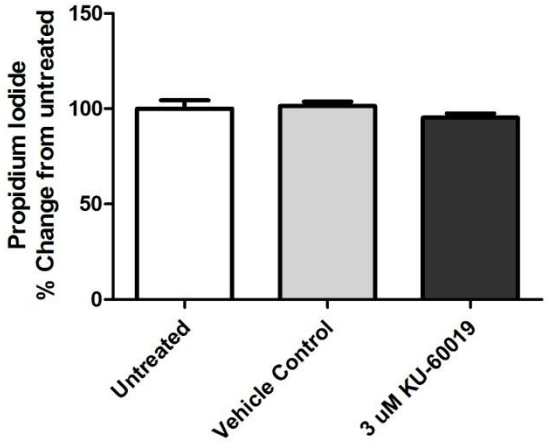

Figure 4.11: Bar graphs showing the percentage change in propidium iodide uptake from untreated cells by isolated cardiomyocytes treated with 3 μM KU-60019 prepared in DMSO or treated with the DMSO alone as vehicle control. (n=2 per group).

4.3 Langendorff perfusions (Balloon model) and global ischaemia

Hearts isolated from control and HCD fed animals were subjected to Langendorff perfusion using the balloon model. These hearts were treated with insulin (1 U/L), wortmannin (100 nM) and KU-60019 (3 μM) after which they underwent 20 minutes of global ischaemia and five or 10 minutes of reperfusion. An inflatable balloon, attached to a pressure transducer, was inserted into the left ventricle to measure cardiac function.

4.3.1 The effect of the vehicle control

We firstly assessed whether the vehicle control, namely DMSO, affected cardiac function. Perfusion with 0.033% DMSO, which is the final concentration of the vehicle used to dissolve KU-60019, had no effect on the LVDevP or RPP. There were no significant changes following the treatment period (before IRI) or in the percentage recovery following IRI (Figure 4.12).

Additionally, the HCD also had no basal effect on cardiac function when compared to the control group.

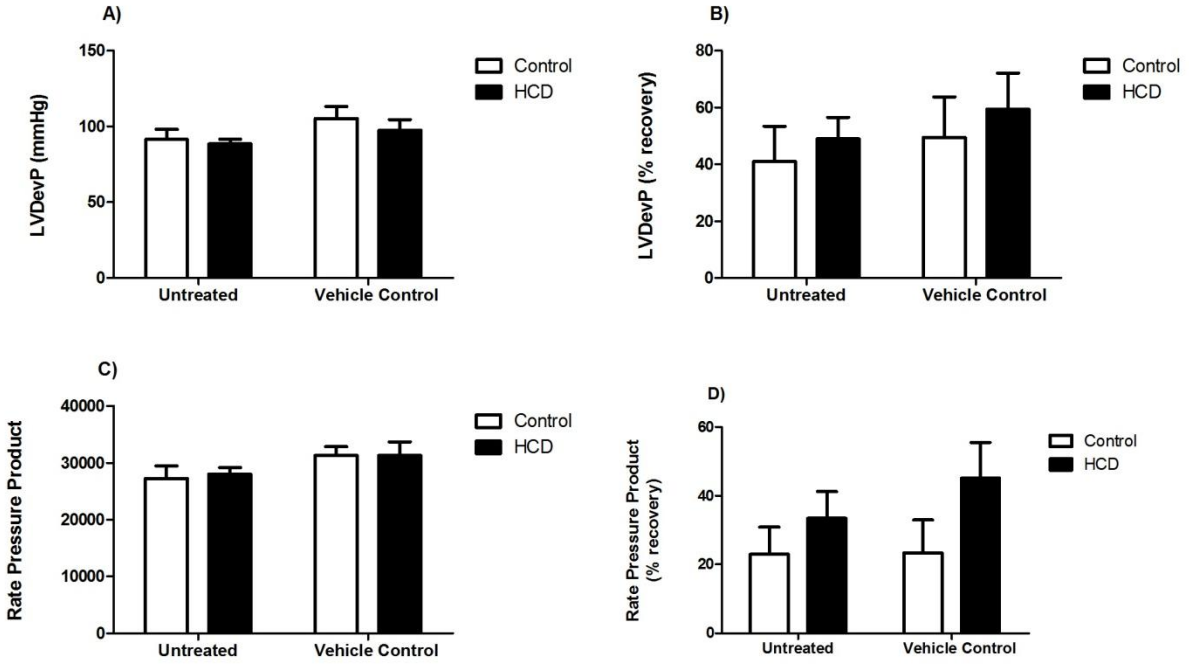

Figure 4.12: Comparison of cardiac function in untreated and DMSO-treated (vehicle control) hearts. A) Left ventricular developed pressure (mm Hg) before IRI. B) Percentage recovery in left ventricular developed pressure following IRI. C) Rate pressure product (mm Hg beats/minute) before IRI. D) Percentage recovery in rate pressure product following IRI. (n=5 per group).

4.3.2 The effect of insulin, wortmannin and KU-60019 on cardiac function of Langendorff perfused control and HCD hearts

The Langendorff perfusion technique was used to perfuse hearts from animals that have been on the HCD for 16 and 25 weeks and their age-matched controls. The length of time on the diet caused no significant differences in cardiac function (data not shown) so the data was pooled together for further analysis.

LVDevP

The treatment groups had no effect on LVDevP prior to ischaemia in either the control or HCD hearts. At both five and 10 minutes reperfusion, the LVDevP was significantly lower compared to before ischaemia. Global ischaemia therefore significantly reduced LVDevP. After five minutes of reperfusion, both wortmannin and KU-60019 treated hearts had significantly higher LVDevP compared to untreated hearts. This effect was observed in control hearts and in HCD hearts, but it was no longer seen at 10 minutes reperfusion. Co-treatment with KU-60019 and insulin resulted in significantly higher LVDevP compared to treatment with insulin alone. This was seen at five and 10 minutes reperfusion in both the control and HCD hearts. Higher LVDevP was also seen in both control and HCD hearts co-treated with wortmannin and insulin compared to treatment with insulin alone. This effect was only observed at 10 minutes and not at five minutes reperfusion. In control and HCD hearts, insulin treatment prior to ischaemia caused significantly reduced LVDevP at 10 minutes reperfusion compared to untreated hearts. HCD insulin treated hearts had significantly higher LVDevP at 10 minutes reperfusion compared to control hearts treated with insulin. Results for LVDeVP are summarised in Table 4.3.

Table 4.3: Left ventricular developed pressure (mm Hg) before and after ischaemia/reperfusion injury in treated control and HCD hearts. Data expressed as mean with standard error of the mean.

		Before Ischaemia (n=9-10)	5 min Reperfusion (n=8-10)	10 min Reperfusion (n=4-5)
Control	Untreated	103.0 ± 6.9	23.5 ± 5.3 (c)	50.0 ± 10.1 (b)
	Insulin	99.9 ± 3.5	24.0 ± 2.2 (c)	17.8 ± 2.5 (c)(*)
	Wortmannin	89.8 ± 3.5	50.9 ± 6.6 (c)(**)	35.2 ± 3.3 (c)
	Wortmannin + Insulin	105.0 ± 4.0 ($)	20.9 ± 4.8 (c)($$)	34.0 ± 5.8 (c)(#)
	KU-60019	101.5 ± 4.0	71.1 ± 10.0 (b)(***)	66.0 ± 5.9 (c)
	KU-60019 + Insulin	109.6 ± 4.8	55.1 ± 6.2 (c)(###)	63.0 ± 17.1 (b)(#)
HCD	Untreated	98.4 ± 4.3	27.4 ± 4.6 (c)	49.5 ± 1.9 (c)
	Insulin	104.3 ± 4.2	25.8 ± 4.4 (c)	30.8 ± 5.1 (c)(*)(+)
	Wortmannin	102.0 ± 7.1	51.7 ± 10.4 (c)(*)	56.2 ± 9.7 (b)
	Wortmannin + Insulin	100.0 ± 5.6	28.1 ± 7.3 (c)	50.3 ± 6.2 (c)(#)
	KU-60019	95.9 ± 4.1	64.0 ± 16.5 (a)(*)	49.3 ± 4.3 (c)
	KU-60019 + Insulin	107.7 ± 5.9	65.4 ± 9.2 (b)(##)	59.5 ± 9.3 (c)(#)

a $p < 0.05$; b $p < 0.005$; c $p < 0.0001$; Compared to Before Ischaemia

$ $p < 0.05$; $$ $p < 0.005$; Compared to Wortmannin

* $p < 0.05$; ** $p < 0.005$; *** $p < 0.001$; Compared to Untreated

# $p < 0.05$; ## $p < 0.005$ ### $p < 0.0005$; Compared to Insulin

+ $p < 0.05$; Compared to Control

RPP

As with LVDevP, none of the treatment groups had a significant effect on RPP before the ischaemic period and all groups had decreased RPP values following both five and 10 minutes reperfusion. At five minutes reperfusion, control hearts that had been treated with wortmannin and KU-60019 had significantly higher RPP values than untreated control hearts. At 10 minutes reperfusion, only KU-60019 treated hearts had increased RPP values compared to untreated control hearts. Neither wortmannin nor KU-60019 treatment had an effect on RPP values in HCD hearts. Treatment with KU-60019 plus insulin resulted in significantly higher RPP values at both five and 10 minutes reperfusion compared to insulin only treated hearts. This effect

observed in both the control and HCD hearts. KU-60019 treatment caused significantly lower RPP values in HCD hearts compared to control hearts. Results for RPP values are summarised in Table 4.4.

Table 4.4: Rate pressure product (mm Hg beats/minute) before and after ischaemia/reperfusion injury in treated control and HCD hearts. Data expressed as mean with standard error of the mean.

		Before Ischaemia (n=9-10)	5 min Reperfusion (n=5-9)	10 min Reperfusion (n=4-5)
Control	Untreated	29120 ± 1454	4478 ± 696 (c)	5858 ± 2127 (c)
	Insulin	27650 ± 1943	6322 ± 829 (c)	4115 ± 694 (c)
	Wortmannin	27000 ± 2061	8978 ± 1388 (c)(*)	8104 ± 2251 (c)
	Wortmannin + Insulin	30290 ± 1776	5540 ± 1549 (c)	6506 ± 991 (c)
	KU-60019	28180 ± 1304	13000 ± 1488 (c)(***)	14800 ± 2166 (c)(*)
	KU-60019 + Insulin	31180 ± 1370	10270 ± 1499 (c)(#)	16190 ± 4535 (c)(#)
HCD	Untreated	28870 ± 1642	7032 ± 1366 (c)	8853 ± 2309 (c)
	Insulin	30650 ± 1934	5472 ± 1225 (c)	6655 ± 816 (c)
	Wortmannin	27300 ± 2444	8022 ± 1946 (c)	11030 ± 2052 (c)
	Wortmannin + Insulin	29790 ± 1757	9972 ± 1548 (c)(#)	8806 ± 2013 (c)
	KU-60019	29400 ± 1123	9870 ± 1393 (c)	7220 ± 928 (c)(+)
	KU-60019 + Insulin	31540 ± 1320	11100 ± 1736 (c)(#)	17650 ± 1574 (c)(##)

c $p < 0.0001$; Compared to Before Ischaemia

* $p < 0.05$; *** $p < 0.0001$; Compared to untreated

# $p < 0.05$; ## $p < 0.005$; Compared to insulin

+ $p < 0.05$; Compared to Control

Heart Rate

None of the treatment groups had a significant effect on heart rate before ischaemia in either control or HCD hearts. At 10 minutes reperfusion, HCD hearts treated with KU-60019 prior to ischaemia had significantly lower heart rates than control hearts treated with KU-60019 prior to ischaemia. Decreased heart rates were observed in both control and HCD hearts at five and 10 minutes reperfusion compared to before ischaemia in all treatment groups. However, at 10

minutes reperfusion, hearts that were treated with insulin alone prior to ischaemia no longer had decreased heart rates compared to prior to the ischaemic period. Additionally, HCD hearts that were treated with wortmannin had unaltered heart rates at five and 10 minutes reperfusion. A two-way ANOVA was performed to further investigate the effect of insulin on heart rate as insulin appeared to increase heart rate during reperfusion. Insulin treatment prior to global ischaemia resulted in significantly increased heart rates at both five and 10 minutes reperfusion compared to untreated hearts (Figure 4.13). Heart rate data is summarised in Table 4.5.

Table 4.5: Heart rate (beats/minute) before and after ischaemia/reperfusion injury in treated control and HCD hearts. Data expressed as mean with standard error of the mean.

		Before Ischaemia (n=9-10)	**5 min Reperfusion (n=4-10)**	**10 min Reperfusion (n=3-5)**
Control	Untreated	288 ± 16	182 ± 18 (c)	164 ± 16 (c)
	Insulin	273 ± 15	217 ± 19 (a)	234 ± 24
	Wortmannin	309 ± 18	183 ± 24 (c)	221 ± 40 (a)
	Wortmannin + Insulin	288 ± 13	171 ± 29 (c)	202 ± 24 (b)
	KU-60019	280 ± 15	179 ± 19 (c)	220 ± 17 (a)
	KU-60019 + Insulin	286 ± 8	173 ± 17 (c)	253 ± 8 (a)
HCD	Untreated	292 ± 18	187 ± 18 (c)	196 ± 29 (a)
	Insulin	312 ± 20	210 ± 29 (b)	263 ± 38
	Wortmannin	277 ± 20	212 ± 29	210 ± 43
	Wortmannin + Insulin	299 ± 14	208 ± 28 (b)	169 ± 15 (c)
	KU-60019	309 ± 10	145 ± 13 (c)	146 ± 7 (c)(+)
	KU-60019 + Insulin	298 ± 14	160 ± 15 (c)	231 ± 35 (a)

a $p < 0.05$; b $p < 0.005$; c $p < 0.0001$; Compared to Before Ischaemia

\+ $p < 0.05$; Compared to Control

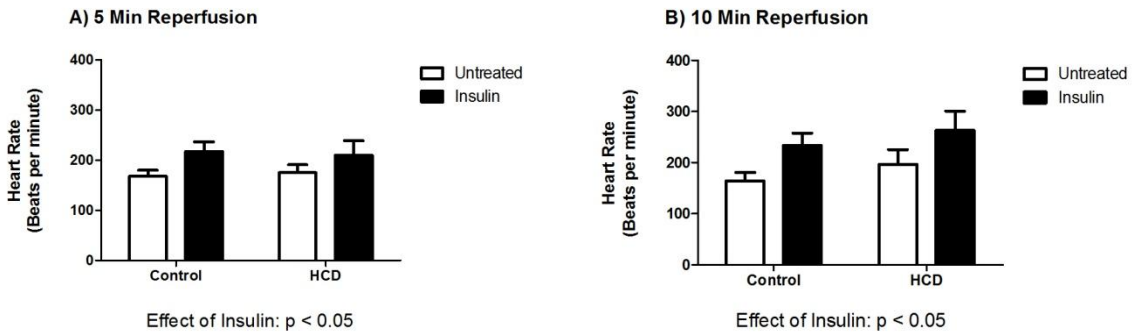

Figure 4.13: The effect of insulin treatment prior to global ischaemia on heart rate during reperfusion. A) Two-way ANOVA to illustrate the effect of insulin treatment on heart rate (beats/minute) at five minutes reperfusion (n=6-9). B) Two-way ANOVA to illustrate the effect of insulin treatment on heart rate (beats/minute) at 10 minutes reperfusion (n=4-5).

Coronary Flow

Treatment with KU-60019 significantly increased CF in both control and HCD hearts immediately once the KU-60019 was administered. This effect of KU-60019 was still observed at five minutes reperfusion. At 10 minutes reperfusion, the effect of KU-60019 on the increase of CF disappeared. Ischaemia had no effect on CF as CF remained unchanged in all other treatment groups. Coronary flow results are summarised in Table 4.6.

Table 4.6: Coronary flow (mL/min) before and after ischaemia/reperfusion injury in treated control and HCD hearts. Data expressed as mean with standard error of the mean.

		Before Ischaemia (n=9-10)	**5 min Reperfusion (n=8-10)**	**10 min Reperfusion (n=3-5)**
Control	Untreated	15.05 ± 0.89	13.75 ± 0.62	12.80 ± 1.11
	Insulin	14.20 ± 1.23	14.25 ± 0.59	14.30 ± 2.06
	Wortmannin	12.90 ± 1.24	15.10 ± 0.60	11.90 ± 0.99
	Wortmannin + Insulin	14.25 ± 1.14	14.22 ± 0.69	13.10 ± 0.29
	KU-60019	20.55 ± 0.95 (***)	18.20 ± 1.09 (**)	16.13 ± 1.28 (a)
	KU-60019 + Insulin	20.35 ± 0.92 (###)	17.00 ± 0.77 (a)(#)	13.50 ± 1.06 (b)
HCD	Untreated	15.40 ± 0.94	14.67 ± 1.18	13.50 ± 1.50
	Insulin	14.22 ± 1.19	14.56 ± 0.80	16.00 ± 1.16
	Wortmannin	14.35 ± 1.22	14.83 ± 1.04	13.80 ± 0.56
	Wortmannin + Insulin	14.80 ± 1.04	15.45 ± 0.82	12.88 ± 0.72
	KU-60019	21.75 ± 0.78 (***)	18.50 ± 0.80 (b)(*)	20.50 ± 5.77
	KU-60019 + Insulin	20.80 ± 0.94 (###)	17.39 ± 1.02 (a)(#)	14.30 ± 1.11 (b)

a $p < 0.05$; b $p < 0.005$; Compared to Before Ischaemia

* $p < 0.05$; ** $p < 0.005$; *** $p < 0.0001$; Compared to untreated

# $p < 0.05$; ### $p < 0.0001$; Compared to insulin

Time to contracture and peak developed pressure during global ischaemia

Control and HCD hearts that were treated with insulin alone had a significantly longer time to onset of contracture during global ischaemia compared to untreated hearts (Table 4.7). Insulin treatment had no effect on the peak developed pressure in either the control or HCD hearts. Wortmannin treatment had no effect on the time to contracture in control hearts. Interestingly, the peak developed pressure was significantly lower in wortmannin treated control hearts compared to untreated control hearts. Co-treatment with insulin and wortmannin resulted in increased developed pressure compared to treatment with wortmannin alone. In HCD hearts, treatment with wortmannin significantly reduced the time to onset of contracture and co-treatment with insulin was not able to inhibit this effect of wortmannin. Wortmannin did not have an effect on the peak developed pressure in HCD hearts when compared to untreated HCD hearts.

Treatment with KU-60019 resulted in a longer time to onset of contracture in control hearts compared to untreated control hearts. This was accompanied with a significantly lower peak developed pressure in control hearts treated with KU-60019 compared to untreated control hearts. In HCD hearts, KU-60019 treatment had no effect on time to onset of contracture when compared to untreated hearts, however, a significantly lower peak developed pressure was observed in KU-60019 treated HCD hearts compared to untreated HCD hearts. Control and HCD hearts that were co-treated with KU-60019 and insulin took significantly longer to reach contracture than hearts treated with insulin alone. Co-treatment also resulted in significantly reduced peak developed pressures compared to hearts treated with insulin alone or KU-60019 alone. This was seen in both the control and HCD hearts (Table 4.7).

Table 4.7: Time to contracture (min) and peak developed pressure (mmHg) achieved during ischaemia in treated control and HCD hearts. Data expressed as mean with standard error of the mean (n=7-10).

	Time To Contracture		Peak Developed Pressure	
	Control	**HCD**	**Control**	**HCD**
Untreated	13 ± 0.5	14 ± 0.7	48.2 ± 5.0	42.8 ± 2.2
Insulin	16 ± 0.5 (***)	16 ± 0.6 (*)	41.0 ± 3.9	41.7 ± 3.6
Wortmannin	15 ± 0.8	11 ± 1.2 (+)(*)	34.3 ± 3.4 (*)	42.5 ± 3.0
Wortmannin + Insulin	14 ± 1.0	12 ± 1.2 (#)	46.7 ± 1.9 ($$)	35.0 ± 2.2 (+++)
KU-60019	16 ± 0.9 (*)	14 ± 0.9	32.57 ± 3.9 (*)	32.2 ± 3.6 (*)
KU-60019 + Insulin	18 ± 0.6 (#)	19 ± 0.6 (#)(¤¤¤)	16.9 ± 3.0 (###)(¤¤)	17.8 ± 4.4 (###)(¤)

* p < 0.05; *** p < 0.0005; Compared to untreated

+ p < 0.05; +++ p < 0.001; Compared to Control

# p < 0.05; ### p < 0.0005; Compared to insulin

$$ p < 0.007; Compared to wortmannin

¤ p < 0.05; ¤¤ p < 0.007; ¤¤¤ p < 0.0001; Compared to KU-60019

4.4 Western blotting

Hearts from age-matched control and HCD animals were perfused using the Langendorff balloon model. ATM signalling was manipulated using insulin (1 U/L), wortmannin (100 nM) and/or KU-60019 (3 μM), and the hearts were freeze-clamped before and after IRI in order to determine the effect of ATM manipulation on signalling networks through Western blot analysis. Proteins of interest included JNK, IRS-1, PI3K, PTEN, PKB/Akt, mTOR, GSK-3β, AS160, GLUT4, AMPK, acetyl-CoA carboxylase (ACC) and ATM. Untreated control hearts were loaded on all HCD gels and the HCD data was normalized to the untreated controls. This was done to enable comparisons between the control data and HCD data. The control data was also normalised to untreated controls.

4.4.1 Signalling before IRI

Western blot analysis of hearts that were freeze-clamped directly following the treatment period, prior to IRI, was performed by Ms A. Seboko, an Honours(MedSci) student that was under Ms. Y. Espach's supervision. The age-matched control and HCD hearts were treated with insulin (activator), KU-60019 (ATM specific inhibitor) and a combination of KU-60019 and insulin.

JNK

In control hearts, ATM inhibition using KU-60019 significantly reduced JNK expression (Untreated 1; KU 0.72 ± 0.02; $p < 0.005$). Co-treatment with both KU-60019 and insulin restored total JNK to untreated levels. None of the treatment groups had an effect on JNK phosphorylation in control hearts. The results of JNK Western blot analysis in control hearts are indicated in Figure 4.14.

There was no significant difference in total or phospho JNK levels between control and HCD hearts. Compared to untreated HCD hearts, treatment with insulin significantly increased total JNK expression (Untreated 0.92 ± 0.02; Ins 1.14 ± 0.04; $p < 0.005$) and decreased JNK phosphorylation (Untreated 1.01 ± 0.01; Ins 0.81 ± 0.01; $p < 0.0001$) in HCD hearts. This translated into a significantly reduced P/T ratio when treating with insulin compared to untreated hearts (Untreated 1.1 ± 0.01; Ins 0.71 ± 0.02; $p < 0.0001$). When HCD hearts were co-treated with KU-60019 and insulin, insulin was still able to significantly reduce JNK phosphorylation compared to treatment with KU-60019 alone (KU 0.99 ± 0.01; KU + Ins 0.87 ± 0.001; $p < 0.005$). Consequently, the P/T JNK ratio was significantly lower in the co-treated group compared to the KU-60019 group (KU 0.97 ± 0.01; KU + Ins 0.74 ± 0.04; $p < 0.0001$). Although KU-60019 treatment had no significant effect on total or phospho JNK levels, it did cause the P/T ratio to be significantly lower compared to untreated hearts (Untreated 1.1 ± 0.01; KU 0.97 ± 0.01; $p < 0.005$). The results of JNK Western blot analysis in HCD hearts are indicated in Figure 4.15.

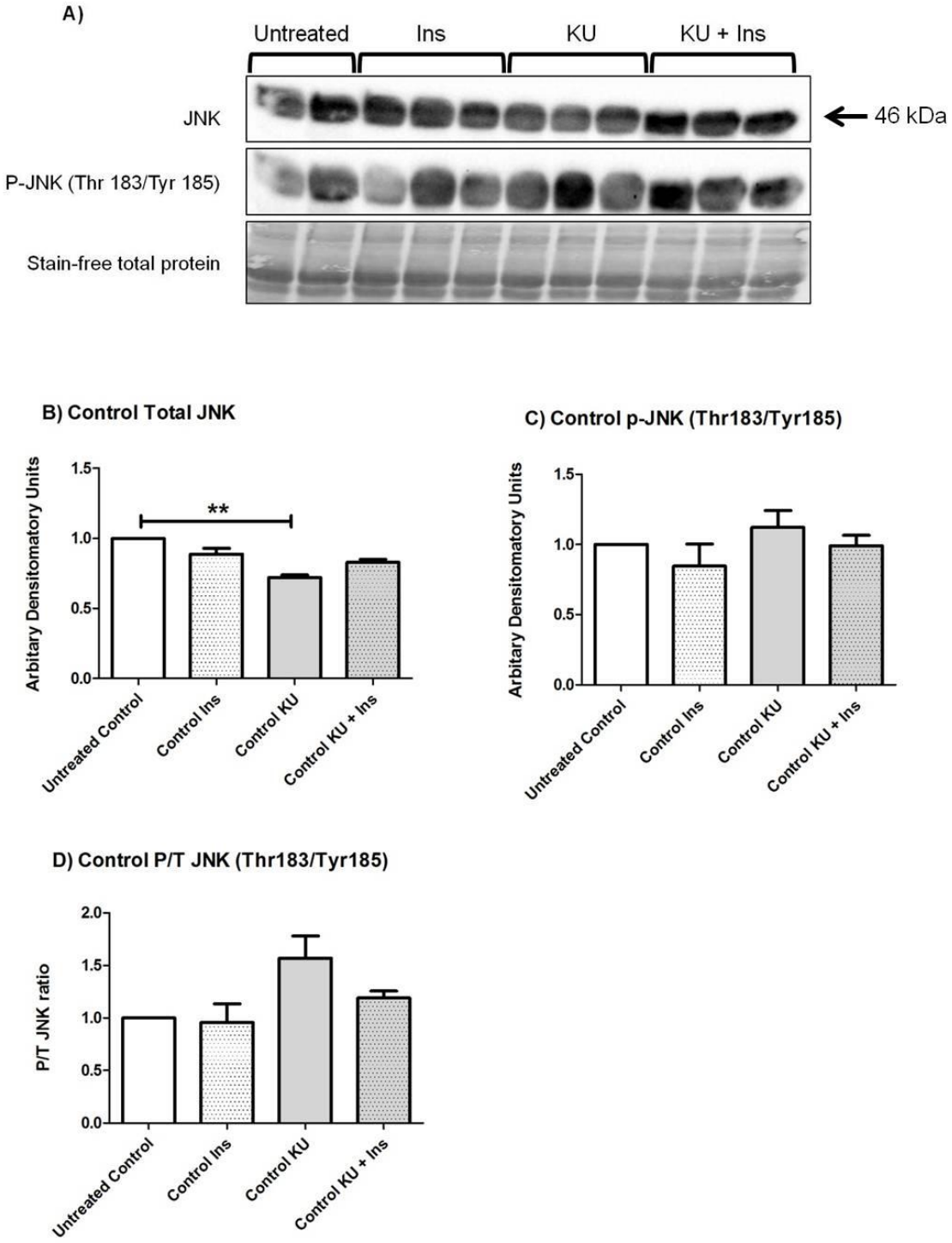

Figure 4.14: JNK expression and phosphorylation levels in control hearts following treatment with insulin, KU-60019 and a combination of insulin and KU-60019. A) Western blot chemiluminescent results of JNK and p-JNK and stain-free total protein stain of the membrane. B) Bar graph depicting analysed results for total JNK. C) Bar graph depicting analysed results for p-JNK (Thr 183/ Tyr 185). D) Bar graph depicting phospho to total ratio of JNK. ** $p < 0.005$ (n=2-3 per group).

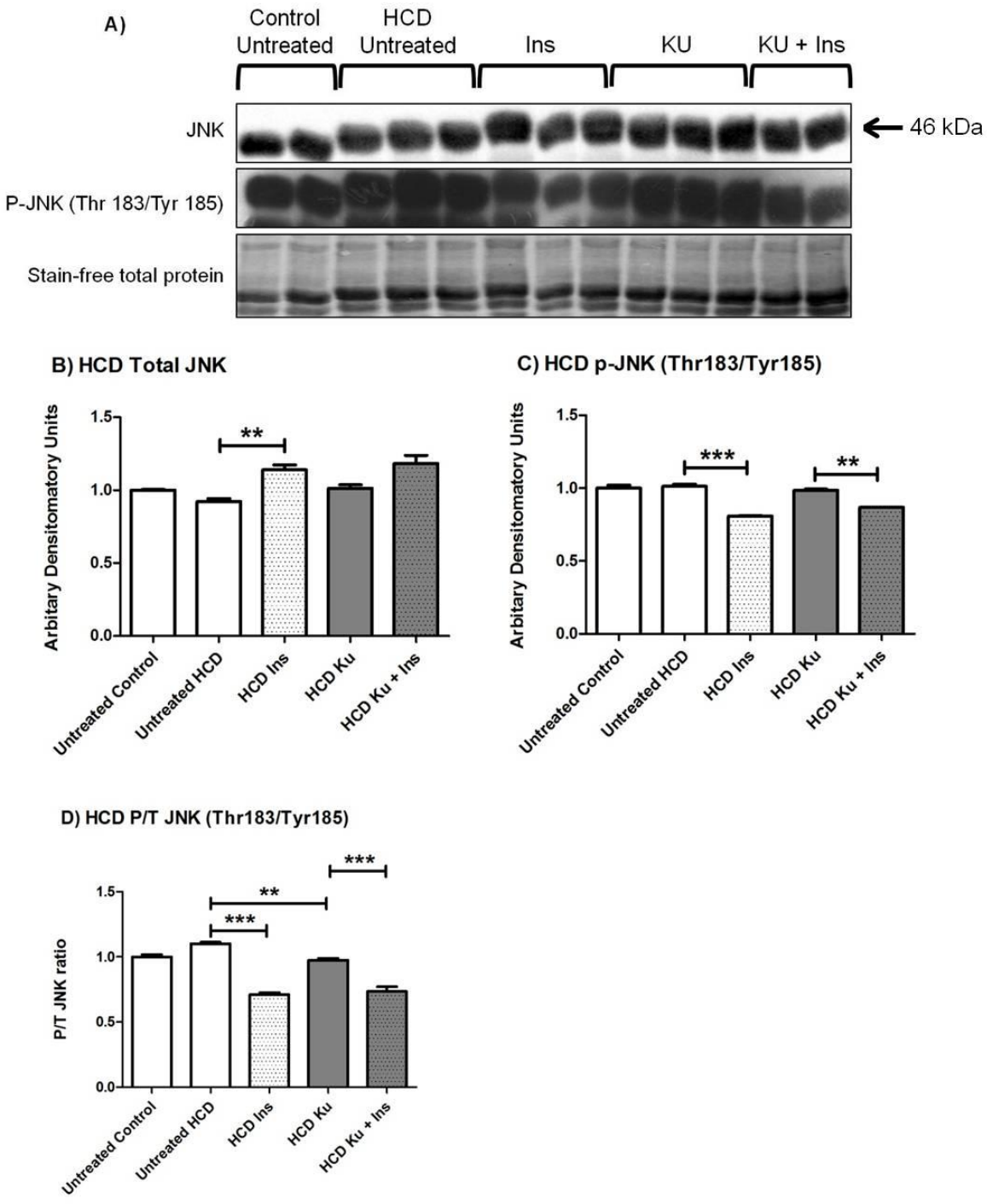

Figure 4.15: JNK expression and phosphorylation levels in HCD hearts normalised to untreated control hearts, following treatment with insulin, KU-60019 and a combination of insulin and KU-60019. A) Western blot chemiluminescent results of JNK and p-JNK and stain-free total protein stain of the membrane. B) Bar graph depicting analysed results for total JNK. C) Bar graph depicting analysed results for p-JNK (Thr 183/ Tyr 185). D) Bar graph depicting phospho to total ratio of JNK. ** $p < 0.005$; *** $p < 0.0001$ (n=2-3 per group).

IRS-1

Insulin treatment significantly increased both the expression (Untreated 1.00 ± 0.16; Ins 2.16 ± 0.08; $p < 0.0001$) and phosphorylation of IRS-1 (serine 307) (Untreated 1.00 ± 0.11; Ins 14.52 ± 0.75; $p < 0.0001$) compared to the untreated group in control hearts. The P/T ratio was also significantly higher in insulin treated hearts compared to untreated control hearts (Untreated 1.01 ± 0.04; Ins 6.48 ± 0.19; $p < 0.005$). Co-treatment with KU-60019 significantly decreased the effect of insulin on total (Ins 2.16 ± 0.08; KU + Ins 1.08 ± 0.04; $p < 0.0001$) and phospho-IRS-1 (Ins 14.52 ± 0.75; KU + Ins 0.07 ± 0.01; $p < 0.0001$) levels and it also resulted in a decreased P/T ratio compared to the group treated with insulin only (Ins 6.48 ± 0.19 ± 0.07 ± 0.02; $p < 0.0001$). Compared to the untreated group, KU-60019 treatment decreased total IRS-1 levels in control hearts (Untreated 1.00 ± 0.16; KU 0.43 ± 0.04; $p < 0.05$), however the p-IRS-1 and P/T IRS-1 ratio remained unchanged by KU-60019 treatment in control hearts. Co-treatment with insulin and KU-60019 resulted in significantly higher total IRS-1 levels compared to the KU-60019 only group (KU 0.43 ± 0.04; KU + Ins 1.08 ± 0.04; $p < 0.005$), which translated into a significantly smaller P/T IRS-1 ratio in the co-treatment group compared to the KU-60019 only group (KU 2.58 ± 0.52; KU + Ins 0.07 ± 0.02; $p < 0.05$). The results of IRS-1 Western blot analysis in control hearts are indicated in Figure 4.16.

Hearts from animals that were on the HCD had significantly higher IRS-1 expression levels compared to hearts from animals on the control diet (Control untreated 1; HCD untreated 4.96 ± 0.08; $p < 0.05$) HCD hearts that were co-treated with KU-60019 and insulin had significantly less total IRS-1 expression compared to hearts that were treated only with insulin (Ins 6.60 ± 1.26; KU + Ins 0.31 ± 0.06; $p < 0.005$). The results of IRS-1 Western blot analysis in HCD hearts are indicated in Figure 4.17.

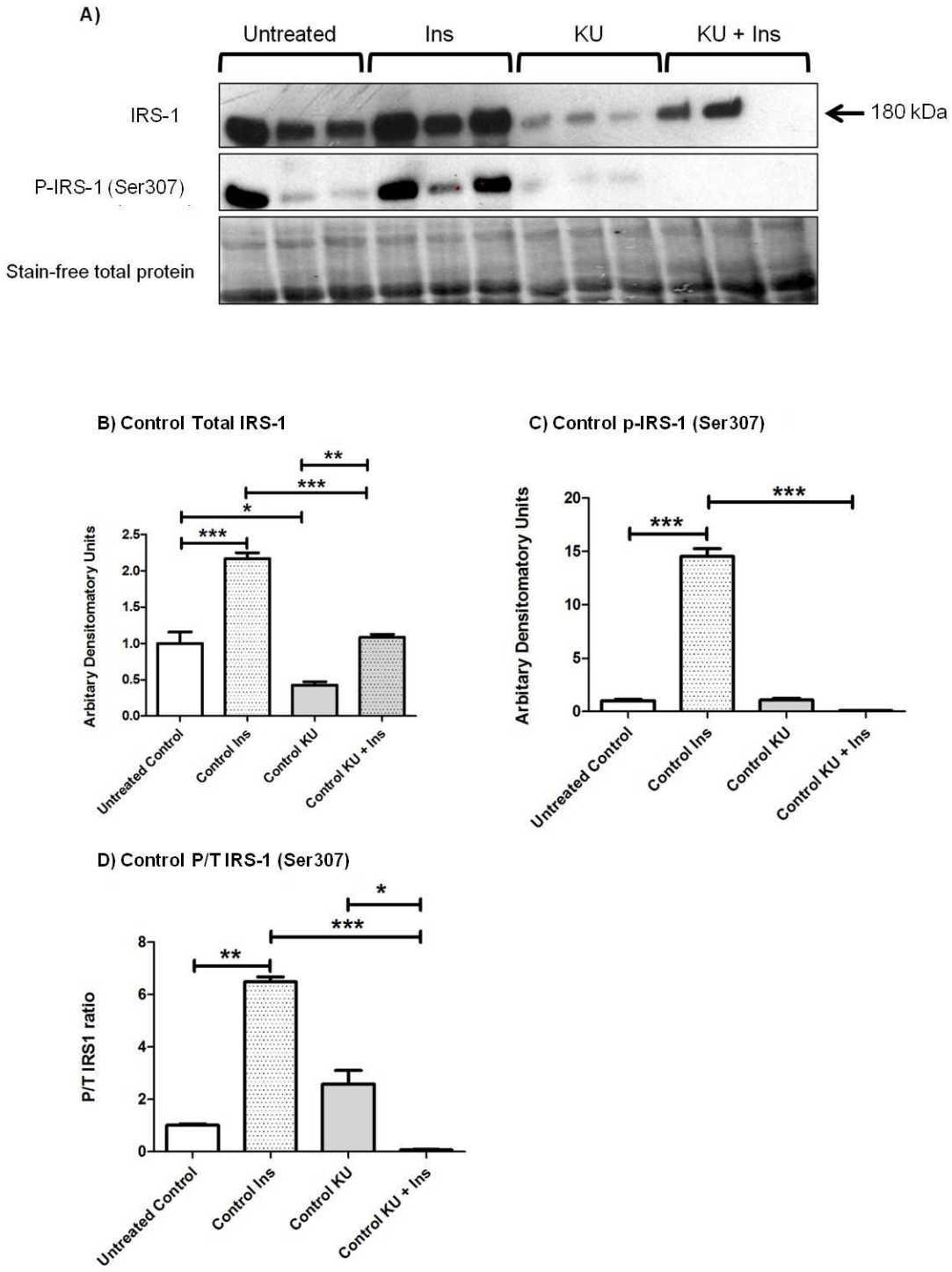

Figure 4.16: IRS-1 expression and phosphorylation levels in control hearts following treatment with insulin, KU-60019 and a combination of insulin and KU-60019. A) Western blot chemiluminescent results of IRS-1 and p-IRS-1 and stain-free total protein stain of the membrane. B) Bar graph depicting analysed results for total IRS-1. C) Bar graph depicting analysed results for p-IRS-1 (Ser307). D) Bar graph depicting phospho to total ratio of IRS-1. * $p < 0.05$; ** $p < 0.005$; *** $p < 0.0001$ (n=3 per group).

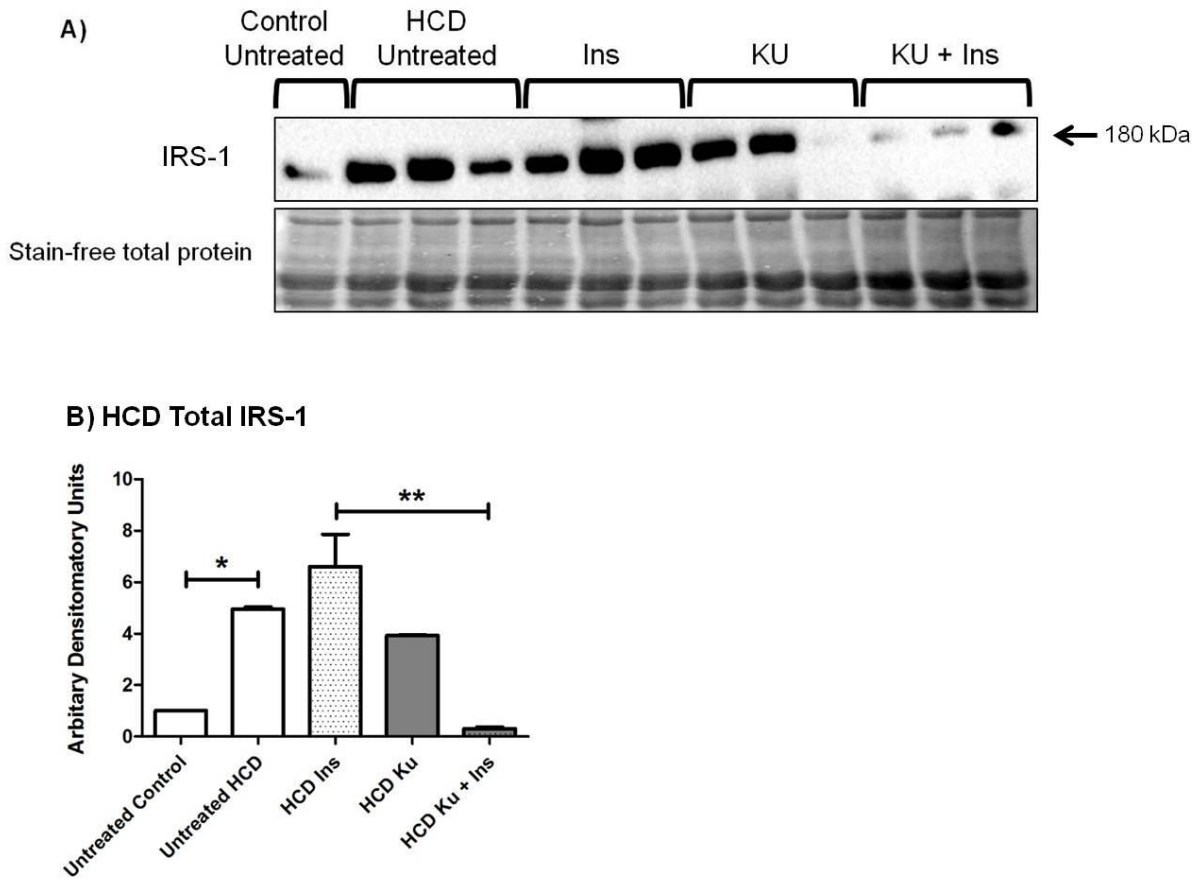

Figure 4.17: IRS-1 expression levels in HCD hearts following treatment with insulin, KU-60019 and a combination of insulin and KU-60019. A) Western blot chemiluminescent results of IRS-1 and stain-free total protein stain of the membrane. B) Bar graph depicting analysed results for total IRS-1 * $p < 0.05$; ** $p < 0.005$ (n=3 per group).

P85 subunit of PI3K

In control hearts, insulin treatment resulted in decreased total PI3K expression levels compared to the untreated group (Untreated 1.00 ± 0.01; Ins 0.81 ± 0.003; $p < 0.0001$). Surprisingly, the insulin group also had a significantly lower P/T PI3K ratio compared to the untreated control group (Untreated 1.00 ± 0.03; Ins 0.75 ± 0.02; $p < 0.05$). When KU-60019 was administered in combination with insulin, total PI3K levels were significantly reduced compared to the insulin only group (Ins 0.81 ± 0.003; KU + Ins 0.62 ± 0.003; $p < 0.0001$). The same effect was seen on the phosphorylation levels of PI3K (Ins 0.83 ± 0.005; KU + Ins 0.37 ± 0.05; $p < 0.005$). However,

the P/T PI3K ratio was unchanged in the KU-60019 + insulin group compared to the insulin only group. Compared to the untreated group, KU-60019 treatment reduced both the total PI3K (Untreated 1.00 ± 0.01; KU 0.75 ± 0.002; $p < 0.0001$) and the phosphorylation of PI3K (Untreated 1.00 ± 0.04; KU 0.69 ± 0.01; $p < 0.005$). The P/T PI3K ratio, however, remained unchanged in the KU-60019 group compared to the untreated group. Compared to the KU-60019 only group, the KU-60019 + insulin group had significantly lower total PI3K (KU 0.75 ± 0.002; KU + Ins 0.62 ± 0.003; $p < 0.005$), lower phosphorylated PI3K (KU 0.69 ± 0.01; KU + Ins 0.37 ± 0.05; $p < 0.005$) and a lower P/T PI3K ratio (KU 0.93 ± 0.01; KU + Ins 0.60 ± 0.08; $p < 0.05$). The results of PI3K Western blot analysis in control hearts are indicated in Figure 4.18.

In HCD hearts, none of the treatment groups had a significant effect on the PI3K total expression levels or on the phosphorylation levels of PI3K. There were, however, significant effects on the P/T PI3K ratio. Insulin treatment significantly reduced the P/T PI3K ratio compared to the untreated group (Untreated 1.72 ± 0.08; Ins 1.05 ± 0.04; $p < 0.0001$). Treatment with KU-60019 also reduced the P/T PI3K ratio compared to the untreated group (Untreated 1.72 ± 0.08; KU 1.22 ± 0.07; $p < 0.005$). Co-treatment with both KU-60019 and insulin resulted in a significantly higher P/T PI3K ratio than when treated with insulin alone (Ins 1.05 ± 0.04; KU + Ins 1.77 ± 0.02; $p < 0.0001$) or with KU-60019 alone (KU 1.22 ± 0.07; KU + Ins 1.77 ± 0.02; $p < 0.0001$). The results of PI3K Western blot analysis in HCD hearts are indicated in Figure 4.19.

The HCD hearts had a significantly higher P/T PI3K ratio compared to the control hearts (Untreated control 1.00 ± 0.03; Untreated HCD 1.72 ± 0.08; $p < 0.0001$) despite the total PI3K and phospho-PI3K levels being unchanged between the two groups (Figure 4.19 D).

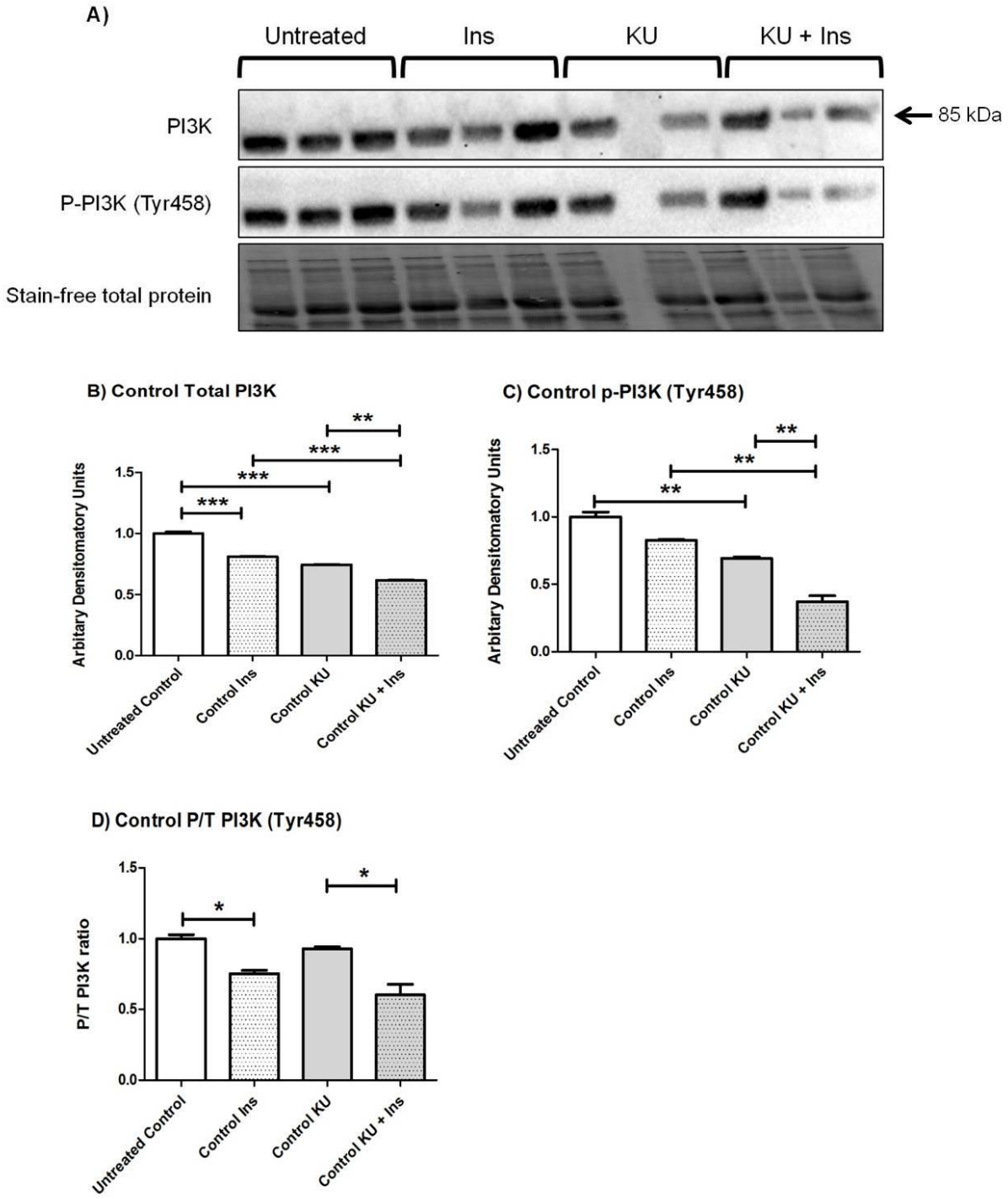

Figure 4.18: PI3K p85 expression and phosphorylation levels in control hearts following treatment with insulin, KU-60019 and a combination of insulin and KU-60019. A) Western blot chemiluminescent results of PI3K and p-PI3K and stain-free total protein stain of the membrane. B) Bar graph depicting analysed results for total PI3K. C) Bar graph depicting analysed results for p-PI3K (Tyr458). D) Bar graph depicting phospho to total ratio of PI3K. * $p < 0.05$; ** $p < 0.005$; *** $p < 0.0001$ (n=2-3 per group).

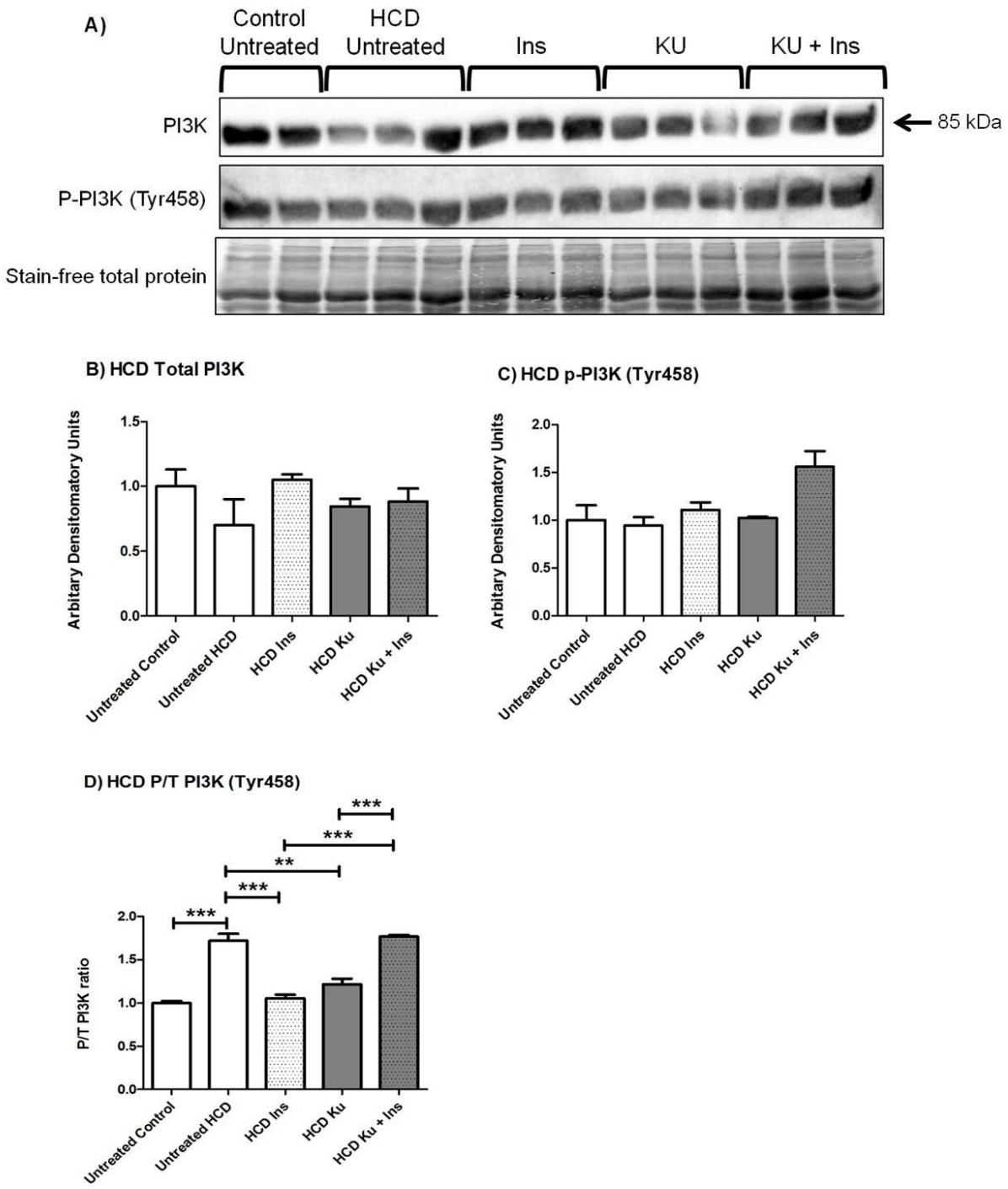

Figure 4.19: PI3K p85 expression and phosphorylation levels in control hearts following treatment with insulin, KU-60019 and a combination of insulin and KU-60019. A) Western blot chemiluminescent results of PI3K and p-PI3K and stain-free total protein stain of the membrane. B) Bar graph depicting analysed results for total PI3K. C) Bar graph depicting analysed results for p-PI3K (Tyr458). D) Bar graph depicting phospho to total ratio of PI3K. ** $p < 0.005$; *** $p < 0.0001$ (n=2-3 per group).

PTEN

The phosphatase PTEN acts as a negative regulator of insulin signalling by dephosphorylating PIP_3. Total PTEN levels were significantly lower in control hearts treated with KU-60019 compared to the untreated control group (Untreated 1.00 ± 0.06; KU 0.55 ± 0.04; $p < 0.05$). When co-treated with insulin and KU-60019, insulin was able to abolish the effect of KU-60019 and restore total PTEN levels to untreated levels (KU 0.55 ± 0.04; KU + Ins 1.03 ± 0.14; $p < 0.05$). Treatment with KU-60019 also caused PTEN phosphorylation (Ser380/Thr382/Thr383) to decrease significantly compared to the untreated group (Untreated 1.00 ± 0.04; KU 0.38 ± 0.04; $p < 0.0001$) and this resulted in the P/T PTEN ratio to be lower in the KU-60019 group compared to the untreated group (Untreated 1.01 ± 0.09; KU 0.69 ± 0.06; $p < 0.05$). Insulin was unable to block the effect of KU-60019 on PTEN phosphorylation as the KU-60019 and insulin group had significantly lower phospho-PTEN levels compared to the insulin only group (Ins 0.87 ± 0.003; KU + Ins 0.51 ± 0.01; $p < 0.0001$). The results of PTEN Western blot analysis in control hearts are indicated in Figure 4.20.

Compared to the untreated control hearts, untreated HCD hearts had significantly lower total PTEN expression levels (Untreated control 1.00; Untreated HCD 0.49 ± 0.005; $p < 0.0001$) as well as lower PTEN phosphorylation levels (Untreated control 1.00; Untreated HCD 0.50 ± 0.09; $p < 0.005$). Total PTEN levels were unaffected by the treatment groups in HCD hearts. Insulin treatment caused PTEN phosphorylation (Ser380/Thr382/Thr383) to be significantly lower than the untreated group (Untreated 0.50 ± 0.09; Ins 0.04 ± 0.02; $p < 0.005$) and this translated into a significantly lower P/T PTEN ratio in the insulin treated HCD group (Untreated 1.20 ± 0.07; Ins 0.06 ± 0.03; $p < 0.001$). KU-60019 treatment had no effect on the total PTEN or the PTEN phosphorylation levels, but the P/T PTEN ratio was significantly lower in the KU-60019 group compared to the untreated group (Untreated 1.20 ± 0.07; KU 0.49 ± 0.06; $p < 0.0001$). The results of PTEN Western blot analysis in HCD hearts are indicated in Figure 4.21.

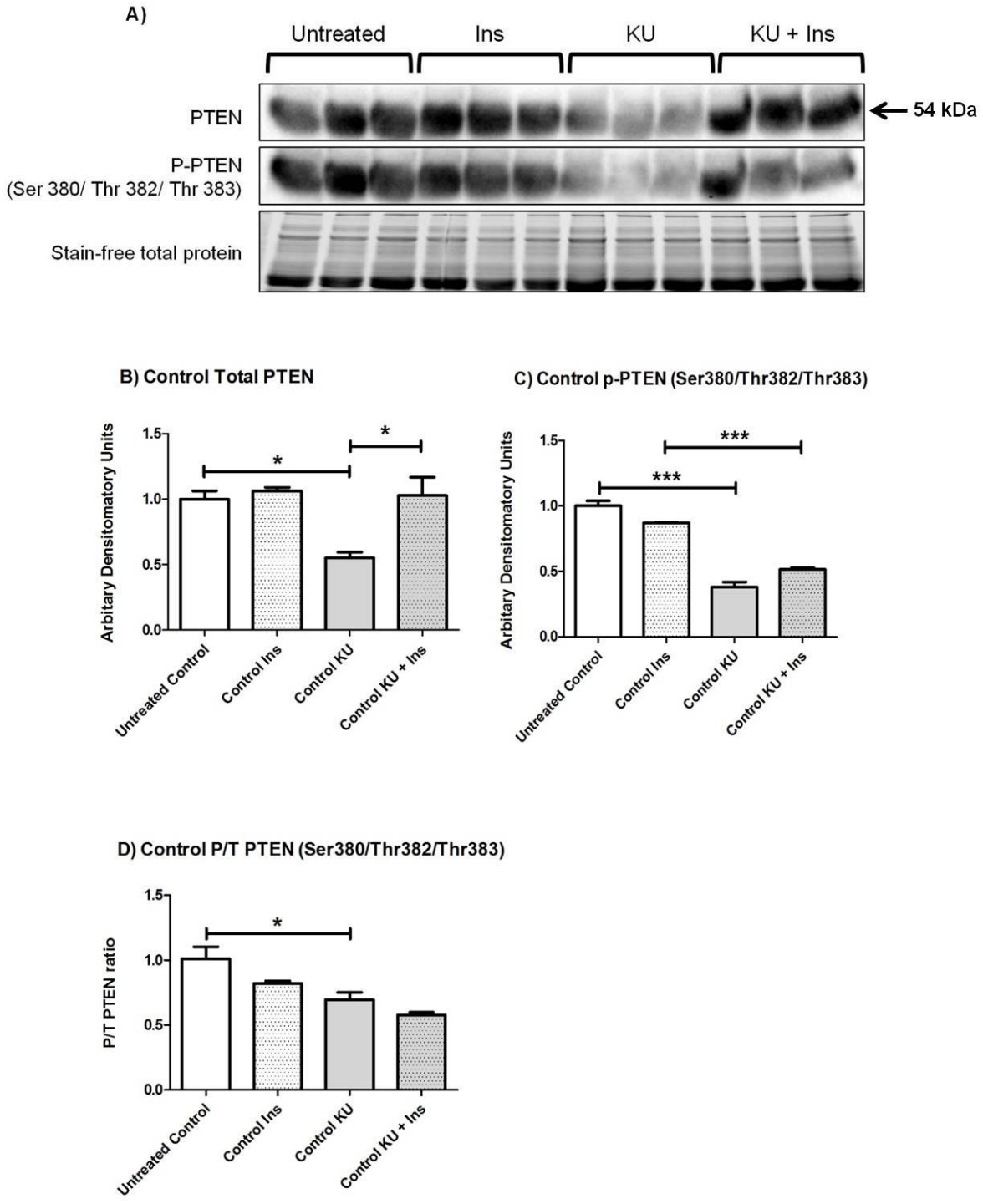

Figure 4.20: PTEN expression and phosphorylation levels in control hearts following treatment with insulin, KU-60019 and a combination of insulin and KU-60019. A) Western blot chemiluminescent results of PTEN and p-PTEN and stain-free total protein stain of the membrane. B) Bar graph depicting analysed results for total PTEN. C) Bar graph depicting analysed results for p-PTEN (Ser380/Thr382/Thr383). D) Bar graph depicting phospho to total ratio of PTEN. * $p < 0.05$; *** $p < 0.0001$ (n=3 per group).

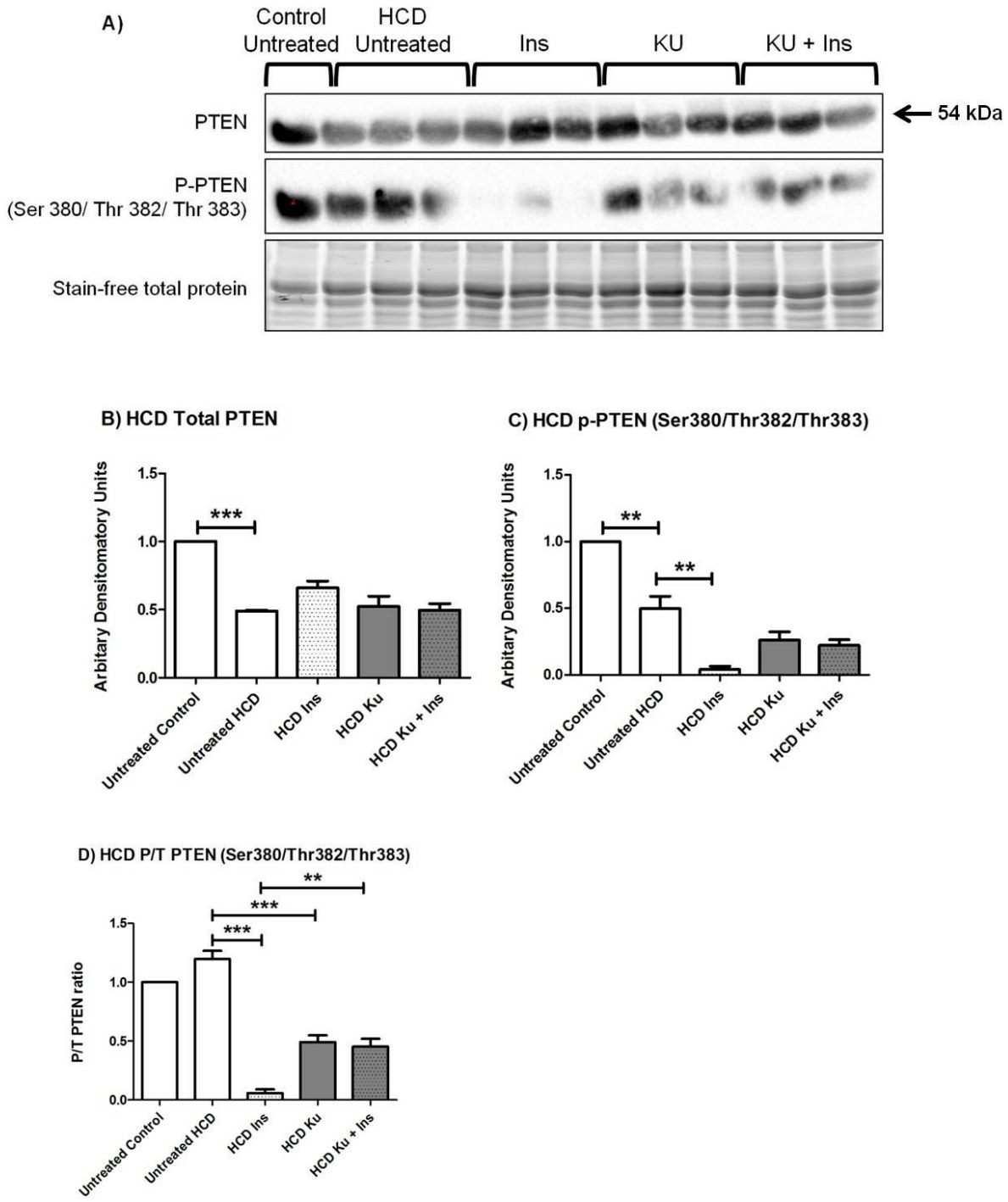

Figure 4.21: PTEN expression and phosphorylation levels in HCD hearts following treatment with insulin, KU-60019 and a combination of insulin and KU-60019. A) Western blot chemiluminescent results of PTEN and p-PTEN and stain-free total protein stain of the membrane. B) Bar graph depicting analysed results for total PTEN. C) Bar graph depicting analysed results for p-PTEN (Ser380/Thr382/Thr383). D) Bar graph depicting phospho to total ratio of PTEN. ** $p < 0.005$; *** $p < 0.0001$ (n=3 per group).

PKB/Akt

PKB/Akt plays a central role in the insulin signalling network. As expected, insulin stimulation resulted in a significant increase in total PKB/Akt expression (Untreated 1.00 ± 0.001; Ins 1.36 ± 0.04; $p < 0.005$), PKB/Akt phosphorylation of Ser473 (Untreated 1.00 ± 0.21; Ins 2.85 ± 0.39; $p < 0.005$) and a significantly higher P/T ratio (Untreated 0.79 ± 0.004; Ins 2.10 ± 0.25; $p < 0.005$) compared to the untreated group in hearts from animals that were on the control diet. Treatment with KU-60019 resulted in an increase in total PKB/Akt compared to the untreated group (Untreated 1.00 ± 0.001; KU 1.34 ± 0.05; $p < 0.05$), but PKB/Akt phosphorylation and the P/T ratio remained unchanged in response to KU-60019. Treatment with a combination of KU-60019 and insulin resulted in a decrease in PKB/Akt expression compared to treatment with only insulin (Ins 1.36 ± 0.04; KU + Ins 0.92 ± 0.05; $p < 0.005$) or with only KU-60019 (KU 1.34 ± 0.05; KU + Ins 0.92 ± 0.05; $p < 0.005$). It also caused increased phosphorylation of PKB/Akt compared to treatment with only KU-60019 (KU 1.38 ± 0.01; KU + Ins 2.77 ± 0.03; $p < 0.05$), resulting in an increased P/T ratio in the KU-60019 + insulin group compared to the KU-60019 only group (KU 1.18 ± 0.12; KU + Ins 3.02 ± 0.12; $p < 0.0001$). The results of PKB/Akt Western blot analysis in control hearts are indicated in Figure 4.22.

As in the control hearts, insulin treatment caused an increase in total PKB/Akt (Untreated HCD 1.15 ± 0.04; Ins 1.57 ± 0.03; $p < 0.005$) in the HCD hearts. Interestingly, KU-60019 treatment also increased PKB/Akt expression (Untreated 1.15 ± 0.04; KU 1.64 ± 0.02; $p < 0.005$) compared to untreated HCD hearts. No differences were observed in PKB/Akt phosphorylation levels or in the P/T PKB/Akt ratio. The results of PKB/Akt Western blot analysis in HCD hearts are indicated in Figure 4.23.

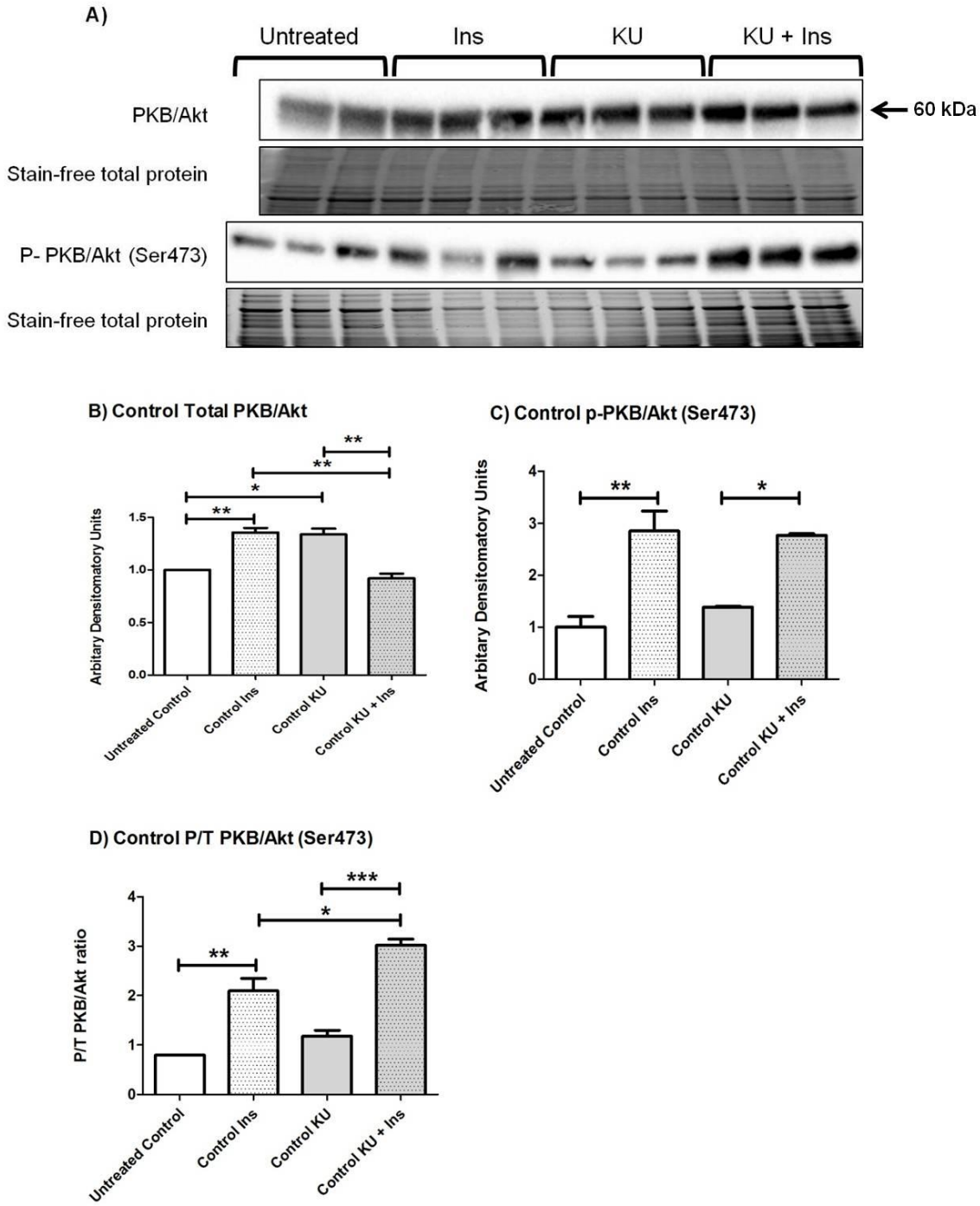

Figure 4.22: PKB/Akt expression and phosphorylation levels in control hearts following treatment with insulin, KU-60019 and a combination of insulin and KU-60019. A) Western blot chemiluminescent results of PKB/Akt and p-PKB/Akt and stain-free total protein stain of the membrane. B) Bar graph depicting analysed results for total PKB/Akt. C) Bar graph depicting analysed results for p-PKB/Akt (Ser473). D) Bar graph depicting phospho to total ratio of PKB/Akt. * $p < 0.05$; ** $p < 0.005$; *** $p < 0.0001$ (n=2-3 per group).

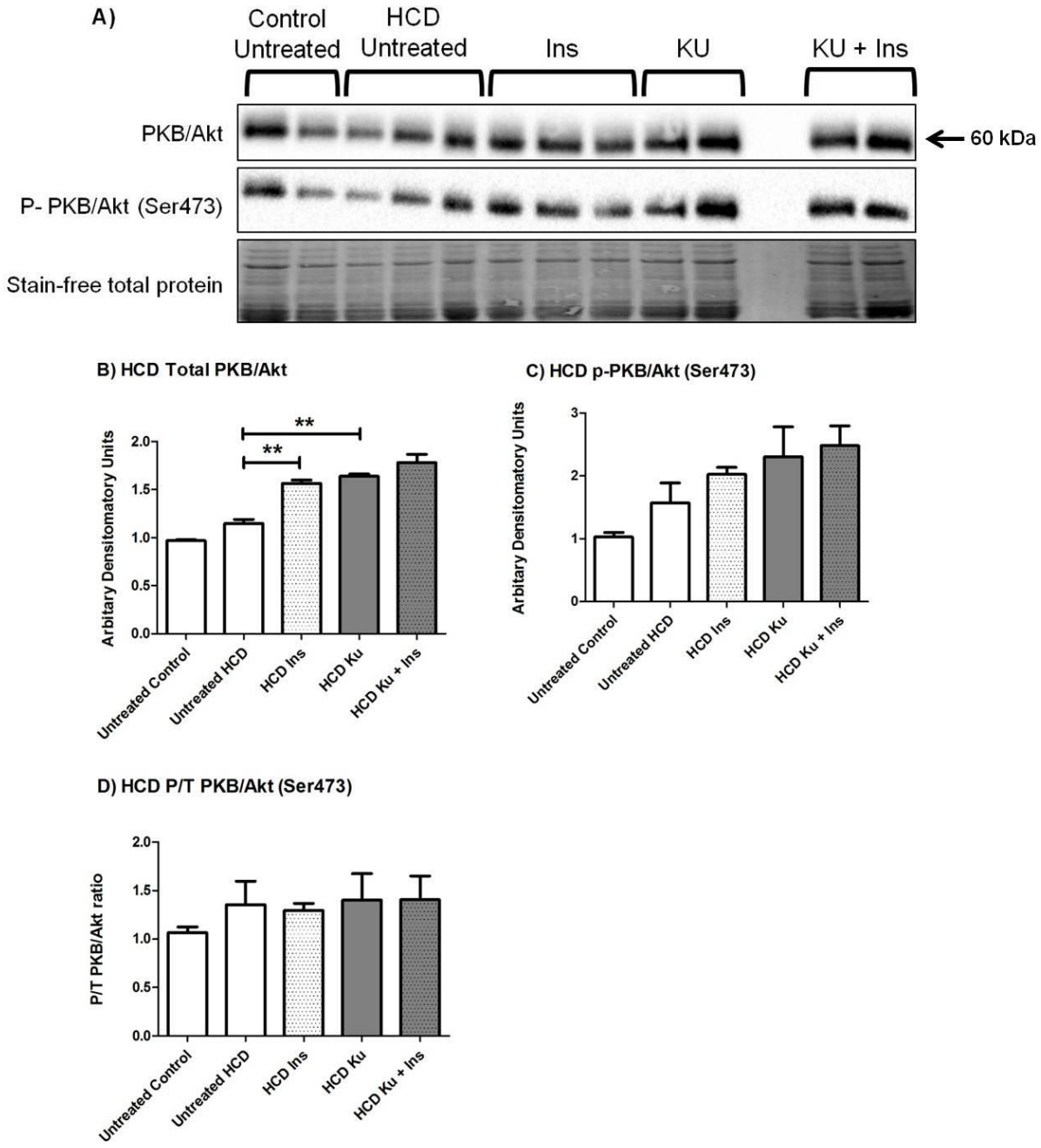

Figure 4.23: PKB/Akt expression and phosphorylation levels in HCD hearts following treatment with insulin, KU-60019 and a combination of insulin and KU-60019. A) Western blot chemiluminescent results of PKB/Akt and p-PKB/Akt and stain-free total protein stain of the membrane. B) Bar graph depicting analysed results for total PKB/Akt. C) Bar graph depicting analysed results for p-PKB/Akt (Ser473). D) Bar graph depicting phospho to total ratio of PKB/Akt. * $p < 0.05$; ** $p < 0.005$; *** $p < 0.0001$ (n=2-3 per group).

mTOR

None of the treatment groups affected total mTOR levels in control hearts. Co-treatment with KU-60019 and insulin resulted in increased phosphorylation of mTOR (Ser2448) compared to treatment with insulin alone (Ins 1.00 ± 0.004; KU + Ins 1.42 ± 0.01; $p < 0.0001$) or compared to treatment with KU-60019 alone (KU 1.10 ± 0.004; KU + Ins 1.42 ± 0.01; $p < 0.0001$). There were no differences in P/T mTOR ratios between the groups. The results of mTOR Western blot analysis in control hearts are indicated in Figure 4.24.

The HCD hearts had significantly more basal total mTOR (Untreated control 1.00 ± 0.01; Untreated HCD 1.80 ± 0.08; $p < 0.0001$) and phosphorylated mTOR (Untreated control 1.00 ± 0.009; Untreated HCD 1.66 ± 0.004; $p < 0.05$) compared to the untreated control hearts. There was, however, no difference in the P/T ratio between the untreated control and HCD groups. Insulin treatment had no effect on total mTOR levels in HCD hearts, but mTOR phosphorylation was significantly higher in insulin treated hearts compared to untreated hearts (Untreated 1.66 ± 0.004; Ins 2.62 ± 0.20; $p < 0.0001$). This resulted in an increased P/T ratio in insulin treated HCD hearts (Untreated 0.93 ± 0.04; Ins 1.29 ± 0.09; $p < 0.005$). Compared to treatment with insulin only, treatment with a combination of insulin and KU-60019 caused an increase in total mTOR (Ins 2.03 ± 0.07; KU + Ins 2.31 ± 0.04; $p < 0.05$), a decrease in mTOR phosphorylation (Ins 2.62 ± 0.20; KU + Ins 2.02 ± 0.02; $p < 0.05$) and a resultant decrease in P/T ratio (Ins 1.29 ± 0.09; KU + Ins 0.88 ± 0.02; $p < 0.005$). Co-treatment with KU-60019 and insulin also significantly increased total mTOR levels compared to treatment with only KU-60019 (KU 1.94 ± 0.008; KU + Ins 2.31 ± 0.04; $p < 0.005$). There was no difference in mTOR phosphorylation or the P/T ratio between the co-treatment and KU-60019 only groups. The results of mTOR Western blot analysis in HCD hearts are indicated in Figure 4.25.

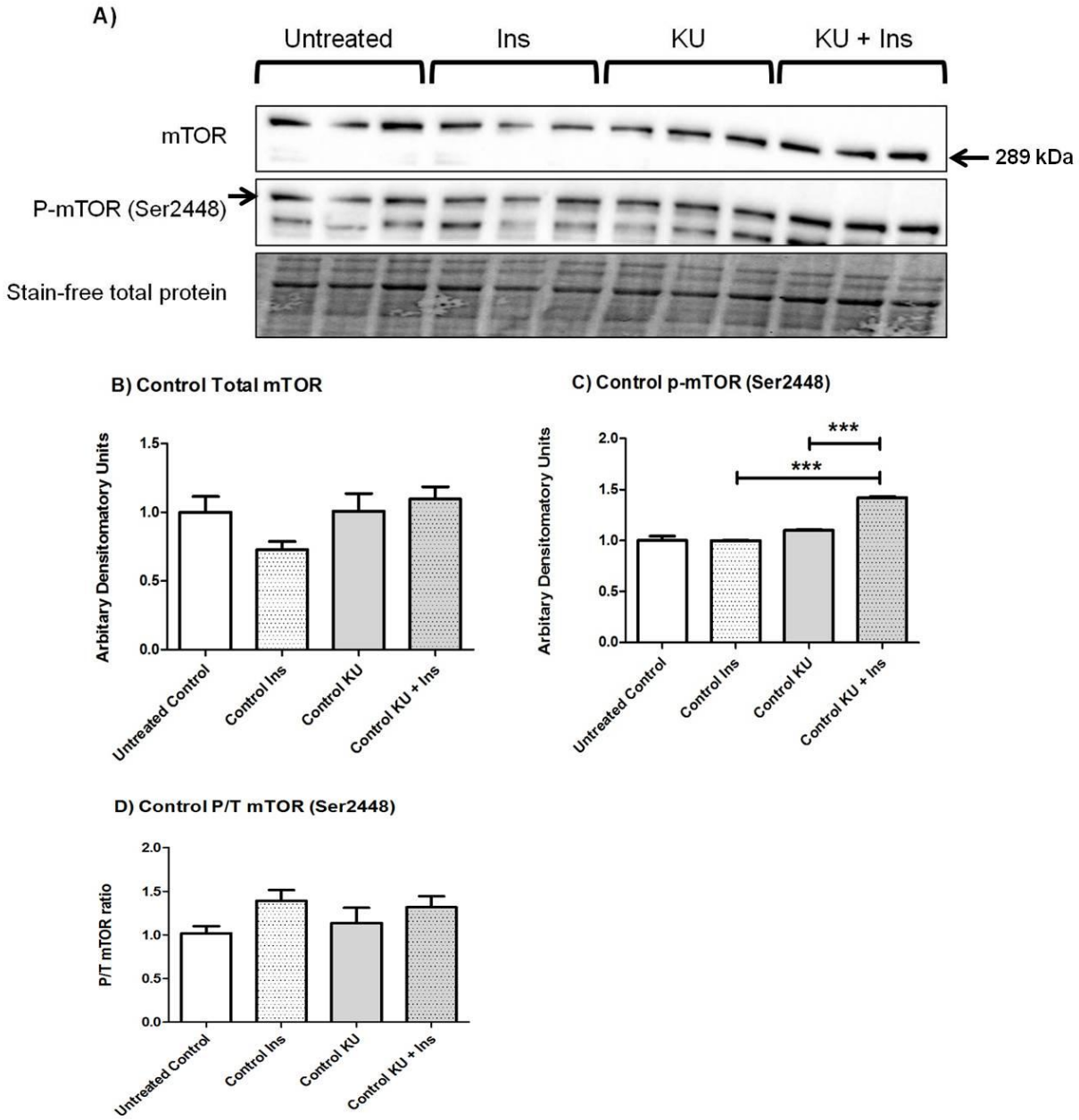

Figure 4.24: mTOR expression and phosphorylation levels in control hearts following treatment with insulin, KU-60019 and a combination of insulin and KU-60019. A) Western blot chemiluminescent results of mTOR and p-mTOR and stain-free total protein stain of the membrane. B) Bar graph depicting analysed results for total mTOR. C) Bar graph depicting analysed results for p-mTOR (Ser2448). D) Bar graph depicting phospho to total ratio of mTOR. *** $p < 0.0001$ (n=3 per group).

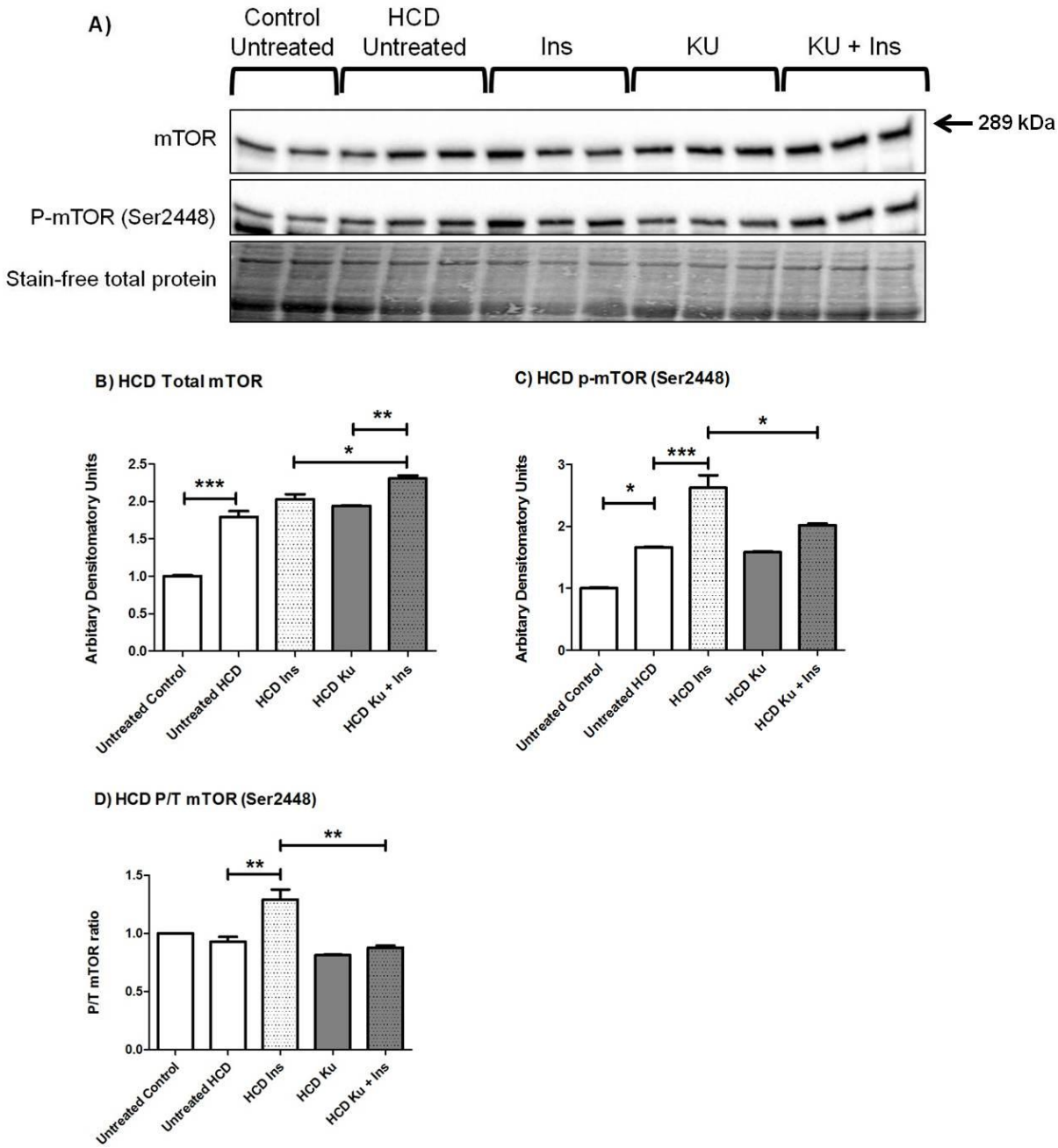

Figure 4.25: mTOR expression and phosphorylation levels in HCD hearts following treatment with insulin, KU-60019 and a combination of insulin and KU-60019. A) Western blot chemiluminescent results of mTOR and p-mTOR and stain-free total protein stain of the membrane. B) Bar graph depicting analysed results for total mTOR. C) Bar graph depicting analysed results for p-mTOR (Ser2448). D) Bar graph depicting phospho to total ratio of mTOR. * $p < 0.05$; ** $p < 0.005$; *** $p < 0.0001$ (n=2-3 per group).

GSK-3β

In response to insulin treatment, total GSK-3β expression levels were decreased compared to the untreated group in control hearts (Untreated 1.00 ± 0.01; Ins 0.66 ± 0.04; $p < 0.0001$). Insulin treatment also decreased GSK-3β phosphorylation (Ser9) compared to the untreated group (Untreated 1.00 ± 0.03; Ins 0.70 ± 0.04; $p < 0.005$), but the P/T ratio remained unchanged by insulin treatment. Treatment with KU-60019 significantly decreased both GSK-3β expression (Untreated 1.00 ± 0.01; KU 0.81 ± 0.01; $p < 0.05$) and phosphorylation (Untreated 1.00 ± 0.03; KU 0.67 ± 0.03; $p < 0.005$), leading to a decreased P/T ratio compared to the untreated group (Untreated 1.00 ± 0.02; KU 0.77 ± 0.06; $p < 0.05$). The results of GSK-3β Western blot analysis in control hearts are indicated in Figure 4.26.

There was no difference in total GSK-3β, GSK-3β phosphorylation or the P/T ratio of GSK-3β between untreated control hearts and untreated HCD hearts. As was seen in control hearts, treatment with KU-60019 significantly decreased total GSK-3β levels (Untreated 0.90 ± 0.07; KU 0.60 ± 0.03; $p < 0.05$) as well as GSK-3β phosphorylation levels (Untreated 1.07 ± 0.08; KU 0.53 ± 0.01; $p < 0.05$) in HCD hearts. The P/T ratio, however, remained unchanged by KU-60019 treatment when compared to the untreated group. The results of GSK-3β Western blot analysis in HCD hearts are indicated in Figure 4.27.

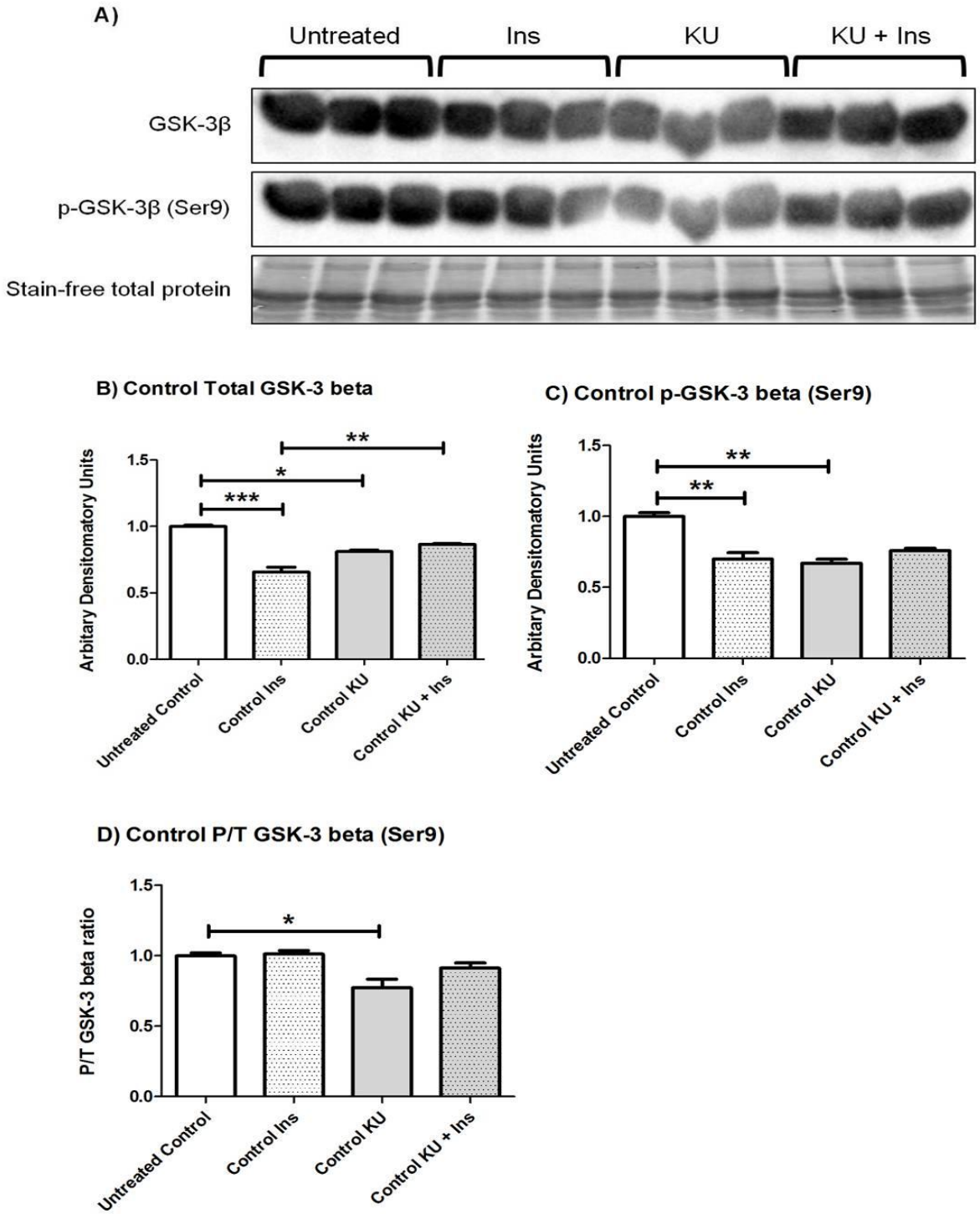

Figure 4.26: GSK-3β expression and phosphorylation levels in control hearts following treatment with insulin, KU-60019 and a combination of insulin and KU-60019. A) Western blot chemiluminescent results of GSK-3β and p-GSK-3β and stain-free total protein stain of the membrane. B) Bar graph depicting analysed results for total GSK-3β. C) Bar graph depicting analysed results for p-GSK-3β (Ser9). D) Bar graph depicting phospho to total ratio of GSK-3β. * $p < 0.05$; ** $p < 0.005$; *** $p < 0.0001$ (n=3 per group).

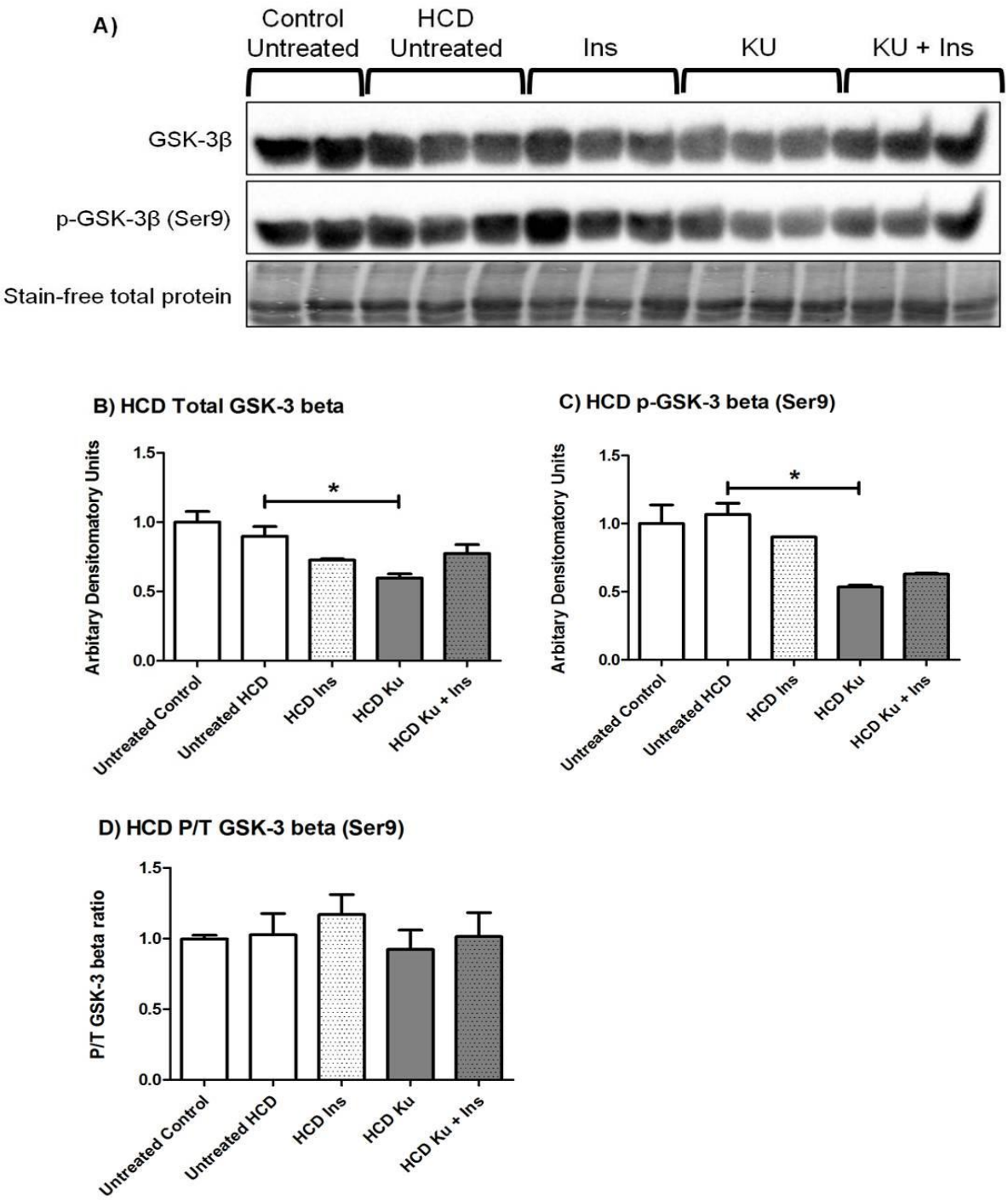

Figure 4.27: GSK-3β expression and phosphorylation levels in HCD hearts following treatment with insulin, KU-60019 and a combination of insulin and KU-60019. A) Western blot chemiluminescent results of GSK-3β and p-GSK-3β and stain-free total protein stain of the membrane. B) Bar graph depicting analysed results for total GSK-3β. C) Bar graph depicting analysed results for p-GSK-3β (Ser9). D) Bar graph depicting phospho to total ratio of GSK-3β. * $p < 0.05$ (n=2-3 per group).

AS160

Insulin treatment caused an increase in total AS160 in control hearts compared to untreated control hearts (Untreated 1.00 ± 0.13; Ins 1.62 ± 0.03; $p < 0.005$). An increase in AS160 phosphorylation was also seen in response to insulin (Untreated 1.00 ± 0.18; Ins 3.07 ± 0.32; $p < 0.05$). There was no difference in P/T ratio between the untreated and insulin groups. Insulin also caused an increase in total AS160 when co-treated with KU-60019 (KU 1.17 ± 0.08; KU + Ins 1.93 ± 0.08; $p < 0.005$). Co-treatment with KU-60019 and insulin caused greater phosphorylation of AS160 than what was observed in samples treated with only insulin (Ins 3.07 ± 0.32; KU + Ins 6.73 ± 0.46; $p < 0.005$) or with KU-60019 treatment alone (KU 3.00 ± 0.20; KU + Ins 6.73 ± 0.46; $p < 0.005$). An increased P/T ratio was observed in samples treated with KU-60019 compared to untreated samples (Untreated 0.99 ± 0.05; KU 2.43 ± 0.37; $p < 0.05$). Co-treatment with KU-60019 and insulin also resulted in a significantly bigger P/T AS160 ratio compared to treatment with insulin alone (Ins 1.90 ± 0.21; KU + Ins 3.48 ± 0.11; $p < 0.005$). The results of AS160 Western blot analysis in control hearts are indicated in Figure 4.28.

Total and phospho-AS160 levels were unaffected by the HCD compared to the control diet. None of the treatment groups had a significant effect on total AS160 levels. Treatment with KU-60019 resulted in a significant decrease in AS160 phosphorylation compared to the untreated group (Untreated 1.03 ± 0.17; KU 0.47 ± 0.01; $p < 0.05$), however, the P/T ratio did not differ between the untreated and KU-60019 treated groups. The results of AS160 Western blot analysis in HCD hearts are indicated in Figure 4.29.

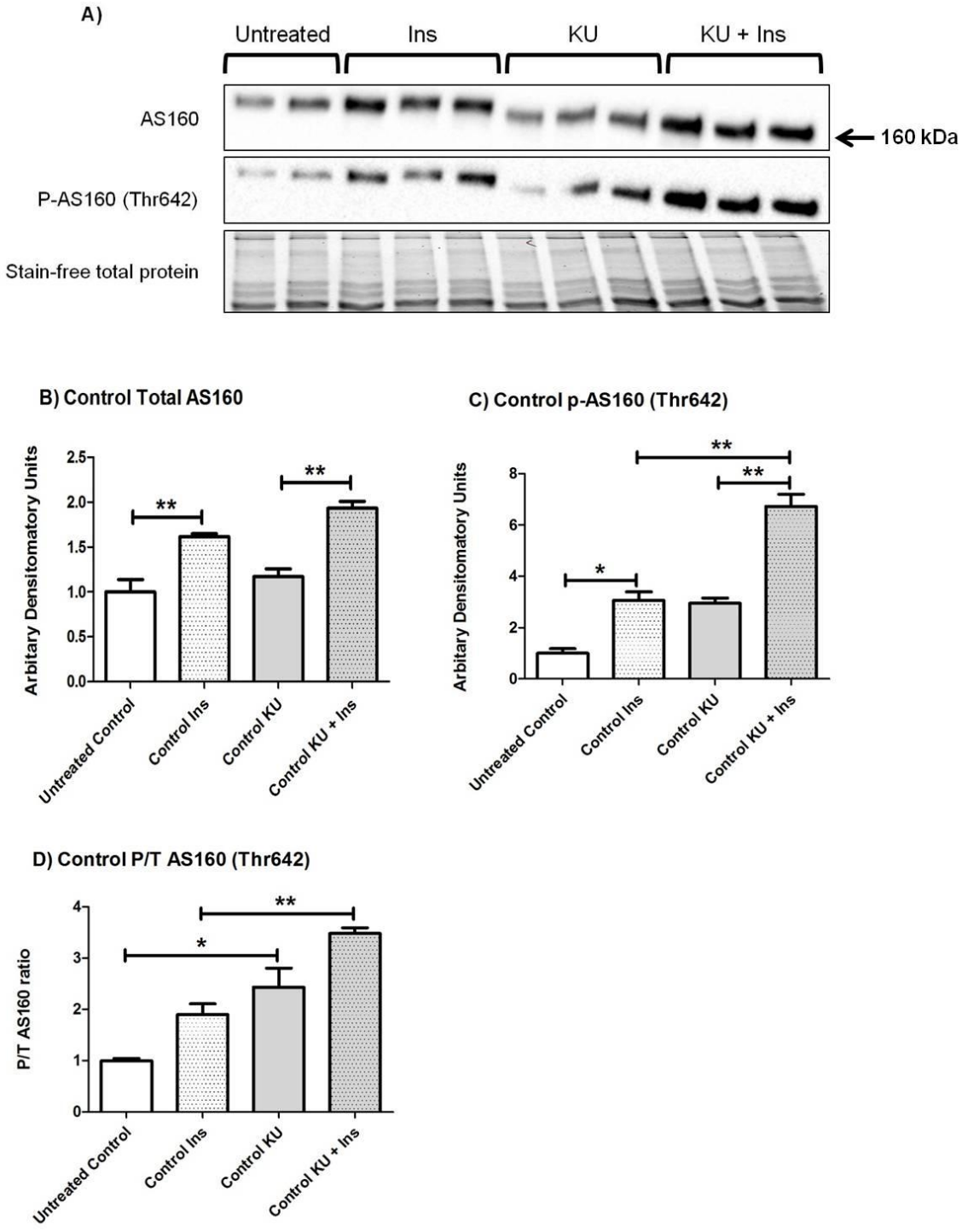

Figure 4.28: AS160 expression and phosphorylation levels in control hearts following treatment with insulin, KU-60019 and a combination of insulin and KU-60019. A) Western blot chemiluminescent results of AS160 and p-AS160 and stain-free total protein stain of the membrane. B) Bar graph depicting analysed results for total AS160. C) Bar graph depicting analysed results for p-AS160 (Thr642). D) Bar graph depicting phospho to total ratio of AS160. * $p < 0.05$; ** $p < 0.005$ (n=2-3 per group).

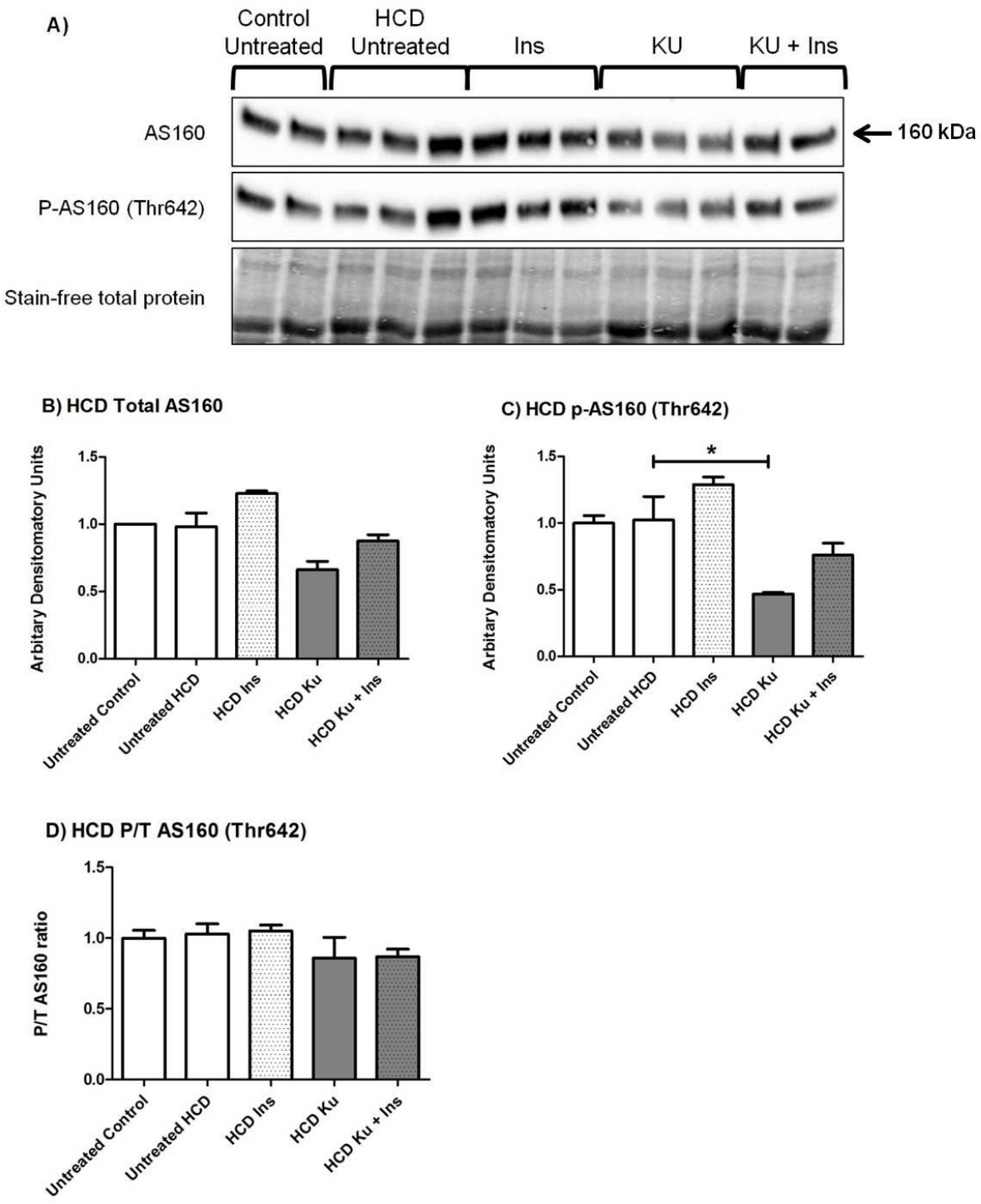

Figure 4.29: AS160 expression and phosphorylation levels in HCD hearts following treatment with insulin, KU-60019 and a combination of insulin and KU-60019. A) Western blot chemiluminescent results of AS160 and p-AS160 and stain-free total protein stain of the membrane. B) Bar graph depicting analysed results for total AS160. C) Bar graph depicting analysed results for p-AS160 (Thr642). D) Bar graph depicting phospho to total ratio of AS160. * $p < 0.05$ (n=2-3 per group).

GLUT4

None of the treatment groups had a significant effect on total GLUT4 levels in either the control or HCD hearts. The untreated HCD hearts did have significantly less total GLUT4 compared to the untreated control hearts. GLUT4 Western blot results are indicated in Figure 4.30.

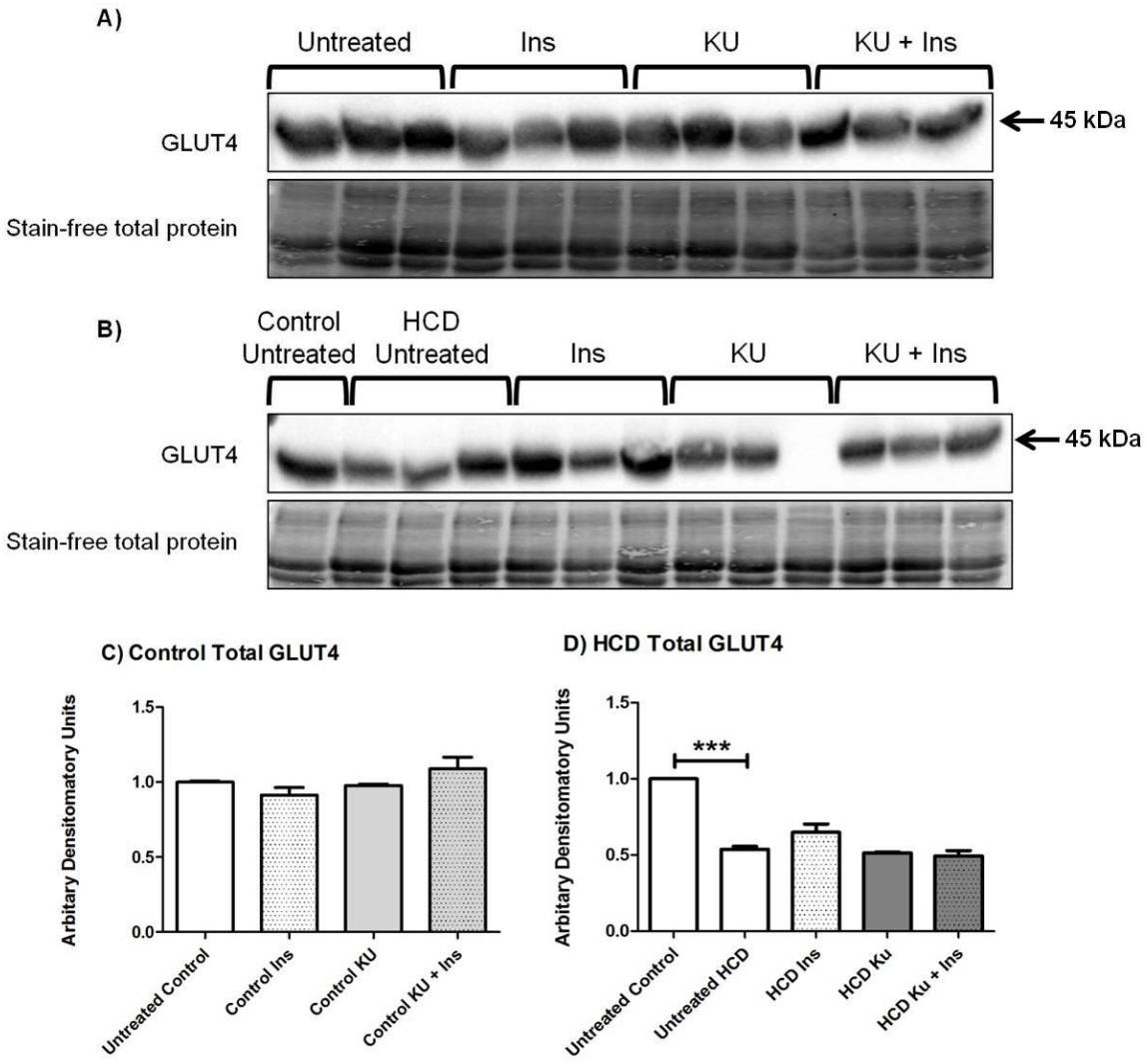

Figure 4.30: GLUT4 expression levels in control diet and HCD hearts following treatment with insulin, KU-60019 and a combination of insulin and KU-60019. A) Western blot chemiluminescent results of GLUT4 and stain-free total protein stain of the membrane of the control diet samples. B) Western blot chemiluminescent results of GLUT4 and stain-free total protein stain of the membrane of the HCD samples. C) Bar graph depicting analysed results for total GLUT4 in control samples. D) Bar graph depicting analysed results for total GLUT4 in HCD samples. *** $p < 0.0001$ (n=3 per group).

AMPK

Treatment with insulin caused a significant increase in total AMPK in control hearts compared to untreated control hearts (Untreated 1.00 ± 0.003; Ins 1.46 ± 0.05; $p < 0.0001$). Insulin had no effect on AMPK phosphorylation, but because of the increased total AMPK, insulin treated hearts had a significantly lower P/T AMPK ratio compare to the untreated group (Untreated 1.00 ± 0.03; Ins 0.72 ± 0.20; $p < 0.05$). KU-60019 had no effect on total AMPK compared to the untreated group, but co-treatment with KU-60019 and insulin resulted in total AMPK levels that were significantly lower than what was seen in the insulin group (Ins 1.46 ± 0.05; KU + Ins 1.16 ± 0.05; $p < 0.05$). This resulted in a higher P/T AMPK ratio in the control KU-60019 + insulin group compared to the insulin only group (Ins 0.72 ± 0.20; KU + Ins 1.05 ± 0.08; $p < 0.05$). Compared to treatment with KU-60019 alone, co-treatment with KU-60019 and insulin resulted in increased total AMPK (KU 0.90 ± 0.01; KU + Ins 1.16 ± 0.05; $p < 0.05$) and increased phosphorylation of AMPK (KU 0.82 ± 0.11; KU + Ins 1.21 ± 0.04; $p < 0.05$). The P/T ratio remained similar between the two groups. The results of AMPK Western blot analysis in control hearts are indicated in Figure 4.31.

Total AMPK levels were similar between the control and HCD groups, but the HCD had significantly less phosphorylation of AMPK compared to the control group (Untreated control 1.00 ± 0.02; Untreated HCD 0.56 ± 0.04; $p < 0.05$). Although there were no changes in total AMPK or AMPK phosphorylation between the two groups, the insulin treated group had a significantly lower P/T ratio than the untreated group (Untreated 0.71 ± 0.09; Ins 0.22 ± 0.10; $p < 0.05$). ATM inhibition through treatment with KU-60019 resulted in reduced total AMPK levels (Untreated 0.91 ± 0.002; KU 0.66 ± 0.03; $p < 0.005$), reduced AMPK phosphorylation levels (Untreated 0.56 ± 0.04; KU 0.12 ± 0.03; $p < 0.05$) and a reduced P/T ratio (Untreated 0.71 ± 0.09; KU 0.18 ± 0.04; $p < 0.005$) compared to the untreated group. The results of AMPK Western blot analysis in HCD hearts are indicated in Figure 4.32.

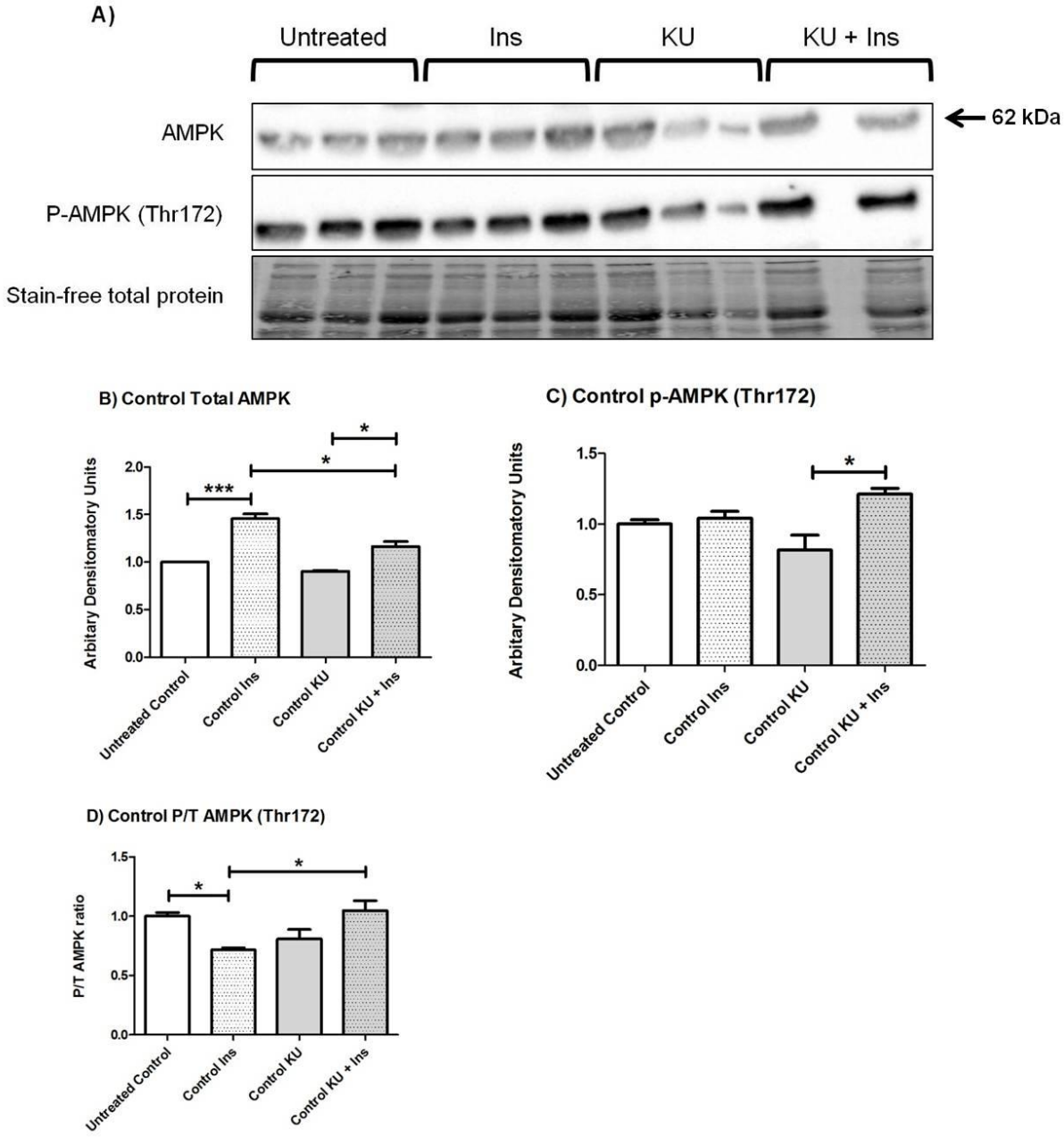

Figure 4.31: AMPK expression and phosphorylation levels in control hearts following treatment with insulin, KU-60019 and a combination of insulin and KU-60019. A) Western blot chemiluminescent results of AMPK and p-AMPK and stain-free total protein stain of the membrane. B) Bar graph depicting analysed results for total AMPK. C) Bar graph depicting analysed results for p-AMPK (Thr172). D) Bar graph depicting phospho to total ratio of AMPK. * $p < 0.05$; *** $p < 0.0001$ (n=2-3 per group).

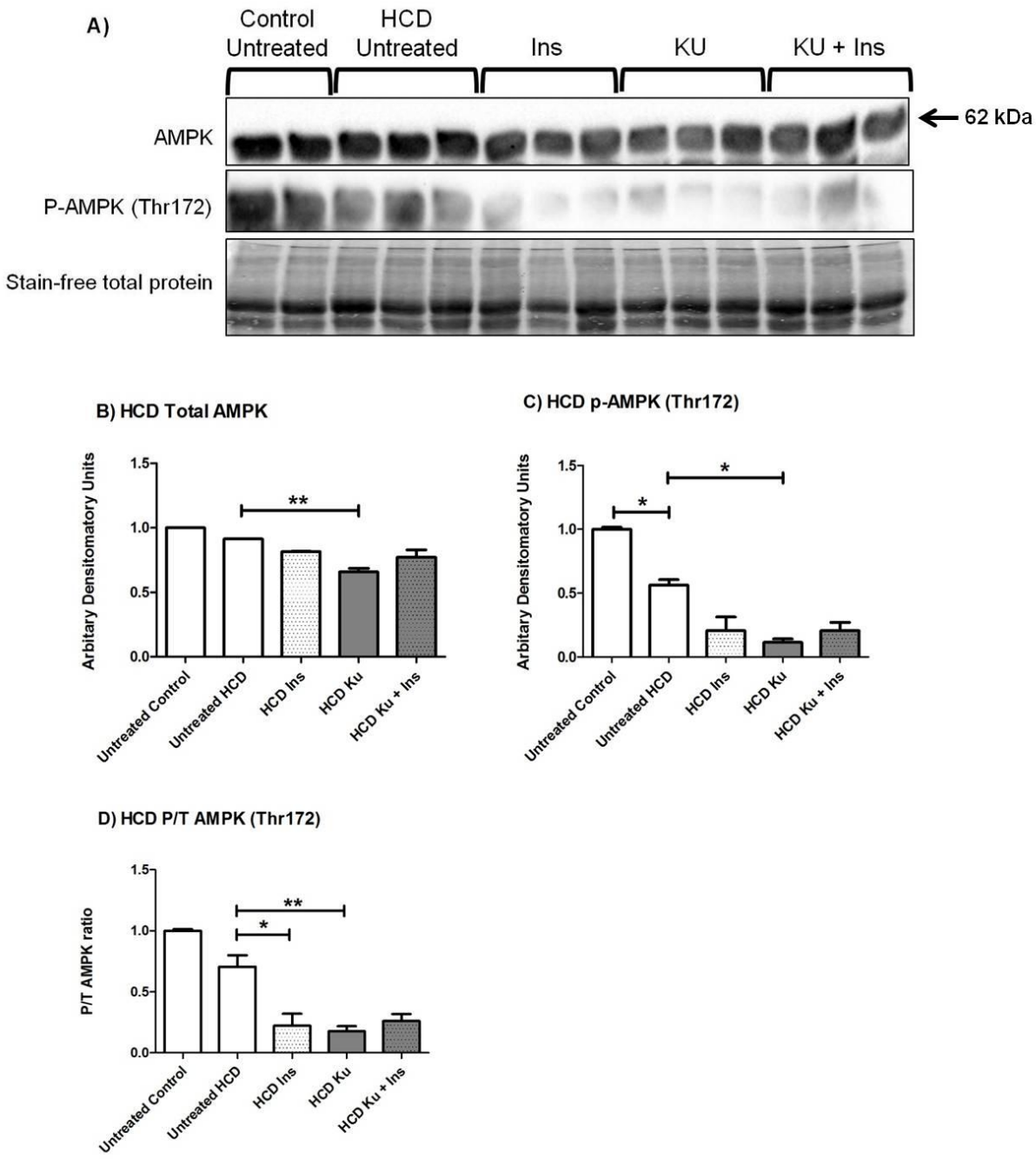

Figure 4.32: AMPK expression and phosphorylation levels in HCD hearts following treatment with insulin, KU-60019 and a combination of insulin and KU-60019. A) Western blot chemiluminescent results of AMPK and p-AMPK and stain-free total protein stain of the membrane. B) Bar graph depicting analysed results for total AMPK. C) Bar graph depicting analysed results for p-AMPK (Thr172). D) Bar graph depicting phospho to total ratio of AMPK. * $p < 0.05$; ** $p < 0.005$ (n=2-3 per group).

ACC

In hearts from animals that were on the control diet, insulin treatment significantly decreased total ACC (Untreated 1.00 ± 0.02; Ins 0.20 ± 0.003; $p < 0.0001$) and decreased phosphorylation of ACC (Untreated 1.00 ± 0.03; Ins 0.38 ± 0.04; $p < 0.0001$) compared to the untreated group. The overall effect was a significantly higher P/T ACC ratio in the insulin treated group compared to the untreated group (Untreated 1.00 ± 0.01; Ins 1.90 ± 0.23; $p < 0.005$). Treatment with KU-60019 resulted in increased ACC levels compared to the untreated group (Untreated 1.00 ± 0.02; KU 1.54 ± 0.06; $p < 0.0001$), however, ACC phosphorylation and the P/T ratio remained similar between the untreated and KU-60019 groups. KU-60019, co-treated with insulin, caused increased total ACC levels compared to the insulin only group (Ins 0.20 ± 0.003; KU + Ins 1.46 ± 0.006; $p < 0.0001$). The KU-60019 plus insulin group also had increased ACC phosphorylation compared to the insulin group (Ins 0.38 ± 0.04; KU + Ins 1.05 ± 0.005; $p < 0.0001$), but the overall effect on the P/T ratio was a decrease in the KU-60019 + insulin group compared to the insulin only group (Ins 1.90 ± 0.23; KU + Ins 0.77 ± 0.05; $p < 0.0001$). The results of ACC Western blot analysis in control hearts are indicated in Figure 4.33.

HCD hearts had significantly higher total ACC compared to control diet hearts (Untreated control 1.00 ± 0.01; Untreated HCD 4.36 ± 0.79; $p < 0.005$). Although he ACC phosphorylation was also higher in the HCD hearts (Untreated control 1.00 ± 0.02; Untreated HCD 1.60 ± 0.16; $p < 0.005$), the P/T ratio was significantly lower in the HCD hearts compared to the control diet hearts (Untreated control 1.00 ± 0.006; Untreated HCD 0.33 ± 0.03; $p < 0.0001$). Compared to untreated HCD hearts, insulin treatment resulted in increased total ACC levels (Untreated HCD 1.60 ± 0.16; Ins 7.74 ± 0.09; $p < 0.005$). Opposite to what was observed in the control hearts, KU-60019 and insulin co-treatment caused a decrease in total ACC levels compared to the insulin treated group (Ins 7.74 ± 0.09; KU + Ins 4.08 ± 0.39; $p < 0.005$) an a decrease in ACC

phosphorylation compared to the insulin only group (Ins 1.81 ± 0.02; KU + Ins 1.11 ± 0.05; p < 0.005). The results of ACC Western blot analysis in HCD hearts are indicated in Figure 4.34.

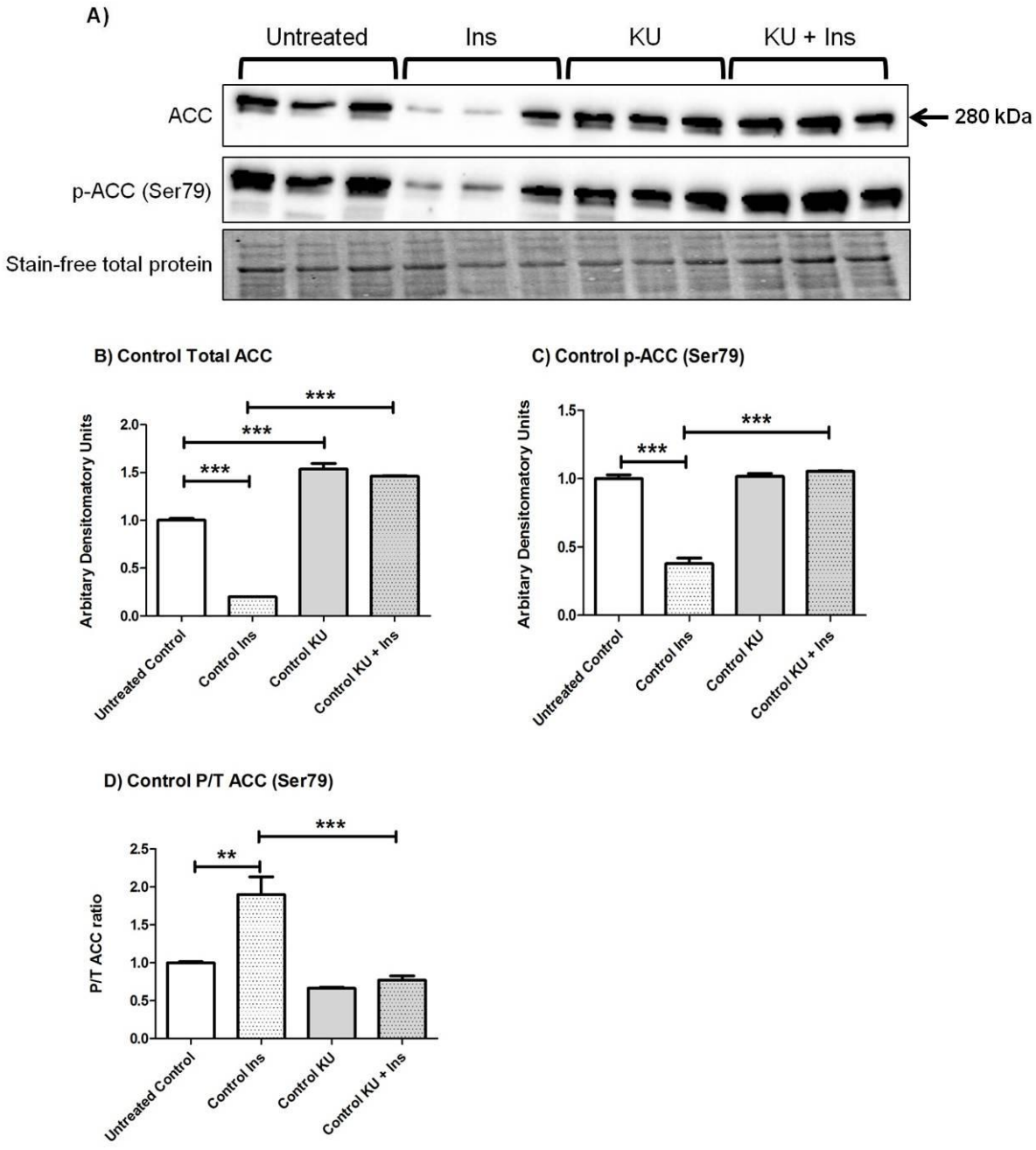

Figure 4.33: ACC expression and phosphorylation levels in control hearts following treatment with insulin, KU-60019 and a combination of insulin and KU-60019. A) Western blot chemiluminescent results of ACC and p-ACC and stain-free total protein stain of the membrane. B) Bar graph depicting analysed results for total ACC. C) Bar graph depicting analysed results for p-ACC (Ser79). D) Bar graph depicting phospho to total ratio of ACC. ** p < 0.005; *** p < 0.0001 (n=3 per group).

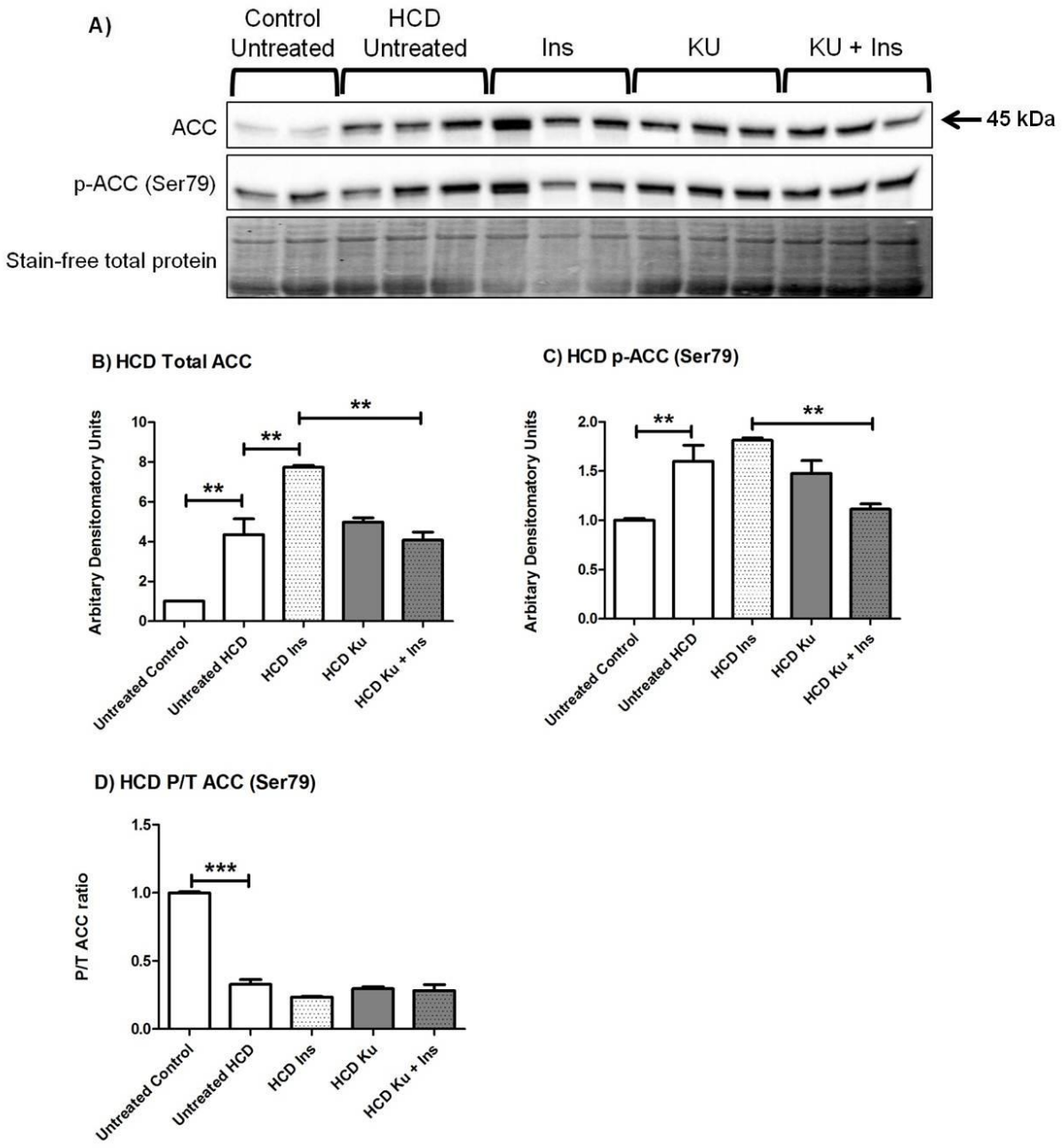

Figure 4.34: ACC expression and phosphorylation levels in HCD hearts following treatment with insulin, KU-60019 and a combination of insulin and KU-60019. A) Western blot chemiluminescent results of ACC and p-ACC and stain-free total protein stain of the membrane. B) Bar graph depicting analysed results for total ACC. C) Bar graph depicting analysed results for p-ACC (Ser79). D) Bar graph depicting phospho to total ratio of ACC. ** $p < 0.005$; *** $p < 0.0001$ (n=2-3 per group).

ATM

In response to insulin treatment, there was a significant increase in total ATM (Untreated 1.00 ± 0.06; Ins 1.57 ± 0.005; $p < 0.0001$) as well as ATM phosphorylation (Untreated 1.00 ± 0.01; Ins 1.20 ± 0.02; $p < 0.0001$) compared to untreated control hearts. The P/T ratio was however significantly lower in the insulin treated group than the untreated control group (Untreated 1.06 ± 0.05; Ins 0.76 ± 0.01; $p < 0.005$). Although KU-60019 treatment surprisingly led to an increase in total ATM levels (Untreated 1.00 ± 0.06; KU 1.22 ± 0.04; $p < 0.05$), phosphorylation of ATM was decreased by KU-60019 treatment (Untreated 1.00 ± 0.01; KU 0.86 ± 0.02; $p < 0.005$), resulting in a lower P/T ATM ratio in KU-60019 treated hearts compared to untreated hearts (Untreated 1.06 ± 0.05; KU 0.72 ± 0.02; $p < 0.005$). Co-treatment with insulin and KU-60019 resulted in more total ATM compared to when hearts were treated with KU-60019 alone (KU 1.22 ± 0.04; KU + Ins 1.49 ± 0.01; $p < 0.05$). The KU-60019 and insulin co-treatment group had significantly less ATM phosphorylation than either the insulin only group (Ins 1.20 ± 0.02; KU + Ins 0.68 ± 0.005; $p < 0.0001$) or the KU-60019 only group (KU 0.86 ± 0.02; KU + Ins 0.68 ± 0.005; $p < 0.005$). In line with this, the KU-60019 and insulin co-treatment group had a lower P/T ratio than both the insulin only group (Ins 0.76 ± 0.01; KU + Ins 0.46 ± 0.0004; $p < 0.005$) and the KU-60019 only group (KU 0.72 ± 0.02; KU + Ins 0.46 ± 0.0004; $p < 0.05$). The results of ATM Western blot analysis in control hearts are indicated in Figure 4.35.

In HCD hearts, none of the treatment groups had an effect on total ATM or ATM phosphorylation levels. The P/T ratios were also similar across all the groups. The results of ATM Western blot analysis in HCD hearts are indicated in Figure 4.36.

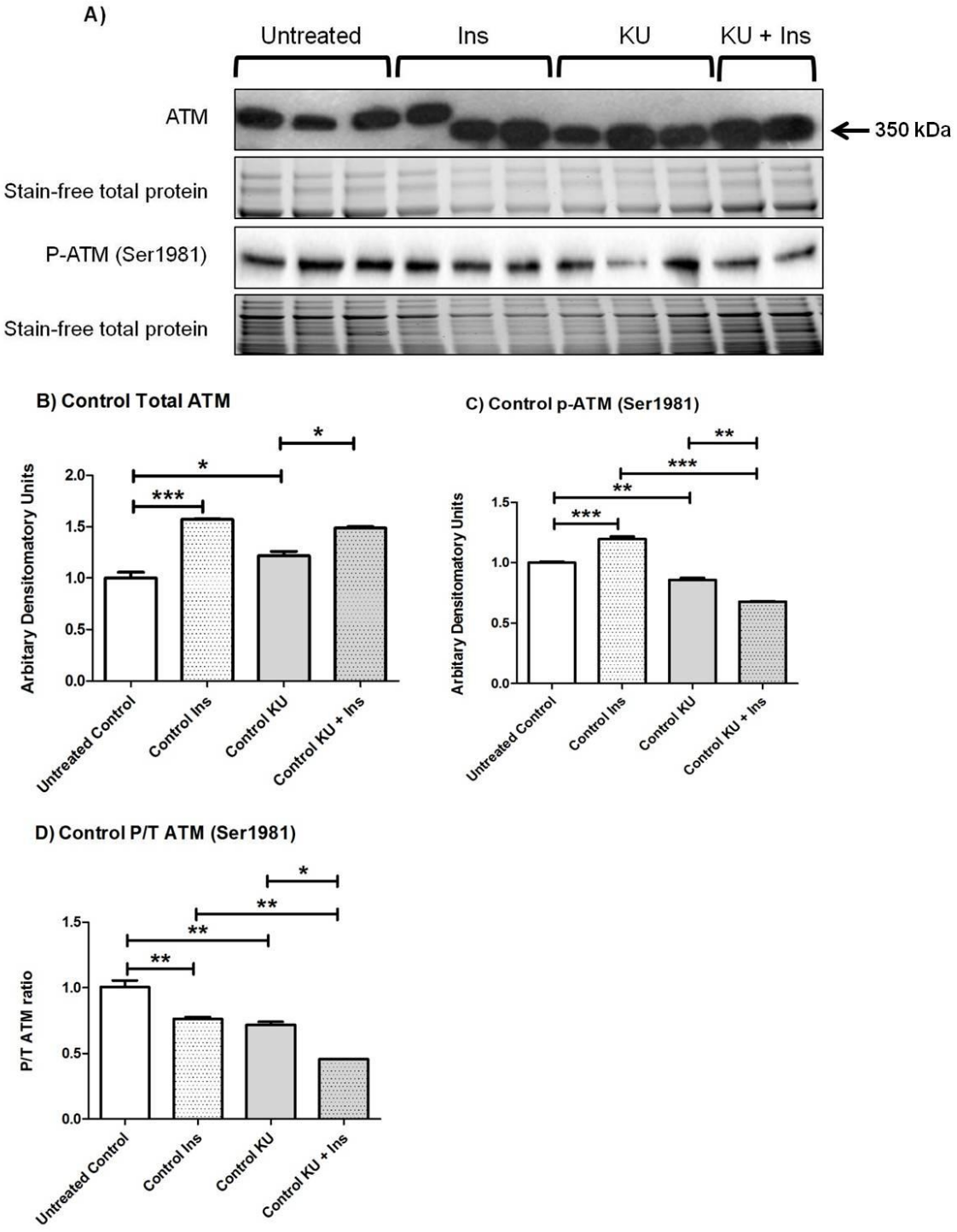

Figure 4.35: ATM expression and phosphorylation levels in control hearts following treatment with insulin, KU-60019 and a combination of insulin and KU-60019. A) Western blot chemiluminescent results of ATM and p-ATM and stain-free total protein stain of the membrane. B) Bar graph depicting analysed results for total ATM. C) Bar graph depicting analysed results for p-ATM (Ser1981). D) Bar graph depicting phospho to total ratio of ATM. * $p < 0.05$; ** $p < 0.005$; *** $p < 0.0001$ (n=2-3 per group).

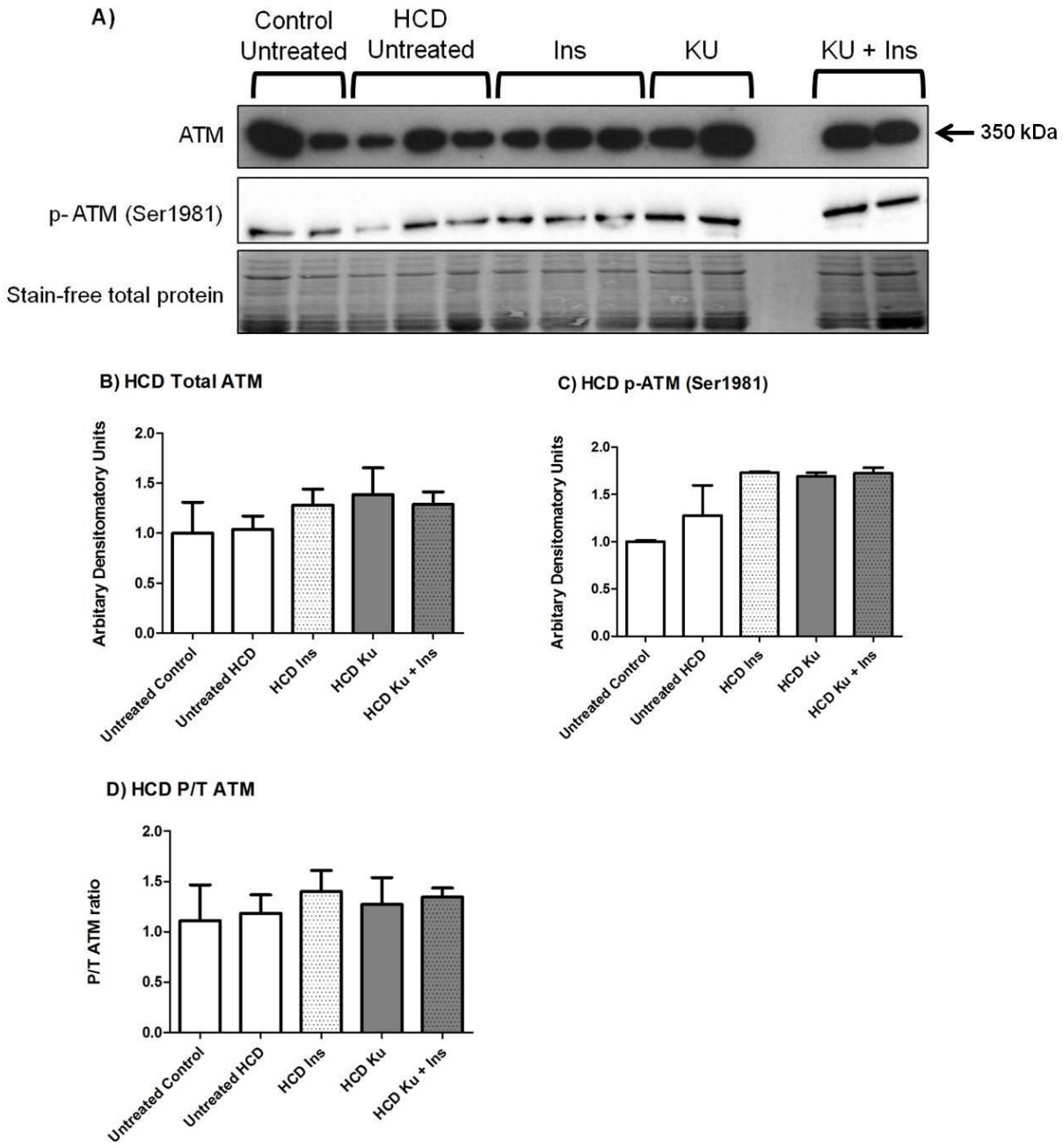

Figure 4.36: ATM expression and phosphorylation levels in HCD hearts following treatment with insulin, KU-60019 and a combination of insulin and KU-60019. A) Western blot chemiluminescent results of ATM and p-ATM and stain-free total protein stain of the membrane. B) Bar graph depicting analysed results for total ATM. C) Bar graph depicting analysed results for p-ATM (Ser1981). D) Bar graph depicting phospho to total ratio of ATM. (n=2-3 per group).

4.4.2 Signalling after IRI

Hearts from age-matched control and HCD animals were perfused with a Langendorff *ex vivo* perfusion protocol. The hearts were treated with insulin (activator), wortmannin (PI3K inhibitor), KU-60019 (ATM inhibitor) and activator-inhibitor combinations. Following the treatment period, the hearts were subjected to 20 minutes global ischaemia after which they were reperfused for 10 minutes. The hearts were freeze-clamped and Western blot analysis used to determine the effect of the treatments on insulin signalling intermediates.

JNK

None of the treatments had a significant effect on total JNK, JNK phosphorylation or the P/T JNK ratio in control hearts (Figure 4.37). In the HCD hearts, co-treatment with KU-60019 and insulin resulted in significantly less total JNK compared to treatment with KU-60019 alone (Figure 4.38 B). None of the treatment groups had an effect on JNK phosphorylation or the P/T ratio in HCD hearts (Figure 4.38 C-D). When comparing only the KU-60019 treated hearts to untreated hearts, KU-60019 significantly reduced JNK phosphorylation in both control and HCD hearts (Figure 4.39 A).

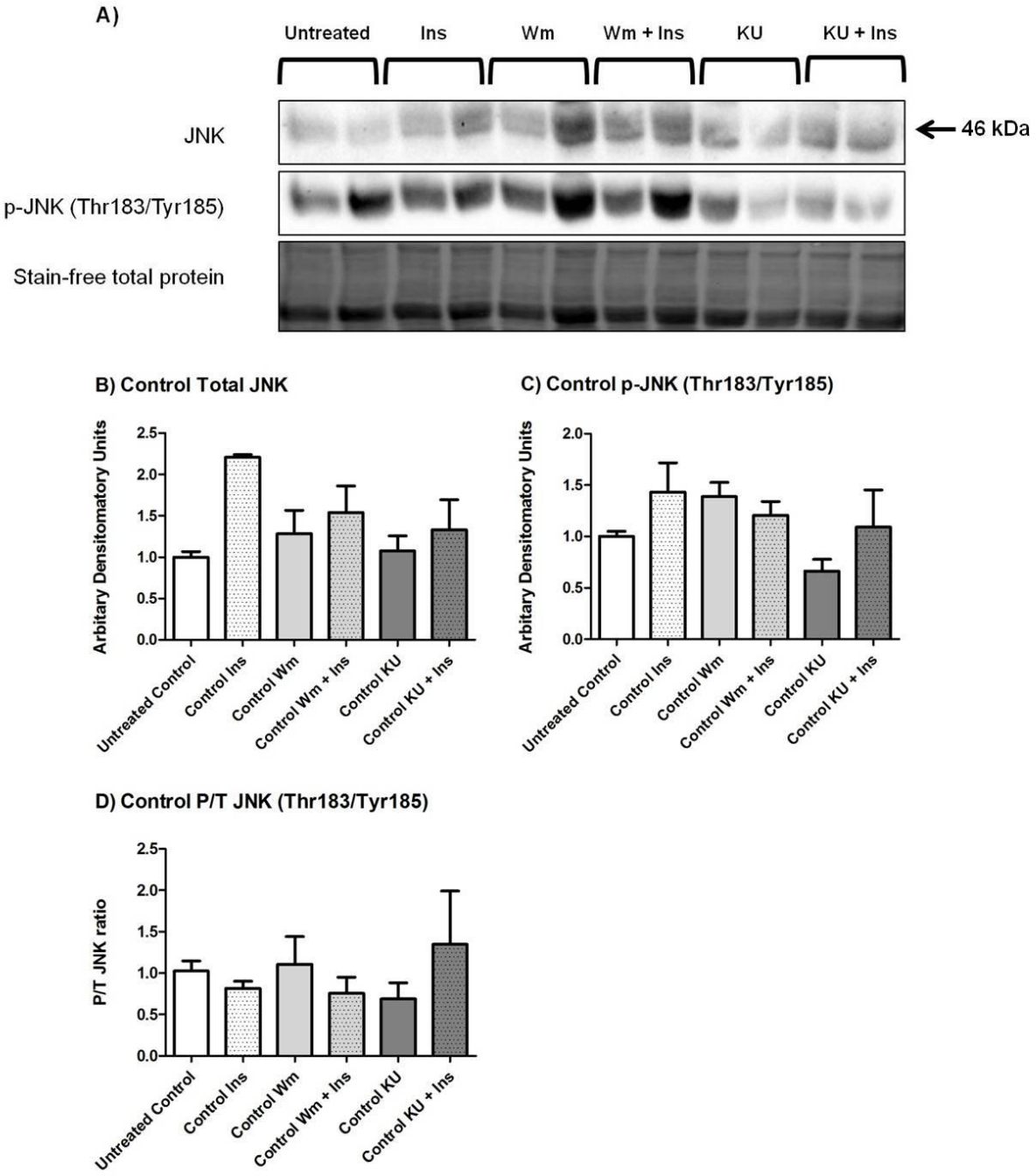

Figure 4.37: JNK expression and phosphorylation levels following ischaemia and reperfusion in control hearts treated with insulin, wortmannin and KU-60019. A) Representative western blot chemiluminescent results of JNK and p-JNK and stain-free total protein stain of the membrane. B) Bar graph depicting analysed results for total JNK. C) Bar graph depicting analysed results for p-JNK (Thr183/Tyr185). D) Bar graph depicting phospho to total ratio of JNK. (n=4 per group).

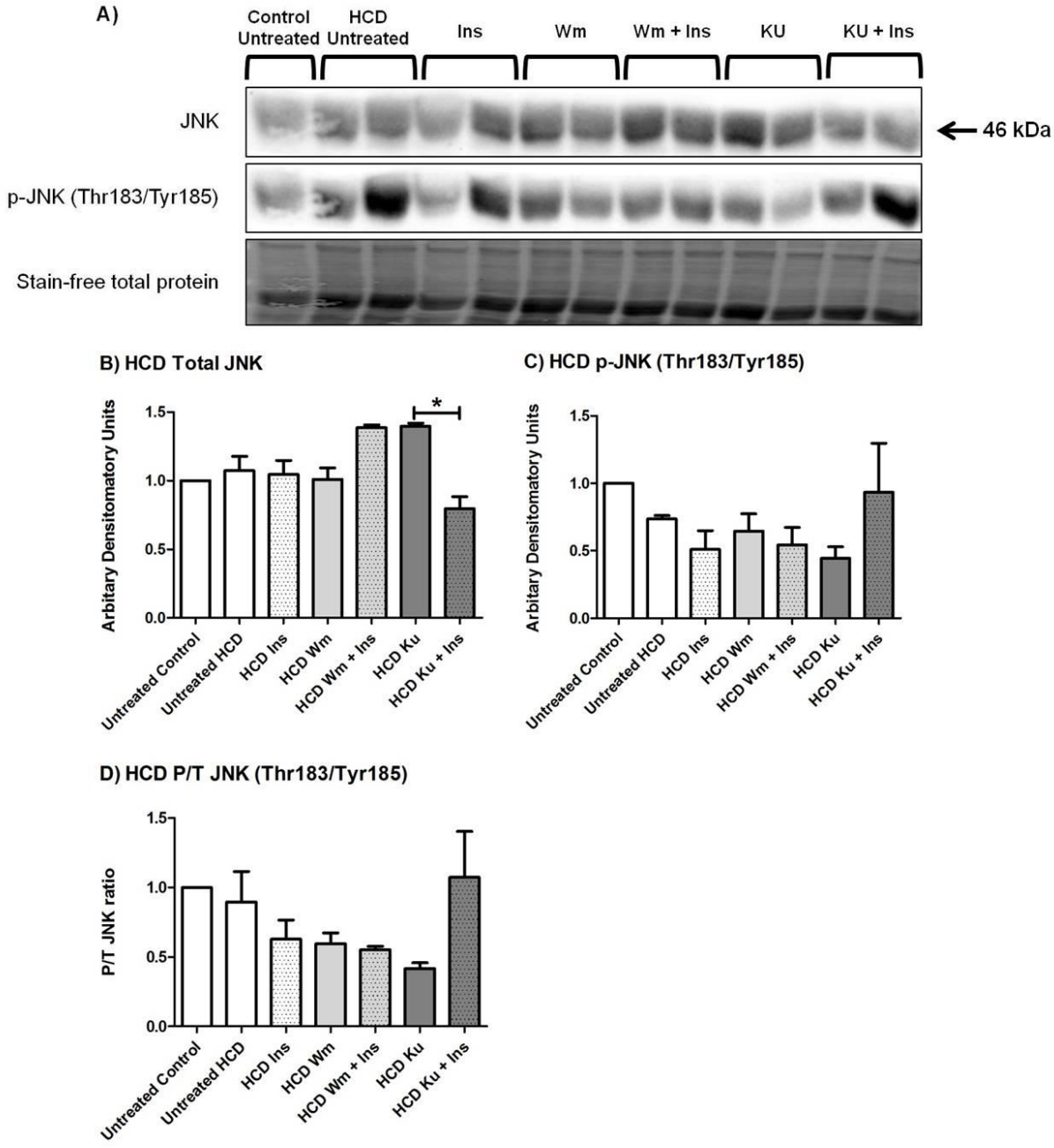

Figure 4.38: JNK expression and phosphorylation levels following ischaemia and reperfusion in HCD hearts treated with insulin, wortmannin and KU-60019. A) Representative western blot chemiluminescent results of JNK and p-JNK and stain-free total protein stain of the membrane. B) Bar graph depicting analysed results for total JNK. C) Bar graph depicting analysed results for p-JNK (Thr183/Tyr185). D) Bar graph depicting phospho to total ratio of JNK. * $p < 0.05$ (n=4 per group, except Control Untreated n=2).

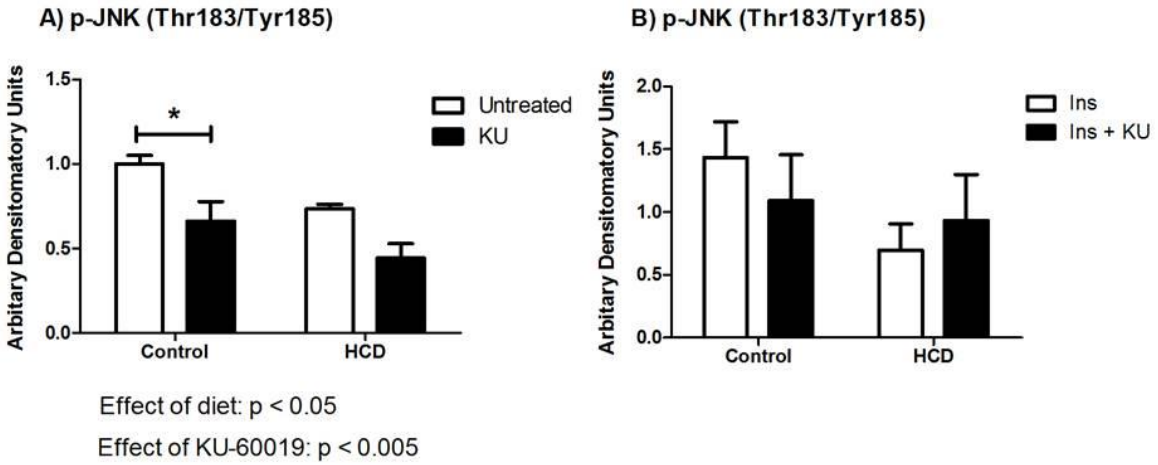

Figure 4.39: The effect of KU-60019 on JNK phosphorylation (Thr183/Tyr185). A) Two-way ANOVA to illustrate the effect of KU-60019 on JNK phosphorylation compared to untreated hearts in control and HCD hearts. B) Two-way ANOVA to illustrate the effect of KU-60019 on insulin stimulated JNK phosphorylation in control and HCD hearts. * $p < 0.05$ (n=4 per group).

IRS-1

The treatment groups had no effect on total IRS-1 levels or on IRS-1 (Ser307) phosphorylation in the control and the HCD hearts (Figures 4.40 & 4.41). In the control hearts, co-treatment with wortmannin and insulin resulted in a higher P/T ratio compared to treatment with insulin or wortmannin alone. KU-60019 also increased the P/T ratio in control hearts when compared to untreated control hearts (Figure 4.40 D). The P/T IRS-1 ratio was unchanged in the treatment groups in HCD hearts. Although no significant difference was detected between the P/T IRS-1 ratio in untreated control and untreated HCD hearts using a one way ANOVA, an unpaired Student's t-test between the two groups indicated that the HCD untreated hearts had a significantly higher P/T IRS-1 ratio compared to the untreated control hearts (Figure 4.41 D). Two-way ANOVA to determine the effect of KU-60019 on IRS-1 phosphorylation detected no significant effect (Figure 4.42).

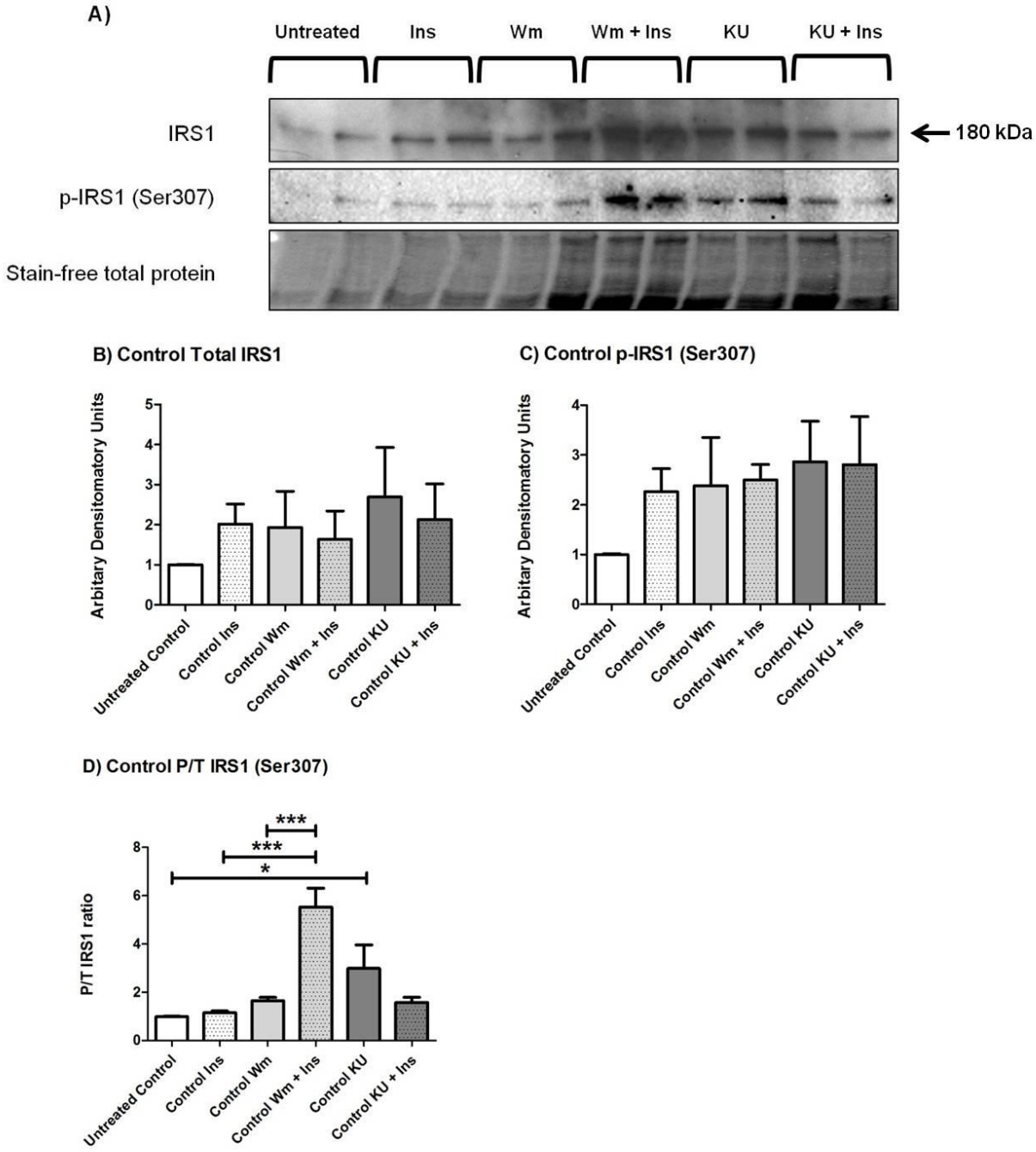

Figure 4.40: IRS-1 expression and phosphorylation levels following ischaemia and reperfusion in control hearts treated with insulin, wortmannin and KU-60019. A) Representative western blot chemiluminescent results of IRS-1 and p-IRS-1 and stain-free total protein stain of the membrane. B) Bar graph depicting analysed results for total IRS-1. C) Bar graph depicting analysed results for p-IRS1 (Ser307). D) Bar graph depicting phospho to total ratio of IRS1. * $p < 0.05$; *** $p < 0.0001$ (n=4 per group).

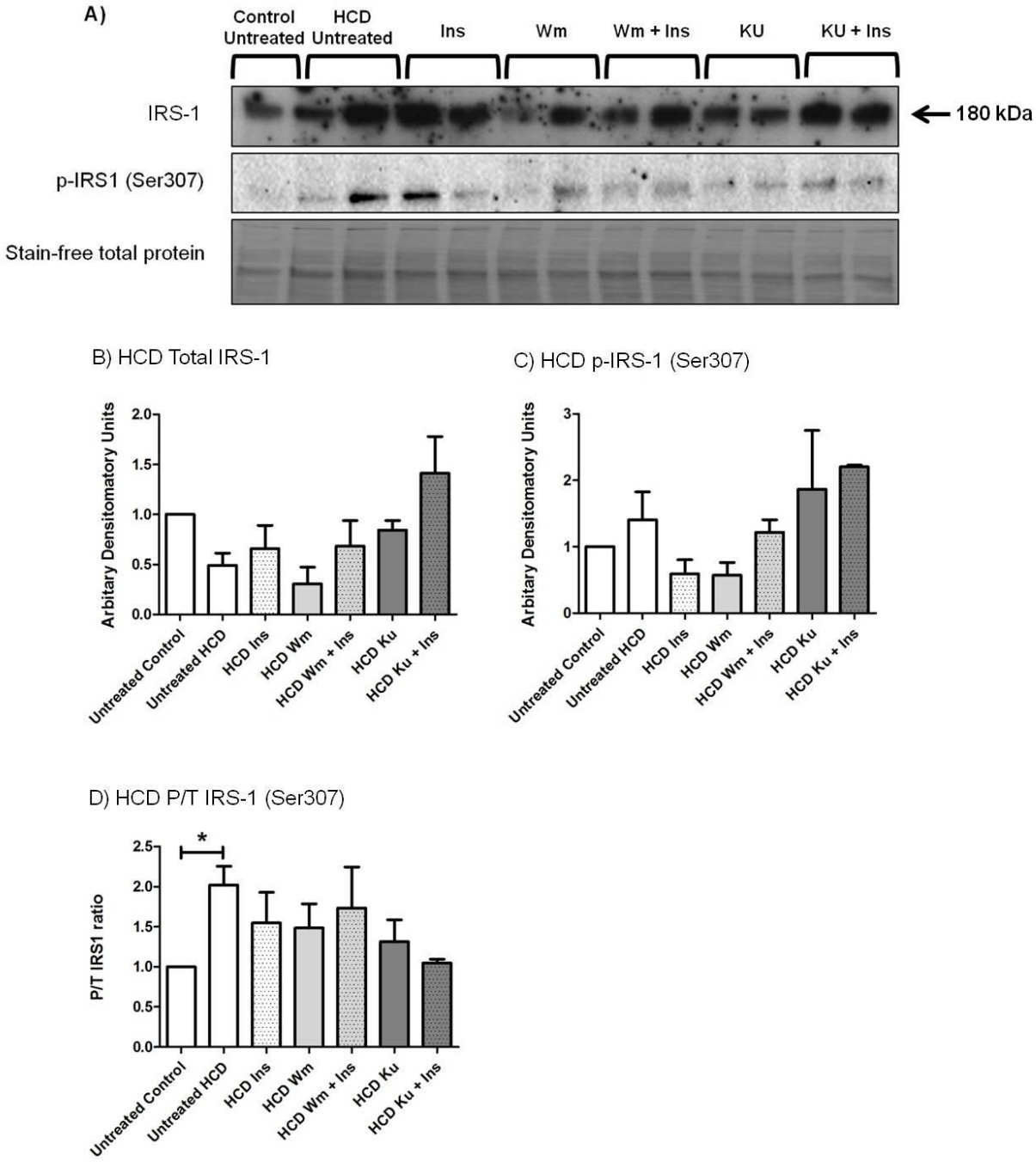

Figure 4.41: IRS-1 expression and phosphorylation levels following ischaemia and reperfusion in HCD hearts treated with insulin, wortmannin and KU-60019. A) Representative western blot chemiluminescent results of IRS-1 and p-IRS-1 and stain-free total protein stain of the membrane. B) Bar graph depicting analysed results for total IRS-1. C) Bar graph depicting analysed results for p-IRS-1 (Ser307). D) Bar graph depicting phospho to total ratio of IRS-1. * $p < 0.05$ (Unpaired Student's t-test) (n=4 per group, except Control Untreated n=2).

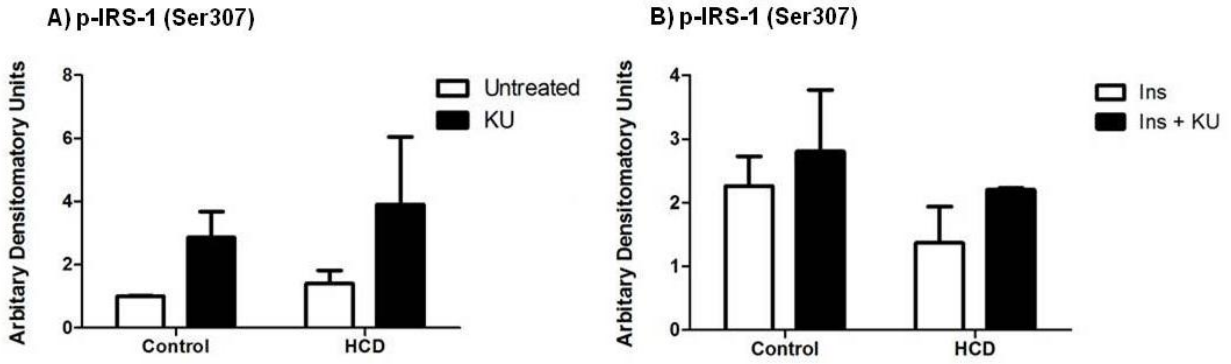

Figure 4.42: The effect of KU-60019 on IRS-1 phosphorylation (Ser307). A) Two-way ANOVA to illustrate the effect of KU-60019 on IRS-1 phosphorylation compared to untreated hearts in control and HCD hearts. B) Two-way ANOVA to illustrate the effect of KU-60019 on insulin stimulated IRS-1 phosphorylation in control and HCD hearts. (n=4 per group).

P85 subunit of PI3K

In control hearts, treatment with wortmannin resulted in significantly increased PI3K phosphorylation following IRI (Untreated 1.00 ± 0.01; Wm 1.72 ± 0.19; $p < 0.005$) (Figure 4.43 C). None of the other groups had an effect on total PI3K, PI3K phosphorylation or P/T PI3K ratio in control hearts (Figure 4.43). The P/T ratio was significantly lower in untreated HCD hearts than in untreated control hearts after IRI (Untreated control 1.00; Untreated HCD 0.48 ± 0.01; $p < 0.05$) (Figure 4.44D). ATM inhibition with KU-60019 resulted in increased insulin stimulated phosphorylation of PI3K (Figure 4.45B).

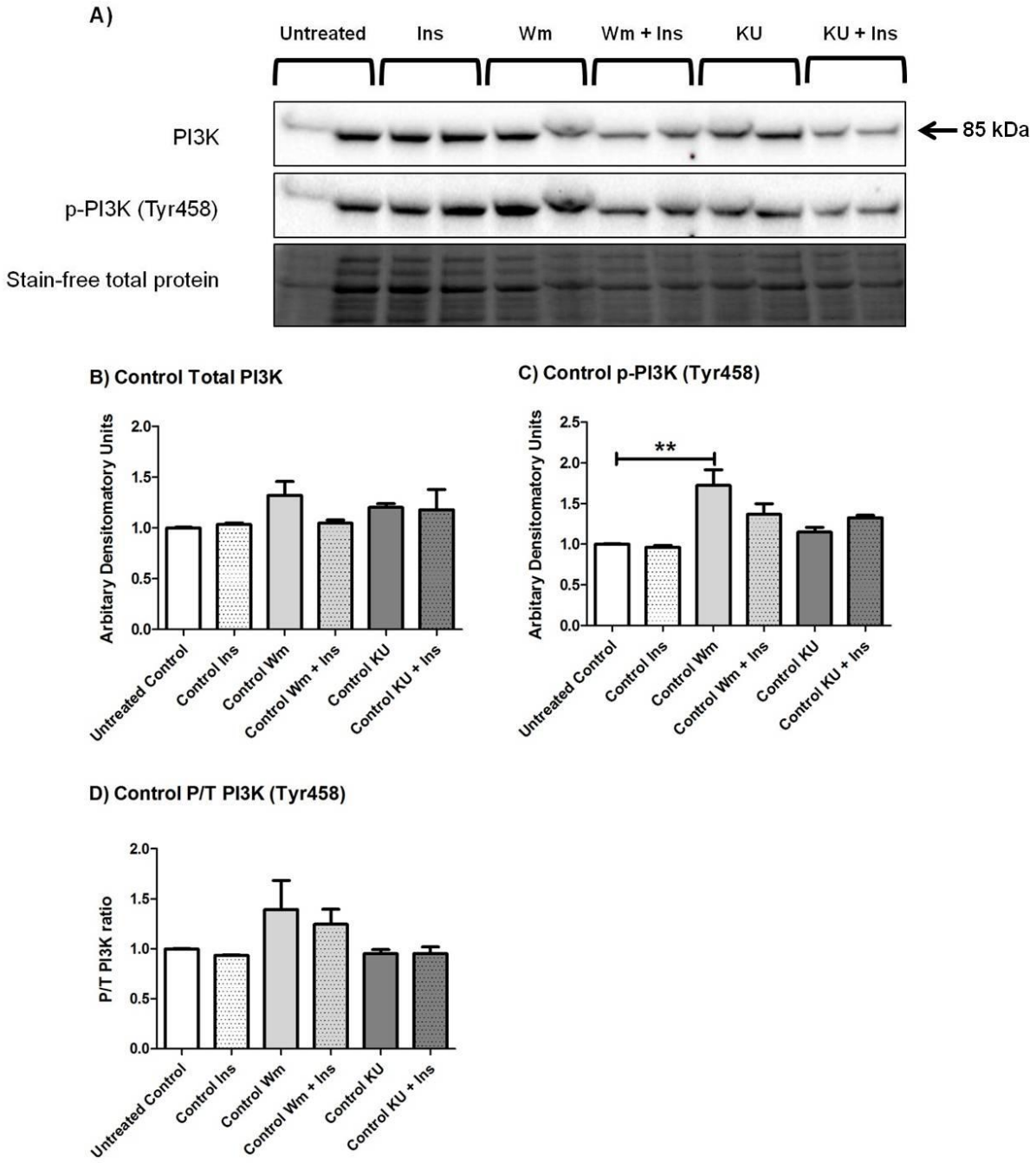

Figure 4.43: PI3K (p85 subunit) expression and phosphorylation levels following ischaemia and reperfusion in control hearts treated with insulin, wortmannin and KU-60019. A) Representative western blot chemiluminescent results of PI3K and p-PI3K and stain-free total protein stain of the membrane. B) Bar graph depicting analysed results for total PI3K. C) Bar graph depicting analysed results for p-PI3K (Tyr458). D) Bar graph depicting phospho to total ratio of PI3K. ** $p < 0.005$ (n=4 per group).

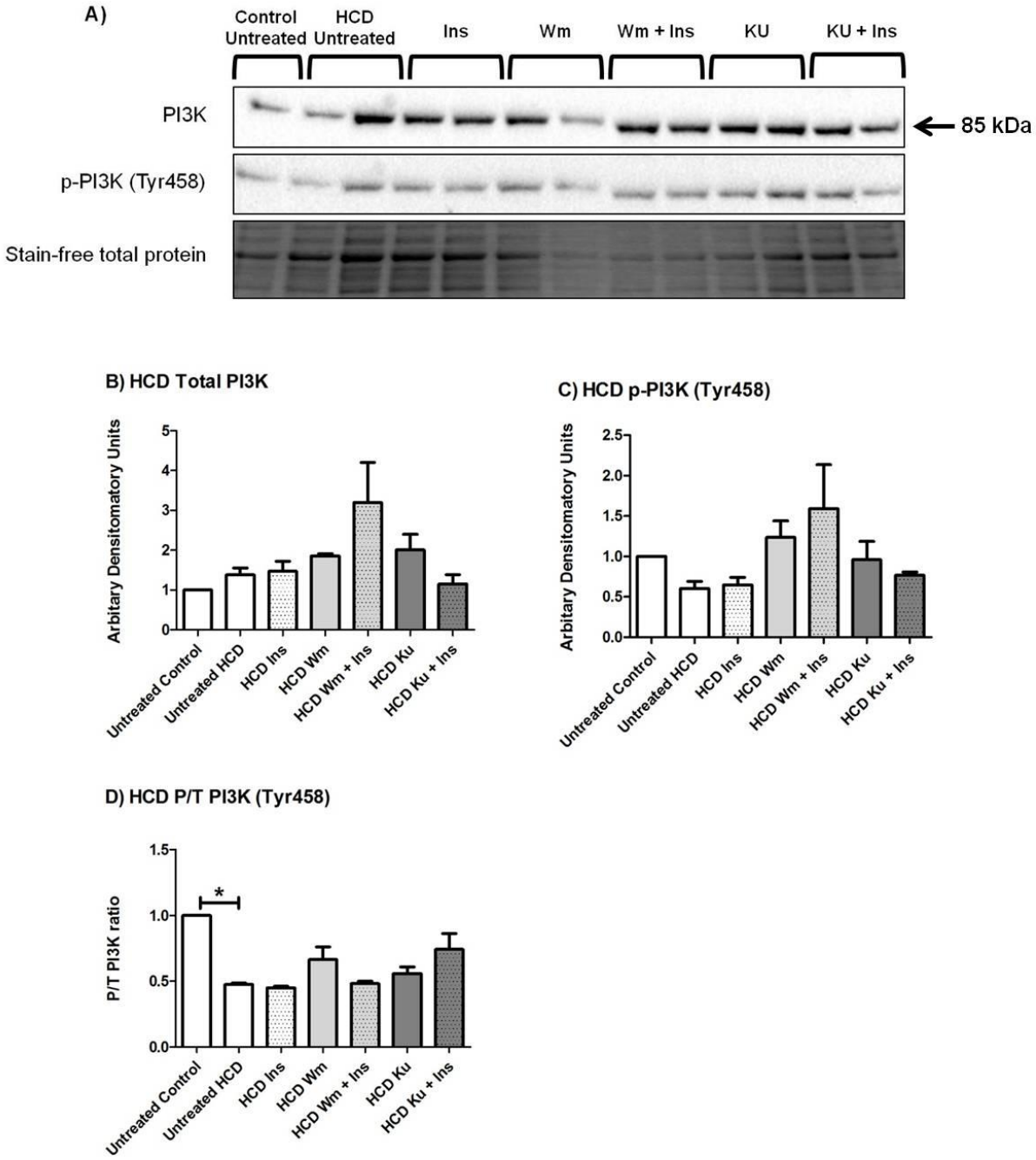

Figure 4.44: PI3K expression and phosphorylation levels following ischaemia and reperfusion in HCD hearts treated with insulin, wortmannin and KU-60019. A) Representative western blot chemiluminescent results of PI3K and p-PI3K and stain-free total protein stain of the membrane. B) Bar graph depicting analysed results for total PI3K. C) Bar graph depicting analysed results for p-PI3K (Tyr458). D) Bar graph depicting phospho to total ratio of PI3K. * $p < 0.05$ (n=4 per group, except Control Untreated n=2).

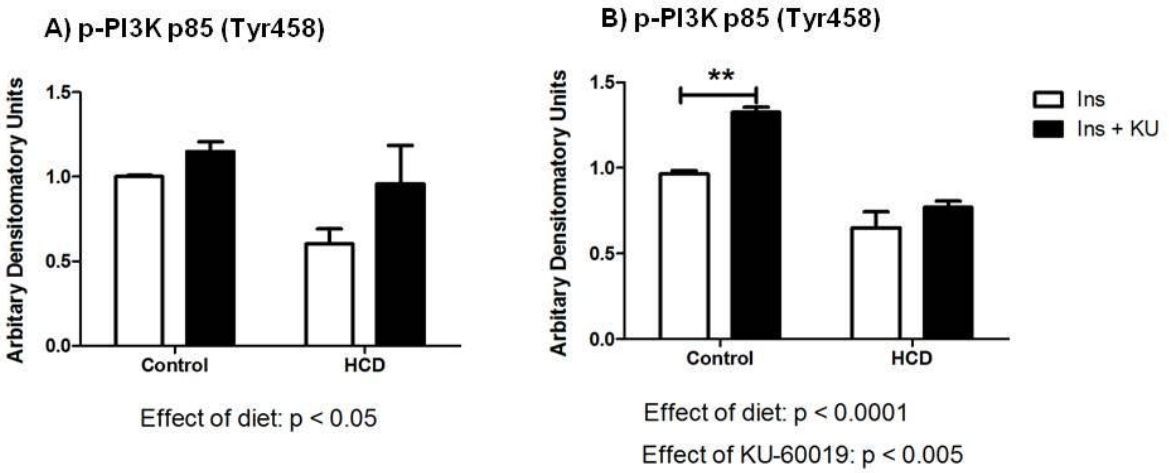

Figure 4.45: The effect of KU-60019 on PI3K p85 phosphorylation (Tyr458). A) Two-way ANOVA to illustrate the effect of KU-60019 on PI3K phosphorylation compared to untreated hearts in control and HCD hearts. B) Two-way ANOVA to illustrate the effect of KU-60019 on insulin stimulated PI3K phosphorylation in control and HCD hearts. ** $p < 0.005$ (n=4 per group).

PTEN

Following IRI, total PTEN, PTEN phosphorylation and the P/T PTEN ratios of all groups were comparable in both the control (Figure 4.46) and HCD (Figure 4.47) hearts. ATM inhibition prior to IRI had no effect on PTEN phosphorylation after ten minutes of reperfusion (Figure 4.48).

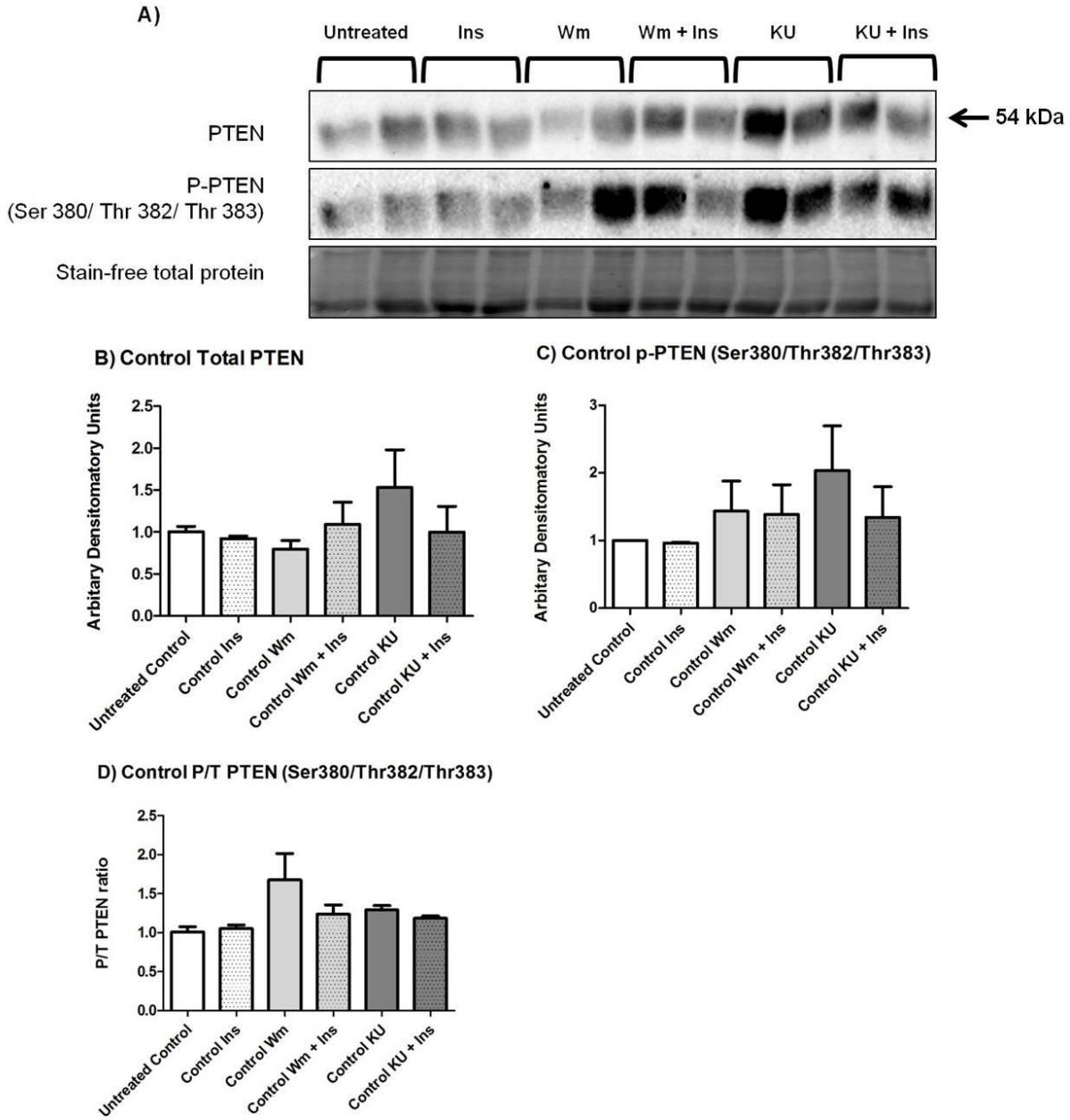

Figure 4.46: PTEN expression and phosphorylation levels following ischaemia and reperfusion in control hearts treated with insulin, wortmannin and KU-60019. A) Representative western blot chemiluminescent results of PTEN and p-PTEN and stain-free total protein stain of the membrane. B) Bar graph depicting analysed results for total PTEN. C) Bar graph depicting analysed results for p-PTEN (Ser380/Thr382/Thr383). D) Bar graph depicting phospho to total ratio of PTEN. (n=4 per group).

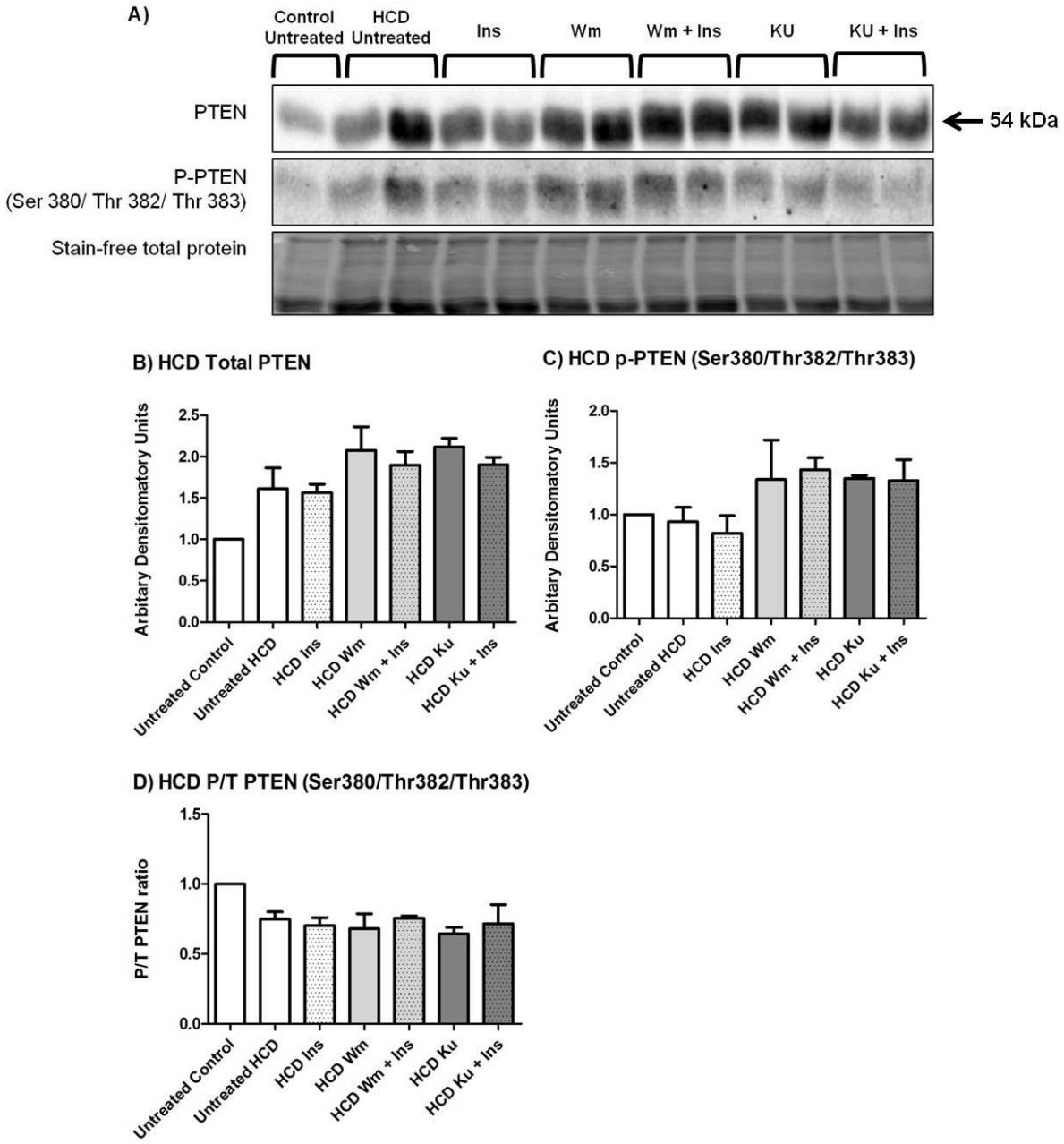

Figure 4.47: PTEN expression and phosphorylation levels following ischaemia and reperfusion in HCD hearts treated with insulin, wortmannin and KU-60019. A) Representative western blot chemiluminescent results of PTEN and p-PTEN and stain-free total protein stain of the membrane. B) Bar graph depicting analysed results for total PTEN. C) Bar graph depicting analysed results for p-PTEN (Ser380/Thr382/Thr383). D) Bar graph depicting phospho to total ratio of PTEN. (n=4 per group, except Control Untreated n=2).

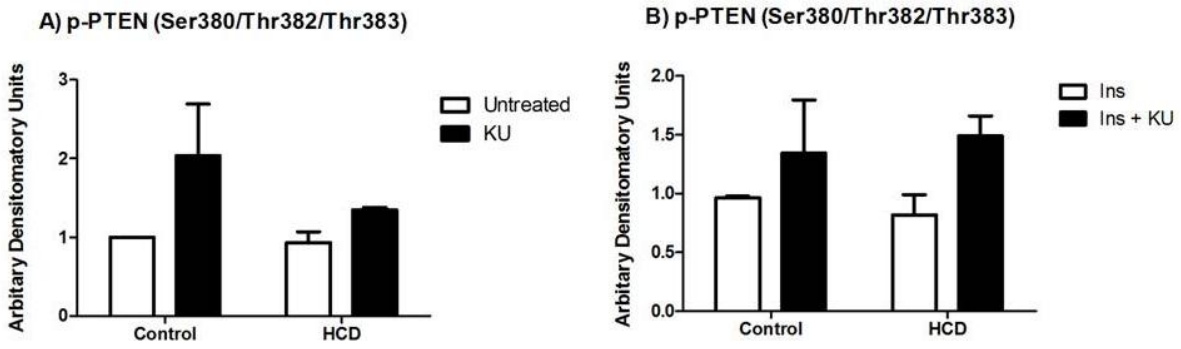

Figure 4.48: The effect of KU-60019 on PTEN phosphorylation (Ser380/Thr382/Thr383). A) Two-way ANOVA to illustrate the effect of KU-60019 on PTEN phosphorylation compared to untreated hearts in control and HCD hearts. B) Two-way ANOVA to illustrate the effect of KU-60019 on insulin stimulated PTEN phosphorylation in control and HCD hearts. (n=4 per group).

PKB/Akt

The treatment groups had no effect on PKB/Akt expression or phosphorylation following IRI in either the control (Figure 4.49) or HCD (Figure 4.50) hearts. A two-way ANOVA revealed that treatment of KU-60019 significantly reduced insulin stimulated PKB/Akt (Ser473) phosphorylation in HCD hearts (Figure 4.51 B).

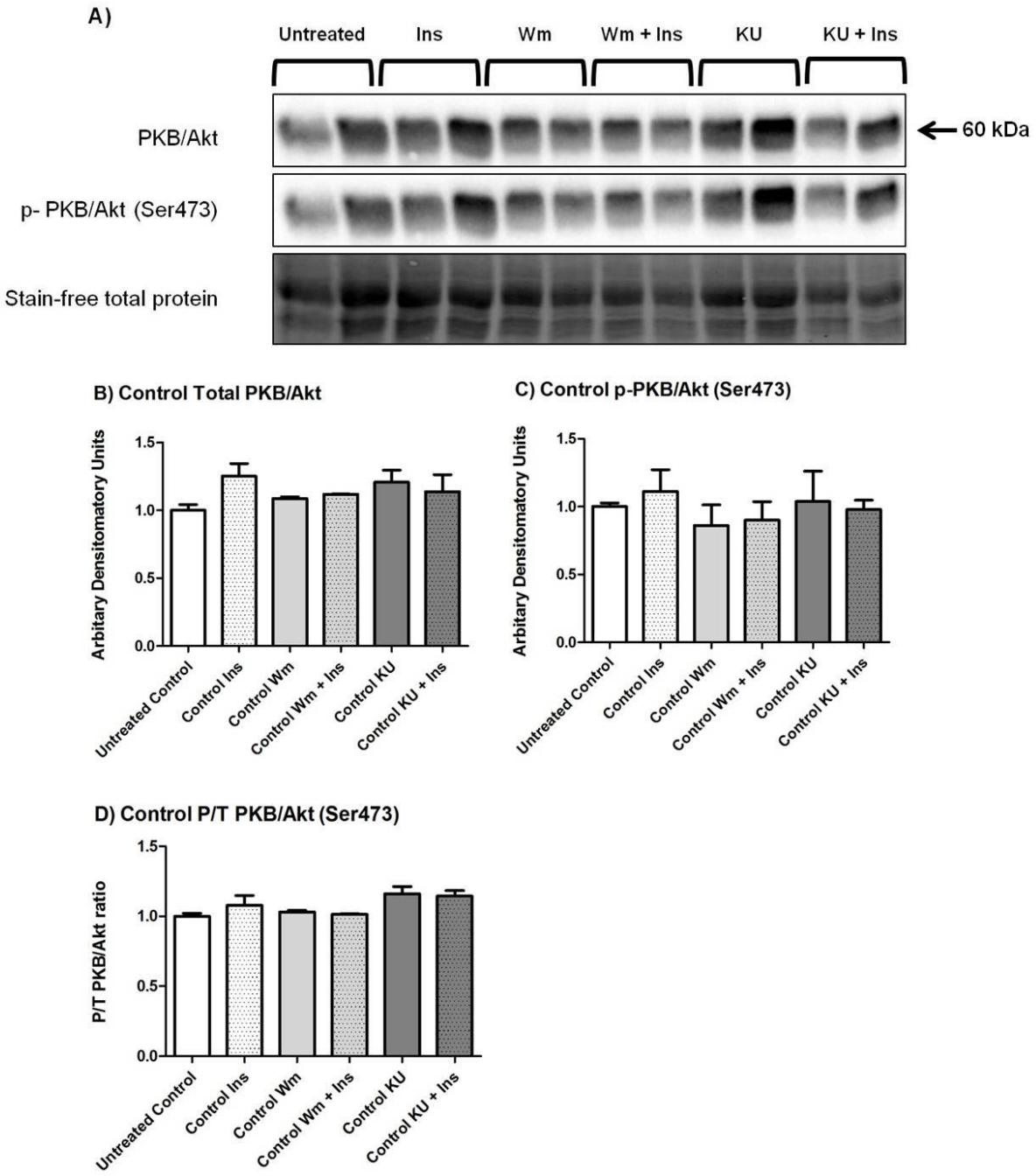

Figure 4.49: PKB/Akt expression and phosphorylation levels following ischaemia and reperfusion in control hearts treated with insulin, wortmannin and KU-60019. A) Representative western blot chemiluminescent results of PKB/Akt and p-PKB/Akt and stain-free total protein stain of the membrane. B) Bar graph depicting analysed results for total PKB/Akt. C) Bar graph depicting analysed results for p-PKB/Akt (Ser473). D) Bar graph depicting phospho to total ratio of PKB/Akt. (n=4 per group).

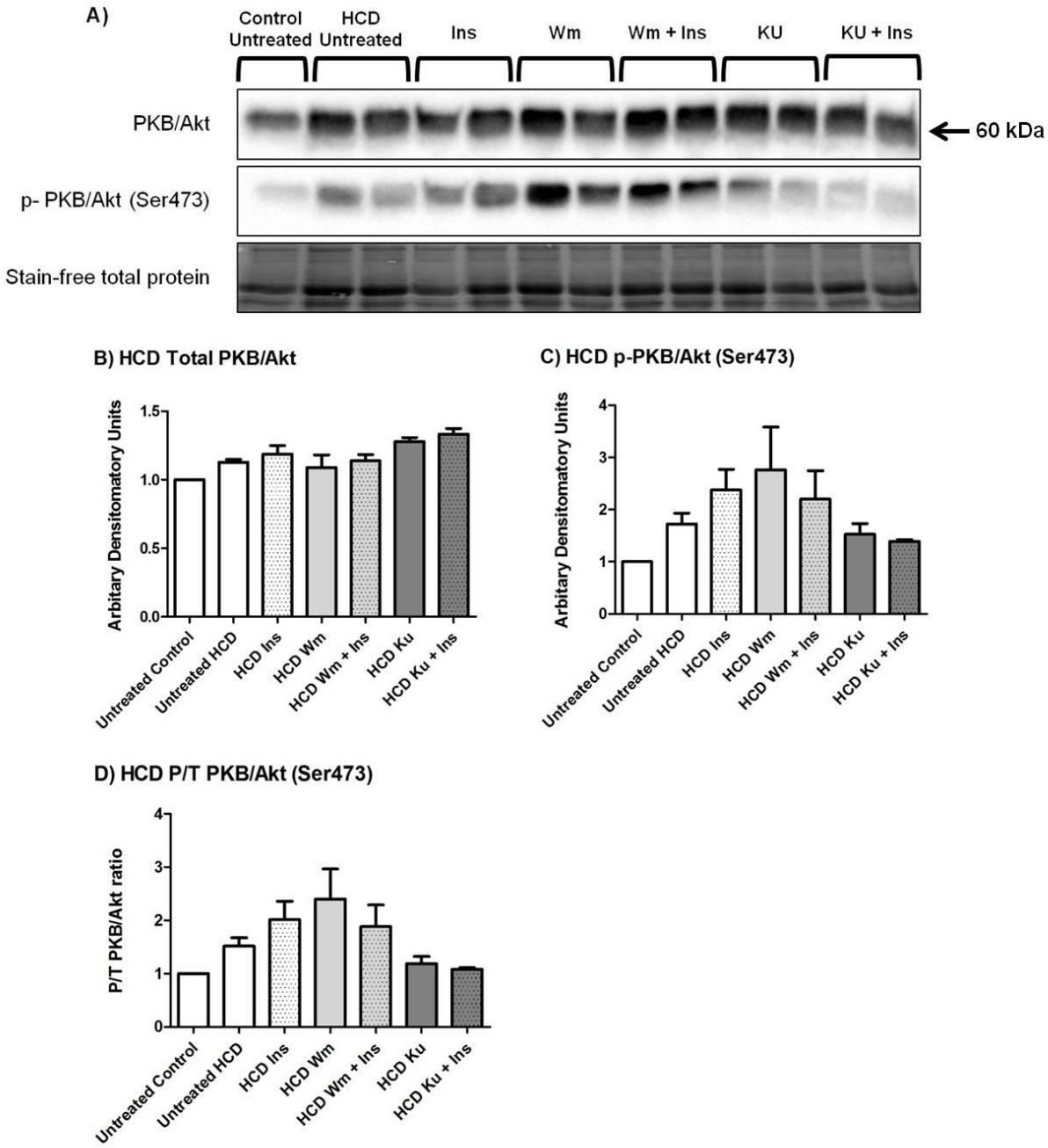

Figure 4.50: PKB/Akt expression and phosphorylation levels following ischaemia and reperfusion in HCD hearts treated with insulin, wortmannin and KU-60019. A) Representative western blot chemiluminescent results of PKB/Akt and p-PKB/Akt and stain-free total protein stain of the membrane. B) Bar graph depicting analysed results for total PKB/Akt. C) Bar graph depicting analysed results for p-PKB/Akt (Ser473). D) Bar graph depicting phospho to total ratio of PKB/Akt. (n=4 per group, except Control Untreated n=2).

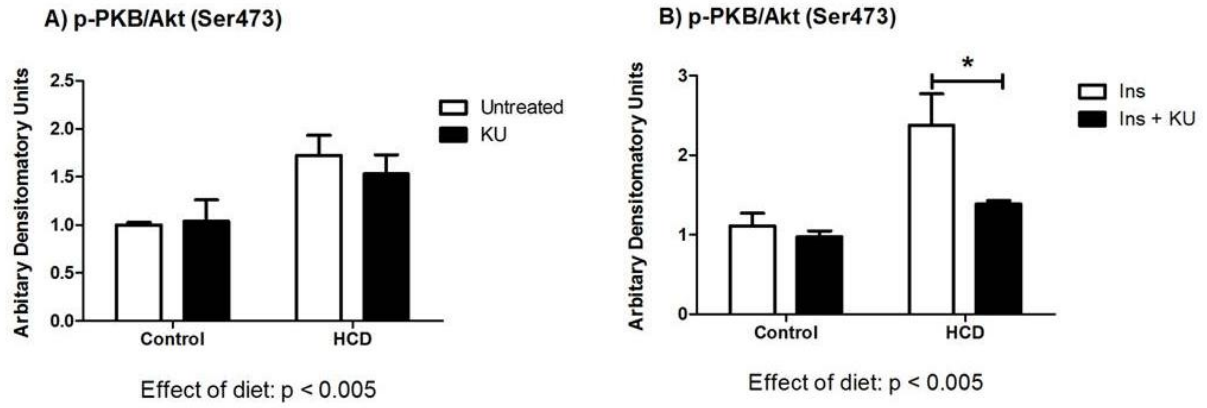

Figure 4.51: The effect of KU-60019 on PKB/Akt phosphorylation (Ser473). A) Two-way ANOVA to illustrate the effect of KU-60019 on PKB/Akt phosphorylation compared to untreated hearts in control and HCD hearts. B) Two-way ANOVA to illustrate the effect of KU-60019 on insulin stimulated PKB/Akt phosphorylation in control and HCD hearts. * $p < 0.05$ (n=4 per group).

mTOR

Expression and activation of mTOR was unaffected by the treatment groups in the control (Figure 4.52) and HCD (Figure 4.53) hearts. Treatment with KU-60019 had no effect on mTOR phosphorylation during reperfusion (Figure 4.54).

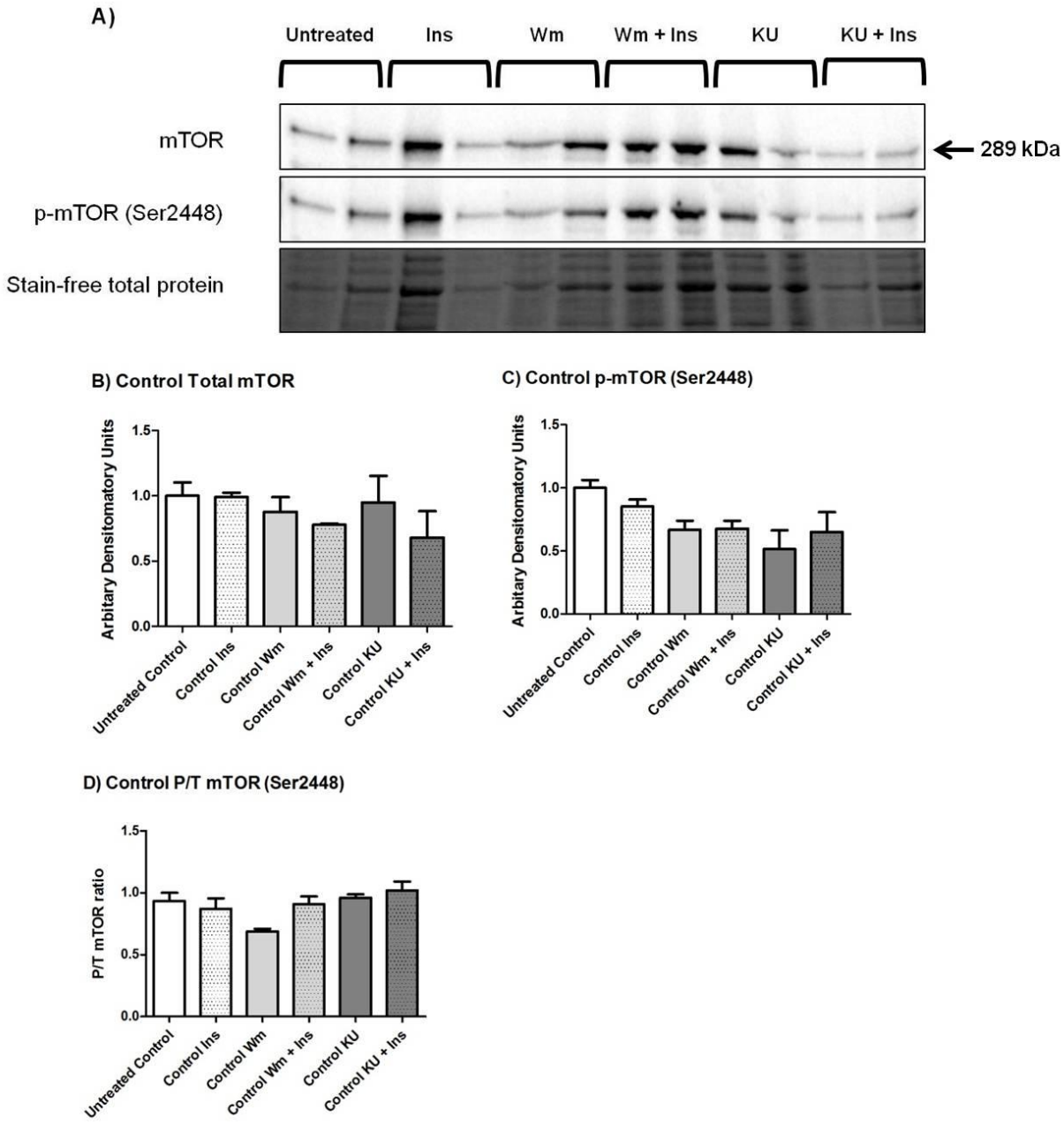

Figure 4.52: mTOR expression and phosphorylation levels following ischaemia and reperfusion in control hearts treated with insulin, wortmannin and KU-60019. A) Representative western blot chemiluminescent results of mTOR and p-mTOR and stain-free total protein stain of the membrane. B) Bar graph depicting analysed results for total mTOR. C) Bar graph depicting analysed results for p-mTOR (Ser2448). D) Bar graph depicting phospho to total ratio of mTOR. (n=4 per group).

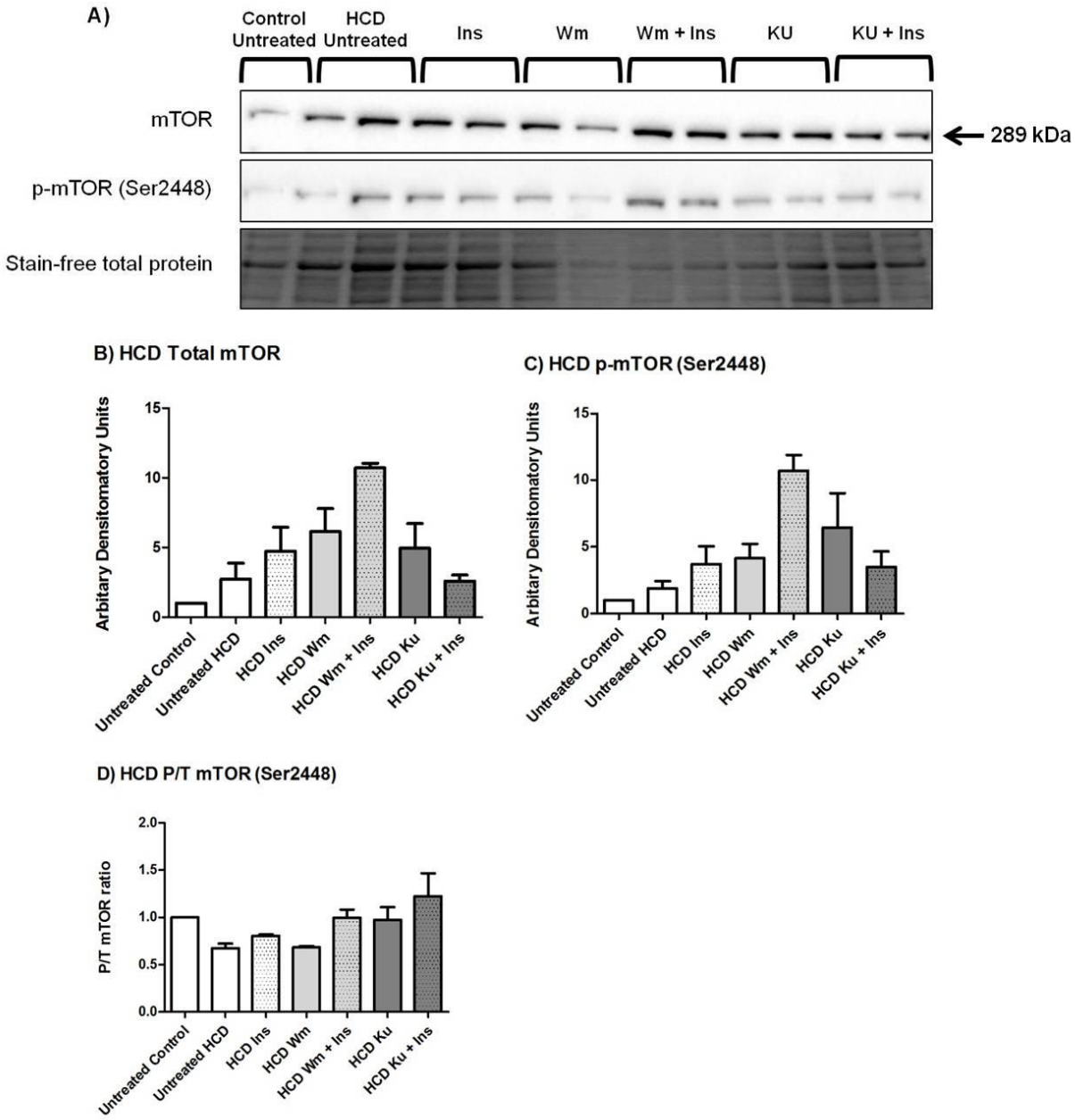

Figure 4.53: mTOR expression and phosphorylation levels following ischaemia and reperfusion in HCD hearts treated with insulin, wortmannin and KU-60019. A) Representative western blot chemiluminescent results of mTOR and p-mTOR and stain-free total protein stain of the membrane. B) Bar graph depicting analysed results for total mTOR. C) Bar graph depicting analysed results for p-mTOR (Ser2448). D) Bar graph depicting phospho to total ratio of mTOR. (n=4 per group, except Control Untreated n=2).

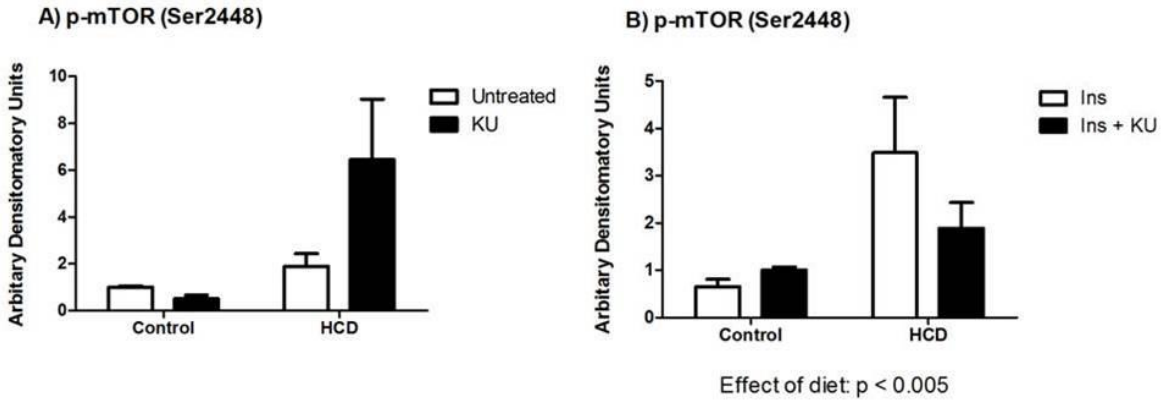

Figure 4.54: The effect of KU-60019 on mTOR phosphorylation (Ser2448). A) Two-way ANOVA to illustrate the effect of KU-60019 on mTOR phosphorylation compared to untreated hearts in control and HCD hearts. B) Two-way ANOVA to illustrate the effect of KU-60019 on insulin stimulated mTOR phosphorylation in control and HCD hearts. (n=4 per group).

GSK-3β

In control hearts, total GSK-3β was unaffected by the treatment groups during reperfusion. Treatment with wortmannin resulted in significantly reduced phosphorylation of GSK-3β compared to the untreated group (Untreated 1.00 ± 0.07; Wm 0.52 ± 0.11; $p < 0.05$). The P/T GSK-3β ratio was unchanged by the treatments in control hearts (Figure 4.55). The untreated HCD hearts had higher total GSK-3β levels compared to the untreated control hearts (Untreated control 1.00; Untreated HCD 1.56 ± 0.07; $p < 0.05$). Treatment with wortmannin significantly reduced total GSK-3β levels during reperfusion in HCD hearts (Untreated 1.56 ± 0.07; Wm 0.96 ± 0.15; $p < 0.05$). Phosphorylation of GSK-3β and the P/T ratios were unchanged by the treatment groups following IRI in HCD hearts (Figure 4.56). Treatment with KU-60019 had no effect on GSK-3β phosphorylation during reperfusion (Figure 4.57).

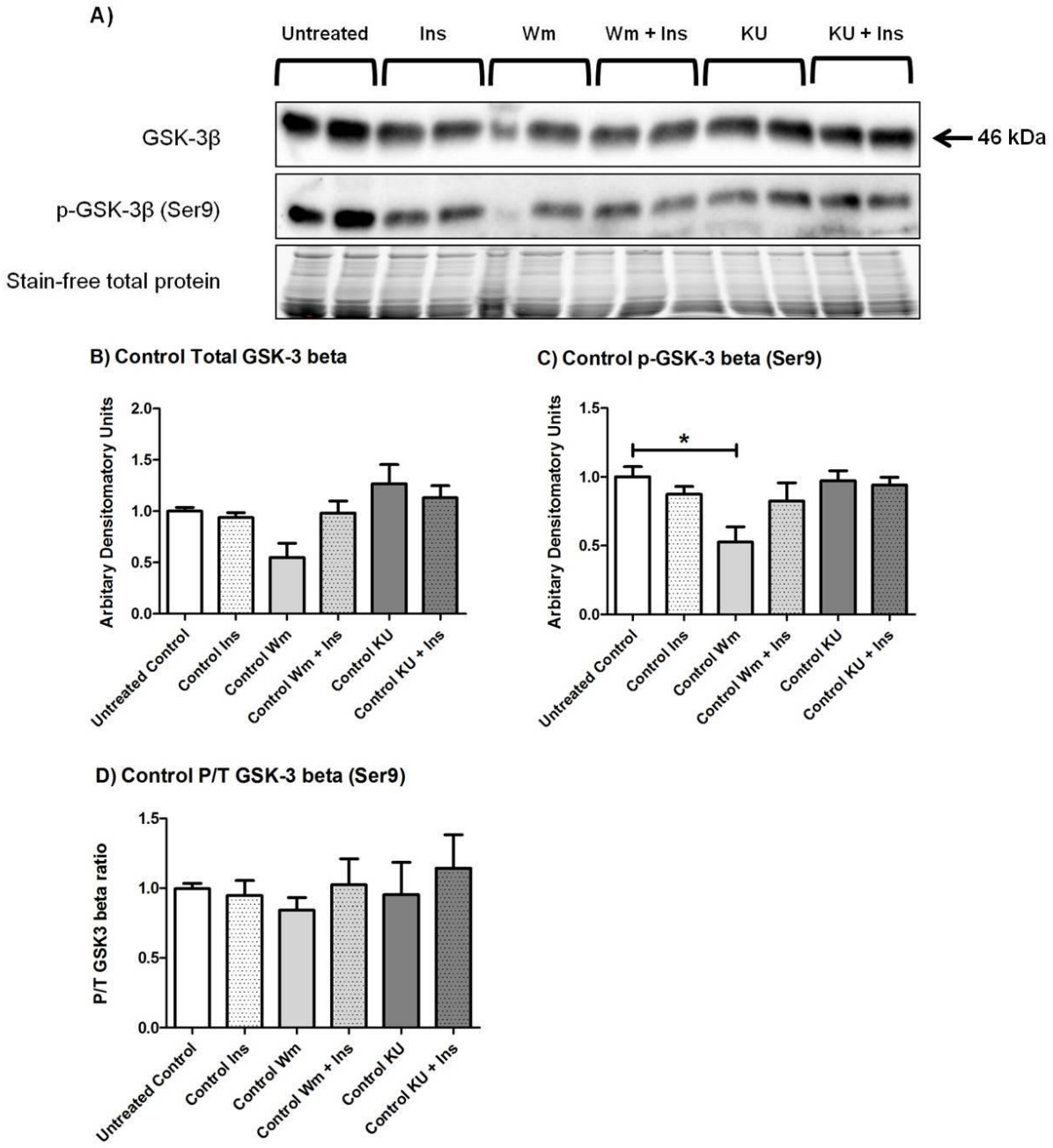

Figure 4.55: GSK-3β expression and phosphorylation levels following ischaemia and reperfusion in control hearts treated with insulin, wortmannin and KU-60019. A) Representative western blot chemiluminescent results of GSK-3β and p-GSK-3β and stain-free total protein stain of the membrane. B) Bar graph depicting analysed results for total GSK-3β. C) Bar graph depicting analysed results for p-GSK-3β (Ser9). D) Bar graph depicting phospho to total ratio of GSK-3β. * $p < 0.05$ (n=4 per group).

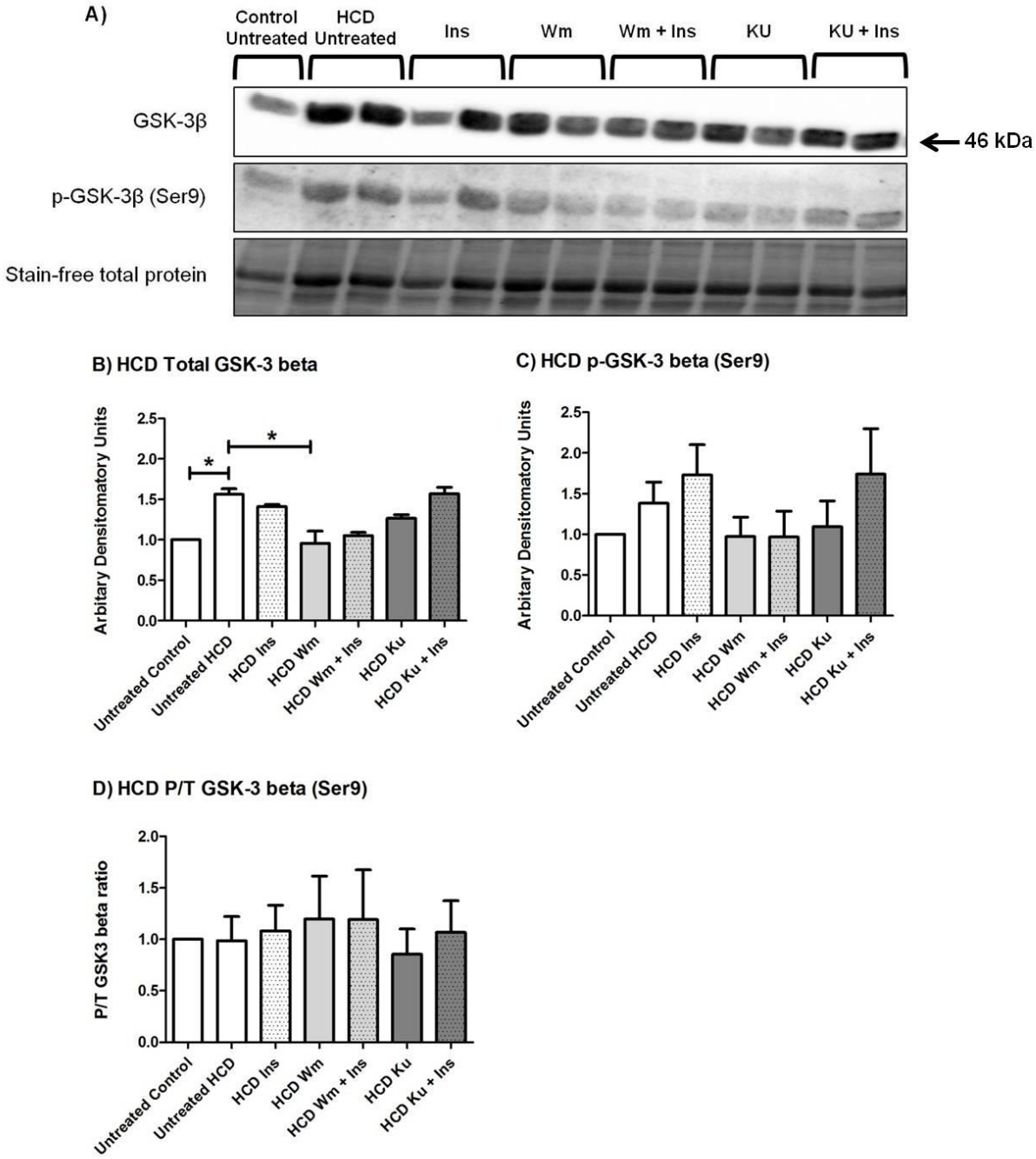

Figure 4.56: GSK-3β expression and phosphorylation levels following ischaemia and reperfusion in HCD hearts treated with insulin, wortmannin and KU-60019. A) Representative western blot chemiluminescent results of GSK-3β and p-GSK-3β and stain-free total protein stain of the membrane. B) Bar graph depicting analysed results for total GSK-3β. C) Bar graph depicting analysed results for p-GSK-3β (Ser9). D) Bar graph depicting phospho to total ratio of GSK-3β. * $p < 0.05$ (n=4 per group, except Control Untreated n=2).

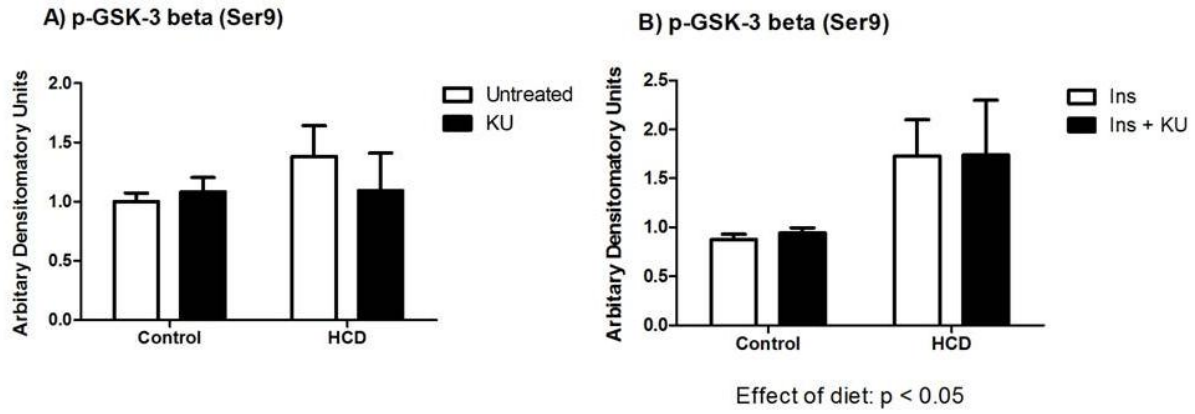

Figure 4.57: The effect of KU-60019 on GSK-3β phosphorylation (Ser9). A) Two-way ANOVA to illustrate the effect of KU-60019 on GSK-3β phosphorylation compared to untreated hearts in control and HCD hearts. B) Two-way ANOVA to illustrate the effect of KU-60019 on insulin stimulated GSK-3β phosphorylation in control and HCD hearts. (n=4 per group).

AS160

There were no changes in total AS160 or phosphorylation of AS160 in control hearts during reperfusion. The P/T ratios were also unchanged (Figure 4.58). Untreated HCD hearts had a significantly lower P/T AS160 ratio compared to untreated control hearts (Untreated control 1.00; Untreated HCD 0.30 ± 0.04; $p < 0.05$) (Figure 4.59 D). Total AS160 was unaffected by the treatment groups during reperfusion. Treatment with KU-60019 significantly increased insulin-stimulated AS160 phosphorylation during reperfusion (Figures 4.59 C and 4.60 B).

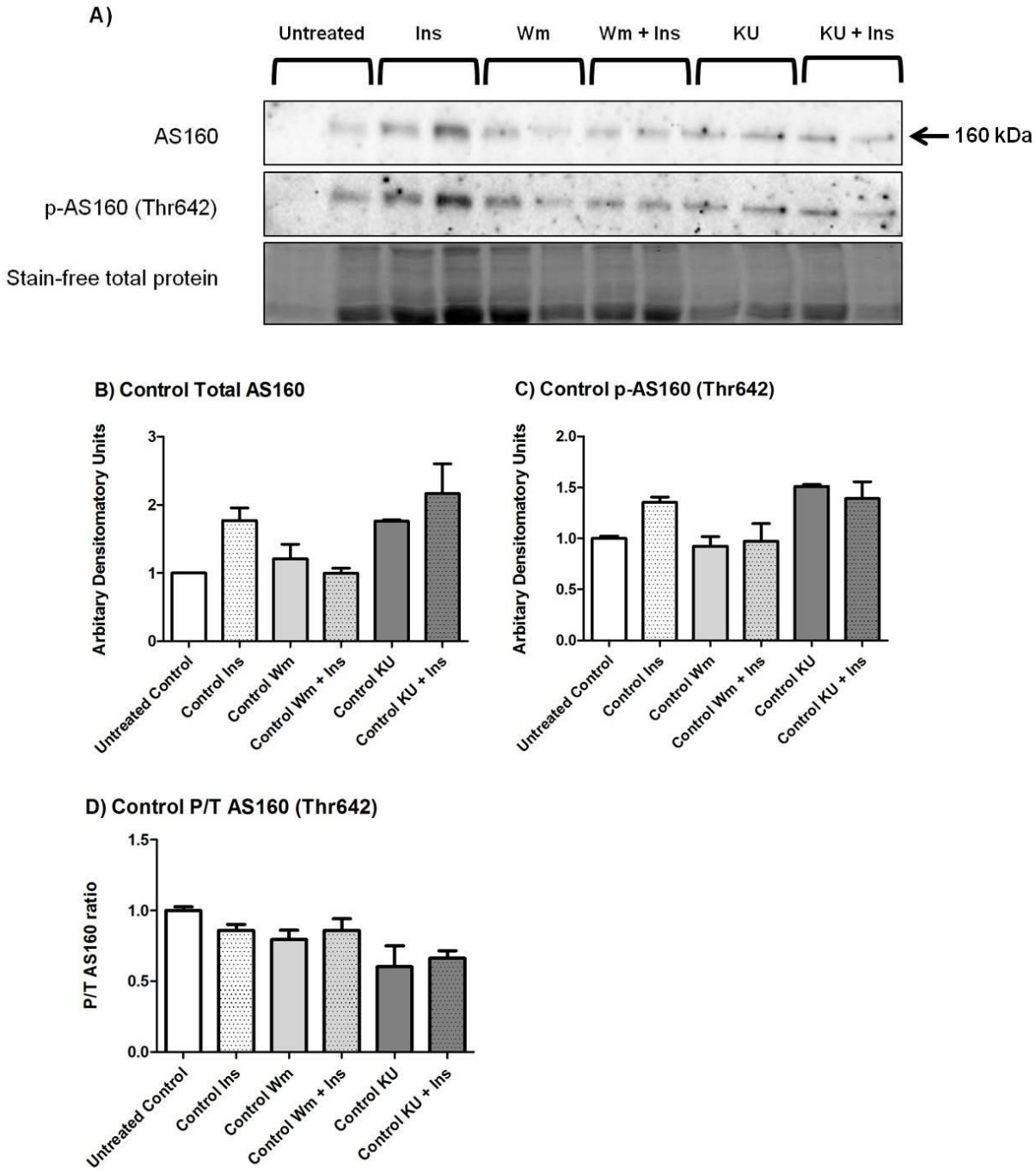

Figure 4.58: AS160 expression and phosphorylation levels following ischaemia and reperfusion in control hearts treated with insulin, wortmannin and KU-60019. A) Representative western blot chemiluminescent results of AS160 and p-AS160 and stain-free total protein stain of the membrane. B) Bar graph depicting analysed results for total AS160. C) Bar graph depicting analysed results for p-AS160 (Thr642). D) Bar graph depicting phospho to total ratio of AS160. (n=4 per group).

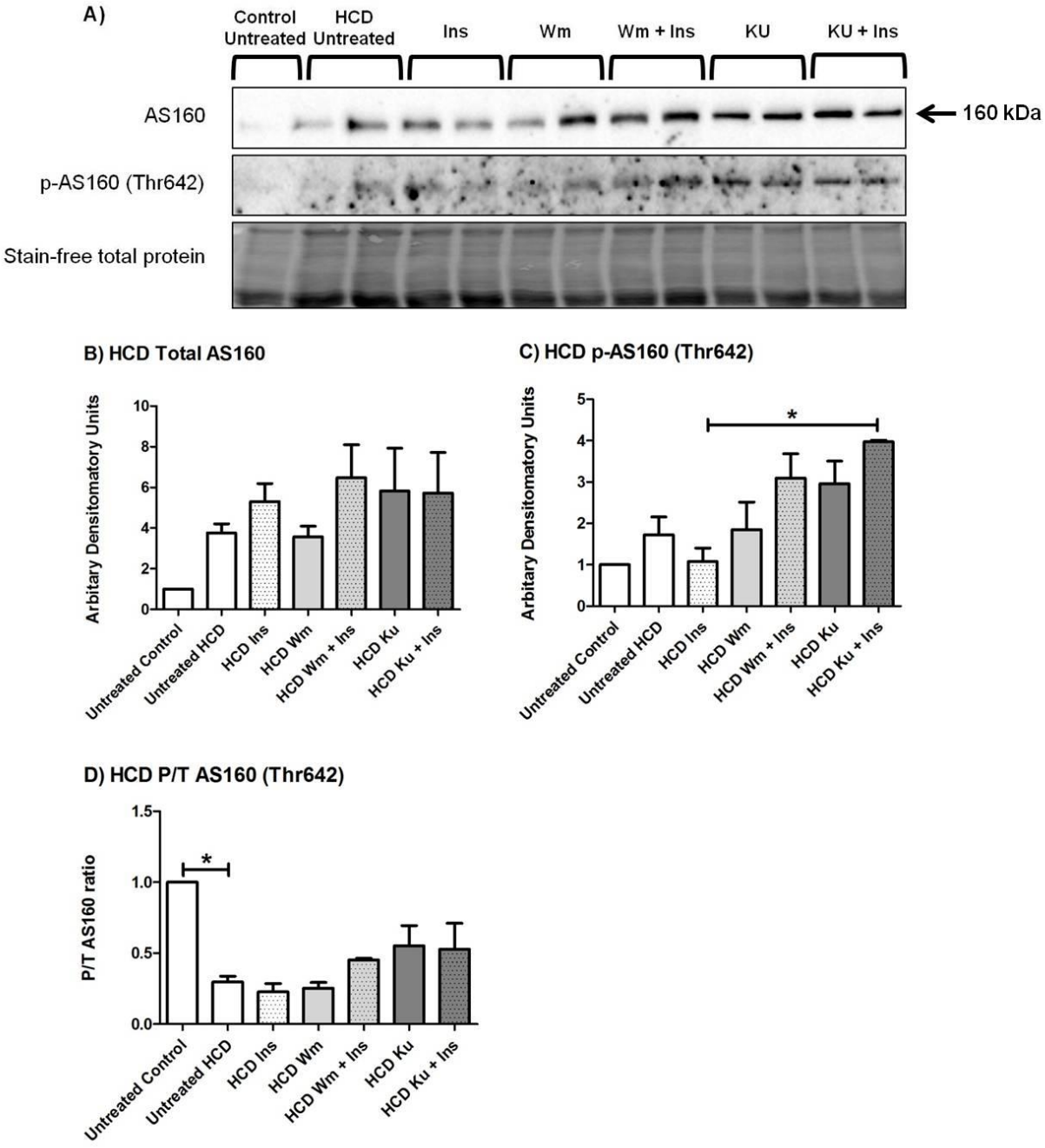

Figure 4.59: AS160 expression and phosphorylation levels following ischaemia and reperfusion in HCD hearts treated with insulin, wortmannin and KU-60019. A) Representative western blot chemiluminescent results of AS160 and p-AS160 and stain-free total protein stain of the membrane. B) Bar graph depicting analysed results for total AS160. C) Bar graph depicting analysed results for p-AS160 (Thr642). D) Bar graph depicting phospho to total ratio of AS160. * $p < 0.05$ (n=4 per group, except Control Untreated n=2).

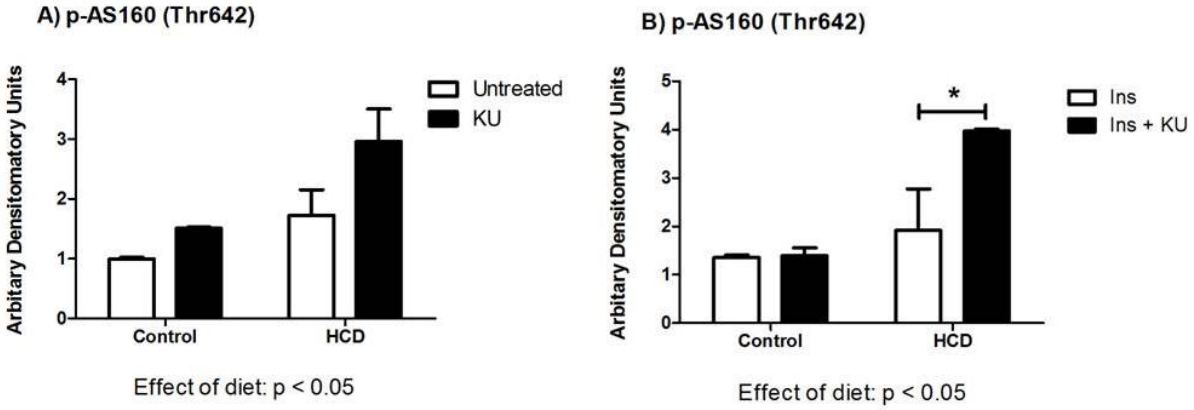

Figure 4.60: The effect of KU-60019 on AS160 phosphorylation (Thr642). A) Two-way ANOVA to illustrate the effect of KU-60019 on AS160 phosphorylation compared to untreated hearts in control and HCD hearts. B) Two-way ANOVA to illustrate the effect of KU-60019 on insulin stimulated AS160 phosphorylation in control and HCD hearts. * $p < 0.05$ (n=4 per group).

GLUT4

Total GLUT4 levels were similar in all the treatment groups during reperfusion in both the age-matched control and HCD hearts (Figure 4.61).

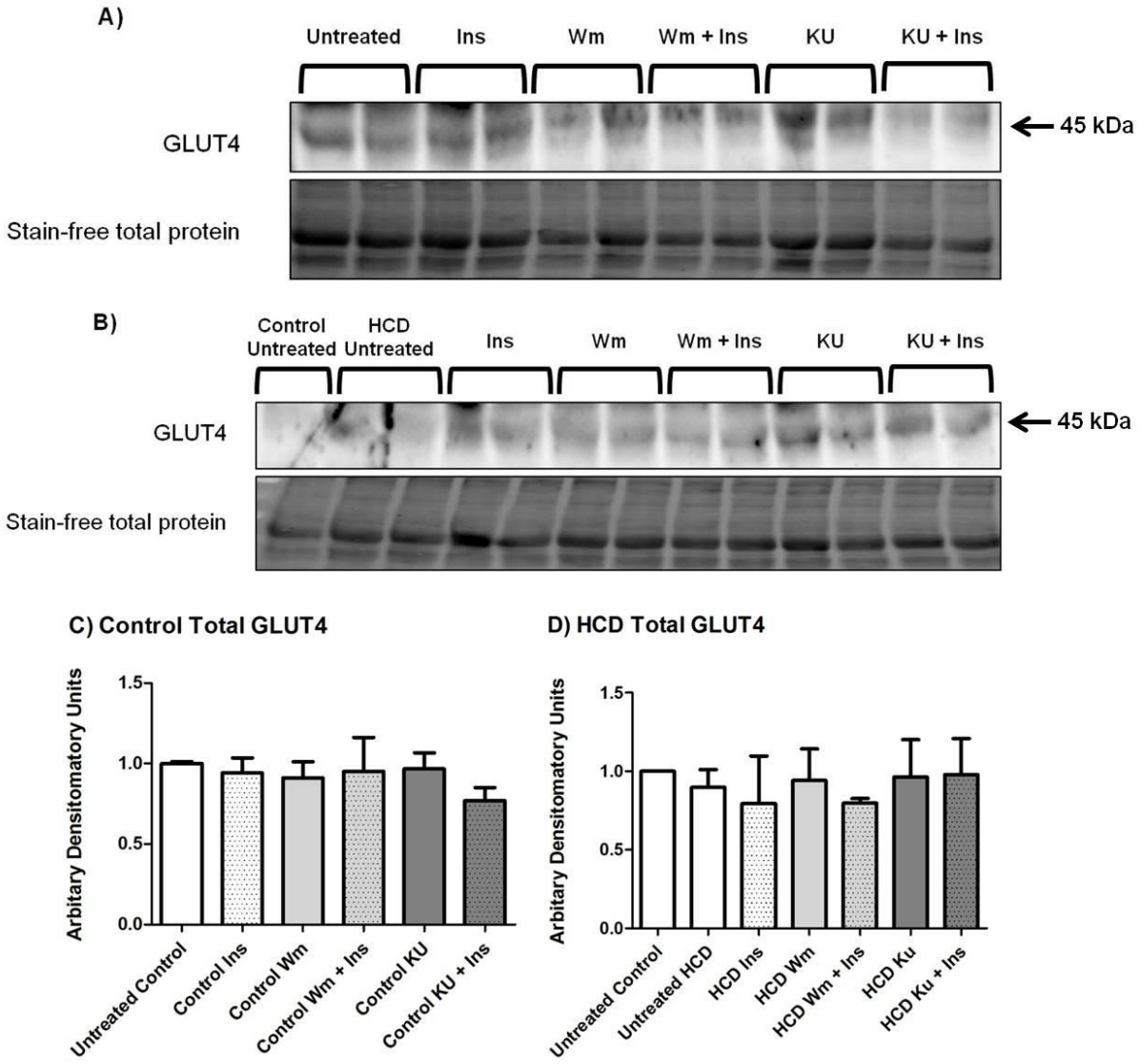

Figure 4.61: Total GLUT4 expression levels following ischaemia and reperfusion in hearts treated with insulin, wortmannin and KU-60019. A) Representative western blot chemiluminescent results of GLUT4 and stain-free total protein stain of the membrane of age-matched control hearts. B) Representative western blot chemiluminescent results of GLUT4 and stain-free total protein stain of the membrane of HCD hearts C) Bar graph depicting analysed results for total GLUT4 in age-matched control hearts. (n=4 per group). D) Bar graph depicting analysed results for total GLUT4 in HCD hearts. (n=4 per group, except Control Untreated n=2).

AMPK

Total AMPK, AMPK phosphorylation and the P/T AMPK ratios were unchanged by the treatment groups in both the control (Figure 4.62) and HCD (Figure 4.63) hearts. Treatment with KU-60019 had no effect on AMPK phosphorylation (Figure 4.64).

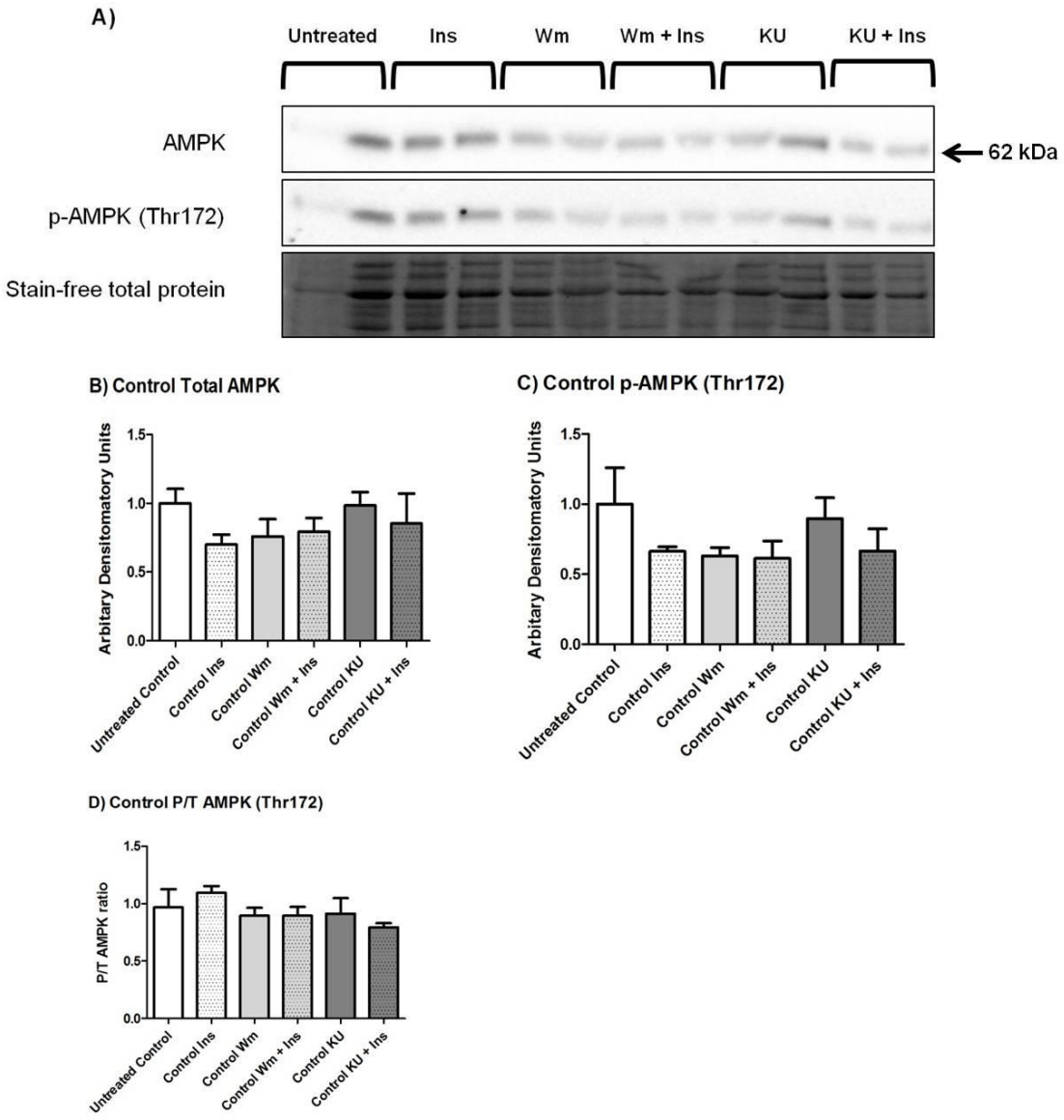

Figure 4.62: AMPK expression and phosphorylation levels following ischaemia and reperfusion in control hearts treated with insulin, wortmannin and KU-60019. A) Representative western blot chemiluminescent results of AMPK and p-AMPK and stain-free total protein stain of the membrane. B) Bar graph depicting analysed results for total AMPK. C) Bar graph depicting analysed results for p-AMPK (Thr172). D) Bar graph depicting phospho to total ratio of AMPK. (n=4 per group).

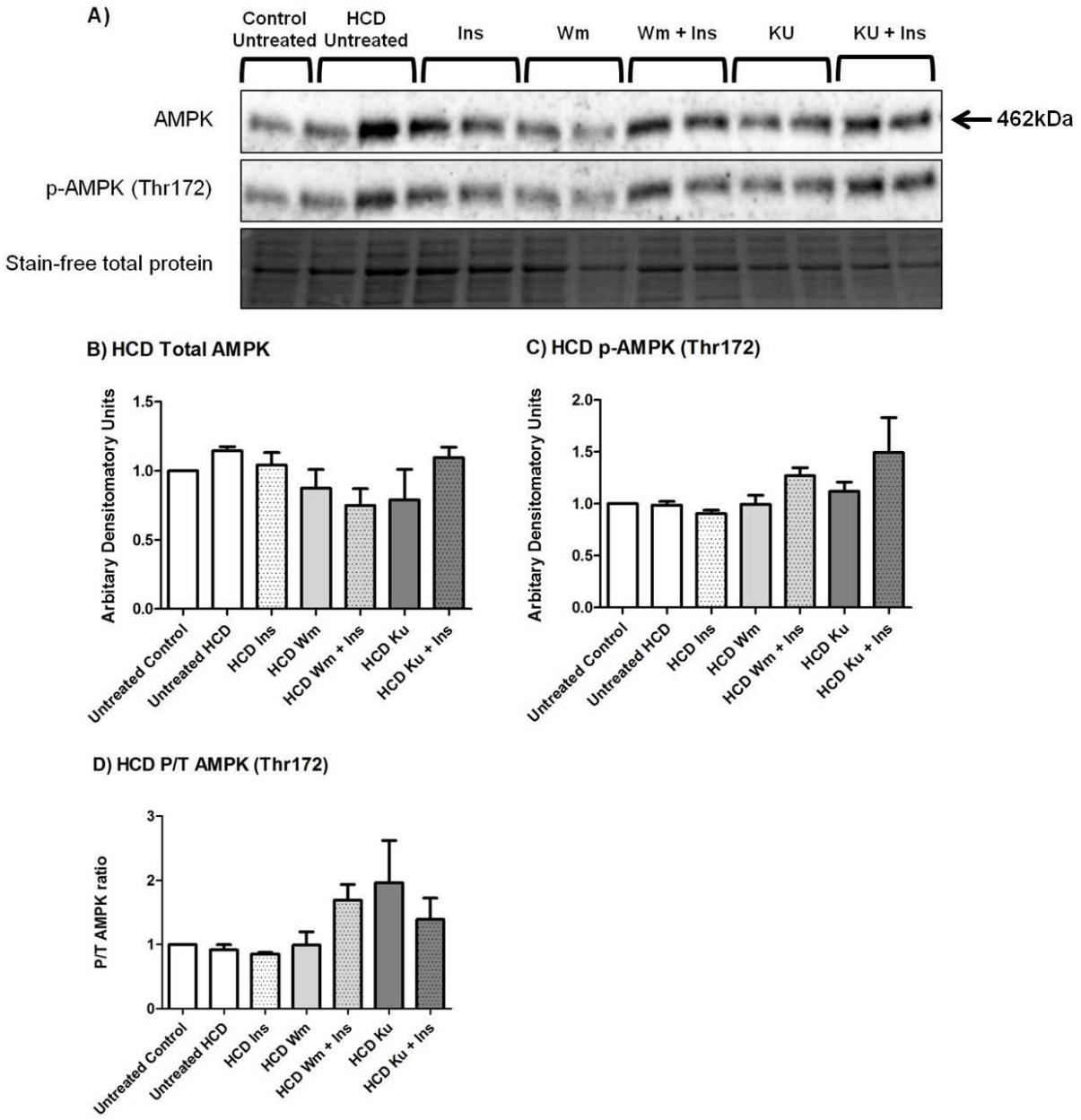

Figure 4.63: AMPK expression and phosphorylation levels following ischaemia and reperfusion in HCD hearts treated with insulin, wortmannin and KU-60019. A) Representative western blot chemiluminescent results of AMPK and p-AMPK and stain-free total protein stain of the membrane. B) Bar graph depicting analysed results for total AMPK. C) Bar graph depicting analysed results for p-AMPK (Thr172). D) Bar graph depicting phospho to total ratio of AMPK. (n=4 per group, except Control Untreated n=2).

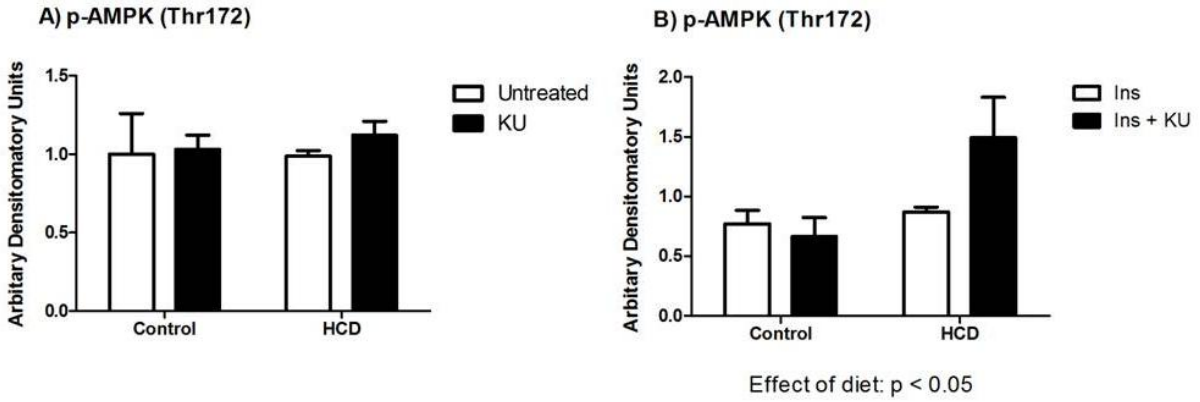

Figure 4.64: The effect of KU-60019 on AMPK phosphorylation (Thr172). A) Two-way ANOVA to illustrate the effect of KU-60019 on AMPK phosphorylation compared to untreated hearts in control and HCD hearts. B) Two-way ANOVA to illustrate the effect of KU-60019 on insulin stimulated AMPK phosphorylation in control and HCD hearts. (n=4 per group).

ACC

KU-60019 treatment increased total ACC levels in control hearts compared to the untreated control hearts (Untreated 1.00 ± 0.13; KU 3.31 ± 0.49; $p < 0.005$). None of the other treatment groups affected total ACC levels (Figure 4.65 B) and there were no changes in ACC phosphorylation during reperfusion in control hearts (Figure 4.65 C). Compared to untreated control hearts, the P/T ACC ratio was reduced in response to treatment with insulin (Untreated 0.99 ± 0.04; Ins 0.40 ± 0.03; $p < 0.0001$), wortmannin (Untreated 0.99 ± 0.04; Wm 0.37 ± 0.03; $p < 0.0001$) and KU-60019 (Untreated 0.99 ± 0.04; KU 0.56 ± 0.07; $p < 0.005$). Co-treatment with KU-60019 and insulin resulted in a higher P/T ratio compared to treatment with insulin alone (Ins 0.40 ± 0.03; KU + Ins 0.88 ± 0.09; $p < 0.0001$) or KU-60019 alone (KU 0.56 ± 0.07; KU + Ins 0.88 ± 0.09; $p < 0.05$) (Figure 4.65 D). Total ACC, ACC phosphorylation and the P/T ACC ratios were unchanged during reperfusion by all the treatment groups in HCD hearts (Figure 4.66). When a two-way ANOVA is performed, it is revealed that KU-60019 treatment significantly increased the phosphorylation of ACC in HCD hearts compared to untreated HCD hearts (Figure 4.67 A).

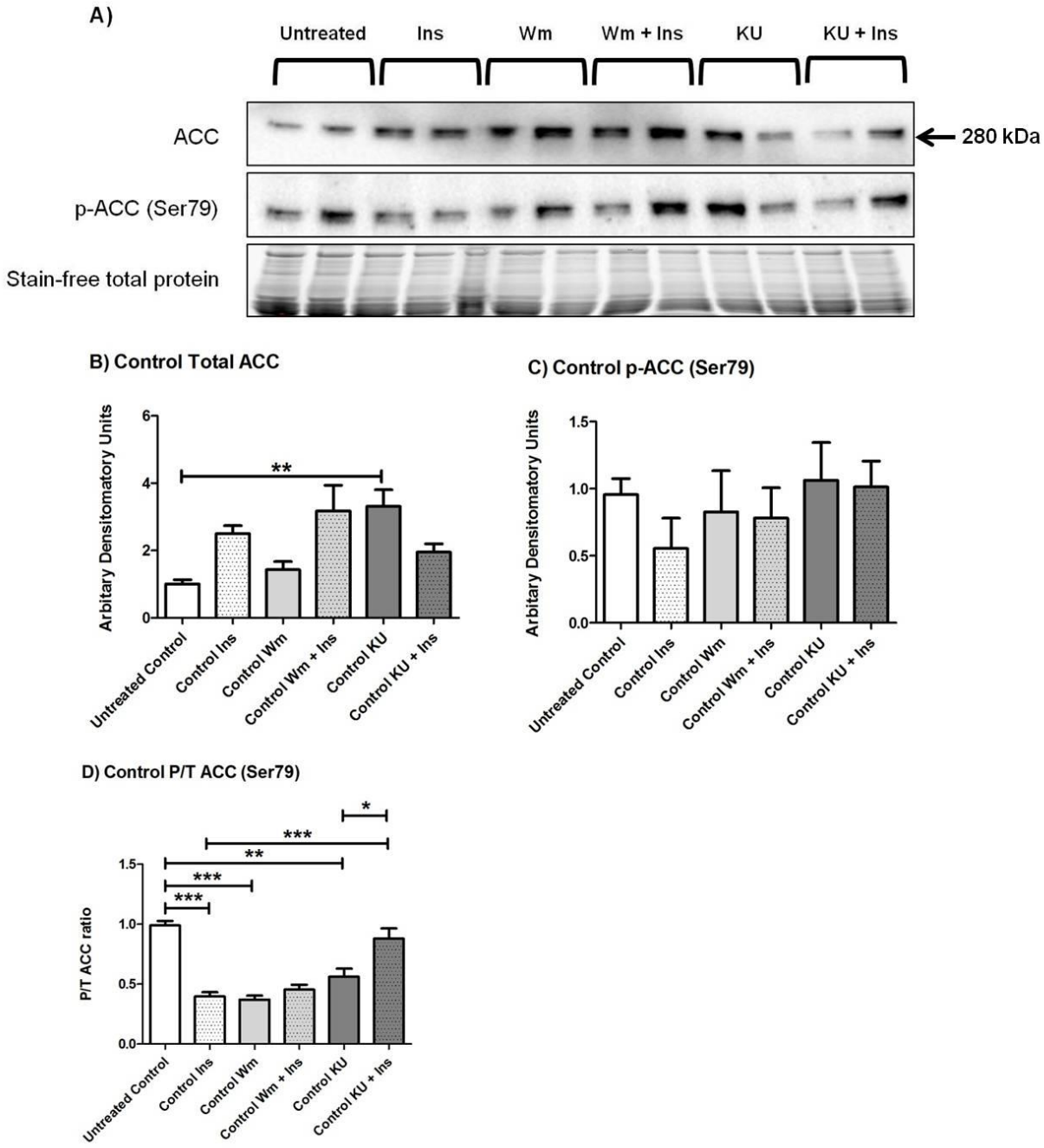

Figure 4.65: ACC expression and phosphorylation levels following ischaemia and reperfusion in control hearts treated with insulin, wortmannin and KU-60019. A) Representative western blot chemiluminescent results of ACC and p-ACC and stain-free total protein stain of the membrane. B) Bar graph depicting analysed results for total ACC. C) Bar graph depicting analysed results for p-ACC (Ser79). D) Bar graph depicting phospho to total ratio of ACC. * $p < 0.05$; ** $p < 0.005$; *** $p < 0.0001$ (n=4 per group).

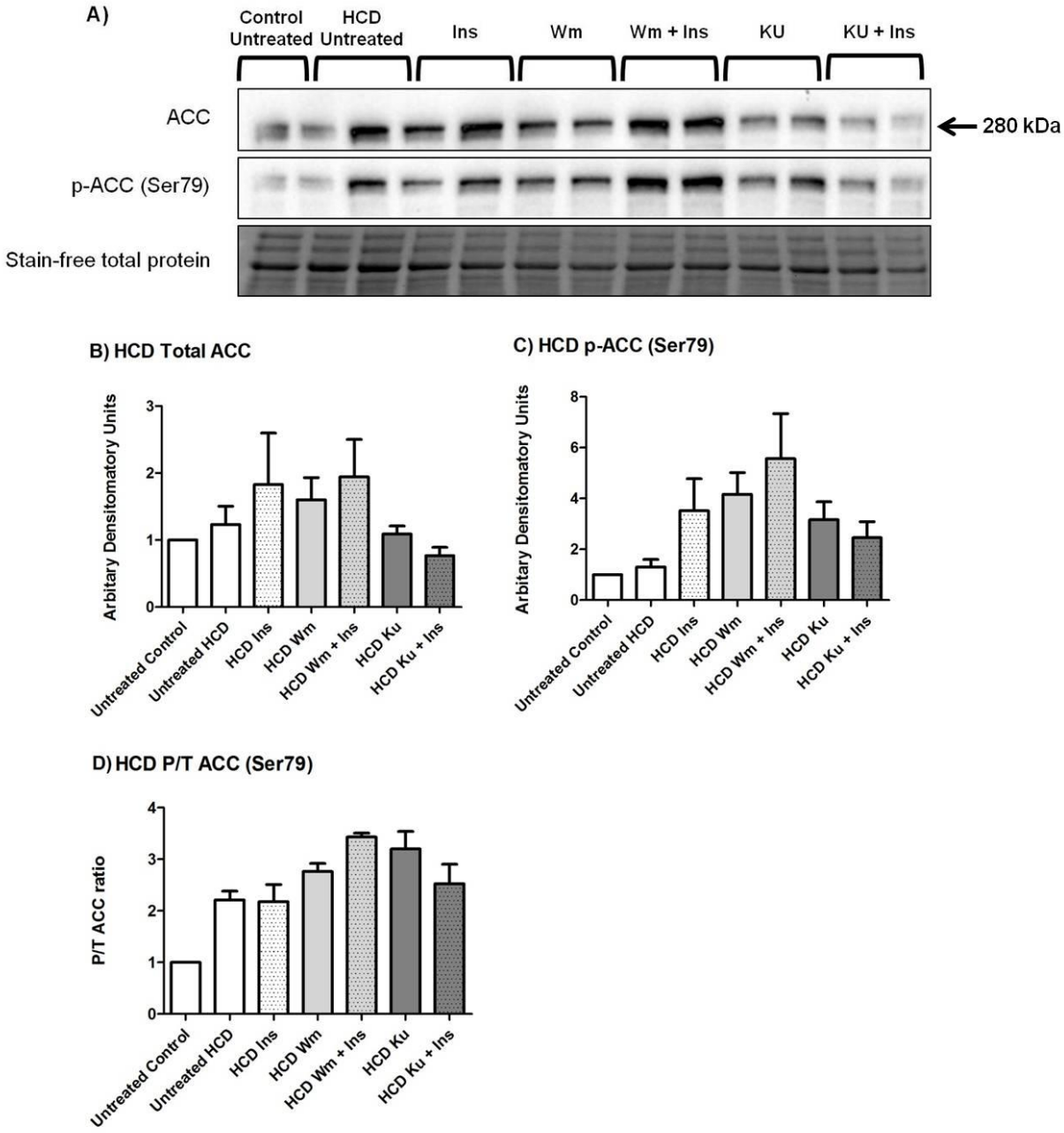

Figure 4.66: ACC expression and phosphorylation levels following ischaemia and reperfusion in HCD hearts treated with insulin, wortmannin and KU-60019. A) Representative western blot chemiluminescent results of ACC and p-ACC and stain-free total protein stain of the membrane. B) Bar graph depicting analysed results for total ACC. C) Bar graph depicting analysed results for p-ACC (Ser79). D) Bar graph depicting phospho to total ratio of ACC. (n=4 per group, except Control Untreated n=2).

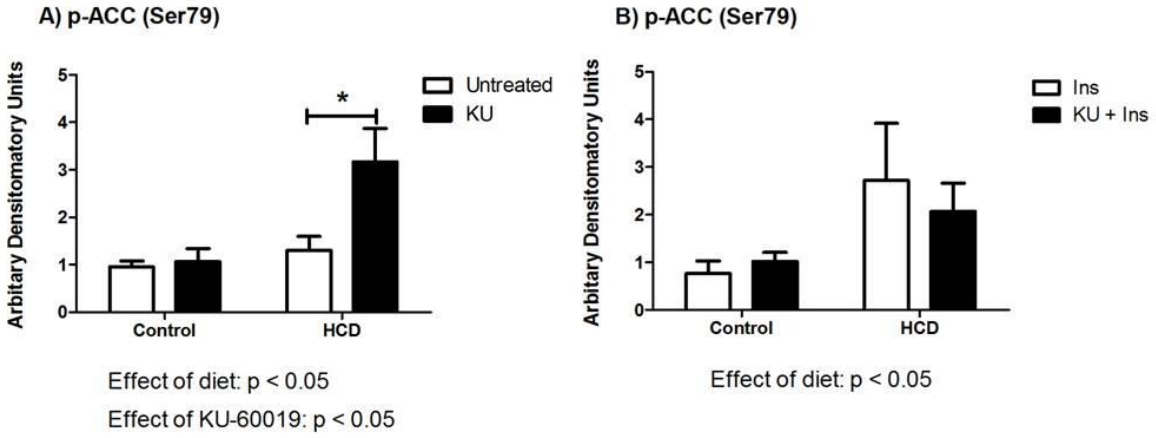

Figure 4.67: The effect of KU-60019 on ACC phosphorylation (Ser79). A) Two-way ANOVA to illustrate the effect of KU-60019 on ACC phosphorylation compared to untreated hearts in control and HCD hearts. B) Two-way ANOVA to illustrate the effect of KU-60019 on insulin stimulated ACC phosphorylation in control and HCD hearts. (n=4 per group).

ATM

Total ATM, ATM phosphorylation and the P/T ATM ratios were unchanged by the treatment groups in both the control (Figure 4.68) and HCD (Figure 4.69) hearts. Treatment with KU-60019 had no effect on ATM phosphorylation during reperfusion (Figure 4.70).

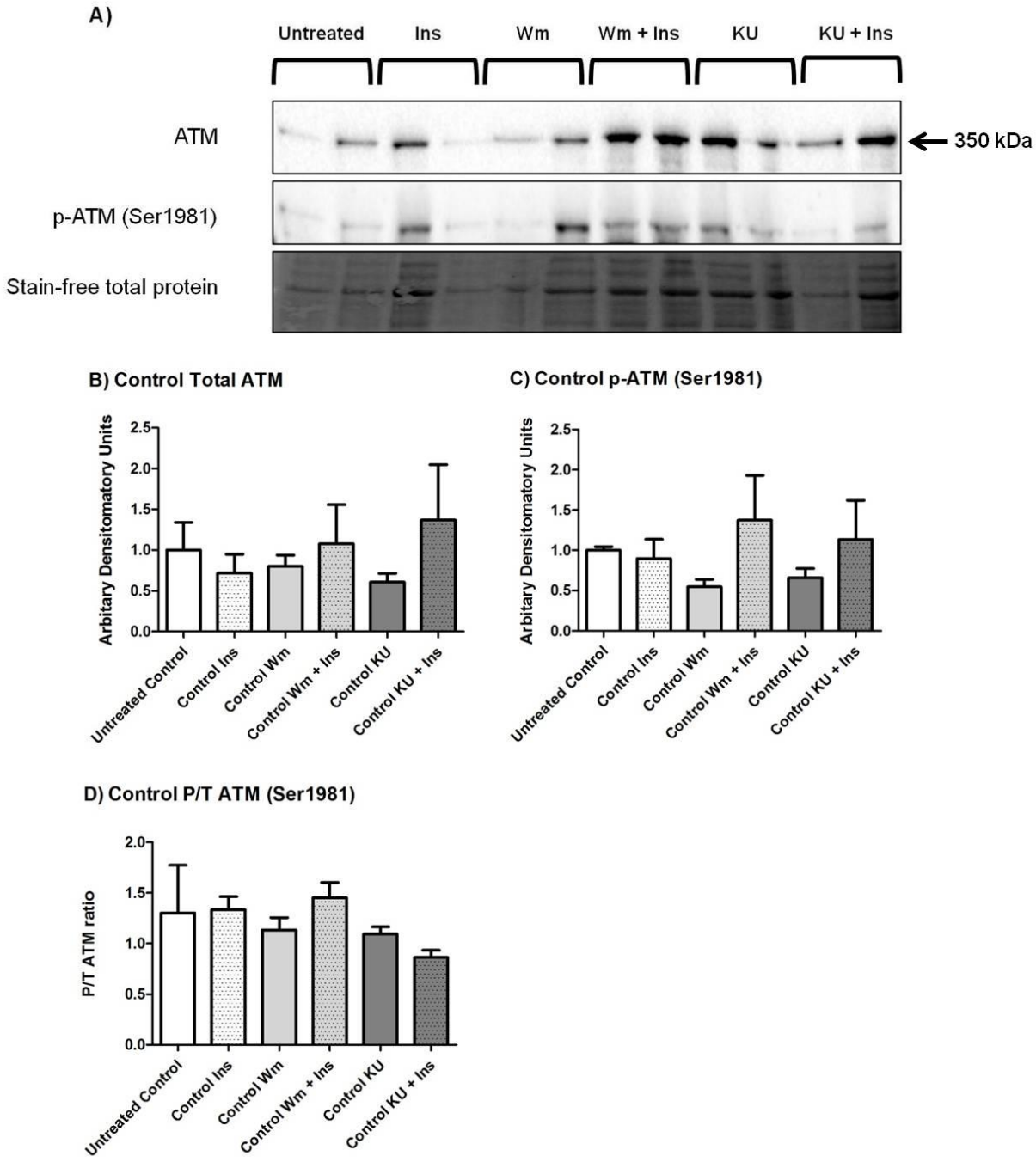

Figure 4.68: ATM expression and phosphorylation levels following ischaemia and reperfusion in control hearts treated with insulin, wortmannin and KU-60019. A) Representative western blot chemiluminescent results of ATM and p-ATM and stain-free total protein stain of the membrane. B) Bar graph depicting analysed results for total ATM. C) Bar graph depicting analysed results for p-ATM (Ser1981). D) Bar graph depicting phospho to total ratio of ATM. (n=4 per group).

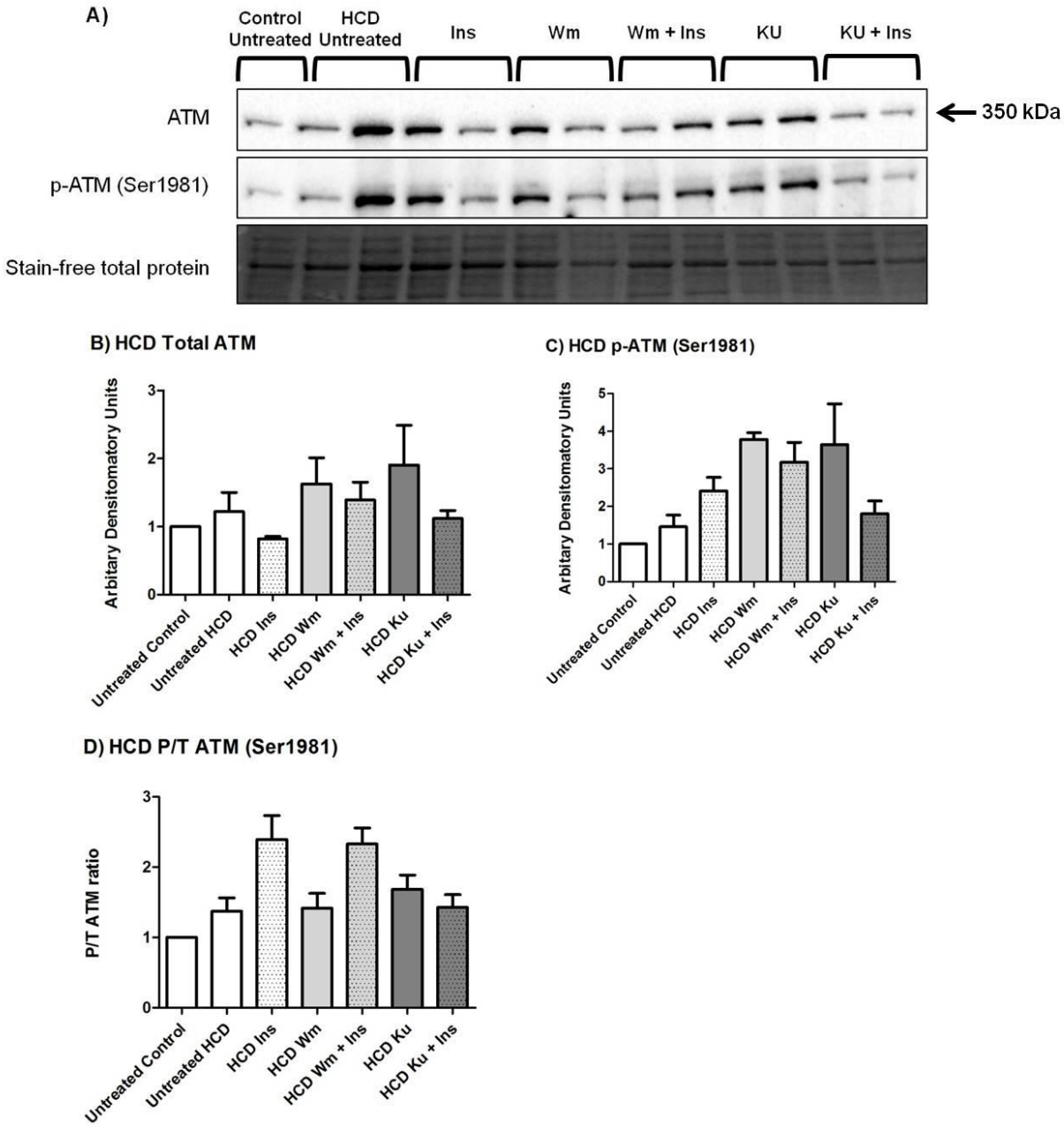

Figure 4.69: ATM expression and phosphorylation levels following ischaemia and reperfusion in HCD hearts treated with insulin, wortmannin and KU-60019. A) Representative western blot chemiluminescent results of ATM and p-ATM and stain-free total protein stain of the membrane. B) Bar graph depicting analysed results for total ATM. C) Bar graph depicting analysed results for p-ATM (Ser1981). D) Bar graph depicting phospho to total ratio of ATM. (n=4 per group, except Control Untreated n=2).

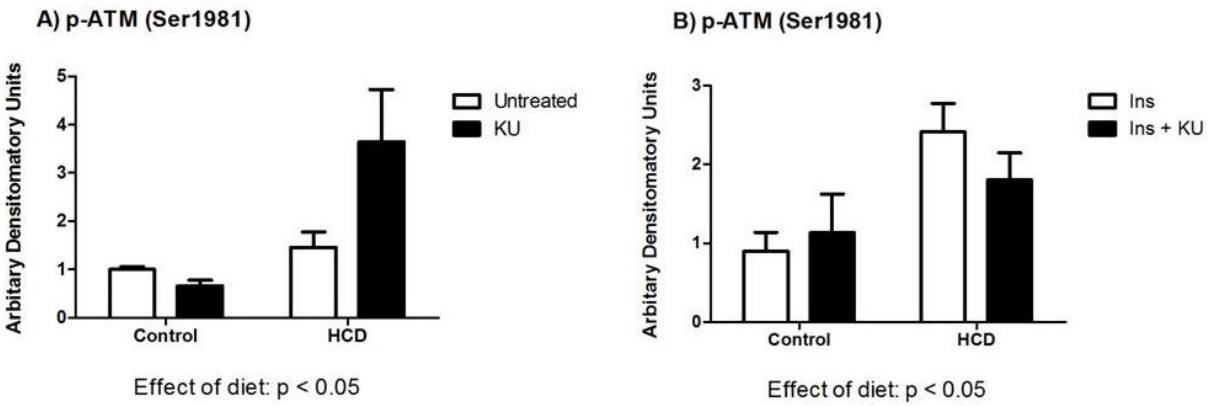

Figure 4.70: The effect of KU-60019 on ATM phosphorylation (Ser1981). A) Two-way ANOVA to illustrate the effect of KU-60019 on ATM phosphorylation compared to untreated hearts in control and HCD hearts. B) Two-way ANOVA to illustrate the effect of KU-60019 on insulin stimulated ATM phosphorylation in control and HCD hearts. (n=4 per group).

4.5 *Ex vivo* working heart perfusions

Hearts were isolated from animals that have been on the HCD for 16 weeks as well as from age-matched control animals. The hearts were perfused in an *ex vivo* fashion and exposed to IRI in order to assess cardiac function before and after IRI as well as the resultant IFS. Cardiac function was assessed after 25 minutes of reperfusion. The hearts were also exposed to various pharmaceutical agents, such as insulin (1 U/L), wortmannin (100nM) and KU-60019 (3 μM), prior to being subjected to IRI in order to manipulate the ATM signalling and to assess the effect thereof on cardiac functioning and IFS. Infarct sizes are displayed as percentage of the AAR with AAR being 51.58 ± 0.73% and not varying between all groups.

4.5.1 The effect of the HCD on cardiac function and infarct size following IRI

The HCD had no effect on any of the measured parameters of cardiac function before or after IRI in untreated hearts compared to the control diet (Table 4.8). Ischaemia/reperfusion injury did, however, significantly reduce AO, heart rate, SP, DP and total work performed by both control and HCD hearts (Table 4.8). Out of the control hearts, 43% did not show functional

recovery following IRI, while 51% of the HCD hearts did not have any functional recovery following IRI. There was no significant difference in IFS between the two groups (Control 33.24 ± 2.6%; HCD 30.60 ± 2.7%; p=0.49) (Figure 4.71).

Table 4.8: Cardiac function before and after ischaemia/reperfusion injury in untreated control and HCD hearts (n=7-8 per group).

Parameter	Diet	Before IRI	After IRI
Coronary Flow (mL/min)	Control	17.8 ± 1.1	16.2 ± 1.5
	HCD	16.9 ± 1.2	15.7 ± 1.1
Aortic Output (mL/min)	Control	36.8 ± 3.4	3.8 ± 2.0 (c)
	HCD	31.3 ± 1.6	4.0 ± 2.7 (c)
Heart Rate (beats/minute)	Control	289.0 ± 11.1	168.3 ± 49.9 (a)
	HCD	263.6 ± 11.1	124.8 ± 47.9 (a)
Aortic Systolic Pressure (mm Hg)	Control	88.4 ± 2.1	49.8 ± 14.6 (a)
	HCD	89.3 ± 1.1	40.9 ± 15.5 (a)
Aortic Diastolic Pressure (mm Hg)	Control	71.8 ± 1.2	38.4 ± 13.6 (a)
	HCD	72.3 ± 0.8	34.0 ± 12.9 (a)
Total Work (mWatts)	Control	10.3 ± 1.2	2.5 ± 0.8 (c)
	HCD	9.8 ± 0.5	2.2 ± 0.9 (c)

a $p < 0.05$; c $p < 0.001$ Compared to Before IRI.

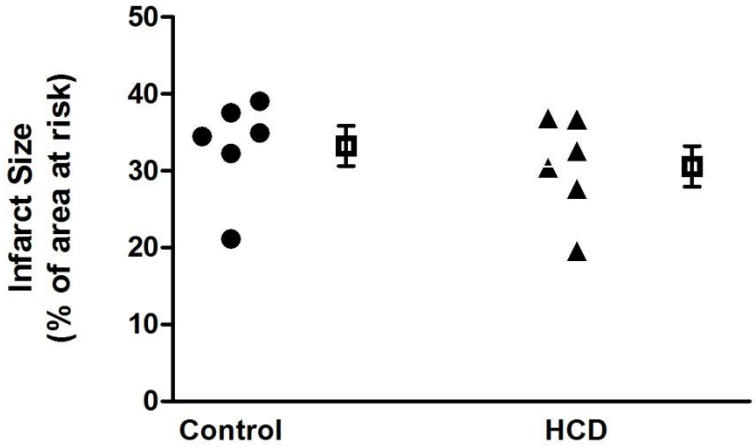

Figure 4.71: The effect of the HCD on infarct size following 35 minutes of regional ischaemia and 60 minutes of reperfusion (n=6 per group).

4.5.2 The effect of insulin, wortmannin and KU-60019 on cardiac function and infarct size following IRI in control and HCD fed rat hearts

Cardiac function results

Ischaemia-reperfusion injury had no effect on CF in either the control or HCD hearts. Additionally, none of the treatments had a significant effect on CF following IRI (Table 4.9). Not all of the hearts recovered functionally following IRI. As indicated in Table 4.10, 57% of control hearts had functional recovery while 49% of HCD hearts recovered functionally after IRI across all the groups. Hearts that failed to generate an AO were excluded from the "After IRI" data analyses. As anticipated, AO was significantly decreased in all groups following IRI in both the control and HCD hearts. The only exception was the control KU-60019 group (Table 4.10). In the control hearts, KU-60019 was able to block the effect of insulin and significantly reduce the AO back to vehicle control levels (Table 4.10). Aortic output was significantly lower in HCD insulin treated hearts compared to control insulin treated hearts.

Total work was significantly decreased following IRI in both the control and HCD hearts in all the treatment groups. Compared to the vehicle control, insulin significantly increased the total work in the control hearts following IRI. This effect of insulin was blocked with the use of both inhibitors (wortmannin and KU-60019) in control hearts. Insulin was unable to increase total work performed by the HCD hearts compared to the untreated hearts and as a result, total work performed by the insulin-treated HCD hearts was significantly reduced compared to the total work performed by insulin-treated control hearts (Table 4.11).

Aortic SP decreased significantly following IRI. Insulin treatment significantly increased aortic SP following IRI compared to vehicle control treated hearts and this effect of insulin was blocked by both wortmannin and KU-60019. Insulin was unable to increase aortic SP in HCD hearts (Table 4.12). Heart rate was not affected by IRI or by any of the treatments used (Table 4.13).

Table 4.9: Coronary flow (mL/min) before and after ischaemia/reperfusion injury in treated control and HCD hearts. Data expressed as mean with standard error of the mean (n=6-8).

		Before IRI[&]	After IRI
Control	Vehicle Control	17.75 ± 1.07	16.20 ± 1.45
	Insulin	20.17 ± 2.01	16.42 ± 1.33
	Wortmannin	16.69 ± 1.48	15.36 ± 1.28
	Wortmannin + Insulin	20.29 ± 2.42	14.50 ± 2.07
	KU-60019	17.94 ± 1.68	16.75 ± 1.06
	KU-60019 + Insulin	18.57 ± 1.25	19.07 ± 2.90
HCD	Vehicle Control	16.94 ± 1.15	15.67 ± 1.11
	Insulin	18.44 ± 1.49	15.81 ± 1.63
	Wortmannin	16.5 ± 1.18	15.75 ± 3.28
	Wortmannin + Insulin	19.06 ± 1.00	17.21 ± 1.71
	KU-60019	18.63 ± 1.92	18.00 ± 2.30
	KU-60019 + Insulin	17.94 ± 1.65	15.25 ± 1.11

[&] Basal coronary flow measurements before treatments were given.

Table 4.10: Aortic output (mL/min) before and after ischaemia/reperfusion injury in treated control and HCD hearts. Data expressed as mean with standard error of the mean (n=6-8).

		Before IRI[&]	After IRI	Hearts Recovered
Control	Vehicle Control	36.79 ± 3.37	10.00 ± 2.78 (b)	3/7 (42.9%)
	Insulin	40.75 ± 3.61	18.10 ± 3.05 (b)	5/6 (83.3%)
	Wortmannin	39.43 ± 3.70	11.13 ± 3.80 (c)	4/7 (57.1%)
	Wortmannin + Insulin	38.00 ± 4.32	8.00 ± 4.00 (a)	2/7 (28.6%)
	KU-60019	35.86 ± 4.36	19.50 ± 6.24	4/8 (50.0%)
	KU-60019 + Insulin	36.57 ± 3.05	10.25 ± 1.78 (c) (#)	6/7 (85.7%)
HCD	Vehicle Control	31.29 ± 1.55	16.00 ± 4.00 (b)	2/7 (28.6%)
	Insulin	33.75 ± 2.89	7.60 ± 1.69 (c) (+)	5/8 (62.5%)
	Wortmannin	36.40 ± 5.56	7.00 ± 4.04 (a)	3/6 (50.0%)
	Wortmannin + Insulin	39.00 ± 4.52	8.75 ± 3.25 (b)	4/7 (57.1%)
	KU-60019	35.00 ± 3.23	8.67 ± 2.67 (b)	3/7 (42.9%)
	KU-60019 + Insulin	35.33 ± 3.04	15.25 ± 8.56 (a)	4/8 (50.0%)

[&] Basal coronary flow measurements before treatments were given.

a $p < 0.05$; b $p < 0.005$; c $p < 0.0001$; Compared to Before IRI

# $p < 0.05$; Compared to Insulin

+ $p < 0.05$; Compared to Control

Table 4.11: Total work (mWatts) before and after ischaemia/reperfusion injury in treated control and HCD hearts. Data expressed as mean with standard error of the mean (n=6-8).

		Before IRI[&]	After IRI
Control	Vehicle Control	11.20 ± 0.98	4.02 ± 0.50 (c)
	Insulin	12.61 ± 1.00	6.44 ± 0.80 (b) (*)
	Wortmannin	10.81 ± 1.38	4.33 ± 0.70 (b)
	Wortmannin + Insulin	12.14 ± 0.89	4.14 ± 1.23 (b)
	KU-60019	11.14 ± 1.39	5.63 ± 1.40 (a)
	KU-60019 + Insulin	11.46 ± 0.81	5.17 ± 0.81 (c)
HCD	Vehicle Control	9.77 ± 0.53	4.32 ± 0.86 (c)
	Insulin	10.19 ± 1.00	4.18 ± 0.62 (c) (+)
	Wortmannin	11.30 ± 1.59	3.85 ± 1.02 (b)
	Wortmannin + Insulin	11.77 ± 0.96	4.79 ± 0.65 (c)
	KU-60019	11.80 ± 0.96	4.02 ± 0.66 (c)
	KU-60019 + Insulin	11.22 ± 0.88	4.55 ± 1.18 (b)

[&] Basal coronary flow measurements before treatments were given.

a $p < 0.05$; b $p < 0.005$; c $p < 0.0001$; Compared to Before IRI

* $p < 0.05$; Compared to Vehicle control

+ $p = 0.05$; Compared to Control

Table 4.12: Aortic systolic pressure (mmHg) before and after ischaemia/reperfusion injury in treated control and HCD hearts. Data expressed as mean with standard error of the mean (n=6-8).

		Before IRI[&]	After IRI
Control	Vehicle Control	88.38 ± 2.08	79.60 ± 1.50 (a)
	Insulin	91.33 ± 1.05	84.20 ± 1.02 (c) (*)
	Wortmannin	91.00 ± 1.67	81.67 ± 1.12 (b)
	Wortmannin + Insulin	90.17 ± 2.27	78.00 ± 2.42 (b)
	KU-60019	90.88 ± 2.11	82.33 ± 1.96 (a)
	KU-60019 + Insulin	91.57 ± 1.86	82.14 ± 0.55 (c)
HCD	Vehicle Control	89.29 ± 1.09	81.75 ± 1.81 (b)
	Insulin	87.13 ± 1.58	81.50 ± 2.46
	Wortmannin	89.14 ± 2.34	82.00 ± 1.23
	Wortmannin + Insulin	89.25 ± 1.41	81.00 ± 0.41 (b)
	KU-60019	90.25 ± 1.91	80.00 ± 0.86 (c)
	KU-60019 + Insulin	89.71 ± 2.04	80.71 ± 0.92 (b)

[&] Basal coronary flow measurements before treatments were given.

a $p < 0.05$; b $p < 0.005$; c $p < 0.0001$; Compared to Before IRI

* $p < 0.05$; Compared to Vehicle control

Table 4.13: Heart rate (beats/minute) before and after ischaemia/reperfusion injury in treated control and HCD hearts. Data expressed as mean with standard error of the mean (n=6-8).

		Before IRI[&]	After IRI
Control	Vehicle Control	289.0 ± 11.1	269.2 ± 12.9
	Insulin	291.8 ± 16.1	281.4 ± 15.7
	Wortmannin	260.4 ± 13.4	263.2 ± 6.6
	Wortmannin + Insulin	286.8 ± 9.7	252.2 ± 22.1
	KU-60019	254.0 ± 15.3	255 ± 13.4
	KU-60019 + Insulin	287.6 ± 9.3	280.6 ± 9.2
HCD	Vehicle Control	263.6 ± 11.1	249.5 ± 18.1
	Insulin	276.1 ± 11.4	296.3 ± 15.9
	Wortmannin	275.6 ± 14.5	268.0 ± 20.8
	Wortmannin + Insulin	306.3 ± 10.7	308.5 ± 13.2
	KU-60019	272.9 ± 11.3	286.5 ± 9.8
	KU-60019 + Insulin	286.0 ± 14.3	302.0 ± 19.6

[&] Basal coronary flow measurements before treatments were given.

Infarct size results

In HCD hearts, both insulin treatment and wortmannin treatment resulted in larger IFS compared to the vehicle control HCD group (HCD vehicle control 30.60 ± 2.65%; HCD Ins 46.74 ± 5.89%, $p < 0.05$; HCD Wm 45.98 ± 6.19%, $p < 0.05$). Although only borderline significant, co-treatment with insulin and wortmannin in HCD hearts resulted in smaller IFS compared to treatment with insulin or wortmannin alone (HCD Wm + Ins 31.24 ± 3.00%; HCD Ins 46.74 ± 5.89%, $p = 0.056$; HCD Wm 45.98 ± 6.19%, $p = 0.058$). Wortmannin had no effect on IFS in control hearts (Figure 4.72).

Insulin treatment also resulted in larger IFS in control hearts compared to the vehicle control group (Control vehicle control 33.24 ± 2.61%; Control ins 53.49 ± 5.30%; $p < 0.005$). KU-60019 reduced this effect of insulin in control hearts (Control ins 53.49 ± 5.30%; Control KU + Ins 39.06 ± 4.07%; $p = 0.056$). In HCD hearts, KU-60019 treatment resulted in significantly reduced

IFS compared to the vehicle control group (HCD vehicle control 30.60 ± 2.65%; HCD KU 22.58 ± 1.75%; $p < 0.05$). KU-60019 treatment was however not able to reduce the insulin-stimulated effect on IFS (HCD KU 22.58 ± 1.75%; HCD KU + Ins 54.31 ± 3.04%; $p < 0.0001$). Hearts from HCD animals had smaller IFS compared to hearts from control animals when treated with KU-60019 (Control KU 36.39 ± 5.14%; HCD KU 22.58 ± 1.75%; $p < 0.05$) while co-treatment with KU-60019 and insulin resulted in larger infarcts in HCD hearts compared to control hearts (Control KU + Ins 39.06 ± 4.07%; HCD KU + Ins 54.31 ± 3.04%; $p < 0.05$) (Figure 4.73).

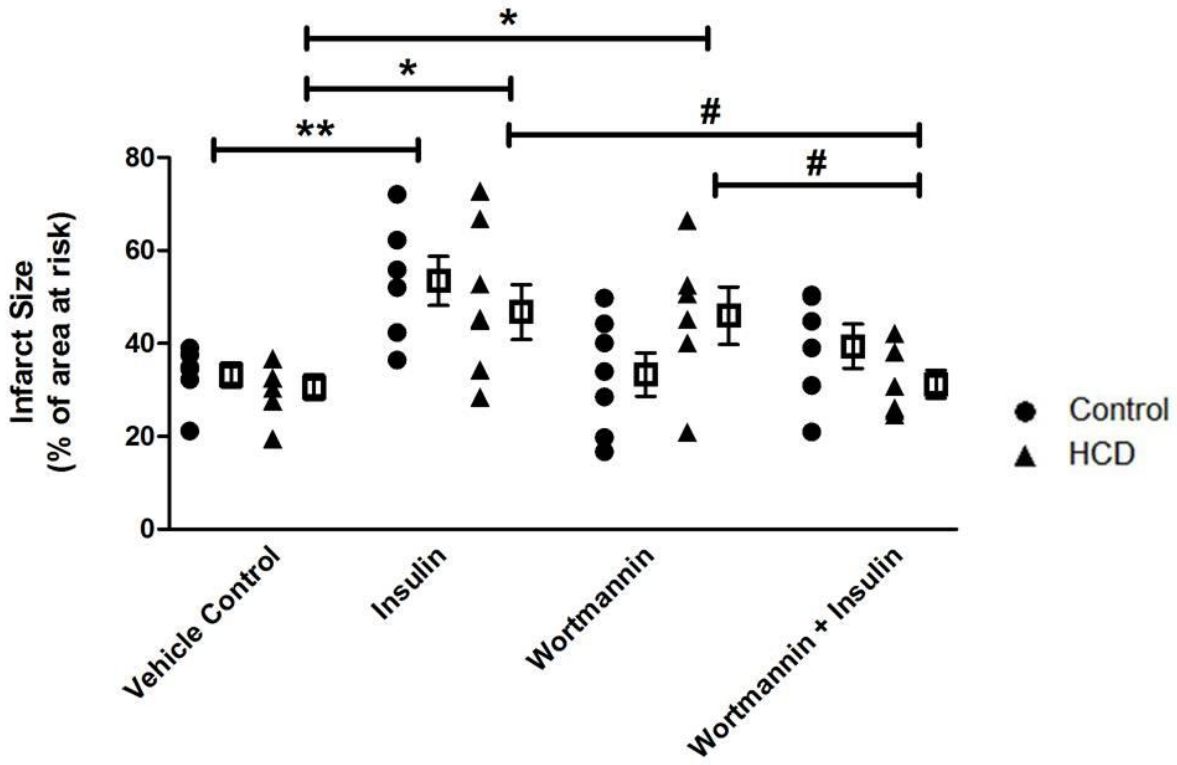

Figure 4.72: The effect of insulin (1 U/L) and wortmannin (100 nM) on infarct size following 35 minutes of regional ischaemia and 60 minutes of reperfusion * $P < 0.05$; ** $p < 0.005$; # $p < 0.06$ (n=6 per group).

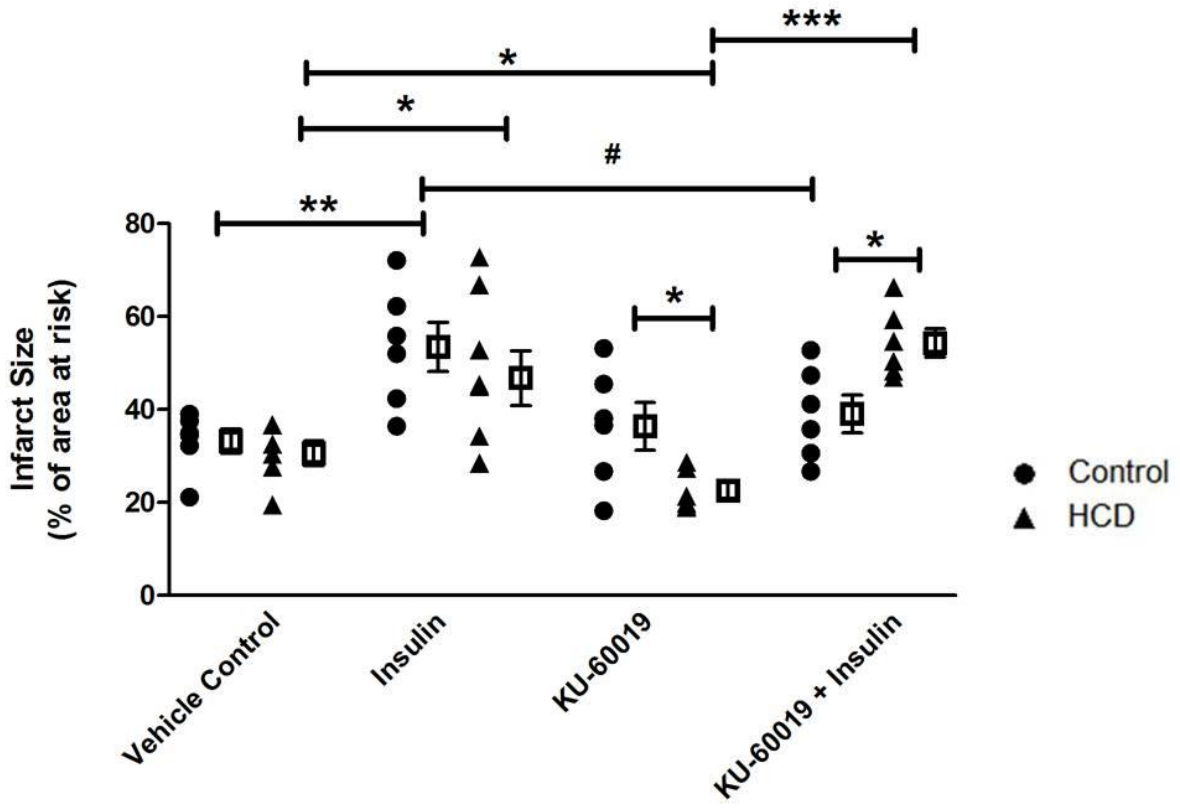

Figure 4.73: The effect of insulin (1 U/L) and KU-60019 (3 μM) on infarct size following 35 minutes of regional ischaemia and 60 minutes of reperfusion * $p < 0.05$; ** $p < 0.005$; *** $p < 0.0001$; # $p = 0.056$ (n=6 per group).

4.5.3 The effect of reduced insulin concentration on infarct size following IRI

Because of the unexpected finding that insulin increased IFS, perfusions were performed in which the hearts were treated with lower insulin concentrations (0.3 U/L vs 1 U/L). With the reduced insulin concentration, insulin treatment no longer resulted in increased IFS (Figure 4.74).

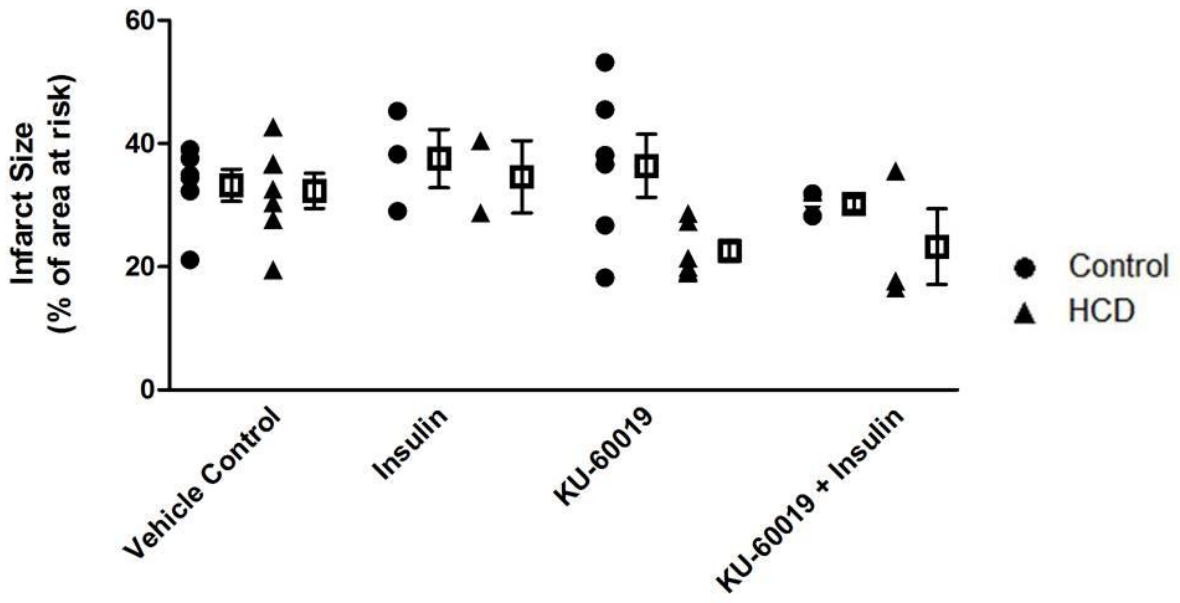

Figure 4.74: The effect of a reduced insulin concentration (0.3 U/L) and KU-60019 (3 μM) on infarct size following 35 minutes of regional ischaemia and 60 minutes of reperfusion (n=3-6 per group).

4.6 Aortic ring studies

Aortic rings were harvested from age-matched control animals and mounted in an organ bath where isometric tension experiments were conducted. This was done to further investigate the possible vasodilatory effect of KU-60019 as KU-60019 significantly increased the CF in the perfusion experiments, without changing the pressure development. Figure 4.75 indicates the percentage relaxation of aortic rings treated with ACh, KU-60019 and DMSO. Acetylcholine was used as a positive control for relaxation. Pre-treatment with L-NAME abolished the vasodilatory effect of ACh, reducing the final relaxation from 74.7 ± 3.8% when treated with ACh alone to 6.9 ± 0.8% when pre-treated with L-NAME ($p < 0.0001$). Although it did not have such a pronounced relaxation effect as ACh, treatment with KU-60019 also resulted in vasodilation. The percentage relaxation when treated with KU-60019 was 44.7 ± 5.4% compared to 74.7 ± 3.8% when treated with ACh ($p < 0.0001$). Pre-treatment with L-NAME was able to abolish the vasodilatory effect of KU-60019, resulting in a final percentage relaxation of only 8.5 ± 1.4% ($p <$

0.0001). At each concentration used, KU-60019 had a significantly greater percentage relaxation than DMSO, indicating that the vasodilatory effect of KU-60019 is not caused by the DMSO vehicle.

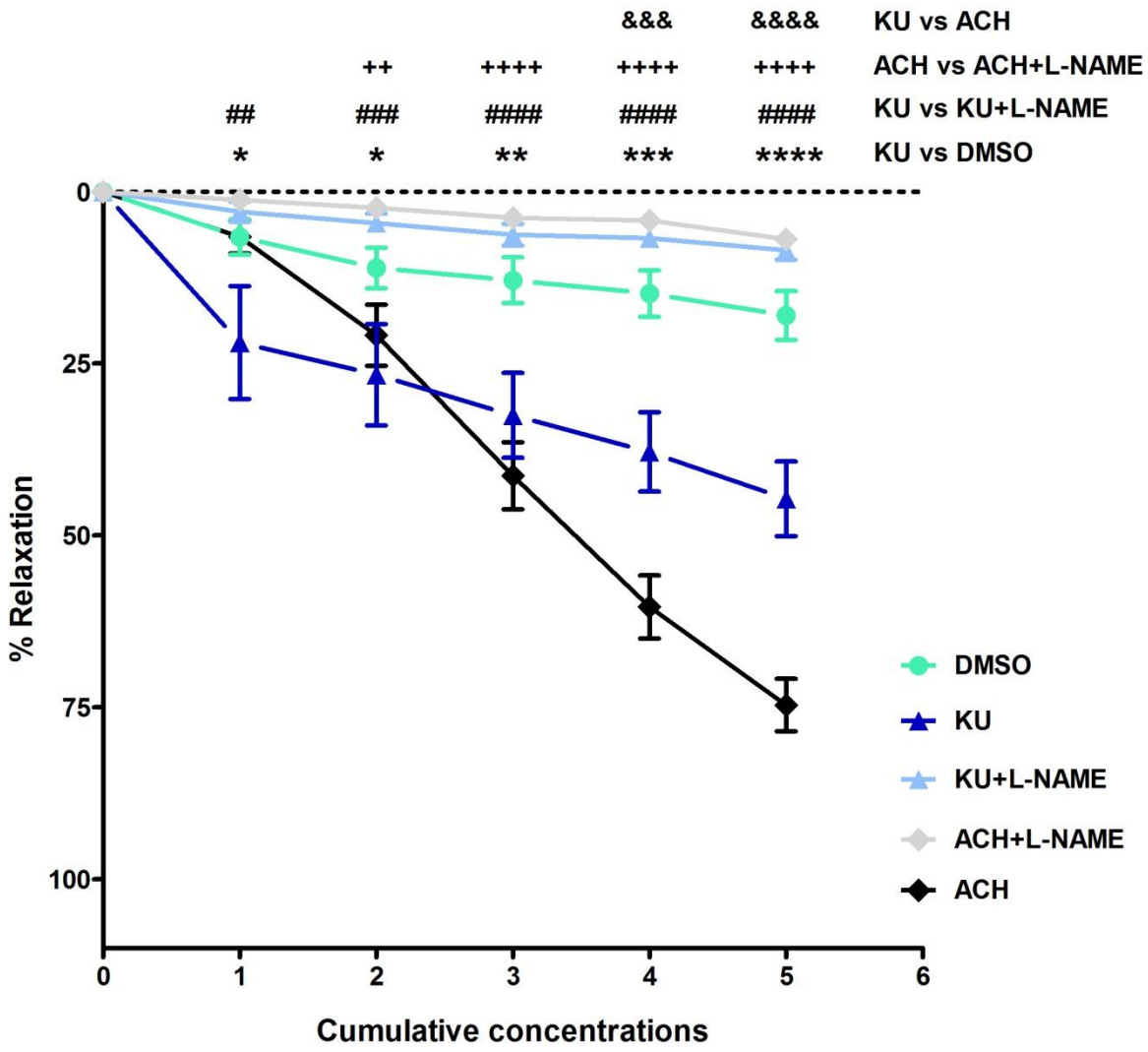

Figure 4.75: Graph indicating percentage relaxation of aortic rings in response to cumulative concentrations of DMSO, KU-60019 and acetylcholine and the effect of pre-incubation with the NOS-inhibitor, L-NAME. * $p < 0.05$; **, ## and ++ $p < 0.005$; ***, ###, &&& $p < 0.0005$; ****, ####, ++++ and &&&& $p < 0.0001$ (n=5-7 per group).

4.7 Results at a glance

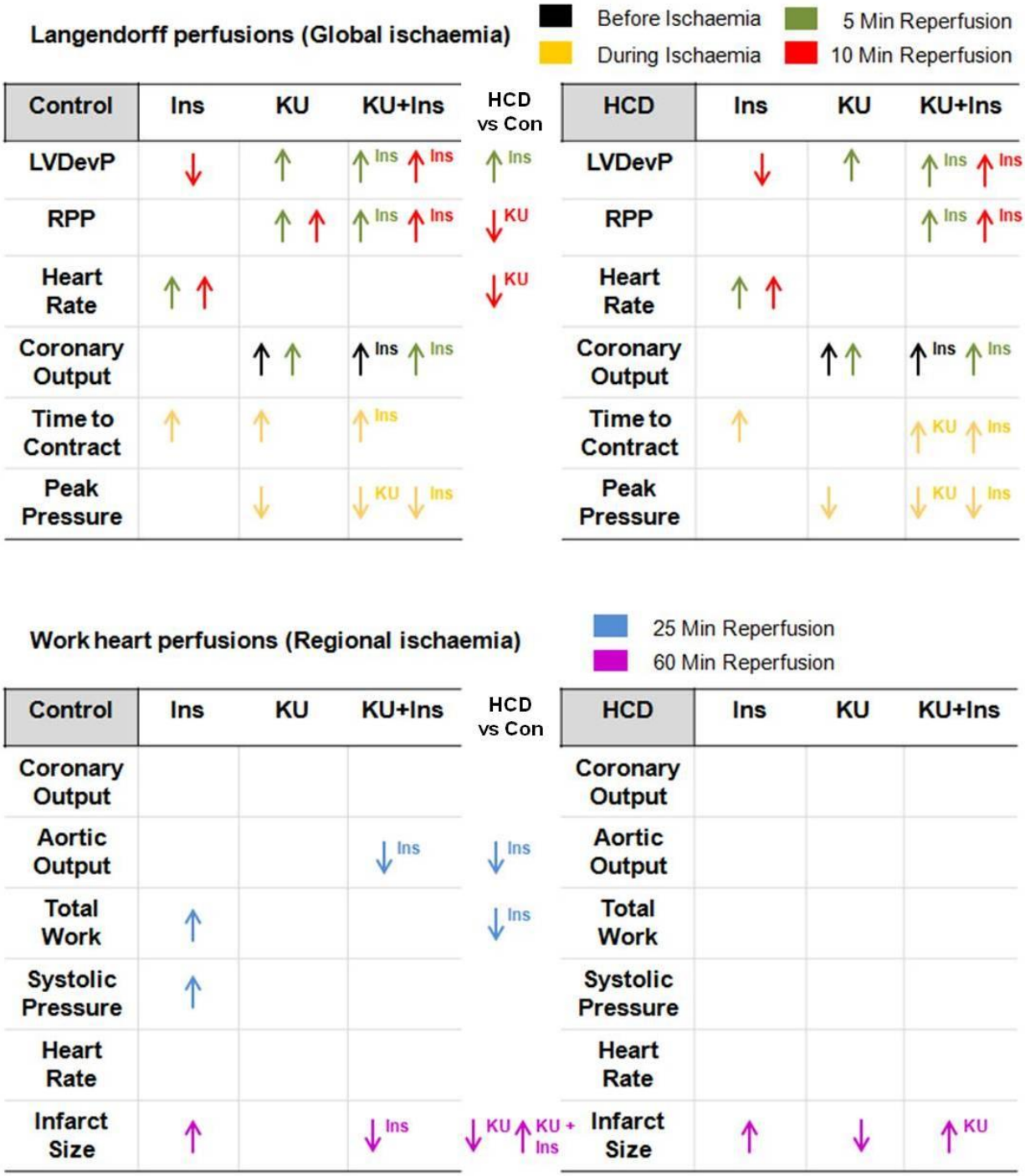

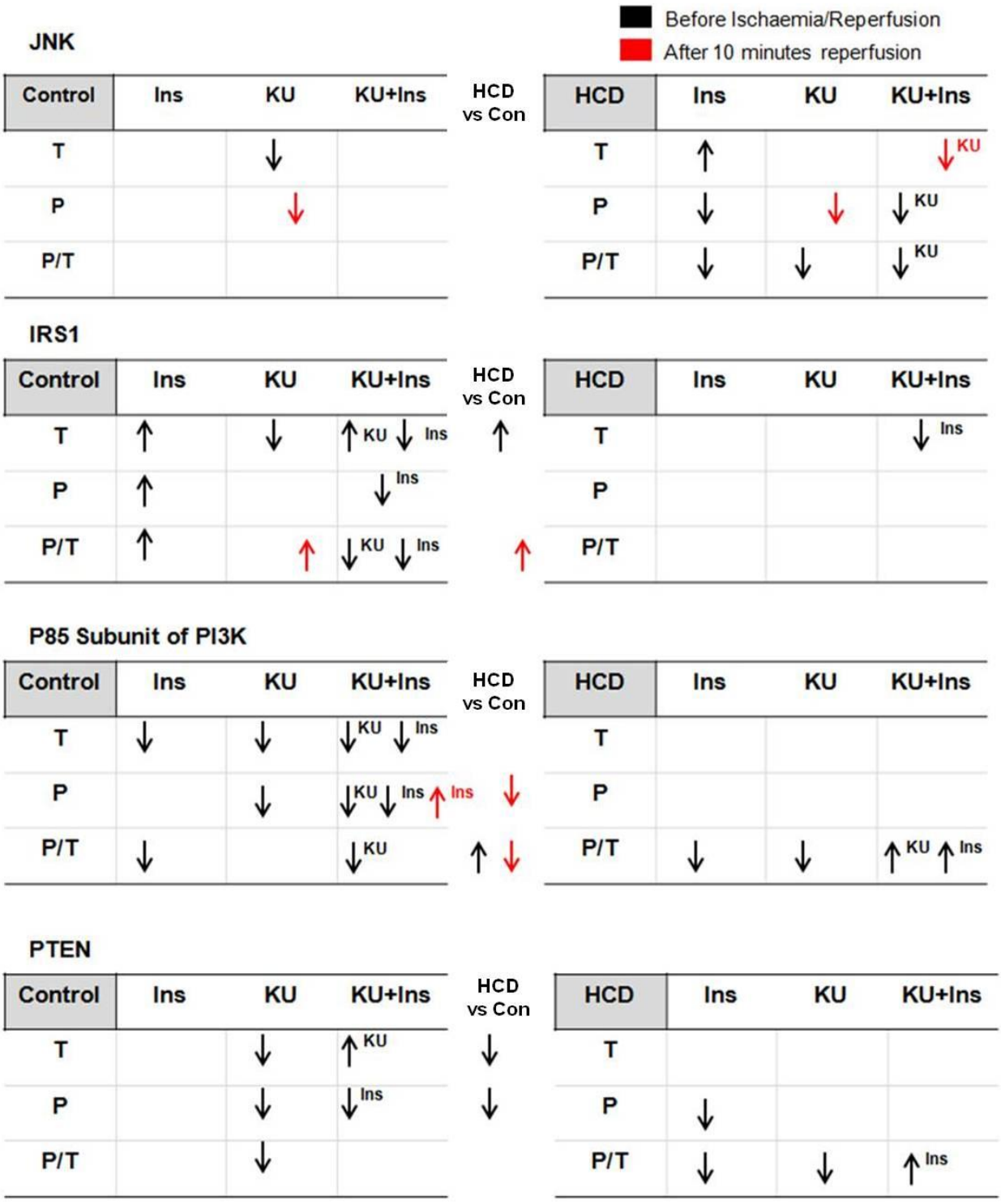

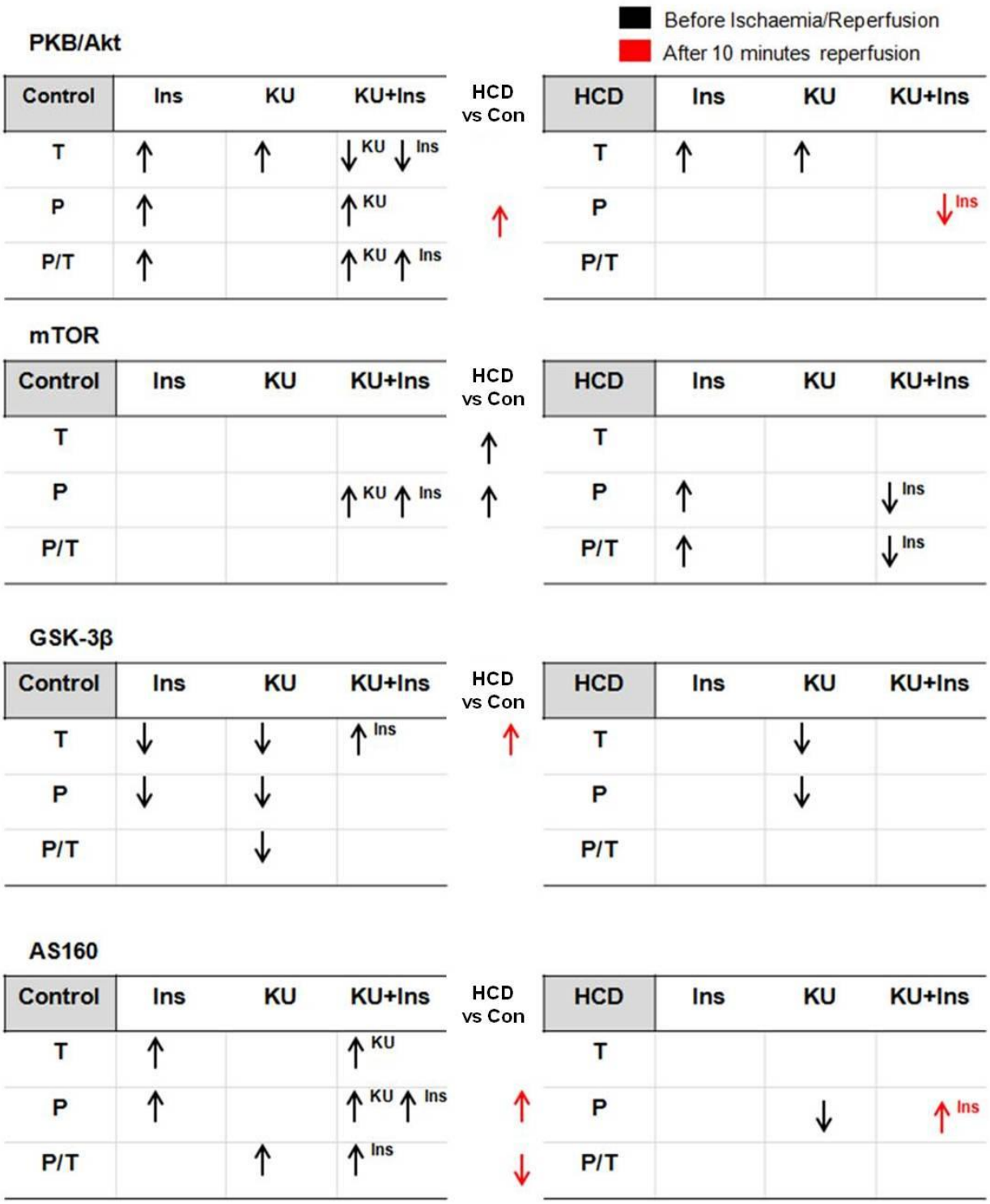

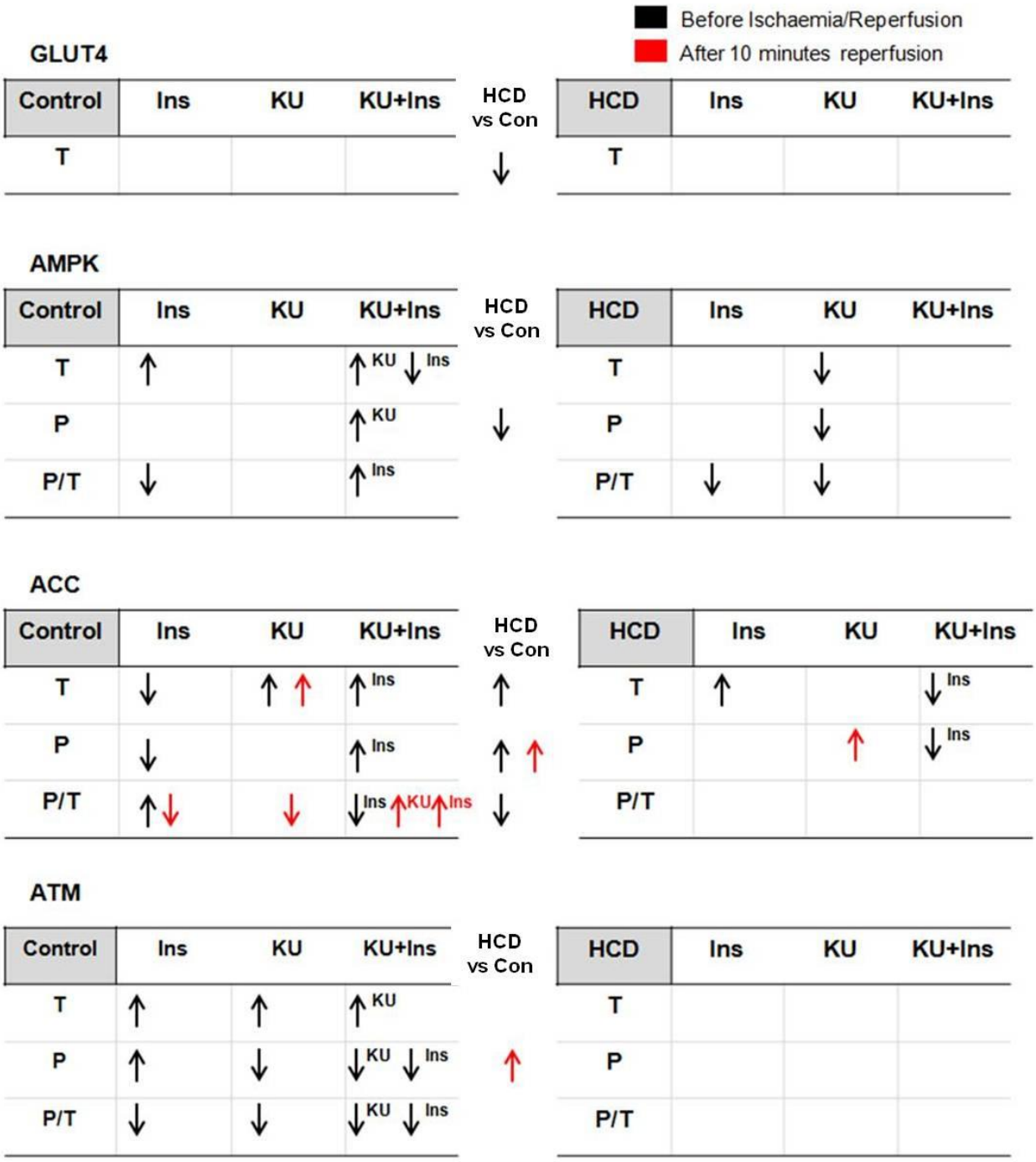

Chapter 5: Discussion

With an increase in urbanization, consumption of a “Western diet” and sedentary lifestyles, the global burden of disease is shifting more towards non-communicable diseases. According to the WHO, there are four main types of non-communicable diseases, including cancer, chronic respiratory diseases, CVD and diabetes (WHO, Noncommunicable Diseases). The latter two conditions are linked as diabetes is considered a major risk factor for the development of CVD. Effective prevention and management of these complex conditions is dependent on a clear understanding of the molecular mechanisms implicated in their aetiologies.

Insulin resistance, glucose intolerance and diabetes are often listed as symptoms of A-T and patients with A-T have been documented to be affected by ischaemic heart disease. There is thus a possibility that ATM deficiency could play a role in the development of these conditions. However, the majority of studies that investigate ATM are focused on its role as an anti-cancer target and as a result, very little is known about the mechanisms in which ATM deficiency lead to insulin resistance, glucose intolerance, diabetes and heart disease.

The aim of the current study was thus to investigate the potential role of ATM in the development of myocardial pathology associated with insulin resistance. We made use of an insulin resistant rat model and manipulated ATM activity using pharmaceutical agents. In the perfusion protocols, insulin, wortmannin and KU-60019 were administered prior to ischaemia, were present during ischaemia and were only washed out at the onset of reperfusion. During administration, all pharmaceutical agents were re-circulated. We made use of a supraphysiological insulin concentration. Western blot analyses to investigate insulin signalling networks were performed in the presence of the pharmaceutical agents prior to ischaemia as well as during reperfusion once the pharmaceutical agents have been washed out of the hearts.

5.1 Summary of key findings

The key findings of the study are listed below:

- The HCD resulted in decreased basal total ATM and PKB/Akt levels, increased body mass, visceral fat mass, non-fasting and fasting glucose levels, increased insulin levels, increased HOMA-IR values and increased glucose levels during an OGTT compared to the control diet.

- Cardiac function and IFS following IRI were comparable in untreated hearts from animals on the control diet and the HCD.

- High concentration insulin treatment increased IFS in control and HCD hearts while lower insulin concentration treatment had no effect on IFS.

- Insulin treatment improved haemodynamic function in control hearts. Insulin had no effect on haemodynamic function in HCD hearts.

- In control hearts, not all proteins of the insulin signalling network were responsive to insulin before ischaemia and the insulin signalling pathway was not activated by insulin during reperfusion.

- In HCD hearts, insulin did not activate the insulin signalling pathway before ischaemia or during reperfusion.

- ATM inhibition increased cardiac function during early reperfusion following global ischaemia in control and HCD hearts.

- ATM had no effect on IFS in control hearts. HCD hearts had smaller infarcts in response to KU-60019 treatment alone, but KU-60019 treatment was unable to reduce insulin-stimulated IFS.

- In control hearts, ATM was activated by insulin and inhibited by KU-60019. Neither insulin nor KU-60019 had an effect on ATM activity in HCD hearts.

- In control hearts, PI3K activation was reduced while PTEN and GSK-3β was activated in response to KU-60019 while PKB/Akt, AMPK and ACC were unaffected.

- Treatment with KU-60019 attenuated the insulin signalling network in HCD hearts.

- ATM inhibition increased CF in perfused hearts and had a NO-dependent vasodilatory effect on isolated aorta rings.

- Chloroquine did not activate cardiac ATM or contribute to increased glucose uptake in cardiomyocytes. Chloroquine treatment led to increased necrosis of cardiomyocytes and reduced cardiac function.

5.2 Comparison between the diets (control, DIO and HCD)

In order to investigate the effect of ATM in the myocardial pathology associated with insulin resistance, we firstly required an animal model that displayed insulin resistance. Two diets were assessed for their ability to induce insulin resistance and obesity in adult male Wistar rats. The first diet had an increased carbohydrate content (DIO) while the second had an increased carbohydrate and fat content (HCD) compared to the control chow diet. These diets generally lead to hyperphagia as the rats find them highly palatable.

Diets were used to induce obesity and insulin resistance in the animal models, as opposed to genetic mutations, as it better resembles the development of obesity in humans. It also

eliminates the possibility of observing unwanted confounding effects of genetic alterations. Furthermore, the use of diets to induce obesity and insulin resistance in animals has been shown to be effective when studying CVD (Rosini et al., 2012).

5.2.1 Biometric data

Although the DIO diet caused an increase in visceral fat mass, the body mass and glucose levels were comparable to that of the control diet. It, therefore, did not have the desired effect and was not used further.

Rats on the HCD had significantly increased body masses and visceral fat masses compared to rats on the control chow diet (Table 4.1). The HCD had a greater fat and carbohydrate content and reduced protein content compared to the control diet. The HCD also had a higher energy content than the control diet (Table 3.1). Although food intake was not measured during this study, a diet high in sugar and fat has been shown to induce hyperphagia in rats (Lucas and Sclafani, 1990). The increased energy content, together with the likely hyperphagia caused by the high sugar and fat content of the diet, resulted in rats on the HCD consuming more energy than they could expend, ultimately leading to weight gain.

A high fat-high sugar diet has previously been shown to successfully induce insulin resistance in Sprague-Dawley rats (Motshakeri et al., 2015). Animals on the HCD had increased fasting and non-fasting glucose levels, together with increased serum insulin levels compared to the control chow-fed group. This scenario is characteristic of insulin resistance as cells are resistant to the effect of insulin, resulting in hyperglycaemia as glucose is not taken up into cells. The increased serum glucose levels in turn result in increased insulin secretion. The presence of insulin resistance in animals that received the HCD is also evident through the increase in the HOMA-IR index compared to animals on the control diet. Furthermore, rats that were on the HCD had

consistently higher glucose levels during an OGTT than animals that were on the control diet, signifying glucose intolerance in the HCD.

Since both diets (DIO and HCD) had increased carbohydrate content, in the form of condensed milk and sucrose, and decreased protein content compared to the control diet, it is likely the high fat content of the HCD that contributed to the increased obesity, insulin resistance and glucose intolerance observed in the HCD but not the DIO diet.

5.2.2 Basal ATM expression and activation levels

Western blot analysis was performed on hearts from animals on the control, DIO and HCD diets in order to determine the ATM and PKB/Akt expression and activation levels. The DIO diet, which had only increased carbohydrates, had no effect on ATM or PKB/Akt. The HCD, which had increased fat content as well as increased carbohydrate content, caused a significant decrease in basal ATM expression in cardiac tissue. Although total ATM was reduced in the HCD, phospho-ATM levels were equal between the diets. This is an indication that ATM phosphorylation is up-regulated in the HCD in order to achieve normal activation levels eventhough there is less total ATM available. This is indicated by the increased P/T ATM ratio in the HCD compared to the control diet (Figure 4.1).

A high fat diet has been shown to cause an increase in oxidative stress and a decrease in antioxidant capacity in heart tissue in rats (Noeman et al., 2011). We speculate that the activity of ATM could be increased in the HCD in response to the oxidative stress associated with a diet high in fat. Oxidative stress is a known activator of ATM (Guo et al., 2010).

A decrease in ATM expression due to high dietary fat intake is consistent with the findings in skeletal muscle by Halaby et al. (2008). They suggested that the decreased ATM expression that is associated with consumption of a high-fat diet contributes to the development of insulin resistance by down-regulation of PKB/Akt activity in skeletal muscle. However, in contrast to

Halaby et al. (2008), who found an associated decrease in PKB/Akt activation, we found no change in phosphorylation of PKB/Akt (Ser473) in the HCD compared to the control diet. In fact, due to a significant decrease in PKB/Akt expression in the HCD, hearts from HCD-fed rats had an increased P/T PKB/Akt ratio compared to hearts from animals on the control diet.

5.2.3 Myocardial function in HCD fed animals

The heart adapts to stress caused by insulin resistance and obesity by altering its structure, function, metabolism and efficiency. Although these changes benefit the heart in the short term, they may contribute to decreased contractility and cardiac dysfunction in the long term (Peterson, 2006). It is well documented that obesity and insulin resistance are risk factors for the development of CVD in humans. However, contradictory results have been obtained in animal models. Park et al. (2005) observed a decline in cardiac function in diet-induced insulin resistant mice and du Toit et al. (2008) observed increased IFS and decreased AO recovery in diet-induced obese rats. In contrast, Wensley et al. (2013) found that there was no difference in the structure and function of hearts from obese and insulin resistant rats compared to control hearts. Nduhirabandi (2014) also found that myocardial function was not adversely affected by a high caloric diet in rats. Paradixically, in our laboratory and elsewhere, there have also been reports of improved cardiac function in obesity.

In the current study, even though the HCD did result in increased insulin resistance, glucose intolerance and obesity and reduced total ATM levels compared to the control diet, we did not observe any noteworthy differences in any of the measured parameters of cardiac function between hearts from the two diets, either before or after IRI (Table 4.8). This indicates that the HCD used in this study did not adversely affect cardiac function following a 16-week feeding period or that the effect of our HCD was not pronounced enough. It is possible that adverse cardiac effects in response to the HCD will only become visible after a longer feeding period. It

is also possible that our age-matched control animals had reduced cardiac function compared to young healthy animals. We did not evaluate the effect of age on cardiac function in the current study, however, in a parallel study van Vuuren (2015) found that cardiomyocytes isolated from the age-matched control animals had reduced insulin-stimulated glucose uptake compared to cardiomyocytes from young control animals. This indicates that, although they are more insulin responsive than hearts from HCD animals, hearts from age-matched control animals did display insulin resistance to some degree. This would minimise the effects seen when comparing the HCD hearts to hearts of the compromised control animals.

Both the control and HCD hearts had AO values lower than what is considered normal in young, healthy control hearts. Usually hearts with AO values lower than 36 mL/min would be discarded in our laboratory. However, we have found that hearts from animals that are older can have reduced AO despite being mounted correctly. Hearts with AO values lower than 36 mL/min were therefore retained in the study if they were optimally mounted on the perfusion rig and were able to maintain the AO for the work heart perfusion time of 15 min.

5.2.4 Infarct sizes in HCD fed animals

Obesity and insulin resistance increase the myocardium's susceptibility to ischaemia-reperfusion injury (Wensley et al., 2013) and obesity is commonly accepted as a risk factor for myocardial infarction (Yusuf et al., 2005). Although the heart uses fatty acid oxidation as its main source of energy production, cardiac metabolism shifts in favour of glycolysis during ischaemia. The insulin resistant heart, however, has a greater dependency on fatty acid oxidation due to its reduced ability to utilize glucose. It is therefore expected that hearts from obese, insulin resistant animals will have larger IFS due to the inability of these hearts to produce energy through anaerobic glycolysis (Thim et al., 2006). However, IFS have varied in

animal studies of diabetes and obesity (Miki et al., 2013). We found IFS to be similar in hearts from animals on the control diet and the HCD (Figure 4.71).

The inconsistency observed in cardiac function and IFS between different studies is possibly due to the use of different diet compositions, different diet feeding durations and the use of animals with different genetic backgrounds as well as to the inherent biological variation in the response of animals.

5.3 Cardiac function following ischaemia/reperfusion injury in response to pre-treatment with insulin, wortmannin and KU-60019

During ischaemia, the lack of oxygen results in cessation of oxidative phosphorylation and an increase in anaerobic glycolysis. This in turn causes an accumulation of lactate and protons and a decrease in pH. By exchanging protons for Na^+, and Na^+ for Ca^{2+}, there is an eventual Ca^{2+} overload in the ischaemic cell (Hausenloy and Yellon, 2013; Kalogeris et al., 2012). Calcium overload plays a significant role in the cardiac dysfunction observed in response to IRI (Nayler, 1981).

Ischaemic contracture, when DP gradually rises during a myocardial ischaemic period, is a marker of ischaemic injury (Reichelt et al., 2007; Torrance et al., 2000). Contracture develops in response to mitochondrial injury, depletion of ATP (which is needed for the dissociation of actin/myosin cross-bridges) and Ca^{2+} overload (Torrance et al., 2000). Delayed onset of contracture and a reduced peak developed pressure is an indication of reduced susceptibility to ischaemic injury.

Calcium overload, together with phosphate overload and the increase in ROS production during reperfusion, contribute to the mitochondrial inner membrane becoming permeable, a phenomenon known as opening of the mitochondrial permeability transition pore. This leads to a loss of protons and subsequently, a loss of the electrochemical proton gradient required for ATP

production (Honda and Ping, 2006). After ATP is depleted, the damaged mitochondria swell and rupture. Ruptured mitochondria can release pro-apoptotic proteins or affected cardiomyocytes will eventually die due to necrosis caused by ATP depletion (Baines, 2009).

Due to the decline in ATP during ischaemia, cardiac contractility is significantly reduced. Contractility is further reduced as a result of proteolysis of proteins that make up the sarcomere and posttranslational modifications caused by ROS (Chen and Ogut, 2006). Upon reperfusion, restoration of myocardial contractility could be delayed as a result of myocardial stunning. In myocardial stunning, post-ischaemic dysfunction is completely reversible and CF is restored to normal rates (Bolli and Marbán, 1999). In contrast, myocardial infarction is the result of irreparable damage to the heart when myocardial cell death has occurred. Both necrosis and apoptosis contribute to cell death during IRI (Yellon and Baxter, 1999). In an attempt to protect the heart against IRI, pro-survival signalling pathways such as the PI3K-PKB/Akt pathway and the ERK1/2 signalling cascades are activated. Both of these pathways have anti-apoptotic effects (reviewed in Hausenloy and Yellon, 2004).

5.3.1 Insulin

Insulin is widely believed to protect the heart against IRI. This is achieved through metabolic optimization and activation of the anti-apoptotic/pro-survival PI3K-PKB/Akt pathway (Sato et al., 2014). It has also been shown that insulin plays a protective role by reducing oxidative stress through increased NO production and reduced superoxide anion production (Ji et al., 2010). In working heart *ex vivo* perfusions, we found that the presence of insulin in the perfusate before ischaemia, increased the total work performed (Table 4.11) and increased the post-ischaemic aortic SP in control hearts (Table 4.12). Although not significant (potentially due to low n-values), insulin treatment also tended to increase the AO in control hearts (Table 4.10). Furthermore, insulin resulted in an increased heart rate during early reperfusion (5 and 10

minutes) following global ischaemia (Figure 4.13) and an increase in the time to contracture in control hearts (Table 4.7). Together, these results indicate improved cardiac haemodynamic function in insulin-treated control hearts.

In contrast, insulin treatment prior to ischaemia did not improve AO, total work or aortic SP in HCD hearts as it did in control hearts (Tables 4.10-a). To the contrary, total work and AO was significantly reduced in HCD hearts compared to control hearts in response to insulin. These results indicate that HCD hearts were resistant to the protective effects of insulin, consistent with the insulin resistant status of the animals. However, as in the control hearts, insulin treatment increased heart rate during early reperfusion (Figure 4.13) and increased time to contracture during global ischaemia (Table 4.7) in HCD hearts. This is an indication that HCD hearts have insulin-stimulated cardiac protection during ischaemia and early reperfusion, but this effect is lost later in reperfusion as was seen in the working heart data.

Compared to vehicle control hearts, the presence of insulin in the perfusate before ischaemia resulted in larger infarcts in both control and HCD hearts (Figure 4.72). These results were unexpected as insulin is believed to be protective against IRI in control and obese hearts (du Toit et al., 2008; Ji et al., 2010). The timing at which insulin is administered has been proposed to have an effect on cardioprotection. Jonassen et al. (2001) found that insulin reduced IFS with 45% when administered at the onset of reperfusion. Protection was, however, lost when insulin was only administered 15 minutes into reperfusion. They further showed that insulin pre-treatment had no effect on IFS. This indicates that the time of insulin administration influences whether or not insulin will have a cardioprotective effect. Insulin administration before ischaemia may enhance the metabolic demand of the heart before and during ischaemia, as insulin is a positive inotrope. This could deplete critical metabolic supplies, such as oxygen and substrates, and result in larger IFS. Cardioprotection, in the form of reduced IFS, has however been observed in response to insulin pre-treatment. Fuglesteg et al. (2009) observed 60% smaller

infarcts in hearts that were pre-conditioned with insulin, in the form of three insulin treatment cycles of five minutes each, compared to untreated hearts. However, in pre-conditioning, the stimulus (insulin) is washed out of the system before the onset of the index ischaemia while insulin was present in our system throughout the ischaemic period and only washed out at the beginning of reperfusion. Furthermore, the metabolic state of the hearts influences the degree of protection offered by insulin as du Toit et al. (2008) observed a greater reduction in IFS in response to insulin in hearts from obese animals than what was seen in hearts from age-matched control animals. Furthermore, the fed/fasted state of animals used also influences the response to insulin administration (Slettom et al., 2016).

It was however demonstrated in some studies that IFS was increased in response to insulin treatment which is consistent with what was found in this study. Fullmer et al. (2013) found that the presence of insulin during pre-conditioning, when the heart is exposed to short periods of ischaemia before a prolonged ischaemic period, resulted in increased IFS. Insulin was present throughout their perfusion protocol. Increased IFS, in spite of improved cardiac function recovery in response to insulin pre-treatment, has previously been observed in our laboratory (Webster, unpublished data). Shimizu et al. (2010) also observed unfavourable cardiac outcomes in response to insulin. They found that excessive insulin-induced signalling resulted in systolic dysfunction.

Although we used an insulin concentration previously used in our research group and shown to result in increased cardiac function (namely 1 U/L; Webster et al., 2014), we suspected that the increased IFS observed in our hearts to which insulin were administered could be due to the insulin concentration used being too high. We therefore performed perfusions using a reduced insulin concentration (0.3 U/L) and determined IFS of the hearts. With the reduced insulin concentration, IFS were no longer larger compared to the untreated hearts (Figure 4.74). However, insulin was still not able to reduce IFS to smaller than what were found in the

untreated group. Consistent with this, Jonassen et al. (2001) also found that pre-treatment with 0.3 U/L insulin had no effect on IFS compared to untreated controls. In a study by du Toit et al. (2008), IFS were found to be significantly reduced compared to the untreated group when treated with 0.03 U/L insulin, while an insulin concentration of 0.05 U/L had no effect on IFS in control hearts. It is thus possible that our reduced insulin concentration of 0.3 U/L was still too high to reduce IFS.

In light of the above, we believe that the effect of insulin varies depending on the timing of administration, the concentration used and the metabolic state of the hearts being treated. Due to different study designs used, it is not possible to directly compare the effect of insulin on IFS observed in different studies (Slettom et al., 2016). In the current study, in which 1 U/L insulin was administered, in a re-circulating manner, 10 minutes prior to ischaemia and washed out at the onset of reperfusion, increased IFS were observed in both control and HCD hearts compared to untreated control hearts.

5.3.2 Wortmannin

Wortmannin is a potent, non-specific inhibitor of the PI3K family, which is able to abrogate insulin signalling (Lam et al., 1994). As it is a member of the PI3K family, ATM has also been shown to be inhibited by wortmannin with an IC_{50} of 100 nM (Chan et al., 2000). We included the use of wortmannin in our study to compare the effects of this known inhibitor of insulin signalling with the effects of an ATM-specific inhibitor, KU-60019. We hypothesised that KU-60019 will also have an effect on insulin signalling.

In our study, cardiac function was enhanced by wortmannin during early reperfusion in control hearts as increased LVDevP and RPP was seen at five minutes reperfusion in Langendorff perfusions. Although RPP remained unaltered in HCD hearts, LVDevP was also increased in early reperfusion in HCD hearts in response to wortmannin treatment (Tables 4.3 and 4.4).

Improved LVDevP following IRI in response to wortmannin treatment has been seen before as wortmannin inhibited the production of superoxide in perfused rat hearts (Young et al., 2000). Young et al. (2000) further showed that wortmannin did not affect cardiac function in the absence of ischaemia and reperfusion, indicating that its effect was dependent on IRI. Wortmannin had no effect on cardiac function later in reperfusion as none of the myocardial mechanical function parameters that were tested in working heart perfusions (namely CO, AO, heart rate, pressure development and total work performed) were altered by wortmannin administration in either the control or HCD hearts (Tables 4.9-4.13). This is an interesting observation as wortmannin is an irreversible inhibitor of PI3K and the effect is thus not expected to be lifted during reperfusion after washout of wortmannin.

Infarct size was not altered by wortmannin treatment, either alone or in conjunction with insulin, in control hearts. In HCD hearts, IFS was larger in wortmannin treated hearts than in untreated hearts. Co-treatment with insulin abolished this effect of wortmannin (Figure 4.72). In line with our findings, Tsang et al. (2004) and Ravingerova et al. (2009) also found that wortmannin did not increase IFS in control rat hearts and Jonassen et al. (2001) did not see a change in IFS in response to wortmannin and insulin co-treatment either. It is possible that wortmannin increased IFS in HCD hearts due to further inhibition of the already compromised insulin signalling network in these hearts. This is however not supported by our Western blot data as none of the proteins that participate in insulin signalling that were analysed, were affected by wortmannin treatment in HCD hearts.

The Western blot analyses were performed following 20 minutes of global ischaemia and 10 minutes of reperfusion. In control hearts, wortmannin treatment did not have the expected effect on insulin signalling intermediates. In the presence of insulin, wortmannin increased serine phosphorylation with consequent inhibition of IRS-1, which is upstream of PI3K, as seen in the P/T IRS-1 ratio (Figure 4.40). However, the p85 subunit of PI3K was phosphorylated following

wortmannin treatment (Figure 4.43). In line with activation of the insulin signalling pathway, the P/T ratio of ACC was reduced with wortmannin treatment, signifying ACC activation and an increase in fatty acid synthesis and reduced oxidation of fatty acids. None of the other proteins downstream of PI3K, namely PKB/Akt, mTOR and AS160, were activated by wortmannin treatment following activation of PI3K. The activity of GSK-3β was increased in control hearts that had been treated with wortmannin (Figure 4.55). This is consistent with inhibition of insulin signalling. The PI3K-PKB/Akt-pathway is activated during reperfusion (Matsui et al., 2001). The activation of PI3K in the presence of wortmannin, a known PI3K inhibitor, indicates that wortmannin was not successful in inhibition of PI3K under the circumstances used in this study, namely in reperfusion following ischaemia.

5.3.3 KU-60019

We made use of a small molecule inhibitor, namely KU-60019, which is specific for ATM inhibition (Golding et al., 2009). No macroscopic or histopathological alterations were observed in rat hearts following administration of 10 mM KU-60019 via an osmotic pump (Vecchio et al., 2014). The metabolic effect of KU-60019 or its predecessor (KU-55933) has never been investigated in the cardiac context and not much is known about the cardiac effect of ATM deficiency or inhibition.

It has been shown that ATM participates in the insulin signalling network in other tissues and that ATM-deficient animal models display insulin resistance similar to that seen in the metabolic syndrome. In skeletal muscle, ATM is involved in the activation of PKB/Akt in response to insulin. ATM also contributes to insulin-stimulated glucose uptake in skeletal muscle by possibly being involved with GLUT4 translocation to the cell surface (Halaby et al., 2008). A role for ATM in adipocyte functioning has been revealed as $ATM^{-/-}$ cells had reduced C/EBPα and PPARγ levels, transcription factors that are crucial for adipocyte differentiation (Takagi et al., 2015). It

was further showed that ATM deficient mice also had reduced adiponectin and leptin levels, reduced subcutaneous fat and increased visceral fat tissue. Interestingly, when adipose functioning was restored, glucose tolerance was improved, suggesting that defective functioning of adipose tissue contributes to the insulin resistance observed in A-T (Takagi et al., 2015). ATM also participates in IGF-1 mediated signalling in skeletal muscle, possibly downstream of IRS-1 (Ching et al., 2013a). ATM inhibition with the use of KU-60019 has been demonstrated to interfere with pro-survival signalling through reduced PKB/Akt phosphorylation in glioma cells (Golding et al., 2009). However, ATM does not participate in insulin-stimulated activation of PKB/Akt in all tissue types as has been shown in skeletal muscle (Ching et al., 2013a).

We were interested to see whether or not ATM is involved in the cardiac pathology associated with IRI and how ATM could be involved in insulin mediated signalling in the heart. During ischaemia, cardiac metabolism shifts from fatty acid oxidation to glucose oxidation. The insulin signalling network is therefore important during ischaemia. Improved cardiac function is seen when glucose oxidation is increased during ischaemia (Traegtmeyer et al., 1997) and it is therefore expected that ATM deficiency would result in decreased cardiac functioning following an ischaemic period due to the associated insulin resistance and glucose intolerance.

Schiekofer et al. (2014) indicated that a single nucleotide polymorphism located near the ATM gene is associated with coronary artery disease in men and they suggested that ATM could thus be associated with CVD. The authors did not elucidate a mechanism in which ATM activity could contribute to cardiovascular health. Another polymorphism, located in the *ATM* promotor region, was associated with ATM expression, the degree of coronary stenosis and the prevalence of diabetes mellitus in a Chinese cohort (Li et al., 2011). A role for ATM in cardiac structure and function has been suggested. ATM deficiency caused increased basal cardiac fibrosis and apoptosis and this was exacerbated in response to β-adrenergic receptor stimulation and following myocardial infarction (Foster et al., 2011; Foster et al., 2012; Daniel et

al., 2014). Interestingly, ATM deficiency delayed the inflammatory response following myocardial infarction, attenuated left ventricular dysfunction and resulted in decreased mortality early following myocardial infarction (Foster et al., 2013). However, decreased activation of PKB/Akt (pro-survival) and increased activation of GSK-3β (pro-apoptotic) was observed in ATM deficient hearts one day following myocardial infarction (Daniel et al., 2014). Although ATM deficiency appeared to be beneficial early post-IRI (1-7 days), ATM deficient animals had a decreased survival rate, increased cardiac dysfunction and remodelling associated with apoptosis, fibrosis and hypertrophy late post-IRI (28 days) (Daniel et al., 2016). Mu et al. (2011) showed that activation of ATM with PE resulted in reduced cardiac remodelling, fibrosis and cardiac dysfunction eight weeks following myocardial infarction.

Long-term ATM deficiency, as seen in ATM knockout mice, resulted in structural cardiac changes. Foster et al. (2012) found that ATM knockout mice had smaller heart weights, reduced septal wall thickness, reduced left ventricular diameters, increased basal fibrosis and increased cross-sectional areas of cardiomyocytes compared to wild type mice. In response to chronic β-adrenergic receptor stimulation, increased apoptosis, possibly due to decreased PKB/Akt activity, was observed in ATM knockout mice (Foster et al., 2012).

In our study, KU-60019, administered prior to regional ischaemia, had no effect on cardiac function during reperfusion in either the control or HCD hearts. We observed no changes in CF, total work, aortic SP or heart rate (Tables 4.9, 4.11 to 4.13). When co-administered with insulin, KU-60019 reduced AO to vehicle control levels compared to when only insulin was administered in control hearts (Table 4.10). Based on these haemodynamic results, ATM inhibition therefore appeared to block the protective effect of insulin in control hearts, suggesting a role for ATM in the signalling network of insulin.

However, KU-60019 administration resulted in improved cardiac outcomes during reperfusion following global ischaemia according to our Langendorff balloon model perfusion studies. Improved RPP values and LVDevP were achieved in both the control and HCD hearts in response to KU-60019 treatment (Tables 4.3 and 4.4). Interestingly, KU-60019 increased insulin-stimulated LVDevP and RPP at both five and ten minutes of reperfusion. Additionally, KU-60019 treatment resulted in increased times to the onset of contracture during global ischaemia as well as lower peak developed pressures that were achieved during global ischaemia in both the control and HCD hearts (Table 4.7). Together, these data indicate that ATM inhibition prior to an ischaemic period resulted in improved cardiac function, at least during early reperfusion. These findings are in agreement with the studies of Foster et al. (2013) and Daniel et al. (2014) who also observed that ATM deficient hearts had reduced cardiac dysfunction early following myocardial infarction.

During ischaemia, oxygen and nutrient supply is prevented, while waste products accumulate (Beauloye et al., 2001). It is possible that the increased CF observed in response to KU-60019 treatment contributed to the improved cardiac function seen in KU-60019 treated hearts as accumulated waste products were cleared, and oxygen and nutrient supply was restored faster.

When looking at cardiac function parameters measured with the Langendorff balloon model, the effect of KU-60019 treatment was smaller at 10 minutes versus at five minutes reperfusion (Table 4.3) or was no longer seen at 10 minutes reperfusion (Table 4.6). KU-60019 is a reversible inhibitor of ATM (Golding et al., 2012), which means its effect disappeared as it was washed out during reperfusion. It is possible that this is why we did not observe changes in cardiac function during our work heart studies as functional parameters were only measured after approximately 25 minutes of reperfusion.

ATM inhibition had no effect on IFS in control hearts. This is in agreement with other studies that also observed no differences in IFS between hearts from wild-type mice and hearts from ATM heterozygous knock-out mice at one, three, seven and 28 days post myocardial infarction (Foster et al., 2013; Daniel et al., 2014; Daniel et al., 2016). However, in contrast to findings in the ATM heterozygous KO animals, acute inhibition of ATM in hearts from HCD animals protected the hearts and infarcts were smaller compared to untreated HCD hearts as well as compared to KU-60019 treated control hearts (Figure 4.73).

5.4 Insulin signalling in control and HCD hearts

Langendorff perfused hearts were treated with insulin, KU-60019 and a combination of insulin and KU-60019 for 20 minutes following a stabilisation period. Proteins that participate in the insulin signalling network were analysed with Western blots to determine what the effects of the treatments are in the absence of IRI (before ischaemia) and following 10 minutes of reperfusion.

5.4.1 Before ischaemia

In control hearts, JNK expression and activation was not altered by insulin (Figure 4.14). However, insulin treatment did increase IRS-1 Ser307 phosphorylation (Figure 4.16). This is possibly due to inhibition in response to hyperinsulinaemia caused by the 1 U/L insulin treatment. In response to insulin, Ser307 phosphorylation of IRS-1 acts as a mechanism for negative feedback to down regulate insulin action (Rajan et al., 2013). PI3K (p85 subunit), which is downstream of IRS-1 in the insulin signalling network, was also down regulated in response to insulin treatment in control hearts (Figure 4.18). In spite of the apparent down regulation of insulin signalling, PKB/Akt activation was increased in response to insulin treatment, as expected in the insulin responsive control hearts (Figure 4.22). Furthermore, AS160, which is a downstream substrate of activated PKB/Akt (Kane et al., 2002), was also activated in response to insulin treatment and PKB/Akt activation (Figure 4.28).

Hirosumi et al. (2002) reported increased JNK activity in liver, adipose and muscle tissue in a diet-induced obesity animal model. JNK plays a central role in the stress-induced insulin resistance observed in obesity. JNK is activated by elevated TNF-α and FFA in obesity, which in turn inhibits IRS-1 through phosphorylation of its Ser307 residue (Hirosumi et al., 2002). Phosphorylation of Ser307 is associated with reduced insulin signalling (Aguirre et al., 2002). We did not see increased activity of JNK in hearts from our obese HCD model compared to the control diet (Figure 4.15). Insulin treatment caused reduced activation of JNK in HCD hearts compared to untreated HCD hearts, suggesting that insulin had a protective effect in the HCD hearts in spite of their insulin resistant state (Figures 4.15). Unfortunately, we were unable to determine IRS-1 Ser307 levels in HCD hearts, even after numerous attempts. It is therefore not known if insulin signalling was reduced in HCD hearts due to IRS-1 inhibition and insulin had no effect on p85 subunit of PI3K in HCD hearts.

The phosphatase, PTEN, antagonises the effect of PI3K by dephosphorylating PIP_3 to PIP_2 and in doing so, PTEN inhibits insulin signalling (Maehama and Dixon, 1998). The phosphatase activity of PTEN is reduced upon phosphorylation at residues Ser380, Thr382 and Thr383 (Yang et al., 2015). Compared to the control hearts, HCD hearts had decreased phosphorylation of PTEN and therefore increased phosphatase activity and increased inhibition of insulin signalling (Figure 4.21). Insulin treatment caused a further increase in PTEN phosphatase activity through a reduction in PTEN phosphorylation in HCD hearts. The increased activity of PTEN, together with reduced PI3K activity in HCD hearts, indicated by a reduced P/T ratio of its regulatory subunit (Figure 4.19), indicate that insulin signalling was ineffective in HCD hearts. Consistent with the insulin resistant state of the HCD hearts, PKB/Akt and AS160 were not phosphorylated in response to insulin treatment (Figures 4.23 and 4.29). Additionally, insulin did not increase GLUT4 expression in HCD hearts (Figure 4.30D) and HCD hearts had reduced GLUT4 levels compared to control hearts.

GSK-3β regulates metabolism by controlling glycogen and protein synthesis (Cross et al., 1995). Insulin signalling inhibits GSK-3β by PKB/Akt-dependent phosphorylation, resulting in increased GS activity and consequently, increased conversion of glucose to glycogen. In contrast to this well-known effect of insulin on GSK-3β, we found that insulin treatment increased GSK-3β activity in control hearts, thereby reducing glucose conversion to glycogen (Figure 4.26). We are not certain why we observed increased GSK-3β activity after insulin treatment and would need to redo the analysis to confirm the results. Insulin had no effect on GSK-3β phosphorylation in the HCD hearts.

Another protein downstream of PKB/Akt in the insulin signalling network is mTOR. Cell growth is regulated by mTOR according to the nutrient and energy status of the cell as well as in response to growth factors such as insulin (Chiang and Abraham, 2005). Although mTOR is activated by insulin signalling, it has been suggested that mTOR is also a negative modulator of insulin signalling (Khamzina et al., 2005). Insulin had no effect on mTOR in control hearts (Figure 4.24). We observed increased expression and phosphorylation of mTOR in hearts from HCD animals compared to hearts from control animals (Figure 4.25). Insulin treatment further increased mTOR phosphorylation in the HCD hearts (Figure 4.25 C). Our results correspond with the findings of Khamzina et al. (2005) who also found that mTOR was hyperphosphorylated in muscle of obese rats fed a diet high in sugar and fat. Chronic activation of mTOR has been associated with the promotion of insulin resistance in muscle as it leads to serine phosphorylation of IRS-1 (Haruta et al., 2000; Tremblay and Marette, 2001).

AMPK acts as an energy sensor that activates ATP generating processes such as fatty acid oxidation and inhibits ATP consuming processes such as fatty acid synthesis (Ruderman et al., 2013). Reduced activation of AMPK was seen in the insulin resistant HCD hearts compared to control hearts (Figure 4.32). This is consistent with previous studies (Gauthier et al., 2011; Steinberg et al., 2006). The increased TNF-α levels associated with obesity, increase the

transcription of the phosphatase PP2C. This in turn leads to the de-activation and suppression of AMPK (Steinberg et al., 2006). Insulin is able to inhibit AMPK through PKB/Akt-dependent phosphorylation of Ser485/491 (Valentine et al., 2014). Although we did not quantify the inhibitory phosphorylation site of AMPK (Ser485/491), we did quantify the activation phosphorylation site of AMPK (Thr172) (Hawley et al., 1996). Insulin treatment did not alter the Thr172 phosphorylation status significantly in control or HCD hearts in our study. The P/T ratio was however lower in both the control and HCD hearts in response to insulin administration (Figures 4.31 & 4.32). In control hearts, the reduced P/T ratio was due to increased AMPK expression in response to insulin. AMPK expression was however unchanged by insulin in HCD hearts. The reduced P/T ratio observed in HCD hearts was possibly due to altered AMPK phosphorylation as AMPK phosphorylation tended to be reduced by insulin in HCD hearts, although not significantly so ($p=0.08$). Reduced P/T AMPK ratios are an indication that AMPK activity was reduced with insulin treatment, however, a reduction in AMPK activity has been seen without an accompanying reduction in AMPK Thr172 phosphorylation (Valentine et al., 2014).

AMPK inactivates ACC by phosphorylation (Davies et al., 1990). In spite of reduced AMPK activity in HCD hearts compared to control hearts, we observed an increase in total ACC and ACC phosphorylation in HCD hearts, however, the P/T ACC ratio was reduced in HCD hearts compared to control hearts (Figure 4.34). It is believed that increased β-oxidation of fatty acids and reduced fatty acid synthesis resulting from inhibition of ACC activity could be protective against cardiovascular risk factors associated with the metabolic syndrome (Harwood, 2000).

In response to insulin, AMPK activity is reduced, leading to activation of ACC due to reduced phosphorylation of ACC (Witters and Kemp, 1992). Our results in control hearts are consistent with this as the reduced P/T AMPK ratio in response to insulin led to reduced phosphorylation, and therefore increased activation, of ACC (Figure 4.33). ACC inhibits β-oxidation of fatty acids

and promotes fatty acid synthesis. This is consistent with the Randle cycle theory, where insulin treatment inhibits fatty acid oxidation while glucose oxidation is favoured (Randle et al., 1963). Taken together, our Western blot data confirms that hearts from animals on the control diet were insulin responsive while the insulin signalling network was not stimulated by insulin in the insulin resistant HCD hearts.

5.4.2 During early reperfusion

Hearts pre-treated with insulin underwent 20 minutes of global ischaemia. After 10 minutes of reperfusion in the absence of insulin, insulin signalling intermediates were analysed with Western blot analysis. Activation of PKB/Akt in response to insulin is inhibited during ischaemia due to reduced pH during ischaemia. Insulin signalling is however resumed quickly upon reperfusion (Beauloye et al., 2001). Activation of the insulin signalling network in reperfusion is associated with improved cardiac outcomes following IRI.

Although ACC was activated during reperfusion in control hearts in response to insulin (Figure 4.65), none of the other proteins analysed (JNK, IRS-1, p85 subunit of PI3K, PTEN, PKB/Akt, mTOR, GSK-3β, AS160, GLUT4 or AMPK) were affected by insulin in control or HCD hearts. This suggests that insulin signalling was not increased during reperfusion in response to insulin treatment before ischaemia and this could explain the increased IFS observed in insulin treated hearts. However, ACC activation during reperfusion is considered to have a protective effect on the heart as fatty acid β-oxidation is inhibited by the increase in malonyl coenzyme-A and the resultant stimulation of glucose oxidation (Lopaschuk, 1997).

We did observe differences in proteins of the insulin signalling network in HCD hearts compared to control hearts. IRS-1 was inhibited in HCD hearts (Figure 4.41) and reduced activation of PI3K was seen (Figures 4.44 and 4.45). Interestingly, PKB/Akt was more active in HCD hearts during reperfusion (Figure 4.51), which led to increased phosphorylation of AS160 (Figure 4.60).

Increased phosphorylation of ACC was also observed in HCD hearts compared to control hearts during reperfusion (Figure 4.67). The decreased activity of ACC suggests that HCD hearts had increased oxidation of fatty acids during reperfusion compared to control hearts in spite of PKB/Akt activation and AS160 phosphorylation. The fact that insulin signalling was not completely blocked in HCD hearts during reperfusion is a possible explanation as to why we did not observe reduced cardiac function and increased IFS in HCD hearts compared to control hearts in our study.

5.5 The role of ATM in the insulin signalling network

ATM is suggested to participate in the insulin signalling network in skeletal muscle, but it is not yet clear if this is the case in cardiac muscle. In order to elucidate the role of ATM in the insulin signalling network in the heart, the effect of ATM inhibition on insulin signalling intermediates was determined in perfused hearts. Our basal Western blot analysis revealed that ATM expression was decreased in the insulin resistant HCD hearts compared to control hearts (Figure 4.1). In line with previous studies that showed increased ATM activity in response to insulin (Yang and Kastan, 2000), we observed increased expression and phosphorylation of ATM in the insulin-responsive control hearts following treatment with insulin. Treatment with KU-60019 reduced ATM phosphorylation in control hearts, implying reduced ATM activity. KU-60019 was able to block the ATM-stimulating effect of insulin (Figure 4.35). These results validate the use of insulin as an ATM activator and the use of KU-60019 as an ATM inhibitor in the study. Although ATM was expressed in HCD hearts, insulin had no effect on ATM expression or activation levels and KU-60019 treatment did not decrease ATM activity further (Figure 4.36). This suggests that the reduced ATM levels in HCD hearts are resistant to manipulation.

An inverse relationship was seen between the amount of ATM expressed and JNK activity by Schneider et al. (2006), while Halaby et al. (2008) detected no difference in JNK activity associated with ATM deficiency. In our study, JNK activity was not altered in control hearts while HCD hearts had reduced JNK activity when ATM was inhibited (Figures 4.14 and 4.15). ATM deficiency was therefore not likely to influence insulin signalling via JNK according to our results.

ATM inhibition reduced IRS-1 expression levels and insulin-stimulated inhibition of IRS-1 in control hearts (Figure 4.16). Ching et al. (2013a) found that IRS-1 activation (Tyr612) was not affected by ATM deficiency and they therefore suggested that ATM participates in insulin signalling downstream of IRS-1. Our results support this notion as ATM inhibition did not increase IRS-1 inhibition.

Reduced phosphorylation of the p85 subunit of PI3K (Figures 4.18 and 4.19) and increased phosphatase activity of PTEN (Figures 4.20 and 4.21) was seen when ATM was inhibited. Although this is suggestive of inhibition of the insulin signalling network, the effect was not seen in PKB/Akt as PKB/Akt activity was not affected by ATM inhibition (Figures 4.22 and 4.23). As previously mentioned, ATM has been shown to participate in activation of PKB/Akt in skeletal muscle and KU-60019 reduced basal phosphorylation of PKB/Akt (Ser473) in human glioma cells (Golding et al., 2009). It was proposed that ATM regulates a phosphatase, which in turn regulates PKB/Akt phosphorylation as PKB/Akt does not have an ATM recognition site. It was, however shown in other studies that PKB/Akt activation is not ATM-dependent and the involvement of ATM appears to be cell type dependent (Jeong et al., 2009). Our results indicate that ATM is not involved in PKB/Akt activation in the heart as PKB/Akt was not affected by ATM inhibition in either the control or HCD hearts (Figures 4.22 and 4.23). This is not entirely consistent with the results of Foster et al. (2012). They found that PKB/Akt activation tended to be reduced in ATM knock-out hearts, however this effect was not significant. Mu et al. (2011)

found increased phosphorylation of PKB/Akt in the areas surrounding infarcted tissue in response to treatment with PE, which is believed to activate ATM. This effect was only observed in response to PE in the presence of myocardial infarction and not in the absence of PE or in the absence of myocardial infarction. This suggests that ATM is only involved in PKB/Akt activation under very specific conditions, which is in agreement with the views of Ching et al. (2013a). This notion is further supported by the findings of Ching et al. (2013b). They found that, in response to insulin, ATM phosphorylates PKB/Akt in skeletal muscle comprised of fast glycolytic fibers, but that AS160, and not PKB/Akt, is phosphorylated by ATM in muscle comprised of slow and fast oxidative-glycolytic fibers.

Although PKB/Akt activation was not affected when ATM was inhibited, AS160 phosphorylation was reduced with KU-60019 treatment in HCD hearts (Figure 4.29). This is an indication that ATM could function on the level of AS160 in HCD cardiomyocytes. AMPK has been shown to be an activator of AS160 and this effect is independent of insulin (Treebak et al., 2006). ATM inhibition resulted in AMPK inhibition in HCD hearts in our study (Figure 4.32) and it is possible that the reduced activity of AMPK also contributed to the reduced activation of AS160 in HCD hearts. ATM is a known activator of AMPK (Fu et al., 2008; Suzuki et al., 2004), which is consistent with our results in HCD hearts. ACC activity was not affected by KU-60019 treatment in HCD hearts (Figure 4.34).

In control hearts, insulin-stimulated phosphorylation of AS160 was further increased by KU-60019 treatment, and the P/T AS160 ratio was increased in hearts by KU-60019 treatment alone as well as in hearts co-treated with insulin and KU-60019 (Figure 4.28). This was an unexpected finding as ATM deficiency led to reduced AS160 phosphorylation in soleus muscle and L6 myotubes (Ching et al. 2010; Jeong et al., 2010). The effect of ATM on AS160 activation needs to be investigated further. Expression levels of GLUT4, which is downstream of AS160,

was unaffected by ATM manipulation (Figure 4.30). Future measurement of GLUT4 translocation could shed more light on the effects elicited by ATM.

KU-60019 treatment alone had no effect on AMPK or ACC phosphorylation in control hearts. The P/T AMPK ratio was higher in the insulin and KU-60019 co-treated hearts compared to hearts treated with insulin alone (Figure 4.31). This suggests that insulin is unable to inhibit AMPK activity in the absence of ATM. The increased activity of AMPK after insulin and KU-60019 co-treatment caused increased phosphorylation of ACC, resulting in increased β-oxidation of fatty acids in co-treated control hearts. These results indicate that insulin action on AMPK and ACC was blocked when ATM was inhibited in control hearts.

According to Foster et al. (2012), activation of GSK-3β was not affected in ATM knockout hearts compared to wild type hearts, while Thornton et al. (2016) found that nuclear GSK-3β is inhibited by ATM in response to DSB. Our results are in agreement with Thornton et al. (2016) as we also observed that ATM inhibition resulted in reduced expression and phosphorylation of GSK-3β in both the control and HCD hearts. (Figures 4.26 and 4.27). This suggests that GSK-3β phosphorylation is increased in the presence of active ATM and that ATM thus acts as a GSK-3β inhibitor in the heart. This is in line with the effect of insulin on GSK-3β and it is thus possible that ATM is involved in insulin mediated inhibition of GSK-3β.

Very few of the analysed proteins were altered during reperfusion in response to ATM inhibition prior to ischaemia. We believe that this is due to the reversible nature of the ATM inhibitor used in this study. The inhibitor was washed out during reperfusion and ATM could thus be activated as normal during reperfusion. In spite of this, hearts in which ATM was inhibited prior to ischaemia had reduced activation of JNK during reperfusion (Figure 4.40). JNK is usually activated during reperfusion (Yin et al., 1997) and JNK-knockout mice have been shown to have better cardiac outcomes following IRI compared to wild-type mice (Kaiser et al., 2005). It is

possible that the reduced activation of JNK seen in KU-60019 treated hearts contributed to the improved cardiac function seen in hearts in which ATM was inhibited.

5.6 The role of ATM in vasoconstriction

The innermost layer of blood vessels, the endothelium, acts as an autocrine, paracrine and endocrine organ to maintain vasomotor balance and vascular-tissue homeostasis (Esper et al., 2006). The endothelium achieves vasodilation and vasoconstriction by modulation of the vascular smooth muscle. One of the most potent endothelium-derived factors is NO, which is an effective vasodilator (Eliseyeva, 1013).

In response to treatment with KU-60019, we observed an immediate increase in CF during Langendorff perfusions (Table 4.6). This effect of KU-60019 was also seen in the work heart perfusions during the treatment period (data not shown), but was lost by the time functional data was collected (~25 minutes into reperfusion; Table 4.9). The increased CF could not be due to increased pressure as Langendorff perfusions were performed at a constant preload pressure of 100 cm H_2O and we also did not observe an increase in LVDevP during the KU-60019 administration period (Table 4.3). The increased CF was an interesting and unexpected observation. We therefore performed aortic ring isometric tension studies to determine if ATM inhibition has a vasodilatory effect.

PE has been shown to increase ATM kinase activity (Mu et al., 2011). PE is commonly used to induce vasoconstriction of smooth muscle cells by acting on α_1-adrenergic receptors. It is thus possible that ATM could participate in the vasoconstriction mechanism of PE. In our study, the ATM inhibitor, KU-60019 induced relaxation of aortic rings (Figure 4.75). Our results therefore suggest a vasoconstrictive role for ATM. The vasodilation induced by KU-60019 was dependent on NO, as vasodilation was inhibited by the non-specific NOS inhibitor, L-NAME. This suggests that NO production is increased when ATM activity is reduced. This is however not consistent

with the study of Oleson et al. (2014) that showed that ATM inhibition reduced NO-induced effects. They, however, looked at the ability of NO to induce DNA damage as a reactive nitrogen species and not at the vasodilative effect of NO. Nevertheless, our results are in agreement with, and can explain the telangiectasias seen especially in the vessels of the eyes of A-T patients.

Together with the increase in CF, the temperature of the heart rose considerably in response to KU-60019 treatment during the Langendorff perfusion studies (data not shown). Heat production is a by-product of mitochondrial respiration, the rate of which increases with increased contractility of muscle (van Beek, 1996; Ricquier and Bouillaud, 2000). Although we did not observe an increase in heart rate or pressure development with the increase in temperature due to KU-60019 treatment, it would be interesting to analyse mitochondria after exposure to KU-60019 to determine if mitochondrial respiration is affected or if there are differences in the expression of the uncoupling proteins induced by inhibition of ATM.

It is however possible that the increased temperature was merely caused by the increased CF as the buffer had less time to cool down between the bubble trap and the heart. Increased temperature leads to increased activity of NOS and subsequently, an increase in NO production (Brown and Borutaite, 2007). In order to reduce the temperature, NO increases blood flow by vasodilation. NO also reduces heat production by reducing mitochondrial respiration through inhibition of complex IV of the electron transport chain (Sarti et al., 2003).

5.7 The use of chloroquine as a pharmaceutical activator of ATM in the heart

Chloroquine has been used as an antimalarial drug since World War II (Tönnesmann et al., 2013). Since then, studies that show glucose lowering effects of chloroquine, specifically in the diabetic state, have emerged (Emami et al., 1999). This effect of chloroquine is mediated, at least in part, by an increase in insulin secretion (Asamoah et al., 1990). Another mechanism in

which chloroquine has been shown to increase glucose tolerance is via activation of ATM and subsequent activation of PKB/Akt (Halaby et al., 2013; Schneider et al., 2006; Zhou et al., 2013).

Chloroquine has been suggested as a therapeutic agent in the treatment of insulin resistance, glucose intolerance and diabetes (Asamoa et al., 1990; Schneider et al., 2006). We aimed to test the feasibility of the use of chloroquine, specifically in the cardiac context.

Unlike the study in L6 muscle cells by Halaby et al. (2013), we did not observe an increase in glucose uptake in response to chloroquine treatment in isolated cardiomyocytes (Figure 4.4). Insulin treatment (100 nM) also did not increase glucose uptake which could imply a possible methodological problem. However, insulin treatment did tend to increase glucose uptake ($p=0.09$) and this effect could have become significant if the n-value was increased from three to six as in the insulin concentration experiments. In addition to not observing an effect of chloroquine on glucose uptake, we also did not observe an increase in ATM expression or activation in response to chloroquine treatment in Langendorff perfused hearts (Figure 4.7). This suggests that chloroquine does not activate ATM in cardiac tissue and, consequently, does not cause an increase in glucose uptake in cardiomyocytes as it does in skeletal muscle tissue. However, the possibility exists that chloroquine requires a longer treatment period to have its effect. In our study, the chloroquine treatment period was 45 minutes for the glucose uptake study and 10 minutes for the perfusion and ATM Western blot analysis, while Halaby et al. (2013) allowed a three-hour treatment period after which they observed chloroquine-dependent effects. Other studies suggest chronic chloroquine treatment (Asamoah et al., 1990; Schneider et al., 2006). Rats in which myocardial infarction had been induced, were administered low-dose chloroquine daily over 12 weeks following the myocardial infarction procedure. Chloroquine was found to significantly increase phosphorylation of PKB/Akt and reduce cardiomyocyte apoptosis (Zhou et al., 2013).

Chronic treatment with chloroquine is, however, problematic as cardiotoxic effects in the form of conduction disorders and cardiomyopathy have been reported (Teixeira et al., 2002; Tönnesmann et al., 2013). Our results are consistent with results where the cardiotoxic effect of chloroquine was observed. A cell viability assay using PI revealed that chloroquine concentrations of 10 μM and 50 μM significantly increased necrosis in isolated cardiomyocytes (Figure 4.5). Furthermore, chloroquine had a severely detrimental effect on cardiac function as observed in Langendorff balloon model perfusion studies. Following 10 minutes of chloroquine perfusion, a significant decrease in LVDevP and heart rate was observed (Figure 4.6). Interestingly, the highest chloroquine concentration, namely 100 μM, did not result in significant necrosis, suggesting a potential concentration-dependent cardiotoxic effect.

Although glucose lowering effects were observed at a higher chloroquine concentration (100 μM) and at a longer treatment period (three hours) in the study conducted by Halaby et al. (2013) in L6 myoblasts, this is not possible in the heart. We found that heart function was adversely affected almost instantaneously with chloroquine perfusion with concentrations as low as 10 μM (data not shown). These results should be followed up by an *in vivo* study where animals are orally treated with chloroquine to substantiate or negate the effects observed with *ex vivo* perfusions.

Taken together, our results strongly argue that chloroquine is not a suitable pharmaceutical agent in the treatment of insulin resistance and glucose intolerance as it has proved to be ineffective in the heart with possible cardiotoxic effects.

Chapter 6: Concluding Chapter

6.1 Conclusion

In this study we made use of a diet with a high carbohydrate and fat content to induce obesity, glucose intolerance and insulin resistance in a rat model. This HCD resulted in reduced ATM and PKB/Akt expression, however, ATM and PKB/Akt activity was increased as seen by the increased P/T ratios. In spite of these effects, the HCD did not have a detrimental effect on cardiac function and IFS was not larger in the HCD hearts compared to control hearts. In response to insulin treatment, control hearts had increased cardiac haemodynamic function during reperfusion. Insulin treatment activated the insulin signalling pathway prior to ischaemia, but not during reperfusion. Furthermore, the insulin concentration used in this study was possibly too high as IFS was larger in insulin treated hearts compared to untreated hearts. Infarct size is considered the golden standard to evaluate cardioprotection. The increased IFS observed in response to insulin therefore indicate that insulin did not protect the control hearts in spite of the improved haemodynamic effect that insulin had on the control hearts. In line with their insulin resistant state, HCD hearts did not have improved cardiac haemodynamic function in response to insulin and insulin-stimulated cardiac function was less efficient in HCD hearts compared to control hearts. This is possibly due to the fact that the animals were insulin resistant, therefore, the insulin signalling pathway was not activated in response to insulin, either before ischaemia or during reperfusion in HCD hearts. Insulin also resulted in larger IFS in HCD hearts.

The main aim of this study was to determine the effect of ATM in cardiac function and the role of ATM in the cardiac insulin signalling network. Insulin was used as an ATM activator and KU-60019 was used to inhibit ATM. In control hearts, ATM activation was increased with insulin and

decreased with KU-60019, as expected. However, neither insulin nor KU-60019 altered ATM activation in HCD hearts. ATM inhibition resulted in increased cardiac function during early reperfusion (10 minutes) following global ischaemia in control and HCD hearts. Following regional ischaemia, later in reperfusion (~25 minutes), ATM inhibition attenuated the improved heamodynamic effect of insulin in control hearts while ATM inhibition had no effect in HCD hearts during later reperfusion.

PKB/Akt activation is said to be ATM-dependent in some tissues while it is ATM-independent in other tissues. We found that ATM inhibition did not reduce insulin-stimulated PKB/Akt activation and we therefore conclude that PKB/Akt activation is not ATM-dependent in cardiac tissue. In both control and HCD hearts, ATM inhibition decreased PI3K activation and increased PTEN and GSK-3β activity. Although these effects are consistent with down-regulation of the insulin signalling pathway, it is still not completely clear how ATM fits into the insulin signalling pathway.

Besides insulin, oxidative stress is another known activator of ATM which will inevitably affect cardiac ATM during IRI. The regulation of signalling networks is complex and elucidating the role of a master regulator such as ATM, which has been said to have close to 500 substrates (Matsuoka et al., 2007), is not a simple task. What complicates matters more is that it has been proposed that different tissues have different responses to ATM deficiency (Hammond and Muschel, 2014) and that the role of ATM in insulin signalling is dependent on the type of cell (Yang and Kastan, 2000). Moding et al. (2014) found that ATM-deficient proliferating endothelial cells of tumours were sensitive to radiation while ATM-deficient quiescent endothelial cells were not sensitive to radiation. This indicates that the state of a cell also influences the role of ATM.

With this study we have only started to scratch at the surface of the cardiac function of ATM and many questions remain to be answered. More in depth and detailed studies would need to be

conducted before we will fully understand the importance of the ATM protein in the myocardial pathology associated with insulin resistance.

6.2 Shortcomings and limitations of the study

- Some of the drug dosage studies (ie. PI studies and KU-60019 concentration perfusions) had an n-value of 2. For statistical reasons, larger n-values should have been used.
- We used hearts from animals on the HCD and age-matched control diet only. We did not include a young control group. Aging Wistar rats have been shown to have signs of the metabolic syndrome (Ghezzi et al., 2012) so our age-matched control group was possibly not completely healthy.
- Western blot analysis to evaluate the insulin signalling intermediates during reperfusion was performed on animals that have been on the diet for 25 weeks. Although we determined that the longer feeding time had no effect on cardiac function, we did not determine if the longer feeding time affected basal protein expression levels.
- Many of the hearts in the working heart studies did not regain cardiac function following regional ischaemia. This resulted in low n-values for the working heart data. Larger n-values would have provided a clearer and more accurate picture of the effects of the treatments. However, because of the large amount of animals already used in the study, we were unable to further increase the n-values.
- We did not look at the effect of the drugs when administered in the beginning of reperfusion. The drugs were washed out during reperfusion which potentially limited or reversed their effects. This especially applies to KU-60019. The reversible nature of the KU-60019 inhibitor meant that its effect was lost during the initial phase of reperfusion. More distinct results would have been obtained if KU-60019, and the other drugs used, could have remained in the perfusate during reperfusion. However, only small amounts of the inhibitor can be acquired which limited our use of it. We had to use KU-60019 in a re-circulating manner and since we reperfused for an hour during the work heart studies, it was not a viable option to have the inhibitor in the perfusate during reperfusion.
- The fact that the treatments were re-circulated could potentially have influenced the effects observed. Webster et al. (2014) reported that different outcomes were observed in response to treatment with sanguinarine, depending on whether the drug was re-

circulated or not. We did not test whether or not re-circulation had an effect on the drugs used in this study.

- We only looked at the effect of acute ATM deficiency on cardiac function and insulin signalling. Insulin resistance, diabetes and CVD develop over time. In has been suggested that the insulin resistance and glucose intolerance observed in A-T patients is due to the accumulation of oxidative damage over time (Armata et al., 2010). Clearer results could possibly have been obtained if ATM was inhibited chronically by treating animals with KU-60019.
- The aortic ring studies were only performed on aortas isolated from age-matched control animals. It would have been interesting to see what the effect would have been on aortas from the HCD animals.

6.3 Future research

- It was shown in several studies that different cell types have different functions for ATM. It could thus be informative to look at the different cardiac cells, namely cardiomyocytes, fibroblasts and endothelial cells separately.
- Our Western blot analyses were done before ischaemia and during reperfusion, not during ischaemia. Hypoxia is a known ATM activator so it will be interesting to observe how ATM responds to hypoxia during cardiac ischaemia.
- It has been proposed that accumulated oxidative stress experienced in ATM deficiency contributes to the disrupted glucose tolerance seen in the ATM deficient state. Oxidative stress is also an ATM activator. Future studies should thus look at the effect of oxidative stress caused specifically by ATM deficiency on insulin signalling.
- KU-60019 treatment does not block ATM activation completely and residual ATM activity could make it difficult to observe effects of ATM deficiency. A-T heterozygotes do not display the debilitating symptoms seen in A-T patients, indicating that even with reduced ATM expression levels, ATM function could be normal. The use of ATM knockout animals will combat this problem.

- During treatment with KU-60019, the temperature of the heart was significantly higher. It will be interesting to further investigate the cause of the increased heat production in response to ATM inhibition.

6.4 Research Outputs

The following publications and conference contributions were produced during this study:

Publication

- **Espach, Y**., Lochner, A., Strijdom, H. and Huisamen, B. 2015. ATM protein kinase signaling, type 2 diabetes and cardiovascular disease. Cardiovascular Drugs and Therapy, 29(1), 51-58. doi: 10.1007/s10557-015-6571-z

Published abstracts

- Huisamen, B., Strijdom, H., Collop, N., **Espach, Y**. 2014. A possible role for the ATM protein in the myocardial pathology associated with obesity and insulin resistance. Cardiovascular Research, 103 (Suppl 1), S118. doi: 10.1093/cvr/cvu098.75
- Huisamen, B., van Vuuren, M.A., Espach, Y., Marais, E. and Lochner, A. 2016. Is low ATM protein responsible for myocardial insulin resistance associated with obesity? Cardiovascular Research. 111(Suppl 1), S88-S89. doi: 10.1093/cvr/cvw147

International conference contributions

- Huisamen, B., van Vuuren, M.A., **Espach, Y.**, Marais, E. and Lochner, A. Is low ATM protein responsible for myocardial insulin resistance associated with obesity? 4th Meeting of the ESC Council on Basic Cardiovascular Science. Florence, Italy. July 8-10, 2016. (Oral presentation by Prof. Huisamen)
- **Espach, Y**. and Huisamen, B. Myocardial functioning and response to ischemia/reperfusion injury following manipulation of the ATM protein kinase. 33rd Meeting of the European Section of the International Society for Heart Research. Bordeaux, France. July 1-4, 2015. (Poster presentation)

- Huisamen, B., Strijdom, H., Collop, N., **Espach, Y**. A possible role for the ATM protein in the myocardial pathology associated with obesity and insulin resistance. Third Congress of the ESC Council on Basic Cardiovascular Science. Barcelona, Spain. July 4-6, 2014. (Poster presented by Prof. Huisamen)

Local conference contributions

- **Espach, Y**. and Huisamen, B. The effect of ATM on myocardial function and cardiac signalling networks following ischemia/reperfusion injury. Diabetes Discovery Platform Research Symposium. MRC, South Africa. November 10, 2014.
- Huisamen B, Strijdom H, Collop N, **Espach Y**. A possible role for the ATM protein in the myocardial pathology associated with obesity and insulin resistance. 15th Annual SA Heart congress in collaboration with the ESC. Durban, South Africa. October 16-19, 2014. SA Heart Journal 11(4):183-184. (Poster presented by Prof. Huisamen)
- **Espach, Y**. and Huisamen, B. An investigation into the importance of the ATM protein in the myocardial pathology associated with insulin resistance and type 2 diabetes. Diabetes Discovery Platform Research Symposium. MRC, South Africa. June 23, 2014.
- **Espach, Y**. and Huisamen, B. The importance of the ATM protein in the myocardial pathology associated with insulin resistance. 41st Conference of the Physiology Society of Southern Africa. Pretoria, South Africa. 15-18 September, 2013. (Poster presentation).

Honours student co-supervised

- Ascentia M. Seboko – Graduated December 2015

  Project title: Elucidating the role of ATM in the insulin signalling pathway.

Chapter 7: References

Abel, E.D. 2004. Glucose transport in the heart. Frontiers in Biochience: A Journal and Virtual Library. 9, 201-215.

Aguirre, V., Werner, E.D., Giraud, J., Lee, Y.H., Shoelson, S.E. and White, M.F. 2002. Phosphorylation of Ser307 in insulin receptor substrate-1 blocks interactions with the insulin receptor and inhibits insulin action. The Journal of Biological Chemistry. 277(2), 1531-1537.

Aksakal, E., Akaras, N., Kurt, M., Tanboga, I.H., Halici, Z., Odabasoglu, F., Bakirci, E.M. and Unal, B. 2011. The role of oxidative stress in diabetic cardiomyopathy: an experimental study. European Review for Medical and Pharmacological Sciences. 15(11), 1241-1246.

Alberts, B., Johnson, A., Lewis, J., Raff, M., Roberts, K. and Walter, P. 2002. The endoplasmic reticulum. In: Gibbs, S. (ed.), Molecular biology of the cell 4th edition: Garland Science, New York.

Alessi, D.R., James, S.R., Downes, C.P., Holmes, A.B., Gaffney, P.R., Reese, C.B. and Cohen, P. 1997. Characterization of a 3-phosphoinositide-dependent protein kinase which phosphorylates and activates protein kinase Bα. Current Biology. 7(4), 261-269.

Alexander, A., Cai, S.L., Kim, J., Nanez, A., Sahin, M., MacLean, K.H., Inoki, K., Guan, K.L., Shen, J., Person, M.D., Kusewitt, D., Mills, G.B., Kastan, M.B. and Walker, C.L. 2010. ATM signals to TSC2 in the cytoplasm to regulate mTORC1 in response to ROS. Proceedings of the National Academy of Sciences of the United States of America. 107(9), 4153-4158.

Alpert, J.S., Thygesen, K., Antman, E. and Bassand, J.P. 2000. Myocardial infarction redefined – a consensus document of The Joint European Society of Cardiology/American College of Cardiology Committee fr the redefinition of myocardial infarction. Journal of the Ricancan College of Cardiology. 36(3), 959-969.

Ambrose, M. and Gatti, R.A. 2013. Pathogenesis of ataxia-telangiectasia: the next generation of ATM functions. Blood. 121(20), 4036-4045.

Ambrose, M., Goldstine, J.V. and Gatti, R.A. 2007. Intrinsic mitochondrial dysfunctions in ATM-deficient lymphoblastoid cells. Human Molecular Genetics. 16(18), 2154-2164.

Andrisse, S., Patel, G.D., Chen, J.E., Webber, A.M., Spears, L.D., Koehler, R.M., Robinson-Hill, R.M., Ching, J.K., Jeong, I. and Fisher, J.S. 2013. ATM and GLUT1-S490 phosphorylation regulate GLUT1 mediated transport in skeletal muscle. PLoS ONE. 8(6), e66027 doi: 10.1371/journal.pone.0066027

Antunes, L.C., Elkfury, J.L., Jornada, M.N., Foletto, K.C. and Bertoluci, M.C. 2016. Validation of HOMA-IR in a model of insulin-resistance induced by high-fat diet in Wistar rats. Archives of Endocrinology and Metabolism. 60(2), 138-142.

Armata, H.J., Golebiowski, D., Jung, D.Y., Ko, H.J., Kim, J.K. and Sluss, H.K. 2010. Requirement of the ATM/p53 tumor suppressor pathway for glucose homeostasis. Molecular and Cellular Biology. 30(24), 5787-5794.

Armstrong, S.C. 2004. Protein kinase activation and myocardial ischemia/reperfusion injury. Cardiovascular Research. 61(3), 427-436.

Arnon, P., Brownstein, Z., Ber, Y., Bialik, S., David, E., Sagir, D., Ulitsky, I., Elkon, R., Kimchi, A., Avraham, K.B., Shiloh, Y. and Shamir, R. 2011. SPIKE: a database of highly curated human signaling pathways. Nucleic Acids Research. 39(Database issue), D793-D799. doi: 10.1093/nar/gkq1167

Arrigoni, O. and De Tullio, M.C. 2002. Ascorbic acid: much more than just an antioxidant. Biochimica et Biophysica Acta. 1569(1-3), 1-9.

Asamoah, K.A., Robb, D.A. and Furman, B.L. 1990. Chronic chloroquine treatment enhances insulin release in rats. Diabetes Research and Clinical Practice. 9(3), 273-278.

Baines, C.P. 2009. The mitochondrial permeability transition pore and ischemia-reperfusion injury. Basic Research in Cardiology. 104(2), 181-188.

Bakkenist, C.J. and Kastan, M.B. 2003. DNA damage activates ATM through intermolecular autophosphorylation and dimer dissociation. Nature. 421(6922), 499-506.

Banin, S., Moyal, L., Shieh, S.Y., Taya, Y., Anderson, C.W., Chessa, L., Smorodinsky, N.I., Prives, C., Reiss, Y., Shiloh, Y. and Ziv, Y. 1998. Enhanced phosphorylation of p53 by ATM in response to DNA damage. Science. 281(5383), 1674-1677.

Banting, F.G. and Best, C.H. 1922. The internal secretion of the pancreas. The Journal of Laboratory and Clinical Medicine 7(5), 251–266.

Barlow, C., Hirotsune, S., Paylor, R., Liyanage, M., Eckhaus, M., Collins, F., Shiloh, Y., Crawley, J.N., Ried, T., Tagle, D. and Wynshaw_Boris, A. 1996. ATM-deficient mice: a paradigm of ataxia telangiectasia. Cell. 86(1), 159-171.

Beauloye, C., Bertrand, L., Krause, U., Marsin, A.S., Dresselaers, T., Vanstapel, F., Vanoverschelde, J.L. and Hue, L. 2001. No-flow ischemia inhibits insulin signaling in heart by decreasing intracellular pH. Circulation Research. 88(5), 513-519.

Belch, J.J., Bridges, A.B., Scott, N. and Chopra, M. 1991. Oxygen free radicals and congestive heart failure. British Heart Journal. 65(5), 245-248.

Bing, R.J. and Michal, G. 1959. Myocardial efficiency. Annals of the New York Academy of Sciences. 72(12), 555-558.

Birnbaum, M.J. and Shaw, R.J. 2011. Genomics: drugs, diabetes and. Nature. 470(7334), 338-339.

Bloch-Damti, A. and Bashan, N. 2005. Proposed mechanisms for the induction of insulin resistance by oxidative stress. Antioxidants & Redox Signaling. 7(11-12), 1553-1567.

Boden, G., Chen, X., Ruiz, J., White, J.V. and Rossetti, L. 1994. Mechanisms of fatty acid-induced inhibition of glucose uptake. The Journal of Clinical Investigation. 93(6), 2438-2446.

Bolli, R. and Marbán, E. 1999. Molecular and cellular mechanisms of myocardial stunning. Physiological Reviews. 79(2), 609-634.

Boudena, S. and Abel, E.D. 2010. Diabetic cardiomyopathy, causes and effects. Reviews in Endocrine & Metabolic Disorders. 11(1), 31-39.

Bozulic, L. and Hemmings, B.A. 2009. PIKKing on PKB: regulation of PKB activity by phosphorylation. Current Opinion in Cell Biology. 21(2), 256-261.

Bradford, M.M. 1976. A rapid and sensitive method for the quantitation of microgram quantities of protein utilizing the principle of protein-dye bidning. Analytical Biochemistry. 72(1-2), 248-254.

Bray, G.A. 2004. Medical consequences of obesity. The Journal of Clinical Endocrinology & Metabolism. 89(6), 2583-2589.

Brown, G.C. and Borutaite, V. 2007. Nitric oxide and mitochondrial respiration in the heart. Cardiovascular Research. 75(2), 283-290.

Bugger, H. and Abel, E.D. 2014. Molecular mechanisms of diabetic cardiomyopathy. Diabetologia. 57(4), 660-671.

Burma, S., Chen, B.P., Murphy, M., Kurimasa, A., Chen, D.J. 2001. ATM phosphorylates histone H2AX in response to double-strand breaks. The Journal of Biological Chemistry. 276(45), 42462-42467.

Buse, M.G., Robinson, K.A., Marshall, B.A. and Mueckler, M. 1996. Differential effects of GLUT1 or GLUT4 overexpression on hexosamine biosynthesis by muscles of transgenic mice. The Journal of Biological Chemistry. 271(38), 23197-23202.

Caballero, B. 1993. Vitamin E improves the action of insulin. Nutrition Reviews. 51(11), 339-340.

Caballero, A.E. 2003. Endothelial dysfunction in obesity and insulin resistance: a road to diabetes and heart disease. Obesity Research. 11(11), 1278-1289.

Cacho, J., Sevillano, J., de Castro, J., Herrera, E. and Ramos, M.P. 2008. Validation of simple indexes to assess insulin sensitivity during pregnancy in Wistar and Spraque-Dawley rats.

American Journal of Physiology. Endocrinology and Metabolism. 295(5), E1269-E1276 doi: 10.1152/ajpendo.90207.2008

Cam, H., Easton, J.B., High, A. and Houghton, P.J. 2010. mTORC1 signaling under hypoxic conditions is controlled by ATM-dependent phosphorylation of HIF-1α. Molecular Cell. 40(4), 509-520.

Carpenter, C.L., Duckworth, B.C., Auger, K.R., Cohen, B., Schaffhausen, B.S. and Cantley, L.C. 1990. Purification and characterization of phosphoinositide 3-kinase from rat liver. Journal of Biological Chemistry. 265(32), 19704-19711.

Cerf, M.E. 2013. Beta cell dysfunction and insulin resistance. Frontiers in Endocrinology. 4, 37. doi: 10.3389/fendo.2013.00037

Chan, D.W., Son. S.C., Block, W., Ye, R., Khanna, K.K., Wold, M.S., Douglas, P., Goodarzi, A.A., Pelley, J., Taya, Y., Lavin, M.F. and Lees-Miller, S.P. 2000. Purification and characterization of ATM from human placenta. A manganese-dependent, wortmannin-sensitive serine/threonine protein kinase. The Journal of Biological Chemistry. 275(11), 7803-7810.

Chen, F.C. and Ogut, O. 2006. Decline of contractility during ischemia-reperfusion injury: actin glutathionylation and its effect on allosteric interaction with tropomyosin. American Journal of Physiology. Cell Physiology. 290(3), C719-C727.

Chen, J.H., Zhang, P., Chen, W.D., Li, D.D., Wu, X.Q., Deng, R., Jiao, L., Li, X., Ji, J., Feng, G.K., Zeng, Y.X., Jiang, J.W. and Zhu, X.F. 2015. ATM-mediated PTEN phosphorylation promotes PTEN nuclear translocation and autophagy in response to DNA-damaging agents in cancer cells. Autophagy. 11(2), 239-252.

Chiang, G.G. and Abraham, R.T. 2005. Phosphorylation of mammalian target of rapamycin (mTOR) at Ser-2448 is mediated by p70S6 kinase. The Journal of Biological Chemistry. 280(27), 25485-25490.

Chiang, S.H., Baumann, C.A., Kanzaki, M., Thurmond, D.C., Watson, R.T., Neudauer, C.L., Macara. I.G., Pessin, J.E. and Saltiel, A.R. 2001. Insulin-stimulated GLUT4 translocation requires the CAP-dependent activation of TC10. Nature. 410(6831), 944-948.

Ching, J.K., Armon, J.L., Renth, A., Collins IV, R.L. and Fisher, J.S. 2010. ATM plays a role in insulin-stimulated phosphorylation of AS160 independent of Akt in mouse soleus muscle. The FASEB Journal. 24(1), 1046.18

Ching, J.K., Luebbert, S.H., Collins, R.L., Zhang, Z., Marupudi, N., Banerjee, S., Hurd, R.D., Ralston, L. and Fisher, J.S. 2013a. Ataxia telangiectasia mutated impacts insulin-like growth factor 1 signalling in skeletal muscle. Experimental Physiology. 98(2), 526-535.

Ching, J.K., Spears, L.D., Armon, J.L., Renth, A.L., Andrisse, S., Collins, I.V. and Fisher, J.S. 2013b. Impaired insulin-stimulated glucose transport in ATM-deficient mouse skeletal muscle. Applied Physiology, Nutrition, and Metabolism. 38(6), 589-596.

Consentino, C., Grieco, D. and Constanzo, V. 2011. ATM activates the pentose phosphate pathway promoting anti-oxidant defense and DNA repair. The EMBO Journal. 30(3), 546-555.

Cortez, D., Wang, Y., Qin, J. and Elledge, S.J. 1999. Requirement of ATM-dependent phosphorylation of brca1 in the DNA damage response to double-strand breaks. Science. 286(5442), 1162-1166.

Coven, D.L., Hu, X., Cong, L., Bergeron, R., Shulman, G.I., Hardie, D.G. and Young, L.H. 2003. Physiological role of AMP-activated protein kinase in the heart: graded activation during exercise. American Journal of Physiology – Endocrinology and Metabolism. 285(3), E629-E636.

Cross, D.A.E., Alessi, D.R., Cohen, P., Andjelkovich, M. and Hemmings, B.A. 1995. Inhibition of glycogen synthase kinase-3 by insulin mediated by protein kinase B. Nature. 378(6559), 785-789.

Dagogo-Jack, S. and Santiago, J.V. 1997. Pathophysiology of type 2 diabetes and modes of action of therapeutic interventions. Archives of internal medicine. 157(16), 1802-1817.

Daniel., L.L., Daniels, C.R., Harirforoosh, S., Foster, C.R., Singh, M. and Singh, K. 2014. Deficiency of ataxia telangiectasia mutated kinase delays inflammatory response in the heart following myocardial infarction. Journal of the American Heart Association. 3(6), e001286 doi: 10.1161/JAHA.114.001286

Daniel, L.L., Scofield, S.L., Thrasher, P., Dalal, S., Daniels, C.R., Foster, C.R., Singh, M. and Singh, K. 2016. Ataxia telangiectasia-mutated kinase deficiency exacerbates left ventricular dysfunction and remodeling late after myocardial infarction. American Journal of Physiology. Heart and Circulatory Physiology. 311(2), H445-H452. doi: 10.1152/ajpheart.00338.2016

Das, A., Durrant, D., Koka, S., Salloum, F.N., Xi, L. and Kukreja, R.C. 2013. mTOR inhibition with rapamycin improves cardiac function in type 2 diabetic mice: potential role of attenuated oxidative stress and altered contractile protein expression. The Journal of Biological Chemistry. 289(7), 4145-4160.

Datta, S.R., Dudek, H., Tao, X., Masters, S., Fu, H., Gotoh, Y. and Greenberg, M.E. 1997. Akt phosphorylation of BAD couples survival signals to the cell-intrinsic death machinery. Cell. 91(2), 231-241.

Davies, S.P., Sim, A.T. and Hardie, D.G. 1990. Location and function of three sites phosphorylated on rat acetyl-CoA carboxylase by the AMP-activated protein kinase. European Journal of Biochemistry / FEBS. 187(1), 183-190.

Deihl, J.A., Cheng, M., Roussel, M.F. and Sherr, C.J. 1998. Glycogen synthase kinase-3beta regulates cyclin D1 proteolysis and subcellular localization. Genes & Development. 12(22), 3499-3511.

De Meyer, J. 1909. Action de la secretion interne du pancreas sur differents organes et en particulier sur la secretion renale. Archivio de Physiologia. 7,96-99.

DeYoung, M.P., Horak, P., Sofer, A., Sgroi, D. and Ellisen, L.W. 2008. Hypoxia regulates TSC1/2-mTOR signaling and tumor suppression through REDD1-mediated 14-3-3 shuttling. Genes & Development. 22(2), 239-251.

Dhalla, N.S., Elmoselhi, A.B., Hata, T. and Makino, N. 2000. Status of myocardial antioxidants in ischemia-reperfusion injury. Cardiovascular Research. 47(3), 446-456.

Dhalla, N.S., Golfman, L., Takeda, S., Takeda, N. and Nagano, M. 1999. Evidence for the role of oxidative stess in acute ischemic heart disease: a brief review. The Canadian Journal of Cardiology. 15(5), 587-593.

Dimmeler, S., Fleming, I., Fisslthaler, B., Hermann, C., Busse, R. and Zeiher, A.M. Activation of nitric oxide synthase in endothelial cells by Akt-dependent phosphorylation. Nature. 399(6736), 601-605.

Ditch, S. and Paull, T,T. 2012. The ATM protein kinase and cellular redox signaling: beyond the DNA damage response. Trends in Biochemical Sciences. 37(1), 15-22.

Duncan, J.G. 2011. Mitochondrial dysfunction in diabetic cardiomyopathy. Biochimica et Biophysica Acta. 1813(7), 1351-1359.

du Toit, E.F., Smith, W., Muller, C., Strijdom, H., Stouthammer, B., Woodiwiss, A.J., Norton, G.R. and Lochner, A. 2008. Myocardial susceptibility to ischemic-reperfusion injury in a prediabetic model of dietary-induced obesity. American Journal of Physiology. Heart and Circulatory Physiology. 294(5), H2336-H2343.

Eguchi, K., Boden-Albala, B., Jin, Z., Rundek, T., Sacco, R.L., Homma, S. and Di Tullio, M.R. 2008. Association between diabetes mellitus and left ventricular hypertrophy in a multiethnic population. The American Journal of Cardiology. 101(12), 1787-1791.

Eldar-Finkelman, H., Schreyer, S.A., Shinohara, M.M., LeBoeuf, R.C. and Krebs, E.G. 1999. Increased glycogen synthase kinase-3 activity in diabetes- and obesity-prone C57BL/6J mice. Diabetes. 48(8), 1662-1666.

Eliseyeva, M.R. 2013. Endothelium: a long road from mystery to discovery. International Journal of BioMedicine. 3(1), 9-11.

Elkon, R., Vesterman, R., Amit, N., Ulitsky, I., Zohar, I., Weisz, M., Mass, G., Orlev, N., Sternberg, G., Bleckman, R., Assa, J., Shiloh, Y. and Shamir, R. 2008. SPIKE – a database, visualization and analysis tool of cellular signaling pathways. BMC Bioinformatics. 9, 110. doi: 10.1186/1471-2105-9-110

Elstrom, R.L., Bauer, D.E., Buzzai, M., Karnauskas, R., Harris, M.H., Plas, D.R., Zhuang, H., Cinalli, R.M., Alavi, A., Rudin, C.M. and Thompson, C.B. 2004. Akt stimulates aerobic glycolysis in cancer cells. Cancer Research. 64(11), 3892-3899.

Emami, J., Gerstein, H.C., Pasutto, F.M. and Jamali, F. 1999. Insulin-sparing effect of hydroxychloroquine in diabetic rats is concentration dependent. Canadian Journal of Physiology and Pharmacology. 77(2), 118-123.

Espach, Y., Lochner, A., Strijdom, H. and Huisamen, B. 2015. ATM protein kinase signaling, type 2 diabetes and cardiovascular disease. Cardiovascular Drugs and Therapy. 29(1), 51-58.

Esper, R.J., Nordaby, R.A., Vilariño, J.O., Paragano, A., Cacharrón, J.L. and Machado, R.A. 2006. Endothelial dysfunction: a comprehensive appraisal. Cardiovascular Diabetology. 5:4 doi: 10.1186/1475-2840-5-4

Evans, J.L., Maddux, B.A. and Goldfine, I.D. 2005. The molecular basis for oxidative stress-induced insulin resistance. Antioxidants and Redox Signaling. 7(7-8), 1040-1052.

Fiorentino, T.V., Prioletta, A., Zuo, P. And Folli, F. 2013. Hyperglycemia-induced oxidative stress and its role in diabetes mellitus related cardiovascular disease. Current Pharmaceutical Design. 19(32), 5695-5703.

Foster, C.R., Daniel, L.L., Daniels, C.R., Dalal, S., Singh, M. and Singh, K. 2013. Deficiency of ataxia telangiectasia mutated kinase modulates cardiac remodeling following myocardial infarction: Involvement in fibrosis and apoptosis. PLOS ONE. 8(12), e83513 doi: 10.1371/journal.pone.0083513

Foster, C.R., Singh, M., Subramanian, V. and Singh, K. 2011. Ataxia telangiectasia mutated kinase plays a protective role in β-adrenergic receptor-stimulated cardiac myocyte apoptosis and myocardial remodeling. Molecular and Cellular Biochemistry. 353(1-2), 13-22.

Foster, C.R., Zha, Q., Daniel, L.L., Singh, M. and Singh, K. 2012. Lack of ataxia telangiectasia mutated kinase induces structural and functional changes in the heart: role in β-adrenergic receptor-stimulated apoptosis. Experimental Physiology. 97(4), 506-515.

Fragasso, G., Sanvito, F., Baratto, F., Martinenghi, S., Doglioni, C. and Margonato, A. 2009. Cardiotoxicity after low-dose chloroquine antimalarial therapy. Heart Vessels. 24(5), 385-387.

Freedman, A. and Steinberg, V.L. 1960. Chloroquine in rheumatoid arthritis: a double blindfold trial of treatment for one year. Annals of the Rheumatic Disease. 19,243-250.

Frustaci, A., Kajstura, J., Chimenti, C., Jakoniuk, I., Leri, A., Maseri, A., Nadal-Ginard, B. and Anversa, P. 2000. Myocardial cell death in human diabetes. Circulation Research. 87(12), 1123-1132.

Fu, X., Wan, S., Lyu, Y.L., Liu, L.F. and Qi, H. 2003. Etoposide induces ATM-dependent mitochondrial biogenesis through AMPK activation. PLoS One. 3(4), e2009 doi: 10.1371/journal.pone.0002009

Fuglesteg, B.N., Tiron, C., Jonassen, A.K., Mjøs, O.D. and Ytrehus, K. 2009. Pretreatment with insulin before ischaemia reduces infarct size in Langendorff-perfused rat hearts. Acta Physiologica. 195(2), 273-282.

Fukushima, A., Milner, K., Gupta, A. and Lopaschuk, G.D. 2015. Myocardial energy substrate metabolism in heart failure: from pathways to therapeutic targets. Current Pharmaceutical Design. 21(25), 3654-3664.

Fullmer, T.M., Pei, S., Zhu, Y., Sloan, C., Manzanares, R., Henrie, B., Pires, K.M., Cox, J.E., Abel, E.D. and Boudina, S. 2013. Insulin suppresses ischemic preconditioning-

mediated cardioprotection through Akt-dependent mechanisms. Journal of Molecular and Cellular Cardiology. 64, 20-29.

Garcia, L., Garcia, F., Llorens, F., Unzeta, M., Itarte, E. and Gómez, N. 2002. PP1/PP2A phosphatases inhibitors okadaic acid and calyculin A block ERK5 activation by growth factors and oxidative stress. FEBS Letters. 523(1-3), 90-94.

Gastaldelli, A. 2011. Role of beta-cell dysfunction, ectopic fat accumulation and insulin resistance in the pathogenesis of type 2 diabetes mellitus. Diabetes Research and Clinical Practice. 93(S1), S60-S65.

Gauthier, M.S., O'Brien, E.L., Bigornia, S., Mott, M., Cacicedo, J.M., Xu, X.J., Gokce, N., Apovian, C. and Ruderman, N. 2011. Decreased AMP-activated protein kinase activity is associated with increased inflammation in visceral adipose tissue and with whole-body insulin resistance in morbidly obese humans. Biochemical and Biophysical Research Communications. 404(1), 382-387.

Geiβler, K.J., Jung, M.J., Riecken, L.B., Sperka, T., Cui, Y., Schacke, S., Merkel, U., Markwart, R., Rubio, I., Than, M.E., Breithaupt, C., Peuker, S., Seifert, R., Kaupp, U.B., Herrlich, P. and Morrison, H. 2013. Regulation of son of sevenless by the membrane-actin linker protein ezrin. Proceedings of the National Academy of Science of the United States of America. 110(51), 20587-20592.

Gertz, E.W., Wisneski, J.A., Stanley, W.C. and Neese, R.A. 1988. Myocardial substrate utilization during exercise in humans. Dual carbon-labeled carbohydrate isotope experiments. The Journal of Clinical Investigation. 82(6), 2017-2025.

Ghee, M., Baker, H., Miller, J.C. and Ziff, E.B. 1998. AP-1, CREB and CBP transcription factors differentially regulate the tyrosine hydroxylase gene. Brain Research. Molecular Brain Research. 55(1), 101-114.

Ghezzi, A.C., Cambri, L.T., Botezelli, J.D, Ribeiro, C., Dalia, R.A. and de Mello, M.A. 2012. Metabolic syndrome markers in Wistar rats of different ages. Diabetology & Metabolic Syndrome. 4(1), 16

Golding, S.E., Rosenberg, E., Adams, B.R., Wignarajah, S., Beckta, J.M., O'Connor, M.J. and Valerie, K. 2012. Dynamic inhibition of ATM kinase provides a strategy for glioblastoma multiforme radiosensitization and growth control. Cell Cycle. 11(6), 1167-1173.

Golding, S.E., Rosenberg, E., Valerie, N., Hussaini, I., Frigerio, M., Cockcroft, X.F., Chong, W.Y., Hummersone, M., Rigoreau, L., Menear, K.A., O'Connor, M.J., Povirk, L.F., van Meter, T. and Valerie, K. 2009. Improved ATM kinase inhibitor KU-60019 radiosensitizes glioma cells, compromises insulin, AKT and ERK prosurvival signaling, and inhibits migration and invasion. Molecular Cancer Therapeutics. 8(10), 2894-2902.

Goodarzi, A.A., Jonnalagadda, J.C., Douglas, P., Young, D., Ruiqiong, Y., Moorhead, G.B.G., Lees-Miller, S.P. and Khanna, K.K. 2004. Autophosphorylation of ataxia-telangiectasia mutated is regulated by protein phosphatase 2A. The EMBO Journal. 23(22), 4451-4461.

Gorr, M.W., Stevens, S.C.W. and Wold, L.E. 2012. Ataxia telangiectasia mutated kinase in the heart: currency for myocyte apoptosis. Experimental Physiology. 97(4), 476.

Gottlieb, R. and Magnus, R. 1904. Digitalis und Herzarbeit. Nach Versuchen am uberlebenden Warmbluterherzen. Path Pharamakol 51, 30-63.

Gray, S. and Kim, J.K. 2011. New insights into insulin resistance in the diabetic heart. Trends in Endocrinology and Metabolism. 22(10), 394-403.

Gueven, N., Keating, K., Fukao, T., Loeffler, H., Kondo, N., Rodemann, H.P. and Lavin, M.F. 2003. Site-directed mutagenesis of the ATM promoter: consequences for response to proliferation and ionizing radiation. Genes, Chromosomes & Cancer. 38(2), 157-167.

Guo, Z., Kozlov, S., Lavin, M.F., Person, M.D. and Paull, T.T. 2010. ATM activation by oxidative stress. Science. 330(6003), 517-521.

Gürtler, A., Kunz, N., Gomolka, M., Hornhardt, S., Friedl, A.A., McDonald, K., Kohn, J.E. and Posch, A. 2013. Stain-free technology as a normalization tool in Western blot analysis. Analytical Biochemistry. 433(2), 105-111.

Hafstad, A.D., Solevåg, G.H., Severson, D.L., Larsen, T.S. and Aasum, E. 2006. Perfused hearts from type 2 diabetic (db/db) mice show metabolic responsiveness to insulin. American Journal of Physiology – Heart and Circulatory Physiology. 290(5), H1763-H1769. doi: 10.1152/ajpheart.01063.2005

Halaby, M.J., Hibma, J.C., He, J. and Yang, D.Q. 2008. ATM protein kinase mediates full activation of Akt and regulates glucose transporter 4 translocation by insulin in muscle cells. Cellular Signalling. 20(8), 1555-1563.

Halaby, M.J., Kastein, B.K. and Yang, D.Q. 2013. Chloroquine stimulates glucose uptake and glycogen synthase in muscle cells through activation of Akt. Biochemical and Biophysical Research Communications. 435(4), 708-713.

Hammond, E.M. and Muschel, R.J. 2014. Radiation and ATM inhibition: the heart of the matter. The Journal of Clinical Investigation. 124(8), 3289-3291.

Haruta, T., Uno, T., Kawahara, J., Takanoa, A., Egawa, K., Sharma, P.M., Olefsky, J.M. and Kobayashi, M. 2000. A rapamycin-sensitive pathway down-regulates insulin signaling via

phosphorylation and proteasomal degradation of insulin receptor substrate-1. Molecular Endocrinology. 14(6), 783-794.

Harwood, H.J Jr. 2000. Acetyl-CoA carboxylase inhibition for the treatment of metabolic syndrome. Current Opinion in Investigational Drugs. 5(3), 283-289.

Hausenloy, D.J. and Yellon, D.M. 2004. New directions for protecting the heart against ischaemia-reperfusion injury: targeting the Reperfusion Injury Salvage Kinase (RISK)-pathway. Cardiovascular Research. 61(3), 448-460.

Hausenloy, D.J. and Yellon, D.M. 2013. Myocardial ischemia-reperfusion injury: a neglected therapeutic target. The Journal of Clinical Investigation. 123(1), 92-100.

Hawley, S.A., Davison, M., Woods, A., Davies, S.P., Beri, R.K., Carling, D. and Hardie, D.G. 1996. Characterization of the AMP-activated protein kinase kinase from rat liver and identification of threonine 172 as a major site at which it phosphorylates AMP-activated protein kinase. The Journal of Biological chemistry. 271(44), 27879-27887.

Hemmings, B.A. and Restuccia, D.F. 2012. PI3K-PKB/Akt pathway. Cold Spring Harbor Perspectives in Biology. 4, a011189. doi: 10.1101/cshperspect.a011189

Hickson, I., Zhao, Y., Richardson, C.J., Green, S.J., Martin, N.M., Orr, A.I., Reaper, P.M., Jackson, S.P., Curtin, N.J. and Smith, G.C. 2004. Identification and characterization of a novel and specific inhibitor of the ataxia-telangiectasia mutated kinase ATM. Cancer Research. 64(24), 9152-9159.

Hirashima, O., Kawano, H., Motoyama, T., Hirai, N., Ohgushi, M., Kugiyama, K., Ogawa, H. and Yasue, H. 2000. Improvement of endothelial function and insulin sensitivity with vitamin C in patients with coronary spastic angina: possible role of reactive oxygen species. Journal of the American College of Cardiology. 35(7), 1860-1866.

Hirosumi, J., Tuncman, G., Chang, L., Görgün, C.Z., Uysal, K.T., Maeda, K., Karin, M. and Hotamisligil, G.S. 2002. A central role for JNK in obesity and insulin resistance. Nature. 420(6913), 333-336.

Hoeben, A., Landuyt, B., Highley, M.S., Wildiers, H., Van Oosterom, A.T. and De Bruijn, E.A. 2004. Vascular endothelial growth factor and angiogenesis. Pharmacological Review. 56(4), 549-580.

Honda, H.M. and Ping, P. 2006. Mitochondrial permeability transition in cardiac cell injury and death. Cardiovascular Drugs and Therapy. 20(6), 425-432.

Hotamisligil, G.S., Arner, P., Caro, J.F., Atkinson, R.L. and Spiegelman, B.M. 1995. Increased adipose tissue expression of tumor necrosis factor-alpha in human obesity and insulin resistance. The Journal of Clinical Investigation. 95(5), 2409-2415.

Hotamisligil, G.S., Peraldi, P., Budavari, A., Ellis, R., White, M.F. and Spiegelman, B.M. 1996. IRS-1-mediated inhibition of insulin receptor tyrosine kinase activity in TNF-alpha- and obesity-induced insulin resistance. Science. 271(5249), 665-668.

Hotamisligil, G.S., Shargill, N.S. and Spiegelman, B.M. 1993. Adipose expression of tumor necrosis factor-alpha: direct role in obesity-linked insulin resistance. Science. 259(5091), 87-91.

Hue, L. and Taegtmeyer, H. 2009. The Randle cycle revisited: a new head for an old hat. American Journal of Physiology. Endocrinology and Metabolism. 297(3), E578-E591.

Huisamen, B., Donthi, R.V. and Lochner, A. 2001. Insulin in combination with vanadate stimulates glucose transport in isolated cardiomyocytes from obese Zucker rats. Cardiovascular Drugs and Therapy. 15(5), 445-452.

Huisamen, B., Genade, S. and Lochner, A. 2008. Signalling pathways activated by glucagon-like peptide-1 (7-36) amide in the rat heart and their role in protection against ischaemia. Cardiovascular Journal of Africa. 19(2), 77-83.

Inoki, K., Li, Y., Zhu, T., Wu, J. and Guan, K.L. 2002. TSC2 is phosphorylated and inhibited by Akt and suppresses mTOR signalling. Nature Cell Biology. 4(9), 648-657.

Jacob, S., Ruus, P., Hermann, R., Tritschler, H.J., Maerker, E., Renn, W., Augustin, H.J., Dietze, G.J. and Rett, K. 1999. Oral administration of RAC-alpha-lipoic acid modulates insulin sensitivity in patients with type 2 diabetes mellitus: a placebo-controlled pilot trial. Free Radical Biology and Medicine 27(3-4), 309-314.

Jagasia, D., Whiting, J.M., Concato, J., Pfau, S. and McNulty, P.H. 2001. Effect of non-insulin-dependent diabetes mellitus on myocardial insulin responsiveness in patients with ischemic heart disease. Circulation. 103(13), 1734-1739.

Jalloh, I., Carpenter, K.L., Grice, P., Howe, D.J., Mason, A., Gallagher, C.N., Helmy, A., Murphy, M.P., Menon, D.K., Carpenter, T.A., Pickard, J.D. and Hutchinson, P.J. 2015. Glycolysis and the pentose phosphate pathway after human brain injury: microdialysis studies using 1,2-(13)C2 glucose. Journal of Cerebral Blood Flow and Metabolism. 35(1), 111-120.

Jennings, R.B., Steenbergen, C. Jr. and Reimer, K.A. 1995. Myocardial ischemia and reperfusion. Monographs in Pathology. 37, 47-80.

Jeong, I., Patel, A.Y., Zhang, Z., Patil, P.B., Nadella, S.T., Nair, S., Ralston, L., Hoormann, J.K. and Fisher, J.S. 2010. Role of ataxia telangiectasia mutated in insulin signaling of muscle-derived cell lines and mouse soleus. Acta Physiologica. 1984), 465-475.

Ji, L., Fu, F., Zhang, L., Liu, W., Cai, X., Zhang, L., Zheng, Q., Zhang, H. and Gao, F. 2010. Insulin attenuates myocardial ischemia/reperfusion injury via reducing oxidative/nitrative

stress. American Journal of Physiology. Endocrinology and Metabolism. 298(4), E871-E880.

Jiao, K., Liu, H., Chen, J., Tian, D., Hou, J. and Kaye, A. 2008. Roles of plasma interleukin-6 and tumour necrosis factor-alpha and FFA and TG in the development of insulin resistance induced by high-fat diet. Cytokine 42(2), 161-169.

Johnson, A.M.F. and Olefsky, J.M. 2013. The origins and drivers of insulin resistance. Cell. 152(4), 673-684.

Jonassen, A.K., Sack, M.N., Mjøs, O.D. and Yellon, D.M. 2001. Myocardial protection by insulin at reperfusion requires early administration and is mediated via Akt and p70s6 kinase cell-survival signaling. Circulation Research. 89(12), 1191-1198.

Julius, U. 2003. Influence of plasma free fatty acids on lipotprotein synthesis and diabetic dysliipidemia. Experimental and Clinical Endocrinology: Official Journal, German Society of Endocrinology & German Diabetes Association. 111(5), 246-250.

Kahn, S.E. 2003. The relative contributions of insulin resistance and beta-cell dysfunction to the pathophysiology of type 2 diabetes. Diabetologia, 46(1), 3-19.

Kaiser, R.A., Liang, Q., Bueno, O., Huang, Y., Lackey, T., Klevitsky, R., Hewett, T.E. and Molkentin, J.D. 2005. Genetic inhibition or activation of JNK1/2 protects the myocardium from ischemia-reperfusion-induced cell death in vivo. The Journal of Biological Chemistry. 280(38), 32602-32608.

Kalogeris, T., Baines, C.P., Krenz, M. and Korthuis, R.J. 2012. Cell biology of ischemia/reperfusion injury. International Review of Cell and Molecular Biology. 298, 229-317.

Kane, S., Sano, H., Liu, S.C., Asara, J.M., Lane, W.S., Garner, C.C. and Lienhard, G.E. 2002. A method to identify serine kinase substrates. Akt phosphorylates a novel adipocyte protein with a Rab GTPase-activating protein (GAP) domain. The Journal of Biological Chemistry. 277(25), 22115-22118.

Katare, R., Oikawa, A., Cesselli, D., Beltrami, A.P., Avolio, E., Muthukrishnan, D., Munasinghe, P.E., Angelini, G., Emanueli, C. and Madeddu, P. 2013. Boosting the pentose phosphate pathway restores cardiac progenitor cell availability in diabetes. Cardiovascular Research. 97(1), 55-56.

Katori, T., Donzelli, S., Tocchetti, C.G., Miranda, K.M., Cormaci, G., Thomas, D.D., Ketner, E.A., Lee, M.J., Mancardi, D., Wink, D.A., Kass, D.A. and Paolocci, N. Peroxynitrite and myocardial contractility: in vivo versus in vitro effects. Free Radical Biology & Medicine. 41(10), 1606-1618.

Katz, G., Pain, W. and Tiller, P. 1939. A new method for coronary perfusion of the mammalian heart. Archives Int Parmacodyn. 61, 109-112.

Karpe, F., Dickmann, J.R. and Frayn, K.N. 2011. Fatty acids, obesity and insulin resistance: time for re-evaluation. Diabetes. 60(10), 2441-2449.

Khamzina, L., Veilleux, A., Bergeron, S. and Marette, A. 2005. Increased activation of the mammalian target of rapamycin pathway in liver and skeletal muscle of obese rats: possible involvement in obesity-linked insulin resistance. Endocrinology. 146(3), 1473-1481.

Khurana, R., Simons, M., Martin, J.F., and Zachary, I.C. 2005. Role of angiogenesis in cardiovascular disease: A critical appraisal. Circulation. 112(12), 1813-1824.

Kim, E.K. and Choi, E.J. 2010. Pathological roles of MAPK signaling pathways in human diseases. Biochimica et Biophysica Acta. 1802(4), 396-405.

Kim, M., Oh, J.K., Sakata, S., Liang, I., Park, W., Hajjar, R.J. and Lebeche, D. 2008. Role of resistin in cardiac contractility and hypertrophy. Journal of Molecular and Cellular Cardiology. 45(2), 270-280.

Kim, S.T., Lim, D.S., Canman, C.E. and Kastan, M.B. 1999. Substrate specificities and identification of putative substrates of ATM kinase family members. The Journal of Biological Chemistry. 274(53), 37538-37543.

Kozlov, S., Gueven, N., Keating, K., Ramsay, J. and Lavin, M.F. 2003. ATP activates ataxia-telangiectasia mutated (ATM) in vitro. Importance of autophosphorylation. The Journal of Biological Chemistry. 278(11), 9309-9317.

Krüger, A. and Ralser, M. 2011. ATM is a redox sensor linking genome stability and carbon metabolism. Science Signaling. 4(167), pe17 doi: 10.1126/scisignal.2001959

Lam, K., Carpenter, C.L., Ruderman, N.B., Friel, J.C. and Kelly, K.L. 1994. The phosphatidylinositol 3-kinase serine kinase phosphorylates IRS-1. Stimulation by insulin and inhibition by Wortmannin. The Journal of Biological Chemistry. 269(32), 20648-20652.

Langendorff, O. 1895. Untersuchungen am uberlebenden Saugethierherzen. Pflügers Archiv – European Journal of Physiology. 66(7), 355-400.

Laplante, M. and Sabatini, D.M. 2012. mTOR signaling in growth control and disease. Cell. 149(2), 274-293.

Lee, J. and Kim, M.S. 2007. The role of GSK3 in glucose homeostasis and the development of insulin resistance. Diabetes Research and Clinical Practice. 77(Supplementary 1), S49-S57.

Lee, B.L., Kim, W.H., Jung, J., Cho, S.J., Park, J.W., Kim, J., Chung, H.Y., Chang, M.S. and Nam, S.Y. 2007. A hypoxia-independent up-regulation of hypoxia-inducible factor-1 by AKT contributes to angiogenesis in human gastric cancer. Carcinogenesis. 29(1), 44-51.

Lee, J.H., Guo, Z., Myler, L.R., Zheng, S. and Paull, T.T. 2014. Direct activation of ATM by resveratrol under oxidizing conditions. PLOS ONE. 9(6), e97969 doi: 10.1371/journal.pone.0097969

Le Guezennec, X., Brichkina, A., Huang, Y.F., Kostromina, E., Han, W. and Bulavin, D.V. 2012. Wip1-dependent regulation of autophagy, obesity, and atherosclerosis. Cell Metabolism. 16(1), 68-80.

Lewis, G.F. 1997. Fatty acid regulation of very low density lipoprotein production. Current Opinion in Lipidology. 8(3), 146-153.

Li, S., Zhang, L., Chen, T., Tian, B., Deng, X., Zhao, Z., Yuan, P., Dong, B., Zhang, Y. and Mo, X. 2011. Functional polymorphism rs189037 in the promoter region of ATM gene is associated with angiographically characterized coronary stenosis. Atherosclerosis. 219(2), 694-697.

Li, Y. and Yang, D.Q. 2010. The ATM inhibitor KU-55933 suppresses cell proliferation and induces apoptosis by blocking Akt in cancer cells with overactivated Akt. Molecular Cancer Therapeutics. 9(1), 113-125.

Liao, R., Podesser, B.K. and Lim, C.C. 2012. The continuing evolution of the Langendorff and ejecting murine heart: new advances in cardiac phenotyping. American Journal of Physiology – Heart and Circulatory Physiology. 303(2), H156-H167. doi: 10.1152/ajpheart.00333.2012

Liberman, Z. and Eldar-Finkelman, H. 2005. Serine 332 phosphorylation of insulin receptor substrate-1 by glycogen synthase kinase-3 attenuates insulin signaling. The Journal of Biological Chemistry. 280(6), 4422-4428.

Lim, Y., Hedayati, M., Merchant, A.A., Zhang, Y., Yu, H.H.M., Kastan, M.B., Matsui, W. and DeWeese, T.L. 2012. Chloroquine improves survival and hematopoietic recovery after lethal low-dose-rate radiation. International Journal of Radiation Oncology, Biology Physics. 84(3), 800-806.

Lopaschuk, G.D. 1997. Alterations in fatty acid oxidation during reperfusion of the heart after myocardial ischemia. The American Journal of Cardiology. 80(3A), 11A-16A.

Lopaschuk, G.D., Ussher, J.R., Folmes, C.D.L., Jaswal, J.S. and Stanley, W.C. 2010. Myocardial fatty acid metabolism in health and disease. Physiological Reviews. 90(1), 207-258.

Lowry, O.H., Rosebrough, N.J., Farr, A.L., Randall, R.J. 1951. Protein measurement with the Folin phenol reagent. The Journal of Biological Chemistry. 193(1), 265-275.

Lucas, F. and Sclafani, A. 1990. Hyperphagia in rats produced by a mixture of fat and sugar. Physiology & Behavior. 47(1), 51-55.

Maehama, T. and Dixon, J.E. 1998. The tumor suppressor, PTEN/MMAC1, dephosphorylates the lipid second messenger, phosphatidylinositol 3,4,5-trisphosphate. The Journal of Biological Chemistry. 273(22), 13375-13378.

Mallat, Z., Philip, I., Lebret, M., Chatel, D., Maclouf, J. and Tedgui, A. 1998. Elevated levels of 8-iso-prostaglandin $F_{2\alpha}$ in pericardial fluid of patients with heart failure: a potential role for in vivo oxidant stress in ventricular dilatation and progression to heart failure. Circulation. 97(16), 1536-1539.

Mandavia, C.H., Aroor, A.R., DeMarco, V.G. and Sowers, J.R. 2013. Molecular and metabolic mechanisms of cardiac dysfunction in diabetes. Life Sciences. 92(11), 601-608.

Manning, B.D. and Cantley, L.C. 2007. Akt/PKB signalling: Navigating downstream. Cell. 129(7), 1261-1274.

Mathews, C.K., van Holde, K.E. and Ahern, K.G. 2000. Carbohydrate Metabolism I: anaerobic processes in generating metabolic energy. In: Roberts, B. (ed.), Biochemistry 3rd edition: Addison Wesley Longman, San Francisco, USA. 446-482.

Matsui, T., Tao, J., del Monte, F., Lee, K.H., Li, L., Picard, M., Force, T.L., Franke, T.F., Hajjar, R.J. and Rosenzweig, A. 2001. Akt activation preserves cardiac function and prevents injury after transient cardiac ischemia in vivo. Circulation. 104(3), 330-335.

Matsuoka, S., Ballif, B.A., Smogorzewska, A., McDonald, E.R., Hurov, K.E., Luo, J., Bakalarski, C.E., Zhao, Z., Solimini, N., Lerenthal, Y., Shiloh, Y., Gygi, S.P. and Elledge, S.J. 2007. ATM and ATR substrate analysis reveals extensive protein networks responsive to DNA damage. Science. 316(5828), 1160-1166.

Matsuoka, S., Huang, M. and Elledge, S.J. 1998. Linkage of ATM to cell cycle regulation by the Chk2 protein kinase. Science. 282(5395), 1893-1897.

Matthews, D.R., Hoskar, J.P., Rudenski, A.S., Naylor, B.A., Treacher, D.F. and Turner, R.C. 1985. Homeostasis model assessment: insulin resistance and β-cell function from fasting plasma glucose and insulin concentrations in man. Diabetologia. 28(7), 412-419.

Mayer, J.P., Zhang, F. and DiMarchi, R.D. 2007. Insulin structure and function. Peptide Science. 88(5), 687-713.

McGavock, J.M., Lingvay, I., Zib, I., Tillery, T., Salas, N., Unger, R., Levine, B.D., Raskin, P., Victor, R.G. and Szczepaniak, L.S. 2007. Cardiac steatosis in diabetes mellitus: a 1H-magnetic resonance spectroscopy study. Circulation. 116(10), 1170-1175.

McLeod, R.S., LeBlanc, A.M., Langille, M.A., Mitchell, P.L. and Currie, D.L. 2004. Conjugated linoleic acids, atherosclerosis, and hepatic very-low-density lipoprotein metabolism. The American Journal of Clinical Nutrition. 79(6), 1169S-1174S.

McNulty, P.H. 2006. Metabolic responsiveness to insulin in the diabetic heart. American Journal of Physiology – Heart and Circulatory Physiology. 290(5), H1749-H1751. doi: 10.1152/ajpheart.00037.2006

Mead, J.R. and Ramji, D.P. 2002. The pivotal role of lipoprotein lipase in atherosclerosis. Cardiovascular Research. 55(2), 261-269.

Mercer, J.R., Cheng, K.K., Figg, N., Gorenne, I., Mahmoudi, M., Griffin, J., Vidal-Puig, A., Logan, A., Murphy, M.P. and Bennett, M. 2010. DNA damage links mitochondrial dysfunction to atherosclerosis and the metabolic syndrome. Circulation Research. 107(8), 1021-1031.

Mercer, J.R., Yu, E., Figg, N., Cheng, K.K., Prime, T.A., Griffin, J.L., Masoodi, M., Vidal-Puig, A., Murphy, M.P. and Bennett, M.R. 2012. The mitochondria-targeted antioxidant MitoQ decreases features of the metabolic syndrome in ATM+/-/ApoE-/- mice. Free Radical Biology & Medicine. 52(5), 841-849.

Michaelides, M., Stover, N.B., Francis, P.J. and Weleber, R.G. 2011. Retinal toxicity associated with hydroxychloroquine and chloroquine: risk factors, screening, and progression despite cessation of therapy. Archives of Ophthalmology. 129(1), 30-39.

Miki, T., Yuda, S., Kouzu, H. and Miura, T. 2013. Diabetic cardiomyopathy: pathophysiology and clinical features. Heart Failure Reviews. 18(2), 149-166.

Miles, P.D., Treuner, K., Latronica, M., Olefsky, J.M. and Barlow, C. 2007. Impaired insulin secretion in a mouse model of ataxia telangiectasia. American Journal of Physiology, Endocrynology and Metabolism. 293(1), E70-E74 doi: 10.1152/ajpendo.00259.2006

Minamino, T. and Komuro, I. 2007. Vascular cell senescence: contribution to atherosclerosis. Circulation Research. 100(1), 15-26.

Miyauchi, H., Minamino, T., Tateno, K., Kunieda, T., Toko, H. and Komuro, I. Akt negatively regulates the in vitro lifespan of human endothelial cells via a p53/p21-dependent pathway. The EMBO Journal. 23(1), 212-220.

Mizukami, Y. and Yoshida, K. 1997. Mitogen-activated protein kinase translocates to the nucleus during ischaemia and is activated during reperfusion. The Biochemical Journal. 323(Pt 3), 785-790.

Mockridge, J.W., Marber, M.S. and Heads, R.J. 2000. Activation of Akt during simulated ischemia/reperfusion in cardiac myocytes. Biochemical and Biophysical Communications. 270(3), 947-952.

Moding, E.J., Lee, C.L., Castle, K.D., Oh, P., Mao, L., Zha, S., Min, H.D., Ma, Y., Das, S. and Kirsch, D.G. 2014. *ATM* deletion with dual recombinase technology preferentially radiosensitizes tumor endothelium. The Journal of Clinical Investigation. 124(8), 3325-3338.

Molavi, B. and Mehta, J.L. 2004. Oxidative stress in cardiovascular disease: molecular basis of its deleterious effects, its detection, and therapeutic considerations. Current Opinion in Cardiology. 19(5), 488-493.

Morbidelli, L., Donnini, S. and Ziche, M. 2003. Role of nitric oxide in the modulation of angiogenesis. Current Pharmaceutical Design. 9(7), 521-530.

Morino, K., Petersen, K.F. and Shulman, G.I. 2006. Molecular mechanisms of insulan resistance in humans and their potential links with mitochondrial dysfunction. Diabetes. 55(Suppl 2), S9-S15.

Morio, T., Takahashi, N., Watanabe, F., Honda, F., Sato, M., Takagi, M., Imadome, K., Miyawaki, T., Delia, D., Nakamura, K. et al. 2009. Phenotypic variations between affected siblings with ataxia-telangiectasia: ataxia-telangiectasia in Japan. International Journal of Hematology. 90(4), 455-462.

Morrel, D., Cromartie, E. and Swift, M. 1986. Mortality and cancer incidence in 263 patients with ataxia-telangiectasia. Journal of the National Cancer Institute. 77(1), 89-92.

Morrish, N.J., Wang, S.L., Stevens, L.K., Fuller, J.H. and Keen, H. 2001. Mortality and causes of death in the WHO Multinational Study of Vascular Disease in Diabetes. Diabetologia. 44(Suppl2), S14-S21.

Motshakeri, M., Goh, Y.M. and Ebrahimi, M. 2015. Metabolic effects of high sucrose and saturated oil feeding on insulin resistance in *Sprague-Dawley* rats. Indian Journal of Experimental Biology. 53(5), 264-272.

Mu, Y., Li, G., Wang, Z.H. and Zhang, C.J. 2011. Up-regulation of phosphorylated ATM/ATR substrate/Akt expression by phenylephrine in peri-infarct myocardium in rats. Acta Cardiologica Sinica. 27(3), 182-188.

Nakagawa, K., Taya, Y., Tamai, K. and Yamaizumi, M. Requirement of ATM in phosphorylation of the human p53 protein at serine 15 following DNA double-strand breaks. Molecular and Cellular Biology. 19(4), 2828-2834.

Nayler, W.G. 1981. The role of calcium in the ischemic myocardium. The American Journal of Pathology. 102(2), 262-270.

Nduhirabandi, F. 2014. The role of melatonin in cardioprotection: an investigation into the mechanisms involved in glucose homeostasis, microvascular endothelial function and mitochondrial function in normal and insulin resistant states. PhD Dissertation.

Neely, J.R., Liebermeister, H., Battersby, E.J. and Morgan, H.E. 1967. Effect of pressure development on oxygen consumption by isolated rat heart. The American Journal of Physiology. 212(4), 804-814.

Nielsen, S., Guo, Z., Johnson, C.M., Hensrud, D.D. and Jensen, M.D. 2004. Splanchnic lipolysis in human obesity. The Journal of Clinical Investigation. 113(11), 1582-1588.

Nieto-Vazquez, I., Fernández-Veledo, S., Krämer, D.K., Vila-Bedmar, R., Garcia-Guerra, L. And Lorenzo, M. 2008. Insulin resistance associated to obesity: the link TNF-alpha. Archives of Physiology and Biochemistry. 114(3), 183-194.

Nikoulina, S.E., Ciaraldi, T.P., Mudaliar, S., Carter, L., Johnson, K. and Henry, R.R. 2002. Inhibition of glycogen synthase kinase 3 improves insulin action and glucose metabolism in human skeletal muscle. Diabetes. 51(7), 2190-2198.

Noeman, S.A., Hamooda, H.E. and Baalash, A.A. 2011. Biochemical study of oxidative stress markers in the liver, kidney and heart of high fat diet induced obesity rats. Diabetology & Metabolic Syndrome. 3(1), 17 doi: 10.1186/1758-5996-3-17

Nolan, C.J., Madiraju, M.S.R., Delghingaro-Augusto, V., Peyot, M.L. and Prentki, M. 2006. Fatty acid signaling in the β-cell and insulin secretion. Diabetes. 55(S2), S16-S23.

Oleson, B.J., Broniowska, K.A., Schreiber, K.H., Tarakanova, V.L. and Corbett, J.A. 2014. Nitric oxide induces ataxia telangiectasia mutated (ATM) protein-dependent γH2AX protein formation in pancreatic β cells. The Journal of Biological Chemistry. 289(16), 11454-11464.

Omura, T., Yoshiyama, M., Shimada, T., Shimizu, N., Kim, S., Iwao, H., Takeuchi, K. and Yoshikawa, J. 1999. Journal of molecular and cellular cardiology. 31(6), 1269-1279.

Opie, L.H. and Lopaschuk, G.D. 2004. Fuels: aerobic and anaerobic metabolism. In: Opie LH, editor. Heart physiology: From cell to circulation. 4th ed.Philadelphia, PA: Lippincott Williams & Wilkins; pp. 306-354.

Ordway, G.A. and Garry, D.J. Myoglobin: an essential hemoprotein in striated muscle. The Journal of Experimental Biology. 207(Pt 20), 3441-3446.

Osborn, O. and Olefsky, J.M. 2012. The cellular and signaling networks linking the immune system and metabolism in disease. Nature Medicine. 18(3), 363-374.

Ott, M., Gogvadze, V., Orrenius, S. and Zhivotovsky, B. 2007. Mitochondria, oxidative stress and cell death. Apoptosis. 12(5), 913-922.

Ousset, M., Bouquet, F., Fallone, F., Biard, D., Dray, C., Valet, P., Salles, B. and Muller, C. 2010. Loss of ATM positively regulates the expression of hypoxia inducible factor 1 (HIF-1) through oxidative stress. Cell Cycle. 9(14), 2814-2822.

Pacher, P., Schulz, R., Liaudet, L. and Szabó, C. 2005. Nitrosative stress and pharmacological modulation of heart failure. Trends in Pharmacological Sciences. 26(6), 302-310.

Park, S.Y., Cho, Y.R., Kim, H.J., Higashimori, T., Danton, C., Lee, M.K., Dey, A., Rothermel, B., Kim, Y.B., Kalinowski, A., Russell, K.S. and Kim, J.K. 2005. Unraveling the temporal pattern of diet-induced insulin resistance in individual organs and cardiac dysfunction in C57BL/6 mice. Diabetes. 54(12), 3530-3540.

Pellegrini, M., Celeste, A., Didilippantonio, S., Guo, R., Wang, W., Feigenbaum, L. and Nussenzweig, A. 2006. Autophosphorylation at serine 1987 is dispensable for murine ATM activation in vivo. Nature. 443(7108), 222-225.

Peng, Y., Woods, R.G., Beamish, H., Ye, R., Lees-Miller, S.P., Lavin, M.F. and Bedford, J.S. 2005. Deficiency in the catalytic subunit of DNA-dependent protein kinase causes down-regulation of ATM. Cancer Research. 65(5), 1670-1677.

Peretz, S., Jensen, R., Baserga, R. and Glazer, P.M. 2001. ATM-dependent expression of the insulin-like growth factor-I receptor in a pathway regulating radiation response. Proceedings of the National Academy of Sciences of the United States of Ameria. 98(4), 1676-1681.

Peterson, L.R. 2006. Obesity and insulin resistance: effects on cardiac structure, function, and substrate metabolism. Current Hypertension Reports. 8(6), 451-456.

Peyssonnaux, C. and Eychène, A. 2012, The Raf/MEK/ERK pathway: new concepts of activation. Biology of the Cell. 93(1-2), 53-62.

Pike, L.J. 2009. The challenge of lipid rafts. The Journal of Lipid Research. 50(supple), S323-S328.

Powis, G., Bonjouklian, R., Berggren, M.M., Gallegos, A., Abraham, R., Ashendel, C., Zalkow, L., Matter, W.F., Dodge, J., Grindley, G. and Vlahos, C.J. 1994. Wortmannin, a potent and selective inhibitor of phosphatidylinositol-3-kinase. Cancer Research. 54(9), 2419-2423.

Quyyumi, A.A. 1998. Endothelial function in health and disease: new insights into the genesis of cardiovascular disease. The American Journal of Medicine. 105(1A), 32S-39S.

Rainey, M.D., Charlton, M.E., Stanton, R.V. and Kastan, M.B. 2008. Transient inhibition of ATM kinase is sufficient to enhance cellular sensitivity to ionizing radiation. Cancer Research. 68(18), 7466-7474.

Rajan, M.R., Fagerholm, S., Jönsson, C., Kjølhede, P., Turkina, M.V. and Strålfors, P. 2013. Phosphorylation of IRS1 at serine 307 in response to insulin in human adipocytes is not likely to be catalyzed by p70 ribosomal s6 kinase. PLoS One. 8(4), e59725 doi: 10.1371/journal.pone.0059725

Randle, P.J., Garland, P.B., Hales, C.N. and Newsholme, E.A. 1963. The glucose fatty-acid cycle. Its role in insulin sensitivity and the metabolic disturbances of diabetes mellitus. Lancet. 1(7285), 785-789.

Rasio, D., Negrini, M. and Croce, C.M. 1995. Genomic organization of the ATM locus involved in ataxia-telangiectasia. Cancer Research. 55(24), 6053-6057.

Ravingerova, T., Matejikova, J., Rancza, D. and Kolar, F. 2009. Reduced susceptibility to ischemia-induced arrhythmias in the preconditioned rat heart is independent of PI3-kinase/Akt. Physiological Research/Academia Scientiarum Bohemoslovaca. 58(3), 443-447.

Razani, B., Feng, C. and Semenkovich, C.F. 2010. p53 is required for chloroquine-induced atheroprotection but not insulin sensitization. Journal of Lipid Research. 51(7), 1738-1746.

Reichebach, J., Schubert, R., Schwan, C., Müller, K., Böhles, H.J. and Zielen, S. 1999. Anti-oxidative capacity in patients with ataxia telangiectasia. Clinical and Experimental Immunology. 117(3), 535-539.

Reichelt, M.E., Willems, L., Peart, J.N., Ashton, K.J., Matherne, G.P., Blackburn, M.R. and Headrick, J.P. 2007. Modulation of ischaemic contracture in mouse hearts: a 'supraphysiological' response to adenosine. Experimental Physiology. 92(1), 175-185.

Ricquier, D. and Bouillaud, F. 2000. Mitochondrial uncoupling proteins: from mitochondria to the regulation of energy balance. The Journal of Physiology. 529(1), 3-10.

Rosenberg, P. 2004. Mitochondrial dysfunction and heart disease. Mitochondrion. 4(5-6), 621-628.

Rosini, T.C., Silvva, A.S. and Moraes, C.D. 2012. Diet-induced obesity: rat model for the study of obesity-related disorders. Revista da Associação Médica Brasileira. 58(3), 383-387.

Rubler, S., Dlugash, J., Yuceoglu, Y.Z., Kumral, T., Branwood, A.W. and Grishman, A. 1972. New type of cardiomyopathy associated with diabetic glomerulosclerosis. The American Journal of Cardiology. 30(6), 595-602.

Ruderman, N.B., Carling, D., Prentki, M. and Cacicedo, J.M. 2013. AMPK, insulin resistance, and the metabolic syndrome. The Journal of Clinical Investigation. 123(7), 2764-2772.

Russell, R.R., Bergeron, R., Shulman, G.I. and Young, L.H. 1999. Translocation of myocardial GLUT-4 and increased glucose uptake through activation of AMPK by AICAR. American Physiological Society – Heart and Circulatory Physiology. 277(2), H643-H649.

Ryle, A.P., Sanger, F., Smith, L.F. and Kitai, R. 1955. The disulphide bonds of insulin. Biochemical Journal. 60(4), 541-556.

Sakamoto, K. and Holman, G.D. 2008. Emerging role for AS160/TBC1D4 and TBC1D1 in the regulation of GLUT4 traffic. American Journal of Physiology, Endocrinology and Metabolism. 295(1), E29-E37.

Saltiel, A.R. and Kahn, C.R. 2001. Insulin signalling and the regulation of glucose and lipid metabolism. Nature. 414(6865), 799-806.

Samuel, V.T. and Shulman, G.I. 2012. Integrating mechanisms for insulin resistance: common threads and missing links. Cell. 148(5), 852-871.

Sanger, F. and Thompson, E.O.P. 1953a. The amino-acid sequence in the glycyl chain of insulin. 1. The investigation of lower peptides from partial hydrolysates. Biochemical Journal. 53(3), 353–366.

Sanger, F. and Thompson, E.O.P. 1953b. The amino-acid sequence in the glycyl chain of insulin. 2. The investigation of peptides from enzymic hydrolysates. Biochemical Journal. 53(3), 366–374.

Sanger, F. and Tuppy, H. 1951a. The amino-acid sequence in the phenylalanyl chain of insulin. 1. The identification of lower peptides from partial hydrolysates. Biochemical Journal. 49(4), 463–481.

Sanger, F. and Tuppy, H. 1951b. The amino-acid sequence in the phenylalanyl chain of insulin. 2. The investigation of peptides from enzymic hydrolysates. Biochemical Journal. 49(4), 481–490.

Sano, H., Kane, S., Sano, E., Mîinea, C.P., Asara, J.M., Lane, W.S., Garner, C.W. and Lienhard, G.E. 2003. Insulin-stimulated phosphorylation of a rab GTPase-activating protein regulates GLUT4 translocation. The Journal of Biological Chemistry. 278(17), 14599-14602.

Sarbassov, D.D., Guertin, D.A., Ali, S.M. and Sabatini, D.M. 2005. Phosphorylation and regulation of Akt/PKB by the rictor-mTOR complex. Science. 307(5712), 1098-1101.

Sarkaria, J.N., Tibbetts, R.S., Busby, E.C., Kennedy, A.P., Hill, D.E. and Abraham, R.T. 1998. Inhibition of phosphoinositide 3-kinase related kinases by the radiosensitizing agent wortmannin. Cancer Research. 58(19), 4375-4382.

Sarti, P., Giuffrè, A., Barone, M.C., Forte, E., Mastronicola, D. and Brunori, M. 2003. Nitric oxide and cytochrome oxidase: reaction mechanisms from the enzyme to the cell. Free Radical Biology & Medicine. 34(5), 509-520.

Sato, T., Sato, H., Oguchi, T., Fukushima, H., Carvalho, G., Latterman, R., Matsukawa, T. and Schricker, T. 2014. Insulin preconditioning elevates p-Akt and cardiac contractility after reperfusion in the isolated ischemic rat heart. Biomedical Research International. 2014, 536510 doi: 10.1155/2014/536510

Savarino, A., Boelaert, J.R., Cassone, A., Majori, G. and Cauda, R. 2003. Effects of chloroquine on viral infections: an old drug against today's diseases? The Lancet. Invectious Diseases. 3(11), 722-727.

Savitsky, K., Bar-Shira, A., Gilad, S., Rotman, G., Ziv, Y., Vanagaite, L., Tagle, D.A., Smith, S., Uziel, T., Sfez, S., Ashkenazi, M., Pecker, I., Frydman, M., Harnik, R., Patanjali, S.R., Simmons, A., Clines, G.A., Sartiel, A., Gatti, R.A., Chessa, L., Sanal, O., Lavin, M.F., Jaspers, N.G., Taylor, A.M., Arlett, C.F., Miki, T., Weissman, S.M., Lovett, M., Collins, F.S. and Shiloh, Y. 1995. A single ataxia-telangiectasia gene with a product similar to PI-3 kinase. Science. 268(5218), 1749-1753.

Schalch, D.S., McFarlin, D.E. and Barlow, M.H. 1970. An unusual form of diabetes mellitus in ataxia telangiectasia. The New England Journal of Medicine. 282(25), 1396-13402.

Schenk, S., Harber, M.P., Shrivastava, C.R., Burant, C.F. and Horowitz, J.F. 2009. Improved insulin sensitivity after weight loss and exercise training is mediated by a reduction in

plasma fatty acid mobilization, not enhanced oxidative capacity. The Journal of Physiology. 587(20), 4949-4961.

Scheuner, D. and Kaufman, R.J. 2008. The unfolded protein response: a pathway that links insulin demand with β-cell failure and diabetes. Endocrine Reviews. 29(3), 317-333.

Schneider, J.G., Finck, B.N., Ren, J., Standley, K.N., Takagi, M., Maclean, K.H., Bernal-Mizrachi, C., Muslin, A.J., Kastan, M.B. and Semenkovich, C.F. 2006. ATM-dependent suppression of stress signaling reduces vascular disease in metabolic syndrome. Cell Metabolism. 4(5), 377-389.

Seger, R. and Krebs, E.G. 1995. The MAPK signaling cascade. FASEB Journal 9(9), 726-735.

Semlitsch, M., Shackelford, R.E., Zirkl, S., Sattler, W. and Malle, E. 2011. ATM protects against oxidative stress induced by oxidized low-density lipoprotein. DNA Repair. 10(8), 848-860.

Shackelford, D.B. and Shaw, R.J. 2009. The LKB1-AMPK pathway: metabolism and growth control in tumour suppression. Nature Reviews: Cancer. 9(8), 563-575.

Shashkin, P., Dragulev, B. and Ley, K. 2005. Macrophage differentiation to form foam cells. Current Pharmaceutical Design. 11(23), 3061-3072.

Sheeram, S., Demidov, O.N., Hee, W.K., Yamaguchi, H., Onishi, N., Kek, C., Timofeev, O.N., Dudgeon, C., Fornace, A.J., Anderson, C.W., Minami, Y., Appella, E. and Bulavin, D.V. 2006. Wip1 phosphatase modulates ATM-dependent signaling pathways. Molecular Cell. 23(5), 757-764.

Shimizu, I., Minamino, T., Toko, H., Okada, S., Ikeda, H., Yasuda, N., Tateno, K., Moriya, J., Yokoyama, M., Nojima, A. et al. 2010. Excessive cardiac insulin signaling exacerbates systolic dysfunction induced by pressure overload in rodents. The Journal of Clinical Investigation. 120(5), 1506-1514.

Shimizu, M., Umeda, K., Sugihara, N., Yoshio, H., Ino, H., Takeda, R., Okada, Y. and Nakanishi, I. 1993. Collagen remodelling in myocardial of patients with diabetes. Journal of Clinical Pathology. 46(1), 32-36.

Shizukuda, Y., Buttrick, P.M., Geenen, D.L., Borczuk, A.C., Kitsis, R.N. and Sonnenblick, E.H. 1998. β-adrenergic stimulation causes cardiocyte apoptosis: influence of tachycardia and hypertrophy. The American Journal of Physiology. 275(3 Pt 2), H961-H968.

Shoelson, S.E. 2002. Banking on ATM as a new target in metabolic syndrome. Cell Metabolism. 4(5), 337-338.

Shrayyef, M.Z. and Gerich, J.E. 2010. Normal glucose homeostasis. In: Poretsky, L. (ed.), Principles of diabetes mellitus 2nd edition: Springer Science & Business Media. 19-35.

Sidhu, A.B.S., Verdier-Pinard, D. and Fidock, D.A. 2002. Chloroquine resistance in *Plasmodium falciparum* malaria parasites conferred by pfcrt mutations. Scinece. 298(5591), 210-213.

Sies, H. 1997. Oxidative stress: oxidants and antioxidants. Experimental Physiology. 82(2), 291-195.

Skrzypiec-Spring, M., Grotthus, B., Szeląg, A. and Schulz, R. 2007. Isolated heart perfusion according to Langendorff – Still viable in the new millennium. Journal of Pharmacological and Taxicological Methods. 55(2), 113-126.

Slater, A.F.G. 1993. Chloroquine: mechanism of drug action and resistance in *Plasmodium falciparum*. Pharmacology & Therapeutics. 57(2-3), 203-235.

Slettom, G., A.K. Jonassen, Dahle, G.O., Seifert, R., Larsen, T.H., Berge, R.K. and Nordrehaug, J.E. 2016. Insulin postconditioning reduces infarct size in the porcine heart in a dose-dependent manner. Journal of Cardiovascular Pharmacology and Therapeutics. doi: 10.1177/1074248416657611

Snel, M., Jonker, J.T., Schoones, J., Lamb, H., de Roos, A., Pijl, H., Smit, J.W.A., Meinders, A.E. and Jazet, I.M. 2012. Ectopic fat and insulin resistance: pathophysiology and effect of diet and lifestyle interventions. International Journal of Endocrinology. 2012, 1-18 doi: 10.1155/2012/983814

Somaratne, J.B., Whalley, G.A., Poppe, K.K., ter Bals, M.M., Wadams, G., Pearl, A., Bagg, W. and Doughty, R.N. 2011. Screening for left ventricular hypertrophy in patients with type 2 diabetes mellitus in the community. Cardiovascular Diabetology. 10, 29 doi: 10.1186/1475-2840-10-29

Sonksen, P. and Sonksen, J. 2000. Insulin: understanding its action in health and disease. British Journal of Anaesthesia. 85(1), 69-79.

Sowers, J.R. and Lester, M.A. 1999. Diabetes and cardiovascular disease. Diabetes Care. 22, C14-C20.

Sowers, J.R., Whaley-Connell, A. And Hayden, M.R. 2011. The role of overweight and obesity in the cardiorenal syndrome. Cardiorenal Medicine. 1(1), 5-12.

Spinale, F.G. 2002. Matrix metalloproteinases: regulation and dysregulation in the failing heart. Circulation Research. 90(5), 520-530.

Staehr, P., Hother-Nielsen, O., Landau, B.R., Chandramouli, V., Holst, J.J. and Beck-Nielsen, H. 2003. Effects of free fatty acids per se on glucose production, gluconeogenesis, and glycogenolysis. Diabetes. 52(2), 260-267.

Stanley, W.C., Lopaschuk, G.D., Hall, J.L. and McCormack, J.G. 1997. Regulation of myocardial carbohydrate metabolism under normal and ischaemic conditions. Potential for pharmacological interventions. Cardiovascular Research. 33(2), 243-257.

Stanley, W.C., Recchia, F.A. and Lopaschuk, G.D. 2005. Myocardial substrate metabolism in the normal and failing heart. Physiological Reviews. 85(3), 1093-1129.

Steinberg, G.R., Michell, B.J., van Denderen, B.J., Watt, M.J., Carey, A.L., Fam, B.C., Andrikopoulos, S., Proietto, J., Görgün, C.Z., Carling, D. et al. 2006. Cell Metabolism. 4(6), 465-474.

Steinberg, H.O., Chaker, H., Leaming, R., Johnson, A., Brechtel, G. and Baron, A.D. 1996. Obesity/insulin resistance is associated with endothelial dysfunction. Implications for the syndrome of insulin resistance. The Journal of Clinical Investigation. 97(11), 2601-2610.

Su, Y. and Swift, M. 2000. Mortality rates among carriers of ataxia-telangiectasia mutant alleles. Annals of Internal Medicine. 133(10), 770-778.

Sutherland, F.J. and Hearse, D.J. 2000. The isolated blood and perfusion fluid perfused heart. Pharmacological Research. 41(6), 613-627.

Suzuki, A., Kusakai, G.I., Kishimoto, A., Shimojo, Y., Ogura, T., Lavin, M.F. and Esumi, H. 2004. IFG-1 phosphorylates AMPK-α subunit in ATM-dependent and LKB1-independent manner. Biochemical and Biophysical Research Communications. 324(3), 986-992.

Swift, M. and Chase, C. 1983. Cancer and cardiac deaths in obligatory ataxia-telangiectasia heterozygotes. Lancet. 321(8332), 1049-1050.

Swift, M., Morrel, D., Cromartie, E., Chamberlin, A.R., Skolnick, M.H. and Bishop, D.T. 1986. The incidence and gene frequency of ataxia-telangiectasia in the United States. American Journal of Human Genetics. 39(5), 573-583.

Taegtmeyer, H. 2000. Metabolism - The lost child of cardiology. Journal of the American College of Cardiology. 36(4), 1386-1388.

Taegtmeyer, H., Goodwin, G.W., Doenst, T. and Frazier, O.H. 1997. Substance metabolism as a determinant for postischemic functional recovery of the heart. The American Journal of Cardiology. 80(3A), 3A-10A.

Takagi, M., Uno, H., Nishi, R., Sugimoto, M., Hasegawa, S., Piao, J., Ihara, N., Kanai, S., Kakei, S., Tamura, Y. et al. ATM regulates adipocyte differentiation and contributes to glucose homeostasis. Cell Reports. 10(6), 957-967.

Tani, M. 1990. Mechanisms of Ca^{2+} overload in reperfused ischemic myocardium. Annual Review of Physiology. S2, S45-S59.

Taniguchi, C.M., Emanuelli, B. and Kahn, C.R. 2006. Critical nodes in signalling pathways: insights into insulin action. Nature Reviews: Molecular Cell Biology. 7(2), 85-96.

Teixeira, R.A., Martinelli Filho, M., Benvenuti, L.A., Costa, R., Pedrosa, A.A. and Nishióka, S.A. 2002. Cardiac damage from chronic use of chloroquine. A case report and review of the literature. Arquivos Brasileiros De Cardiologia. 79(1),85-88.

Temsah, R.M., Netticadan, T., Chapman, D., Takeda, S., Mochizuki, S. and Dhalla, N.S. 1999. Alterations in sarcoplasmic reticulum function and gene expression in ischemic-reperfused rat heart. The American Journal of Physiology. 277(2 Pt 2), H584-H594.

Thim, T., Bentzon, J.F., Kristiansen, S.B., Simonsen, U., Anderson, H.L., Wassermann, K. and Falk, E. 2006. Size of myocardial infarction induced by ischaemia/reperfusion is unaltered in rats with metabolic syndrome. Clinical Science. 110(6), 665-671.

Thornton, T.M., Delgado, P., Chen, L., Salas, B., Krementsov, D., Fernandez, M., Vernia, S., Davis, R.J., Heimann, R., Teuscher, C. et al. 2016. Inactivation of nuclear GSK3β by Ser(389) phosphorylation promotes lymphocyte fitness during DNA double-strand break response. Nature Communications. 7, 10553 doi: 10.1038/ncomms10553

Thygesen, K., Alpert, J.S. and White, H.D. 2007. ESC/ACCF/AHA/WHF Expert Consensus Document: Universal definition of myocardial infarction. Journal of the American College of Cardiology. 50(22), 2173-2195.

Tomasovic, A., Kurrle, N., Banning, A. And Tikkanen, R. 2012. Role of Cbl-associated protein/ponsin in receptor tyrosine kinase signaling and cell adhesion. Journal of Molecular Biochemistry. 1(3), 171-182.

Tönnesmann, E., Kandolf, R. and Lewalter, T. 2013. Chloroquine cardiomyopathy – a review of the literature. Immunopharmacology and Immunotoxicology. 35(3), 434-442.

Torrance, S.M., Belanger, M.P., Wallen, W.J. and Wittnich, C. 2000. Metabolic and functional response of neonatal pig hearts to the development of ischemic contracture: is recovery possible? Pediatric Research. 48(2), 191-199.

Tran, H., Brunet, A., Griffith, E.C. and Greenberg, M.E. 2003. The many forks in FOXO's road. Science's STKE: Signal Transduction Knowledge Environment. 2003(172), RE5.

Treebak, J.T., Glund, S., Deshmukh, A., Klein, D.K., Long, Y.C., Jensen, T.E., Jørgensen, S.B., Viollet, B., Andersson, L., Neumann, D. et al. 2006. AMPK-mediated AS160 phosphorylation in skeletal muscle is dependent on AMPK catalytic and regulatory subunits. Diabetes. 55(7), 2051-2058.

Tremblay, F. and Marette, A. 2001. Amino acid and insulin signaling via the mTOR/p70S6 kinase pathway. A negative feedback mechanism leading to insulin resistance in skeletal muscle cells. The Journal of Biological Chemistry. 276(41), 28052-28060.

Tsang, A., Hausenloy, D.J., Monanu, M.M. and Yellon, D.M. 2004. Postconditioning: a form of "modified reperfusion" protects the myocardium by activating the phosphatidylinositol 3-kinase-Akt pathway. Circulation Research. 95(3), 230-232.

Tzanavari, T., Giannogonas, P. and Karalis, K.P. 2010. TNF-alpha and obesity. Current Directions in Autoimmunity. 11, 145-156.

Utriainen, T., Takala, T., Luotolahti, M., Rönnemaa, T., Laine, H., Ruotsalainen, U., Haaparanta, M., Nuutila, P. and Yki-Järvinen, H. 1998. Insulin resistance characterizes glucose uptake in skeletal muscle but not in the heart in NIDDM. Diabetologia. 41(5), 555-559.

Uziel, T., Lerenthal, Y., Moyal, L., Andegeko, Y., Mittelman, L. and Shiloh, Y. 2003. Requirement of the MRN complex for ATM activation by DNA damage. The EMBO Journal. 22(20), 5612-5621.

Valentine, R.J., Coughlan, K.A., Ruderman, N.B. and Saha, A.K. 2014. Insulin inhibits AMPK activity and phosphorylates AMPK $Ser^{485/491}$ through Akt in hepatocytes, myotubes and incubated rat skeletal muscle. Archives of Biochemistry and Biophysics. 562, 62-69.

Valentin-Vega, Y.A., MacLean, K.H., Tait-Mulder, J., Milasta, S., Steeves, M., Dorsey, F.C., Cleveland, J.L., Green, D.R. and Kastan, M.B. 2012. Mitochondrial dysfunction in ataxia-telangiectasia. Blood. 199(6), 1490-1500.

Van Beek, J.H.G.M. 1996. Heat generation and transport in the heart. Journal fo Engineering Physics and Thermophysics. 69(3), 287-297.

Van Vuuren, M.A. 2015. The role of ATM in the regulation of cardiomyocyte glucose utilization under normal and insulin resistant conditions. MSc Dissertation.

van Weel, V., Deckers, M.M.L., Grimbergen, J.M., van Leuven, K.J., Lardenoye, H.H., Schlingemann, R.O., van Nieuw Amerongen, G.P., van Bockel, J.H., van Hinsbergh, V.W. and Quax, P.H. 2004. Vascular endothelial growth factor overexpression in ischemic skeletal muscle enhances myoglobin expression in vivo. Circulation Research. 95(1), 58-66.

Vatier, C., Kadiri, S., Muscat, A., Chapron, C., Capeau, J. and Antoine, B. 2012. Visceral and subcutaneous adipose tissue from lean women respond differently to lipopolysaccharide-induced alteration of inflammation and glyceroneogenesis. Nutrition and Diabetes. 2(12), e51 doi: 10.1038/nutd.2012.29

Vecchio, D., Daga, A., Carra, e., Marubbi, D., Baio, G., Neumaier, C.E., Vagge, S., Corvò, R., Brisigotti, M.P., Ravetti, J.P. et al. 2014. Predictability, efficacy and safety of radiosensitization of glioblastoma-initiating cells by the ATM inhibitor KU-60019. International Journal of Cancer. 135(2), 479-491.

Vecchio, D. and Frosina, G. 2014. Targeting the Ataxia Telangiectasia Mutated protein in cancer therapy. Current Drug Targets. PMID 25382204.

Viniegra, J.G., Martínez, N., Modirassari, P., Losa, J.H., Cobo, C.P., Lobo, V.J.S.A., Luquero, C.I.A., Álvarez-Vallina, L., y Cajal, S.R., Rojas, J.M. and Sánchez-Prieto, R. 2005. Full activation of PKB/Akt in response to insulin or ionizing radiation is mediated through ATM. The Journal of Biological Chemistry. 280(6), 4029-4036.

von Zglinicki, T., Saretzki, G., Ladhoff, J., d'Adda di Fagagna, F. and Jackson, S.P. 2005. Human cell senescence as a DNA damage response. Mechanisms of Ageing and Development. 126(1), 111-117.

Wang, J.C. and Bennett, M. 2012. Aging and atherosclerosis: mechanisms, functional consequences, and potential therapeutics for cellular senescence. Circulation Research. 111(2), 245-259.

Wattanapitayakul, S.K. and Bauer, J.A. 2001. Oxidative pathways in cardiovascular disease. Roles, mechanisms, and therapeutic implications. Pharmacology & Therapeutics. 89(2), 187-206.

Watters, D.J. 2003. Oxidative stress in ataxia telangiectasia. Redox Report: Communications in Free Radical Research. 8(1), 23-29.

Webster, I., Smith, A., Lochner, A. and Huisamen, B. 2014. Sanguinarine non- versus re-circulation during isolated heart perfusion – a Jekyll and hyde effect? Cardiovascular Drugs and Therapy. 28(5), 489-491.

Weisberg, S.P., McCann, D., Desai, M., Rosenbaum, M., Leibel, R.L. and Ferrante, A.W. 2003. Obesity is associated with macrophage accumulation in adipose tissue. The Journal of Clinical Investigation. 112(12), 1796-1808.

Weiss, R.G. and Maslov, M. 2004. Normal myocardial metabolism: fueling cardiac contraction. Advanced Studies in Medicine. 4(6B), S457-S463.

Welbourn, C.R.B., Goldman, G., Paterson, I.S., Valeri, C.R., Shepro, D. and Hechtman, H.B. 1991. Pathophysiology of ischaemia reperfusion injury: central role of the neutrophil. The British Journal of Surgery. 78(6), 651-655.

Welsh, G.I., Hers, D.C., Berwick, D.C., Dell, G., Wherlock, M., Birkin, R., Leney, S. and Tavaré, J.M. 2005. Role of protein kinase B in insulin-regulated glucose uptake. Biochemical Society Transactions. 33(2), 346-349.

Wensley, I., Salaveria, K., Bulmer, A.C., Donner, D.G. and du Toit, E.F. 2013. Myocardial structure, function and ischaemic tolerance in a rodent model of obesity with insulin resistance. Experimental Physiology. 98(11), 1552-1564.

White, M.F. 1998. The IRS-signalling system: a network of docking proteins that mediate insulin action. Molecular and Cellular Biochemistry. 182(1-2), 3-11.

White, M.F. 2003. Insulin signalling in health and disease. Science. 302(5651), 1710-1711.

Williams, S.B., Cusco, J.A., Roddy, M.A., Johnstone, M.T. and Creager, M.A. 1996. Impaired nitric oxide-mediated vasodilation in patients with non-insulin-dependent diabetes mellitus. Journal of the American College of Cardiology. 27(3), 567-574.

Witters, L.A. and Kemp, B.E. 1992. Insulin activation of acetyl-CoA carboxylase accompanied by inhibition of the 5'-AMP-activated protein kinase. The Journal of Biological Chemistry. 265(5), 2864-2867.

Wiza, C., Nascimento, E.B. and Ouwens, D.M. 2012. Role of PRAS40 in Akt and mTOR signaling in health and disease. American Journal of Physiology, Endocrinology and Metabolism. 302(12), E1453-E1460.

Wu, D., Yang, H., Xiang, W., Zhou, L., Shi, M., Julies, G., Laplante, J.M., Ballard, B.R. and Guo, Z. 2005. Heterozygous mutation of ataxia-telangiectasia mutated gene aggravates hypercholesterolemia in apoE-deficient mice. Journal of Lipid Research. 46(7), 1380-1387.

Xie, Z., He, C. and Zou, M.H. AMP-activated protein kinase modulates cardiac autophagy in diabetic cardiomyopathy. Autophagy. 7(10), 1254-1255.

Xu, F.P., Chen, M.S., Wang, Y.Z., Yi, Q., Lin, S.B., Chen, A.F. and Luo, J.D. 2004. Leptin induces hypertrophy via endothelin-1-reactive oxygen species pathway in cultured neonatal rat cardiomyocytes. Circulation. 110(10), 1269-1275.

Yang, D.Q., Halaby, M., Li, Y., Hibmam, J.C. and Burn, P. 2011. Cytoplasmic ATM protein kinase: an emerging therapeutic target for diabetes, cancer and neuronal degeneration. Drug Discovery Today. 16(7-8), 332-338.

Yang, D.Q. and Kastan, M.B. 2000. Participation of ATM in insulin signaling through phosphorylation of eIF-4E-binding protein 1. Nature Cell Biology. 2(12), 893-898.

Yang, Z., Xie, C., Xu, C., Liu, G., Cao, X., Li, W., Chen, J., Zhu, Y., Luo, S., Luo, Z. et al. 2015. Phosphorylation and inactivation of PTEN at residues Ser380/Thr382/383 induced by Helicobacter pylori promotes gastric epithelial cell survival through PI3K/Akt pathway. Oncotarget. 6(31), 191601926.

Yellon, D.M. and Baxter, G.F. 1999. Reperfusion injury revisiter: is there a role for growth factor signaling in limiting lethal reperfusion injury? Trends in Cardiovascular Medicine. 9(8), 245-249.

Yin, T., Sandhu, G., Wolfgang, C.D., Burrier, A., Webb, R.L., Rigel, D.F., Hai, T. and Whelan, J. 1997. Tissue-specific pattern of stress kinase activation in ischemic/reperfused heart and kidney. The Journal of Biological Chemistry. 272(32), 19943-19950.

Young, L.H., Ikeda, Y., Scalia, R. And Lefer, A.M. 2000. Wortmannin, a potent antineutrophil agent, exerts cardioprotective effects in myocardial ischemia/reperfusion. The Journal of Pharmacology and Experimental Therapeutics. 295(1), 37-43.

Ytrehus, K. 2006. Models of myocardial ischemia. Drug Discovery Today: Disease Models. 3(3), 263-271.

Yu, X.H., Fu, Y.C., Zhang, D.W., Yin, K. and Tang, C.K. 2013. Foam cells in atherosclerosis. Clinica Chimica Acta. 424, 245-252.

Yusuf, S., Hawken, S., Ounpuu, S., Bautista, L., Franzosi, M.G., Commerford, P., Lang, C.C., Rumboldt, Z., Onen, C.L., Lisheng, L. et al. 2005. Obesity and the risk of myocardial infarction in 27,000 participants from 52 countries: a case-control study. The Lancet. 366(9497), 1640-1649.

Zakikhani, M., Bazile, M., Hashemi, S., Javeshghani, S., Avizonis, D., St Pierre, J., Pollak, M.N. 2012. Alterations in cellular energy metabolism associated with the antiproliferative effects of the ATM inhibitor KU-55933 and with metformin. PloS one. 7(11), e49513. doi: 10.1371/journal.pone.0049513

Zhan, H., Suzuki, T., Aizawa, K., Miyagawa, K. and Nagai, R. 2010. Ataxia telangiectasia mutated (ATM)-mediated DNA damage response in oxidative stress-induced vascular endothelial cell senescence. The Journal of Biological Chemistry. 285(38), 29662-29670.

Zhou, J., Li, G., Wang, Z.H., Wang, L.P. and Dong, P.J. 2013. Effects of low-dose hydroxychloroquine on expression of phosphorylated Akt and p53 proteins and cardiomyocyte apoptosis in peri-infarct myocardium in rats. Experimental and Clinical Cardiology. 18(2), e95-e98.

Zhou, K., Bellenguez, C., Spencer, C.C.A. et al. 2011. Common variants near ATM are associated with glycemic response to metformin in type 2 diabetes: The GoDARTS and UKPDS Diabetes Pharmacogenetics Study Group and the Wellcome Trust Case Control Consortium 2. Nature Genetics. 43(2), 117-120.

Zhou, Y.T., Grayburn, P., Karim, A., Shimabukuro, M., Higa, M., Baetens, D., Orci, L. and Unger, R.H. 2000. Lipotoxic heart disease in obese rats: implications for human obesity. Proceedings of the National Academy of Sciences of the United States of America. 97(4), 1784-1789.

Internet Resources:

International Diabetes Federation. IDF diabetes atlas sixth edition poster update 2014. http://www.idf.org/sites/default/files/Atlas-poster-2014_EN.pdf (Accessed 28/07/2015)

National Center for Biotechnology Information. http://www.ncbi.nlm.nih.gov/protein/AAB65827.1 (Accessed 12/10/2015)

Privett, K., Kunert, M.P. and Lombard, J.H. 2004. Vascular phenotypes: high throughput characterization of vascular reactivity in rats conditioned on 0.4% and 4.0% NaCl diet. User manual for vascular tension studies. Medical College of Wisconsin. http://pga.mcw.edu/pga2/documents/vascular_protocol_manual_020304.pdf (Accessed 26/02/2016)

SPIKE: Signaling Pathway Integrated Knowledge Engine. http://www.cs.tau.ac.il/~spike/ (Accessed 13/10/2015)

The Jackson Laboratory mouse strain datasheet. 129S6/SvEvTac-*ATM*^{tm1Awb}/J. https://www.jax.org/strain/002753 (Accessed 16/10/2015)

World Health Orgaization. 10 Facts on noncommunicable diseases. http://www.who.int/features/factfiles/noncommunicable_diseases/en/ (Accessed 07/07/2016)

World Health Organization. Cardiovascular diseases (CVDs). Fact sheet number 317. http://www.who.int/mediacentre/factsheets/fs317/en/ (Accessed 27/07/2015)

World Health Organization. Obesity and overweight. Fact sheet number 311. http://www.who.int/mediacentre/factsheets/fs311/en/ (Accessed 12/09/2015)

World Health Organization. The top 10 causes of death. Fact sheet number 310. http://www.who.int/mediacentre/factsheets/fs310/en/ (Accessed 27/07/2015)